Solar heating in Greenland

Resource assessment and potential

Dragsted, Janne; Furbo, Simon

Publication date:
2011

Document Version
Også kaldet Forlagets PDF

Citation (APA):
Dragsted, J., & Furbo, S. (2011). Solar heating in Greenland: Resource assessment and potential. Kgs. Lyngby, Denmark: Technical University of Denmark (DTU). (DTU Civil Engineering Report; Nr. R-240).

Solar heating in Greenland

Resource assessment and potential

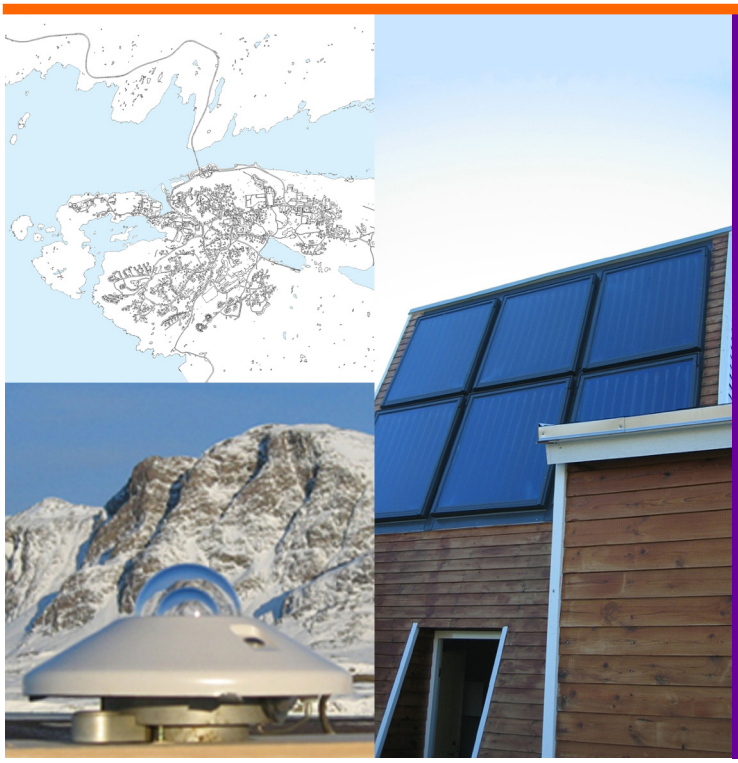

Janne Dragsted

PhD Thesis

Department of Civil Engineering

2011

DTU Civil Engineering Report R-240 (UK)
May 2011

DTU Civil Engineering
Department of Civil Engineering

Solar heating in Greenland

Resource assessment and potential

Printed by

Building Physics and Services
Department of Civil Engineering
Technical University of Denmark

Report R-240
ISBN: 978877973203
March 2011

Preface

This thesis is submitted for the degree of Doctor of Philosophy at the Technical University of Denmark.

The thesis focuses on solar heating in Greenland, and presents an investigation of the available solar radiation and the potential for solar heating in Greenland.

The project was performed from 1st of March 2007 until 28th of March 2011. It should be mentioned that during the process of working on the thesis leaves of absence totaling 9 months occurred in order to carry out work on other solar energy related projects. The funding for this PhD was provided by the Technical University of Denmark.

The work was carried out at the Section for Building Physics and Services at the Department of Civil Engineering at the Technical University of Denmark. The field work in connection with this PhD took place in Sisimiut, Greenland, where solar radiation measurements and data from operating solar heating systems were collected.

The supervisor for this PhD is Associate Professor Simon Furbo.

Kongens Lyngby, 28 March 2011

Acknowledgements

A great deal of help and support has been given to me over the past four years while working on this PhD. Without it I would not have been able to complete my thesis and I would therefore like to give my deepest thanks and appreciation to the following:

- My supervisor, Simon Furbo, for his guidance and support, and for always taking the time to discuss my methods and results.
- My colleagues in the solar group, Bengt Perers, Elsa Andersen, Ziqian Chen and Jianhua Fan, for offering their help and support.
- My colleagues at the Section for Building Physics and Services for their good company and friendly discussions.
- My 'extended' colleagues at ARTEK, for their support and good spirit.
- My colleagues in the laboratory, Martin Dandanell, Lars Kokholm Andersen, Poul Linnert Christiansen and Klaus Myndal for their assistance both in Denmark and in Greenland.
- My friends and family for their support and patience, especially my mother for proof reading this thesis.
- The staff at the Knud Rasmussen Folk High School for allowing me time and time again to barge into the boiler room.
- The occupants of the Low Energy House for their patience.
- Asiaq for providing me with solar radiation data from Greenland.
- DTU for granting me the PhD scholarship.

List of papers

Main author

J. Dragsted, S. Furbo, E. Andersen, B. Karlsson (2007)	*"Measured reflection from snow"* ISES solar world congress 2007, Beijing, China, September 18-21
J. Dragsted, S. Furbo, J. Fan (2008)	*"Solar heating systems in the Arctic"* Conference: Sustainable energy supply in the Arctic, Sisimiut, Greenland, March 1-3
J. Dragsted, S. Furbo, E. Andersen (2008)	*"Investigation of solar radiation models for high northern latitudes"* Conference: Sustainable energy supply in the Arctic, Sisimiut, Greenland, March 1-3
J. Dragsted. S. Furbo, J. Fan (2008)	*"Performance investigations of differently designed heat-pipe evacuated tubular collectors in the Arctic climate"* Eurosun 2008 – International conference on Solar heating, Cooling and Buildings, Lisbon, Portugal, October 7-10
J. Dragsted, S. Furbo (2009)	*"Applying measured reflection from the ground to simulations of thermal performance of solar collectors"* ISES solar world congress 2009, Johannesburg, South Africa, October 11-14
J. Dragsted, S. Furbo, Z. Chen, B. Perers (2010)	*"Pressure and temperature development in solar heating system during stagnation"* Conference: Eurosun 2010 – International conference on Solar heating, Cooling and Buildings, Graz, Austria, September 28th – October 1st

Co-author

J. Fan, J. Dragsted, S. Furbo (2007) *"Validation of simulation models for differently designed heat-pipe evacuated tubular collectors"* ISES solar world congress 2007, Beijing, China, September 18-21

J. Fan, J. Dragsted, S. Furbo (2007) *"Side-by-side tests of differently designed evacuated tubular collectors"* ISES solar world congress 2007, Beijing, China, September 18-21

J. Fan, J. Dragsted, S. Furbo (2008) *"A long term test of differently designed evacuated tubular collectors"* Eurosun 2008 – International conference on Solar heating, Cooling and Buildings, Lisbon, Portugal, October 7-10

C. Rode, J. Kragh, E. Borchersen, P. Vladyková, S. Furbo, J. Dragsted (2009) *"Performance of the Low-energy House in Sisimiut"* Cold Climate HVAC 2009, Sisimiut, Greenland

Reports

J. Dragsted, S. Furbo, B. Perers, Z. Chen (2009) *"Solfangerkreds med stor ekspansionsbeholder og fordampning i solfanger ved faretruende høje temperaturer til sikring af solfangervæske og anlæg - Kvalitetssikring af solvarme, Fase 3"* Department of Civil Engineering, report no. SR-10-04

J. Fan, S. Furbo, J. Andersen (now Dragsted, R. Jørgensen, L. J. Shah (2006) *"Bæredygtigt arktisk byggeri i det 21. århundrede. Vakuumrørsolfangere – slutrapport til VILLUM KANN RASMUSSEN FONDEN".* Department of Civil Engineering, report no. SR-06-10

Abstract

Solar energy is a clean and natural energy source. The solar radiation on earth – including at Arctic latitudes – is so large that it is possible to utilize solar energy on a large scale. Using solar energy means reducing the use of fossil fuels. The use of solar energy varies from country to country, as does the design of the solar heating systems.

The purpose of this study is to investigate the solar radiation potential in Greenland, and to investigate how a solar heating system for Greenland should be designed.

In the Arctic several conditions must be taken into account in terms of solar radiation at these latitudes. The sun is positioned low on the sky, which means that the optimum tilt angle of a receiving surface will increase. Also most solar radiation appears in the summertime, where there, at latitudes above the Arctic Circle, is solar radiation 24 hours a day and radiation from all directions. The reflection from the snow will increase the solar radiation on tilted surfaces.

The potential of utilizing solar radiation is evaluated based on measurements from several different climate stations in Greenland. An investigation of solar radiation models and their suitability for locations in Greenland is carried out. The investigation analyses the diffuse correlation methods developed by 'Erbs et al.' and 'Orgill and Hollands'. The results show that the two correlations both underestimate the diffuse radiation and overestimate the beam radiation, with 'Orgill and Hollands' as the most accurate. Further an investigation of four different radiation models is carried out and shows that they are not suitable for the conditions in Greenland. Of the four models the 'Liu and Jordan' model - the simple isotropic model - is the most accurate.

In Sisimiut measurements of the total radiation and the ground reflected radiation have been carried out since 2003. This data provides the basis for an investigation of the reflection coefficient for the ground for periods with and without snow. The measurements show that snow reflects solar radiation like a mirror. The effective albedo is therefore given as a function of the difference between the solar azimuth and the surface azimuth. Equations for the effective albedo is determined for each month of the year based on the measurements, and can be used as input for simulation models.

The solar heating systems respectively in the Low Energy House and at the Knud Rasmussen Folk High School in Sisimiut have both provided practical experience of operation and performance of solar heating systems in an Arctic climate. Experience from the installation and repair of the systems showed that trained installers are of vital importance to insure a good performance of the systems. The operation of the solar heating system at the Low Energy House showed that thermosyphoning was a problem during the cold winter months. This is now prevented by a magnetic valve controlled by the pump in the solar collector loop.

The system in the Low Energy House has over the course of five years undergone several changes to improve the performance of the system. At present further improvements are still possible regarding utilising the energy from the solar heating system in the space heating loop. The thermal performance of the system at the Knud Rasmussen Folk High School has not reached its optimum potential which is partly due to an electrical error. Measurements from the system have shown that the system is capable of covering most of the hot water consumption for four months during the summer, while also providing energy to the space heating loop.

Both systems have pressurised solar collector loops with an expansion vessel, and have proved that this design works well under Arctic conditions, where power-outage is more frequent.

Resumé

Energi fra solen er en ren og naturlig energikilde. Solstrålingen på jordens overflade – inklusive i det Arktiske klima – er så stor, at det er muligt at udnytte solens energi i stor skala. Ved at udnytte solens energi nedsættes brugen af fossile brændstoffer. Anvendelsen af solenergi varierer fra land til land, lige som udformningen af et solvarmeanlæg.

Formålet med dette forskningsprojekt er at undersøge solstråling i Grønland og undersøge, hvordan et solvarmeanlæg bør udformes til brug i Grønland.

I det Arktiske klima er der flere faktorer som gør sig gældende i forhold til solstrålingen ved disse breddegrader. Solen står lavere på himlen, hvilket bevirker at den optimale hældning på en flade er større. Størstedelen af solstrålingen forekommer om sommeren, hvor der ved breddegrader over den Arktiske Cirkel er solstråling 24 timer i døgnet og stråling fra alle retninger. Reflektion fra sneen øger endvidere solstrålingen på en hældende flade.

Potentialet for anvendelsen af solenergi bliver undersøgt på basis af målinger fra flere forskellig målestationer i Grønland. Derudover undersøges solstrålingsmodeller i relation til deres egnethed på Grønland. Den diffuse korrelation udviklet af 'Erbs et al.' og 'Orgill and Hollands' bliver undersøgt. Resultatet viser, at begge korrelationer overvurdere den diffuse stråling og overvurderer den direkte solstråling. 'Orgill and Hollands' er dog den mest præcise. Derudover bliver fire forskellige strålingsmodeller undersøgt, og resultatet viser, at de ikke er anvendelige på forholdene i Grønland. Af de fire modeller er 'Liu and Jorden's model – den simple isotropiske model – dog den mest præcise.

Siden 2003 er der i Sisimiut udført målinger af den totale solstråling og den reflekterede solstråling. Disse målinger danner baggrund for undersøgelsen af reflektionskoefficienten både med og uden snedække. Målingerne viser, at sne reflekterer solstrålingen som et spejl. Den effektive albedo bliver givet som en funktion af forskellen mellem solens azimut og fladens azimut. Funktionerne for den effektive albedo bliver bestemt på månedsbasis på baggrund af målingerne og kan anvendes som input i simuleringsmodeller.

Solvarmeanlæggene i henholdsvis Lavenergihuset og på Knud Rasmussen Højskolen i Sisimiut har tilvejebragt praktisk erfaring med drift og ydelse af solvarmeanlæg i et Arktisk klima. Erfaringen fra installation og reparation af anlæggene har vist, at det er yderst vigtig at have uddannede installatører for at sikre en god ydelse fra anlæggene. Driften af solvarmeanlægget i Lavenergihuset viser, at selvcirkulation er et problem i de kolde vintermåneder. Dette er nu forhindret ved at installere en magnetisk ventil, der styres af pumpen i solfangerkredsen. Solvarmeanlægget i Lavenergihuset har gennemgået flere ændringer for at forbedre ydelsen. På nuværende tidspunkt er der fortsat mulighed for at forbedre anlægget ved at koble solvarmeanlægget på rumopvarmningen. Anlægget på Knud

Rasmussen Højskolen yder ikke optimalt, hvilket til dels skyldes en elektrisk fejl. Målinger viser, at anlægget kan dække størstedelen af varmtvandsbehovet i fire måneder om sommeren samt forsyne rumopvarmningskredsen med energi fra solvarmeanlægget.

Begge anlæg er installeret med ekspansionsbeholder og solfangerkredse under tryk, hvilket har vist sig at fungere i det Arktisk klima, hvor der oftere forekommer strømsvigt.

Symbols and abbreviations

A_i	Anisotropy index	[-]
a	Constants	[-]
b	Constants	[-]
F_1	Circumsolar brightness coefficient	[-]
F_2	Horizontal brightness coefficient	[-]
f	Modulating factor	[-]
G	Solar radiation on the collector	[W/m²]
I	Global radiation	[W/m²]
I_b	Beam radiation	[W/m²]
I_{bn}	Beam radiation normal	[W/m²]
I_d	Diffuse radiation	[W/m²]
$I_{d,T}$	Diffuse radiation on tilted surface	[W/m²]
I_R	Reflected radiation from the ground	[W/m²]
I_T	Solar radiation on tilted surface	[W/m²]
I_o	Extraterrestrial radiation	[W/m²]
I_{on}	Extraterrestrial radiation normal	[W/m²]
k_T	Clearness index	[-]
k_θ	Incidence angle modifier	[-]
R_b	View factor	[-]
S_ρ	Uncertainty of the albedo	[-]
S_{I_R}	Uncertainty of the measurement of the ground reflected radiation	[-]
S_I	Uncertainty of the measurement of the global radiation	[-]
T_a	Ambient temperature	[°C]
T_m	Mean solar collector fluid temperature in the solar collector	[°C]
β	Tilt of the surface	[°]
ρ	Albedo	[-]
η	Efficiency expression	[-]
θ	Incidence angle	[°]

Content

Chapter 1 Introduction

1.1 Background

Solar energy is a clean and natural energy source. The solar radiation on the earth, including at Arctic latitudes, is so large that it is possible to utilize solar energy in a large scale. Substituting the use of fossil fuels with solar energy will - if the energy consumption does not increase - reduce the emission of CO^2 which is the aim of the majority of nations around the world.

In the Arctic several factors must be taken into account regarding the use of solar energy. The sun is positioned low on the sky, which means that the optimum tilt angle of a receiving surface will increase. Also most solar radiation appears in the summertime, where there is solar radiation 24 hours a day and radiation from all directions. The reflection from the snow will increase the solar radiation on tilted surfaces.

The annual number of hours with potential sunshine is the same all over the world. The higher the latitude, the more solar radiation will occur in the summer time. This can be seen on Figure 1.1 where the earth's elliptic path around the sun is shown. In the summer months, the northern hemisphere is tilted towards the sun, causing midnight sun at latitudes above the Arctic Circle (66.56°). During the winter months the northern hemisphere is facing away from the sun, causing the sun to stay under the horizon all day, for latitudes above the Arctic Circle.

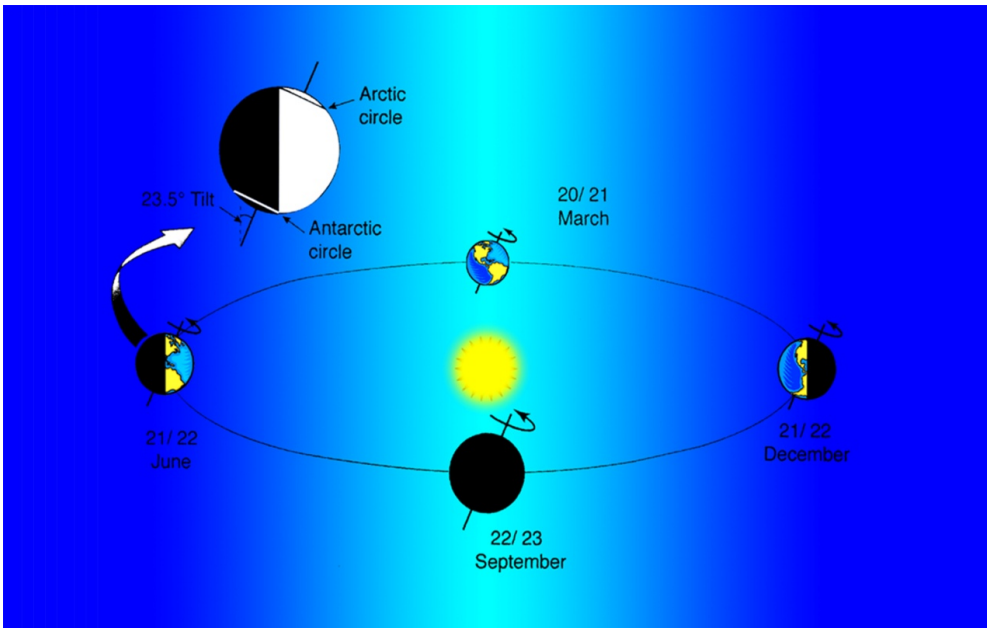

Figure 1.1 The earth's elliptic path around the sun.

Greenland is located on the northern hemisphere spanning from latitude 60.1° to 83.2°. Greenland has a population of 56,452 and is the least densely populated country in the world. The towns and settlements in Greenland are all located along the coast, and most are located on the west coast because of the harsh climate on the east coast. The capital of Greenland Nuuk is located on the southern part of the west coast and has15,487 inhabitants. The second largest town is Sisimiut. It is located on the west coast just north of the Arctic Circle and has 5,460 inhabitants. Qaanaaq is the most northern settlement in Greenland at latitude 77.47° with 626 inhabitants.

Utilizing solar radiation in Greenland and at high latitudes must take these mentioned factors into consideration and make use of the specific conditions.

1.2 Objective

The purpose of this study is to investigate the solar radiation in Greenland, and to elucidate how the design of a solar heating system for Greenland can be optimised.

Based on measurements from several different climate stations in Greenland provided by Asiaq[1], an analysis of the data in comparison with the Danish Reference Year is given. Also an investigation of the diffuse radiation is given, to ensure that the different simulation models used for solar radiation are suited for locations in the northern hemisphere. In Sisimiut measurements of the solar radiation and the ground reflected radiation have been carried out since 2003. This data provides the basis for an investigation of the reflection coefficient for periods with and without snow.

To determine the best design of a solar heating system for the conditions in Greenland an analysis based on simulation calculations will be given. Also experience from the existing solar heating systems in Sisimiut will provide knowledge for future solar heating systems in Greenland.

1.3 Structure of the thesis

This thesis consists of 7 chapters each describing an aspect of the use of solar thermal energy in Greenland.

Chapter 2 gives an analysis of the solar radiation in Greenland and evaluates calculation methods used regarding solar radiation. First the global radiation is presented along with the potential of radiation on tilted surfaces based on reference years. Then the accuracy of two commonly used diffuse fractions and four commonly used radiation models are investigated.

[1] Asiaq is a public enterprise under the Government of Greenland and the Department of Infrastructure and Environment that provides mapping, geographic information, hydrology, climate, environment, and surveying and geotechnical investigation at many locations in Greenland.

Chapter 3 gives an analysis of the ground albedo, both how it is presented and used in calculations, and the effects of implementing an albedo described as a function of the suns position and the orientation of the surface.

In chapter 2 and 3, the measurements used in the different analyses is not presented chronologically; instead they are linked with each individual analysis to maintain a more logic approach to the subject of solar radiation and the use of radiation models.

Chapter 4 is an investigation of the yearly thermal performance of a domestic hot water solar heating system using the simulation tool MantlSim. The investigation is carried out for 4 locations: Uummannaq, Sisimiut, Nuuk and Copenhagen, where the thermal performance for differently designed solar heating systems is evaluated.

Chapter 5 and Chapter 6 present the solar heating systems of the Low Energy House and the solar heating system on the Knud Rasmussen Folk High School, both in Sisimiut. The measured data are analysed and the performance is evaluated. The experiences from both the installation and operation of the solar heating systems are described.

Chapter 7 presents an investigation on the expansion vessel in pressurised solar collector loops, along with a dimensioning tool for the expansion vessel.

Chapter 8 is a conclusion for the investigations presented in this thesis and gives an outlook for future investigations within solar heating in Greenland.

Chapter 2 Solar radiation and radiation models

2.1 The solar potential

Global radiation is the most available measurement of solar radiation at the earth's surface, and can give a good indication of the potential for solar heating and other solar related products. In Greenland measurements of the global radiation are collected by Asiaq at many locations. From the measured value of the global radiation it is possible to calculate the total radiation on a tilted surface facing any direction using radiation models.

The towns in Greenland are all located at the coast. Compared with inland locations, the reflected radiation is higher by the coast because of increased reflection from the sea. This is further enhanced by the low solar altitude. Locations along the coast are also strongly influenced by the weather and the frequent formation of clouds, which influence the global radiation. Locations nearer the inland ice experience fewer clouds and increased global radiation. This benefits towns which are close to the ice. This is especially true for Uummannaq which is a cluster of islands just off the main country and located close to the inland ice. This means that there is both an increase in the reflection from the sea and fewer clouds.

In this chapter the measured global radiation in Greenland is assessed and compared with values from Denmark. Then the method of calculating the total radiation on a tilted surface is investigated to assess if the radiation models take the special conditions of Arctic locations into account.

2.1.1 Global radiation

The global radiation from four locations in Greenland and one location in Denmark is investigated, see Figure 2.1. The locations in Greenland are: Qaanaaq, Uummannaq, Sisimiut and Nuuk, where Nuuk is located below the Arctic Circle and the other three locations above the Arctic Circle. The Arctic Circle marks the border between the occurrence of polar nights and polar days. Polar night is when the sun is below the horizon for 24 continuous hours, and polar day is when the sun is above the horizon for 24 continuous hours and undertakes all cardinal directions in the course of one day.

Figure 2.1 Map of Greenland and Denmark showing the locations from which the global radiation is analysed.

In Figure 2.2 the global radiation for the five locations is compared from the years 2007 to 2009. The measurements from Greenland are supplied by Asiaq and the measurements from Denmark are from the weather station at the Technical University of Denmark. It shows a slight variation between the measurements from the different years. In all the three years the global radiation measured in Lyngby is the highest. The global radiation measured in Uummannaq is higher than the global radiation measured in both Nuuk and Sisimiut. This is contrary to the normal trend for solar radiation on the horizontal plane which is: the higher the latitude the less solar radiation. The reason for the increase in solar radiation in Uummannaq is due to both fewer cloud formations - because of the location close to the inland ice - and the inter-reflection from the sea and the snow. The global radiation measured in Qaanaaq during 2007 is slightly higher than Uummannaq, but lower in 2008 and 2009. The global radiation in Qaanaaq during 2009 is at the same level as Sisimiut and Nuuk, also contradicting the normal trend. Again this is most

likely due to both less clouds because of the location close to the inland ice and inter-reflection from the sea and the snow. Also at this high latitude, the part of the year where this site is coved with snow is longer, and thereby the period with reflection from the snow and ice is longer as well.

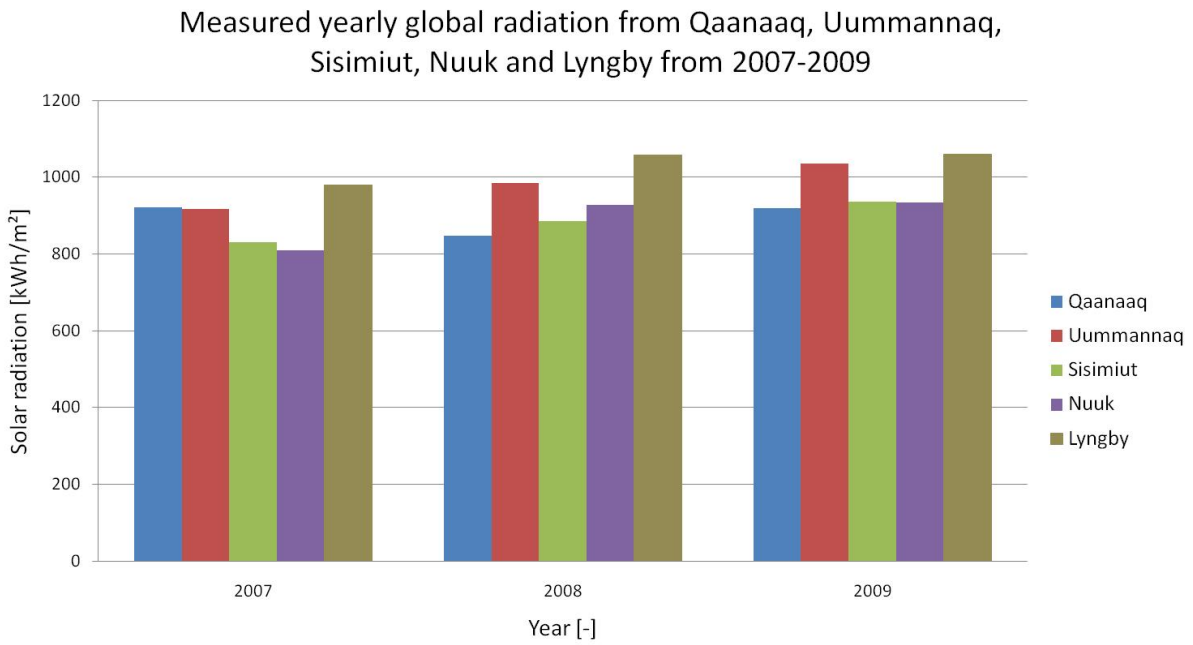

Figure 2.2 Yearly global radiation measurements - 2007 to 2009 from Qaanaaq, Uummannaq, Sisimiut, Nuuk and Lyngby.

In Table 2.1 the values of the global radiation are shown along with the average value. Lyngby has the highest values, with Uummannaq coming in second followed by Qaanaaq, then Nuuk and last Sisimiut.

Table 2.1 The yearly global radiation measurements - 2007 to 2009 and the average value over the 3 years for the locations of Qaanaaq, Uummannaq, Sisimiut, Nuuk and Lyngby.

Global radiation	2007	2008	2009	Average
	[kWh/m²]	[kWh/m²]	[kWh/m²]	[kWh/m²]
Qaanaaq	923	849	920	897
Uummannaq	918	986	1037	980
Sisimiut	833	895	941	890
Nuuk	809	928	935	891
Lyngby	980	1059	1059	1033

The monthly variations of the measured global ration in the same five locations are shown in Figure 2.3 as an average of the measurements from 2007 to 2009. It can here be seen that the higher the latitude the more solar radiation occurs in the summer months. In the months, June, July and August, the measured radiation from Qaanaaq and Uummannaq exceeds the measured radiation in Lyngby. This is due to polar days at these latitudes, with sun above the horizon for 24 continuous hours.

The measurements from Lyngby shows as expected higher values in the winter months compared to the measurements from Greenland.

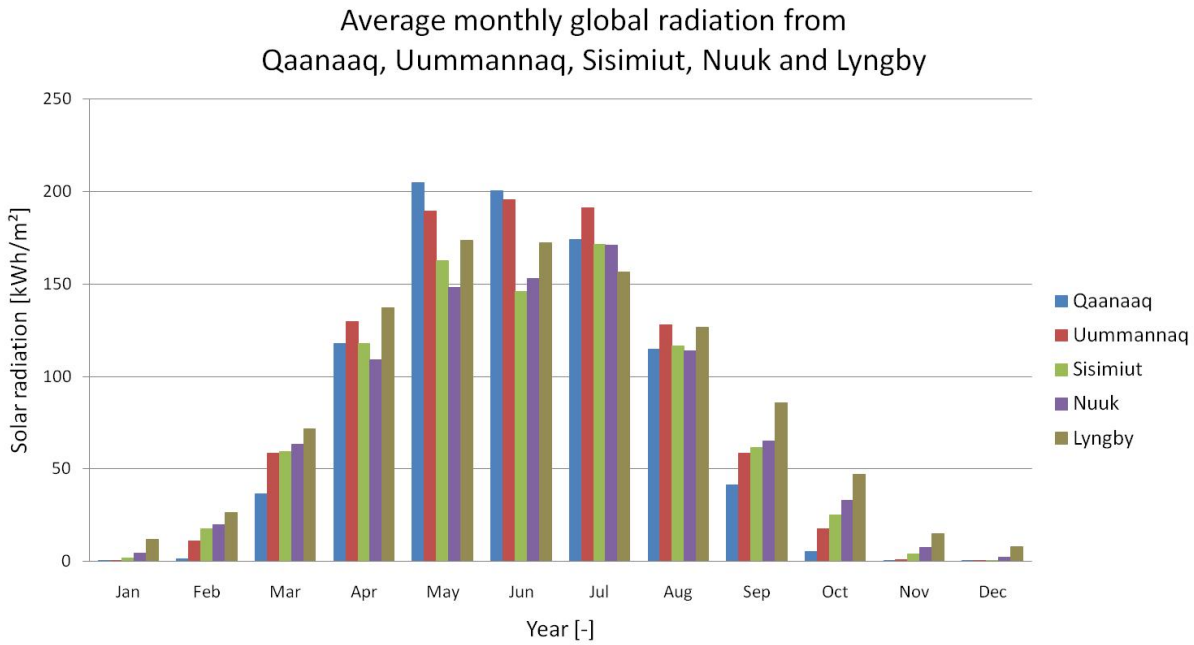

Figure 2.3 Monthly global radiation measurements- 2007 to 2009 from Qaanaaq, Uummannaq, Sisimiut, Nuuk and Lyngby.

2.1.2 Reference years

In 2002 reference years for Uummannaq, Sisimiut and Nuuk where developed based on measurements from Asiaq [Krag et al. 2002]. The reference years are based on 10 years of measurements of the global radiation, ambient temperature, relative humidity, wind speed and atmospheric pressure. Using a diffuse correlation method the beam normal radiation and the diffuse radiation is calculated. The accuracy of two diffuse correlations for the Arctic conditions is analysed in section 2.2.1.

Data from the reference years for Uummannaq, Sisimiut, Nuuk and Copenhagen can be seen in Figure 2.4 to Figure 2.7. The figures show the hour values of the beam normal radiation, the global radiation and the diffuse radiation on a horizontal surface. The reference year from Uummannaq in Figure 2.4 shows that there is no solar radiation in January and December and part of November, which is because of polar nights at this high latitude. Also it can be seen that there is a higher amount of beam radiation in spring

months compared with the fall. The concentration of beam radiation in the spring in Uummannaq exceeds that of the other 3 locations analysed here, which is also seen in Table 2.2.

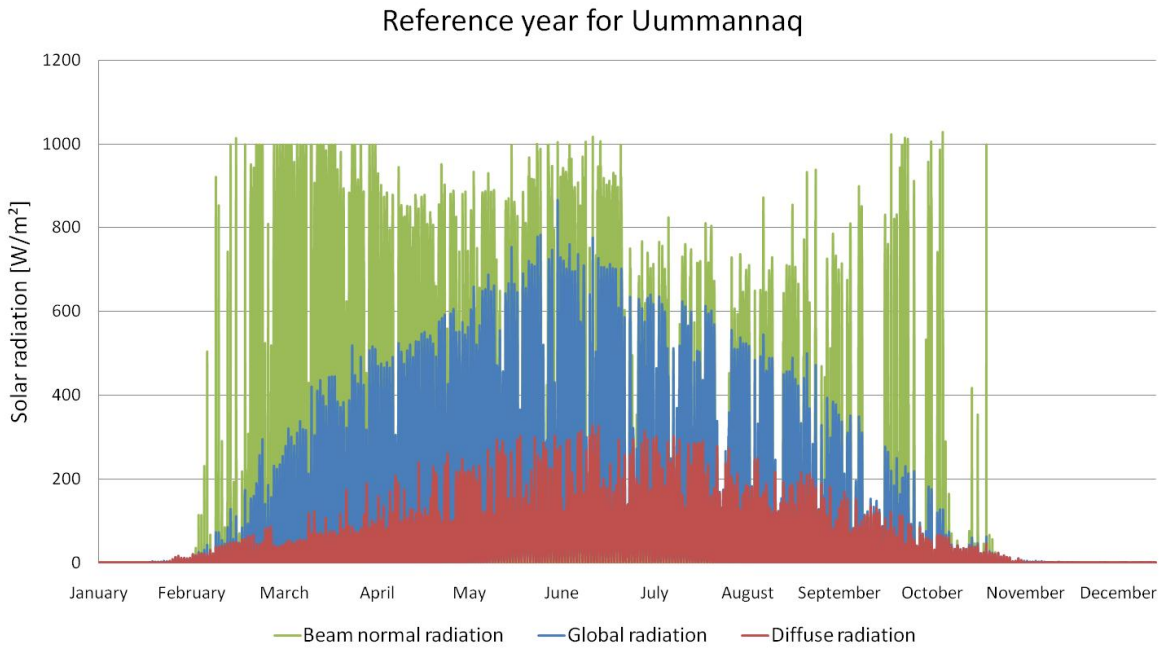

Figure 2.4 The reference year for Uummannaq.

The reference year for Sisimiut in Figure 2.5 shows that there is no solar radiation in December and part of January. Also in Sisimiut there is a higher amount of beam radiation in the spring compared to the fall.

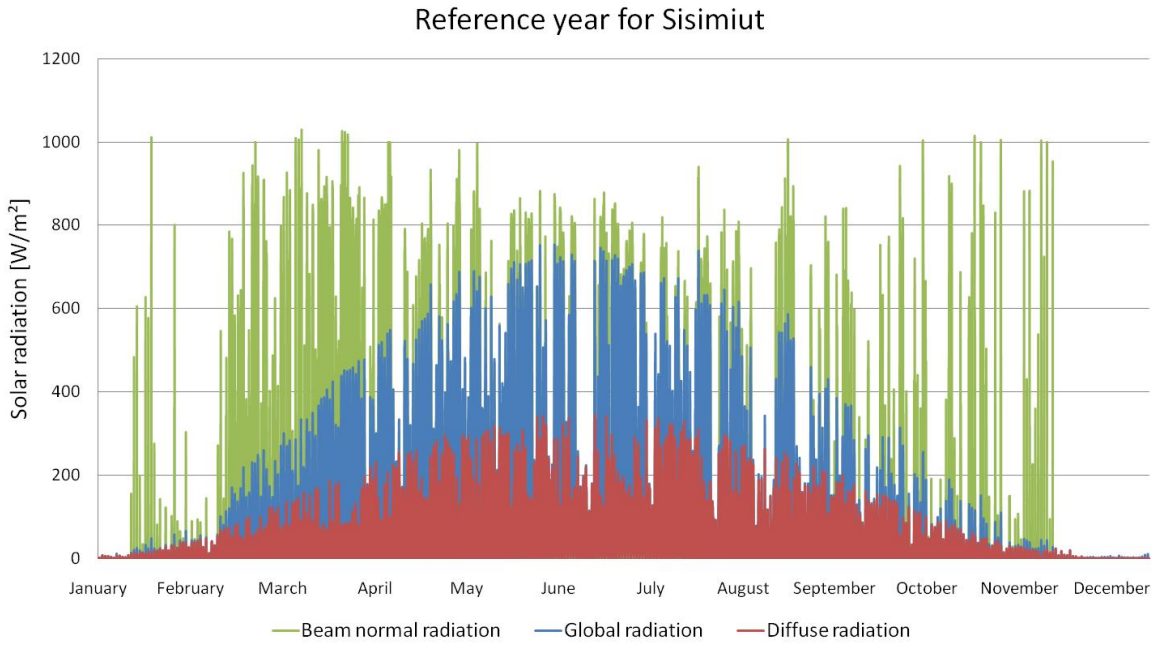

Figure 2.5 The reference year for Sisimiut.

In Figure 2.6 the reference year for Nuuk shows that there here is solar radiation throughout the year, which is because Nuuk is located below the Arctic Circle and therefore not subject to polar nights. The beam radiation in Nuuk is again slightly higher in the spring compared to the fall.

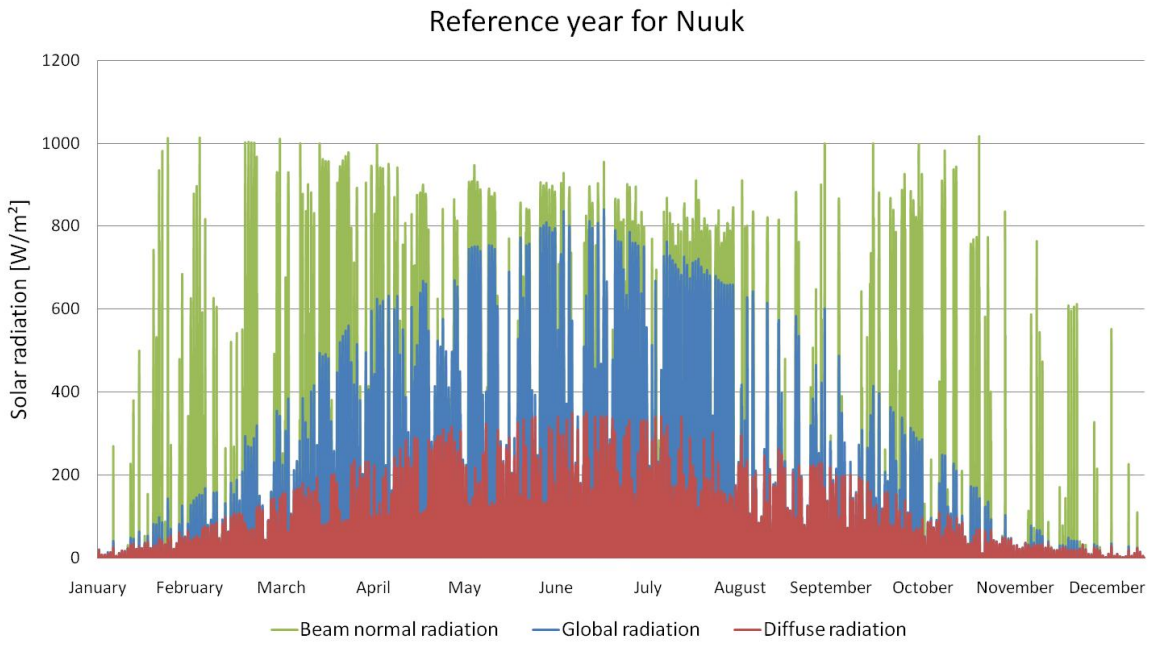

Figure 2.6 The reference year for Nuuk.

The reference year for Copenhagen can be seen in Figure 2.7, and shows solar radiation throughout the year. The beam radiation is more scattered throughout the year with the highest values in the spring.

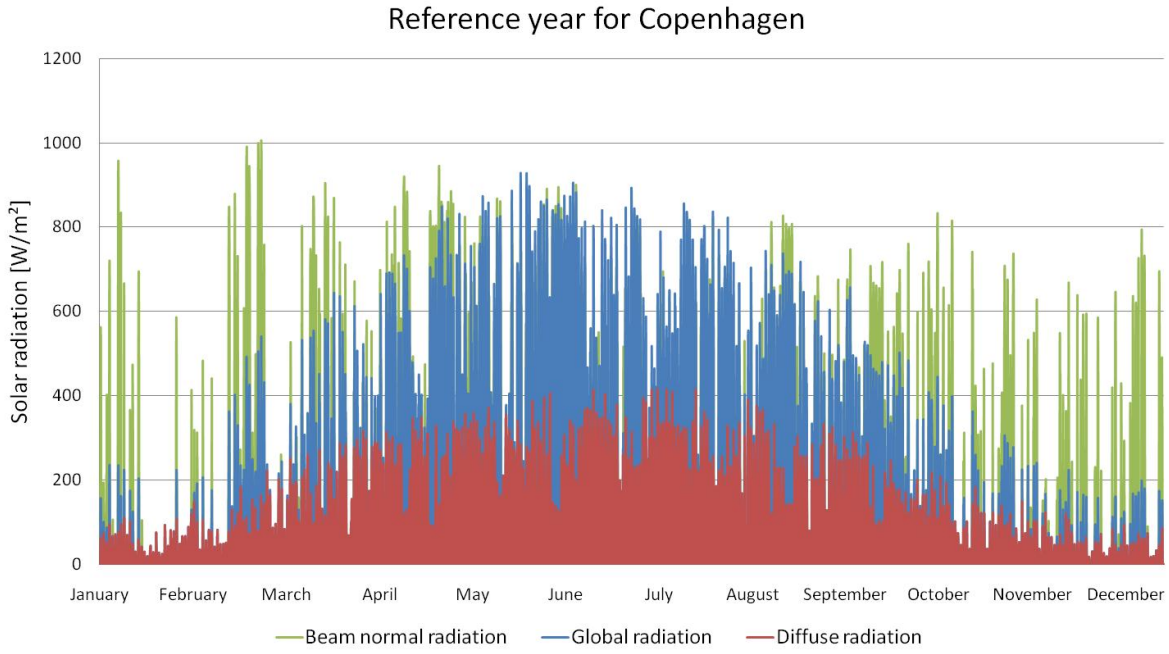

Figure 2.7 The reference year for Copenhagen.

The yearly global radiation in the reference years for the 4 locations can be seen in Table 2.2. The global radiation in Copenhagen is highest followed by Uummannaq, then Nuuk and last Sisimiut, which is the same sequence seen in the measurements from 2007 to 2009 presented in section 2.1.1. The diffuse radiation on horizontal is also highest in Copenhagen, but this time followed by Sisimiut, then Nuuk and last Uummannaq. The beam normal radiation is higher in Uummannaq than Copenhagen, then followed by Nuuk and last Sisimiut.

Table 2.2 Solar radiation in the reference years for Uummannaq, Sisimiut, Nuuk and Copenhagen.

	Global radiation	Diffuse radiation on horizontal	Beam normal radiation
	[kWh/m²]	[kWh/m²]	[kWh/m²]
Uummannaq	926	390	1387
Sisimiut	822	411	1013
Nuuk	900	410	1141
Copenhagen	1018	495	1088

The monthly variation of the global radiation in the reference years can be seen in Figure 2.8. The figure shows that the majority of the global radiation in the Greenlandic locations is concentrated around the spring and summer months. The same trend is seen in the measurements from 2007 to 2009. The global radiation in July in the reference year from Nuuk deviates from the measurements by exceeding the values from Uummannaq.

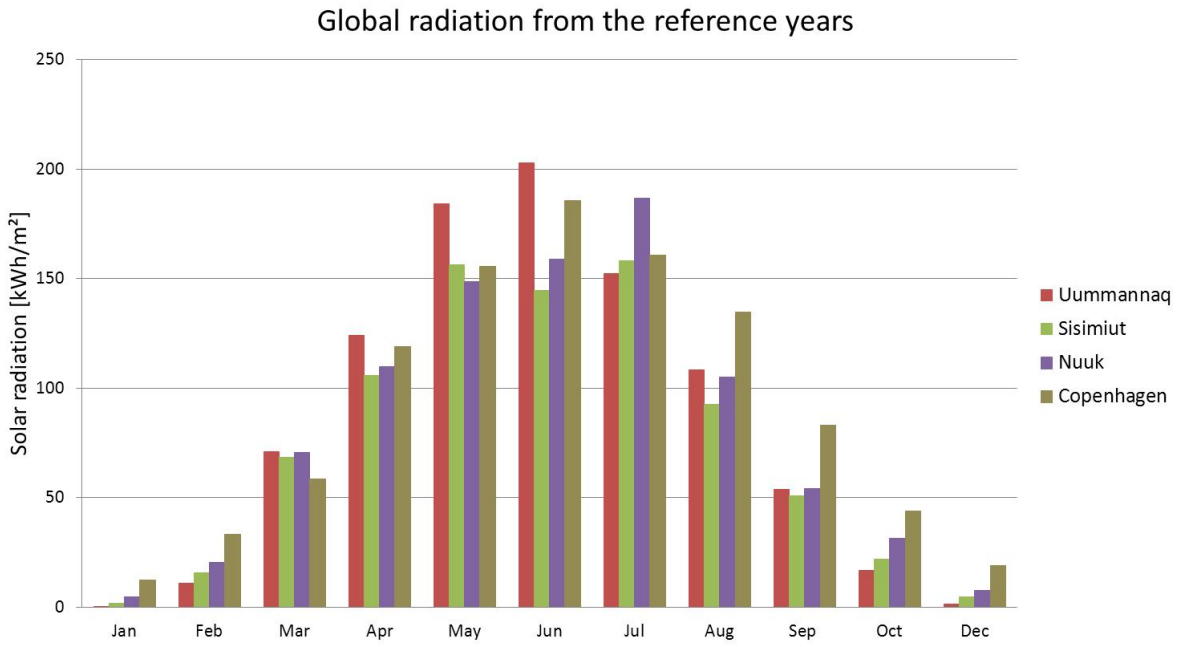

Figure 2.8 The global radiation in the reference years.

Figure 2.9 shows the monthly variation in the diffuse radiation in the reference years on the four locations. The diffuse radiation is higher in the fall compared to the spring, because there is more beam radiation in the spring.

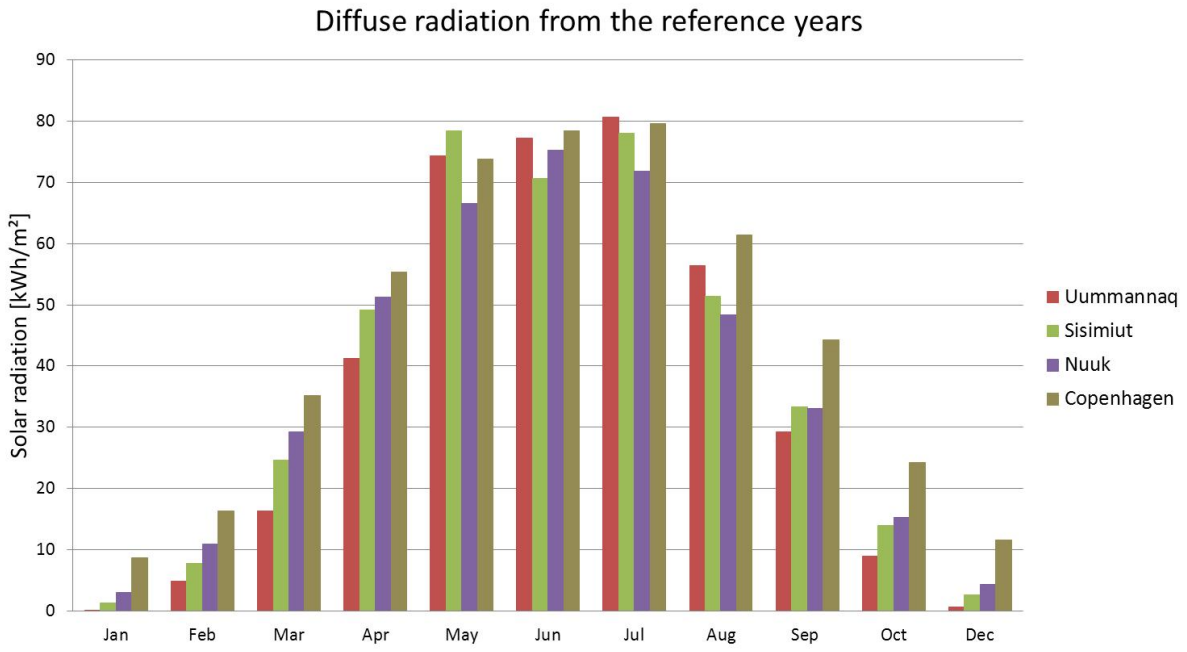

Figure 2.9 The diffuse radiation in the reference years.

The beam normal radiation in the reference years on the four locations is shown in Figure 2.10. Here it can be seen that the beam radiation in the spring in Uummannaq exceeds that of the other locations. In July the beam normal radiation in Nuuk shows the highest value.

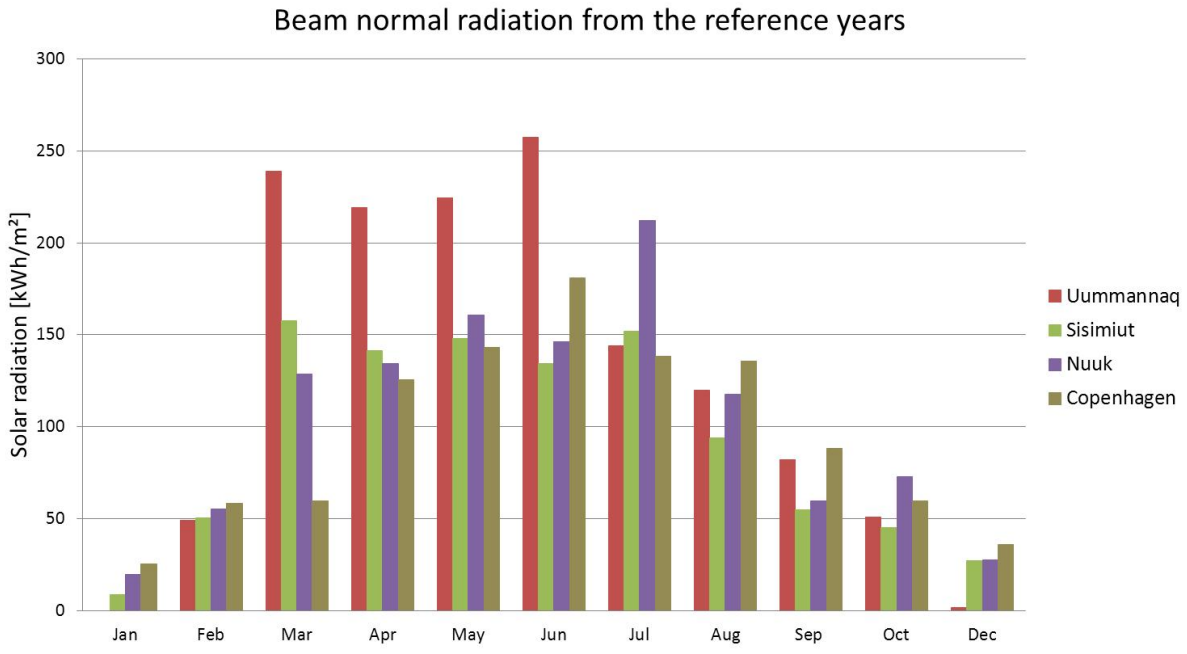

Figure 2.10 The beam normal radiation in the reference years.

2.1.3 Available solar radiation

Based on the information of the global, diffuse and beam normal radiation given in the reference years the total radiation on a titled surface is calculated. The reflected radiation from the ground is based on equations, which are described in chapter 3. Figure 2.11 shows the calculated total radiation on a surface facing south with variation to the tilt of the surface. Here it can be seen that the higher the latitude the higher the optimum tilt for the surface. The optimum tilt for a surface in Copenhagen is around 45 ° and for Uummannaq the optimum is around 55 °.

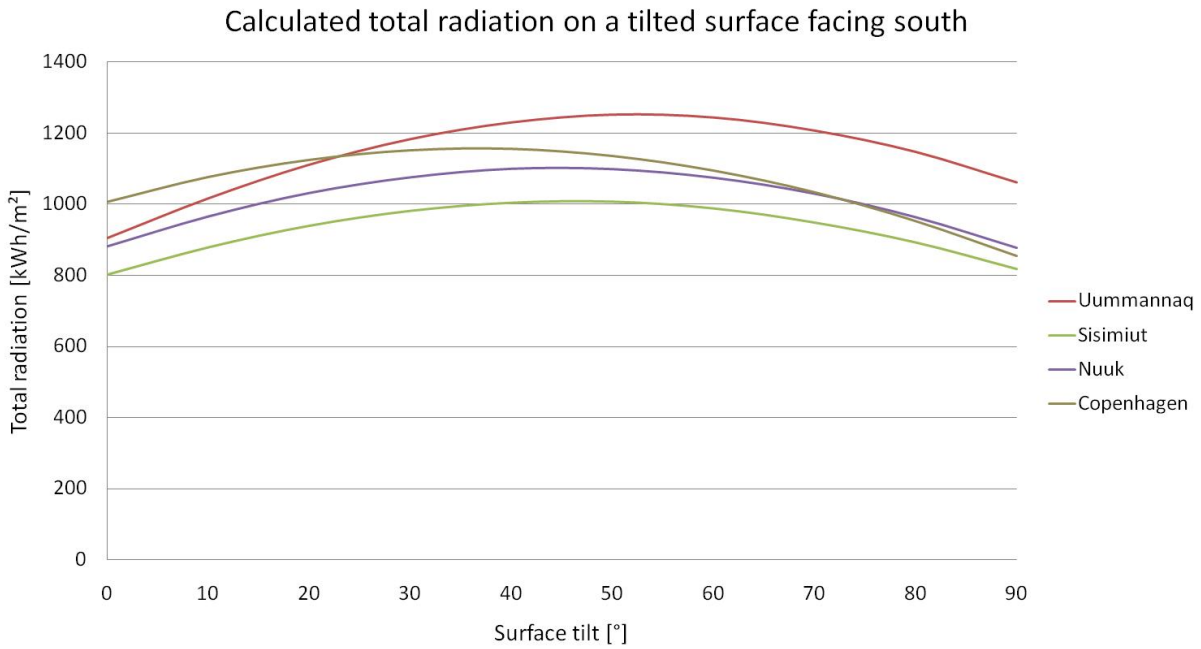

Figure 2.11 Solar radiation on a south facing surface as a function of the tilt of the surface in Uummannaq, Sisimiut, Nuuk and Copenhagen.

In Table 2.3 the calculated total radiation for different tilt angles are given. On a surface with a tilt angle of 0 ° the surface receiving the most is the one in Copenhagen. If the surface is placed vertically the surface in Uummannaq receives the highest amount of solar radiation.

Table 2.3 Calculated total radiation on a south facing surface for different tilt angles in Uummannaq, Sisimiut, Nuuk and Copenhagen.

Total radiation on a south facing tilted surface	0°	30°	45°	60°	90°
	[kWh/m²]	[kWh/m²]	[kWh/m²]	[kWh/m²]	[kWh/m²]
Uummannaq	926	1184	1246	1245	1062
Sisimiut	822	981	1008	988	817
Nuuk	900	1076	1103	1075	878
Copenhagen	1018	1151	1148	1094	854

The table also shows that for a tilt angle higher than 25 ° a surface in Uummannaq receives more solar radiation than a surface with the same tilt would in Copenhagen. The same is true for a vertical surface in Nuuk compared with a vertical surface in Copenhagen. This means that if the conditions of location are taken in to account the solar radiation in Greenland is high enough to support utilizing energy form the sun.

2.2 Solar radiation models

Since the most available measured solar radiation is the global radiation, and this, per definition, is on the horizontal plane, it is necessary to be able to calculate the received radiation on any given surface in terms of tilt and orientation in order to determine the potential of for instance a solar collector.

The calculation of the total radiation on a given surface based on a measured value of the global radiation is done in two steps. First step is to divide the measured global radiation into beam and diffuse radiation on the horizontal plane. The next step is to transfer the beam and diffuse radiation onto the given surface, and add ground reflected radiation.

The division of global radiation into beam and diffuse radiation is determined by a correlation between the global and extraterrestrial radiation, and the global and diffuse radiation. The reason why the beam and diffuse radiation is not measured alongside the global radiation is because this is often both costly and time consuming.

In the following: two diffuse correlations and four radiation models are investigated and compared with the measured values of the total and diffuse radiation.

2.2.1 Correlation determining diffuse and beam radiation on horizontal

Diffuse correlations have been determined on an hourly, daily and monthly basis in several studies, based on different data-sets and locations. Here the correlations developed by ‘Orgill and Hollands’ and ‘Erbs et al.’ [Orgill and Hollands 1977, Erbs et al. 1981] are investigated in terms of their suitability at high latitudes and Greenlandic conditions.

The diffuse correlations are given as the relationship between the extraterrestrial radiation (I_o) and the global radiation (I), and the diffuse radiation (I_d) and the global radiation. The correlations depend on a term called the clearness index (k_T), where k_T is determined by measured global radiation divided by the calculated extraterrestrial radiation on horizontal, $k_T = I / I_o$, thereby describing how much of the potential solar radiation is received.

Orgill and Hollands

The Orgill and Hollands correlation is based on hourly measurements from Toronto Airport in Canada from September 1967 to August 1971 at latitude 43.83°.

$$\frac{I_d}{I} = \begin{cases} 1.0 - 0.249 \cdot k_T & For\ k_T < 0.35 \\ 1.557 - 1.84 \cdot k_T & For\ 0.35 \leq k_T \leq 0.75 \\ 0.177 & For\ k_T > 0.75 \end{cases} \quad (2\text{-}1)$$

Erbs et al.

The Erbs correlation is based on hourly measurement from five locations in USA: Fort Hood, Livermore, Raleigh, Maynard and Albuquerque. The time span from which the data is collected is from 1961 to the end of 1974, and the latitudes vary from 31.08° to 42.42°.

$$\frac{I_d}{I} = \begin{cases} 1.0 - 0.09 \cdot k_T & For\ k_T \leq 0.22 \\ 0.9511 - 0.1604 \cdot k_T + 4.388 \cdot k_T^2 - 16.638 \cdot k_T^3 + 12.336 \cdot k_T^4 & For\ 0.22 < k_T \leq 0.80 \\ 0.165 & For\ k_T > 0.80 \end{cases} \quad (2\text{-}2)$$

In Figure 2.12 the two correlations can be seen as a function of the clearness index.

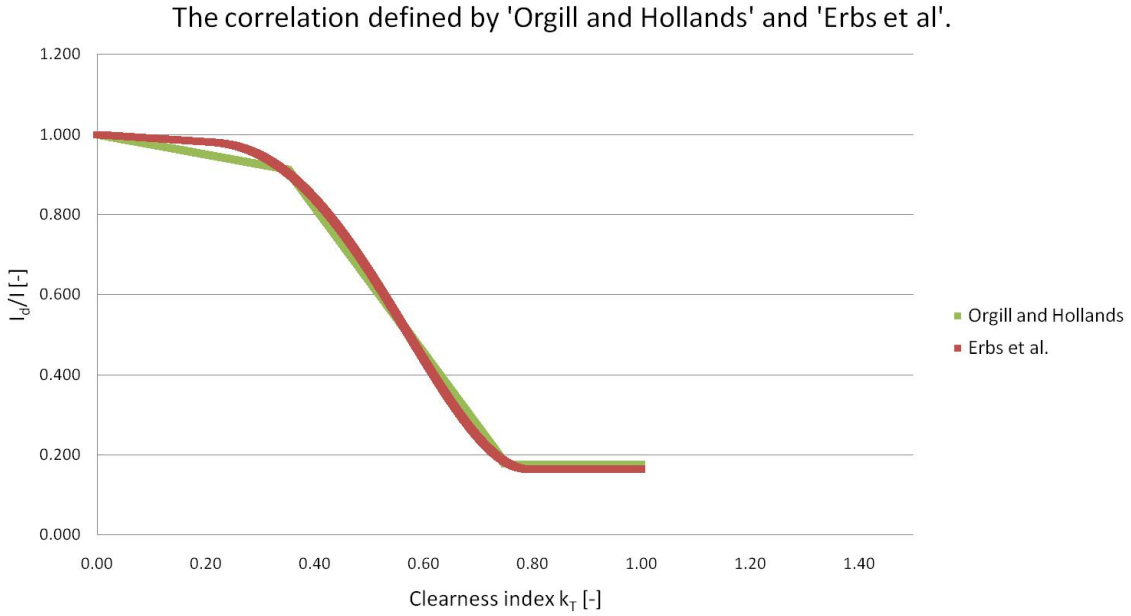

Figure 2.12 The correlations defined by 'Orgill and Hollands' and 'Erbs et al'.

In order to evaluate the accuracy of the two correlations when determining the diffuse radiation, and thereby the beam radiation, the calculated values are compared with measured values of the diffuse radiation. The measured data was collected in Sisimiut from the end of May 2009 to the end of December 2010 with a SPN1 pyranometer.

Measurements from SPN1 in Sisimiut

The SPN1 pyranometer from Delta-T Devices is shown in Figure 2.13 right, and is installed on the roof of Knud Rasmussen Folk High School in Sisimiut, see Figure 2.13 left. The SPN1 pyranometer has 7 sensors registering the incoming radiation on the horizontal plane with a timestep of 10 minutes. Because of the mesh on the glass dome, each sensor only receives radiation from half of the sky-dome. At least one sensor will receive beam radiation and at least one will be shaded from direct sun light and only receive diffuse radiation. The global radiation is determined as the highest reading of the 7 sensors plus the lowest reading. The diffuse radiation on the horizontal plane is determined as the lowest reading multiplied with 2. The accuracy on the global and diffuse radiation measurement is 5 % on an hourly basis and 8 % on individual readings.

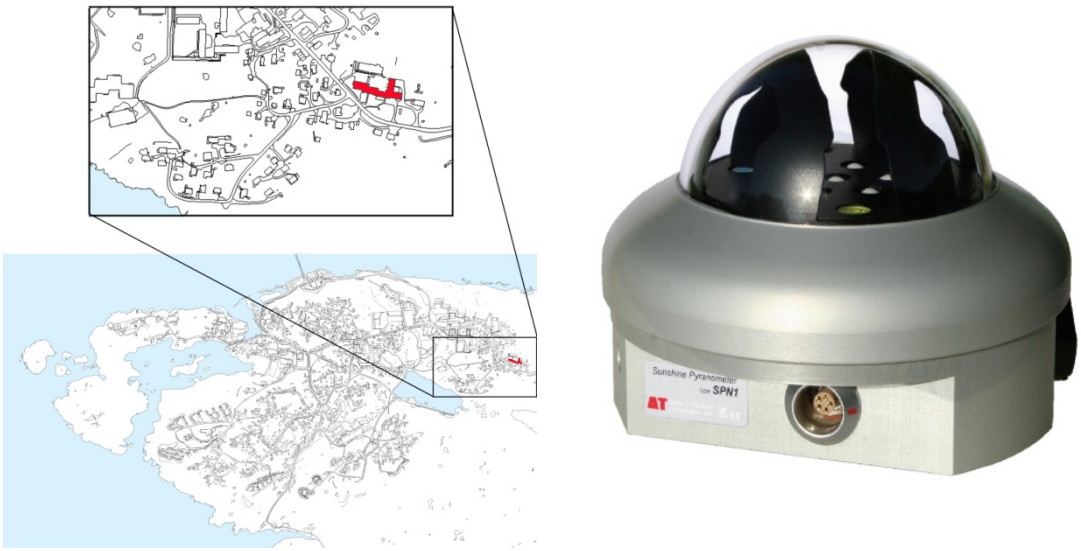

Figure 2.13 SPN1 pyranometer, which is installed on the roof of Knud Rasmussen Folk High School. The Knud Rasmussen Folk High School is marked with red on the map on left.

The measurements from SPN1 from Knud Rasmussen Folk High School from 2009 and 2010 can be seen in Figure 2.14 and Figure 2.15, both with a timestep interval of 10 minutes.

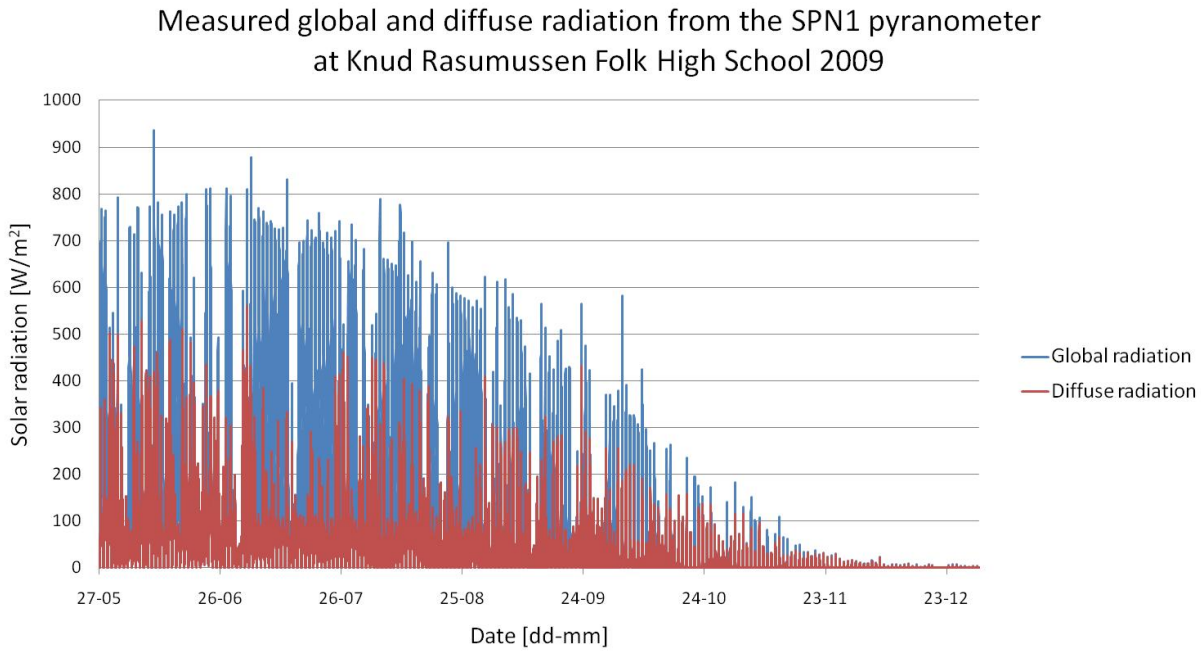

Figure 2.14 2009 measurements from SPN1 installed at the Knud Rasmussen Folk High School.

The difference between global and diffuse radiation is highest in the summer months and decreases in the winter both because of increase in cloud formation and decrease of inter-reflection.

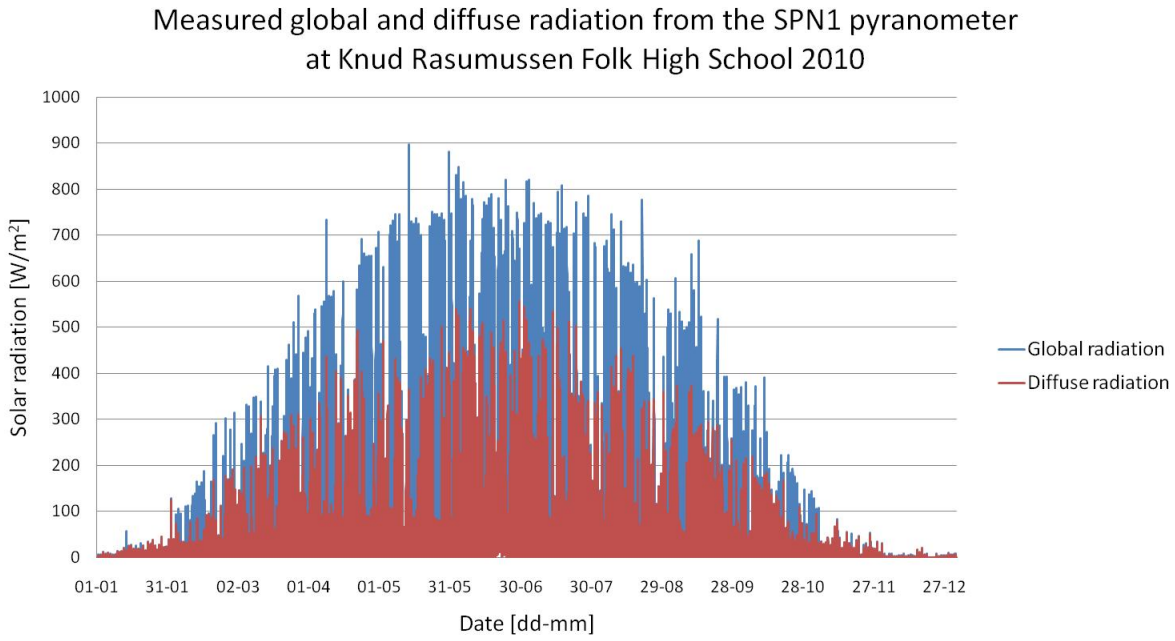

Figure 2.15 2010 measurements from SPN1 installed at the Knud Rasmussen Folk High School.

Comparison between the measurements and the two correlations

The diffuse fraction based on the measurements from the SPN1 is shown in Figure 2.16 as a function of the clearness index. The red dots represent the diffuse fraction calculated with the instantaneous values based on the measurements with a time step of 10 minutes. The green dots shows the diffuse fraction calculated from hourly mean values based on the measurements. A high clearness index indicates clear skies and therefore the ratio of diffuse radiation to global radiation is low. When the clearness index is low the indication is overcast skies and therefore the ratio between diffuse and global radiation is close to 1. A clearness index higher than 1, indicates that the measured global radiation exceeds the calculated extraterrestrial radiation. This occurs when a location on the ground receives both beam radiation and second order reflected radiation, which originates from drifting clouds or the surrounding mountains. During the measuring period from May 2009 to December 2010 this is only registered a few times.

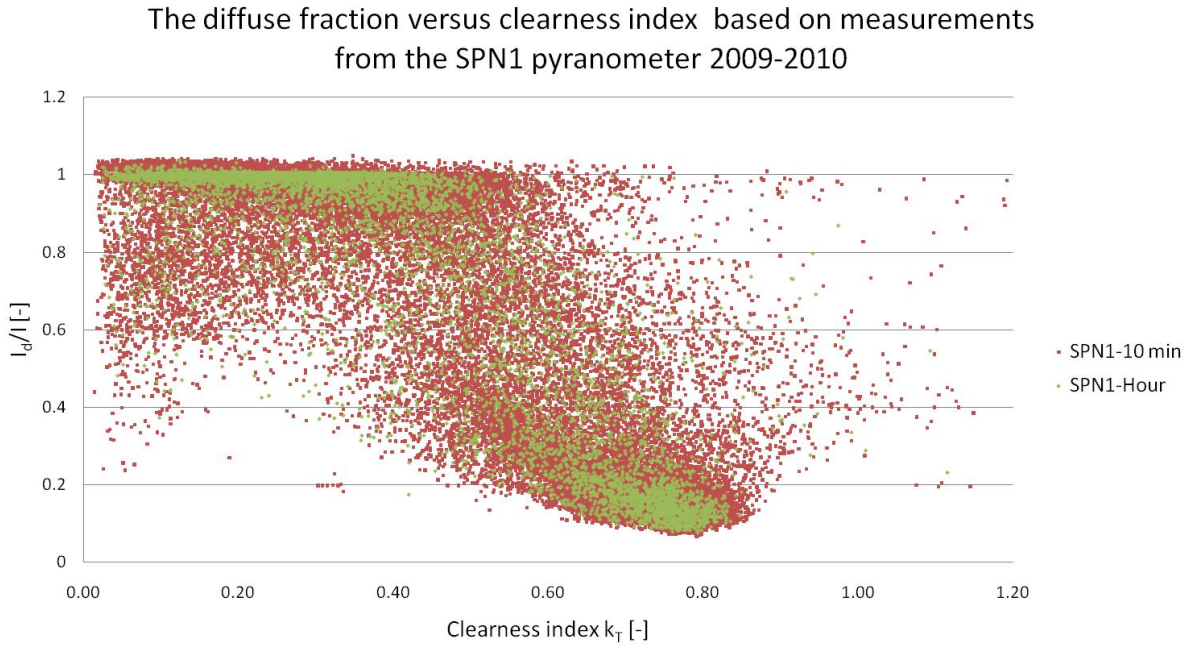

Figure 2.16 The diffuse fraction versus clearness index based on the measurements from the SPN1 pyranometer at Knud Rasmussen Folk High School from 2009 and 2010.

The accuracy of the correlations is compared with the weighted values of the diffuse fraction from the measurements. The weighting is carried out with the global radiation. For a specific value of the clearness index, k_T, the value of diffuse fraction, I_d/I, is weighted against the global radiation, I.

For a specific value of k_T, the weighted term $\frac{I_d}{I}$ is:

$$\frac{\sum\left(\frac{I_d}{I}\cdot I\right)}{\sum I} \qquad (2\text{-}3)$$

The result of the weighting is seen in Figure 2.17, where the green dots are based on the hourly mean values and the black dots are weighted values of the diffuse fraction based on the measurements.

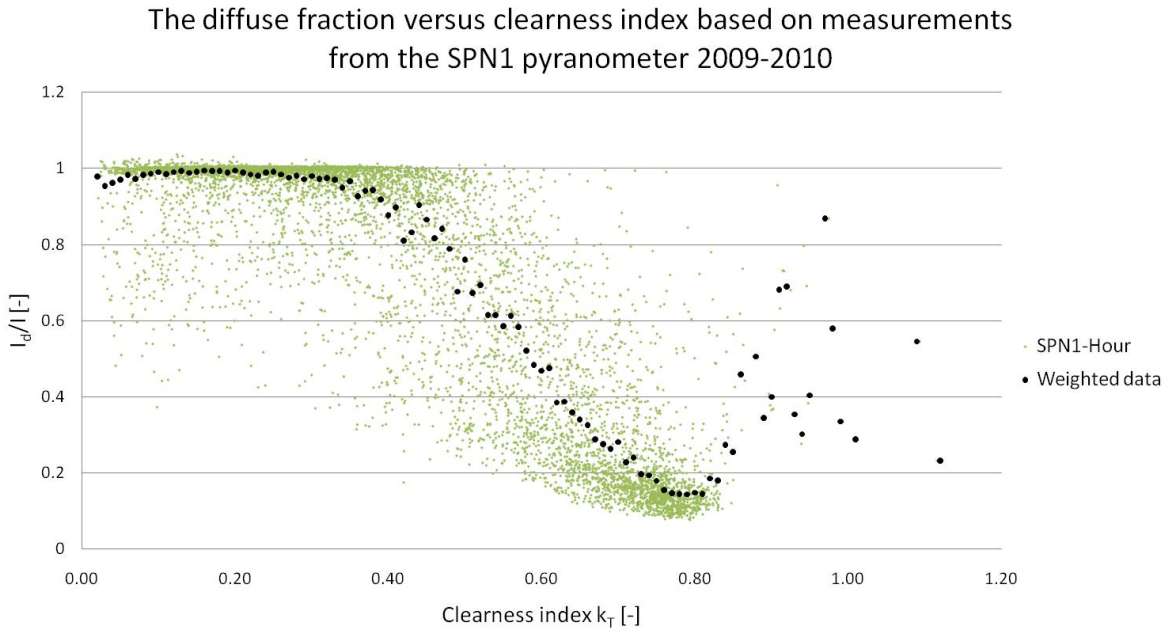

Figure 2.17 The weighted diffuse fraction versus clearness index based on the measurements from Knud Rasmussen Folk High School from 2009 and 2010.

In Figure 2.18 the measurements of the global and diffuse radiation (10 minutes values) for the 9th of August 2009, are shown along with the calculated values for the extraterrestrial radiation and the clearness index.

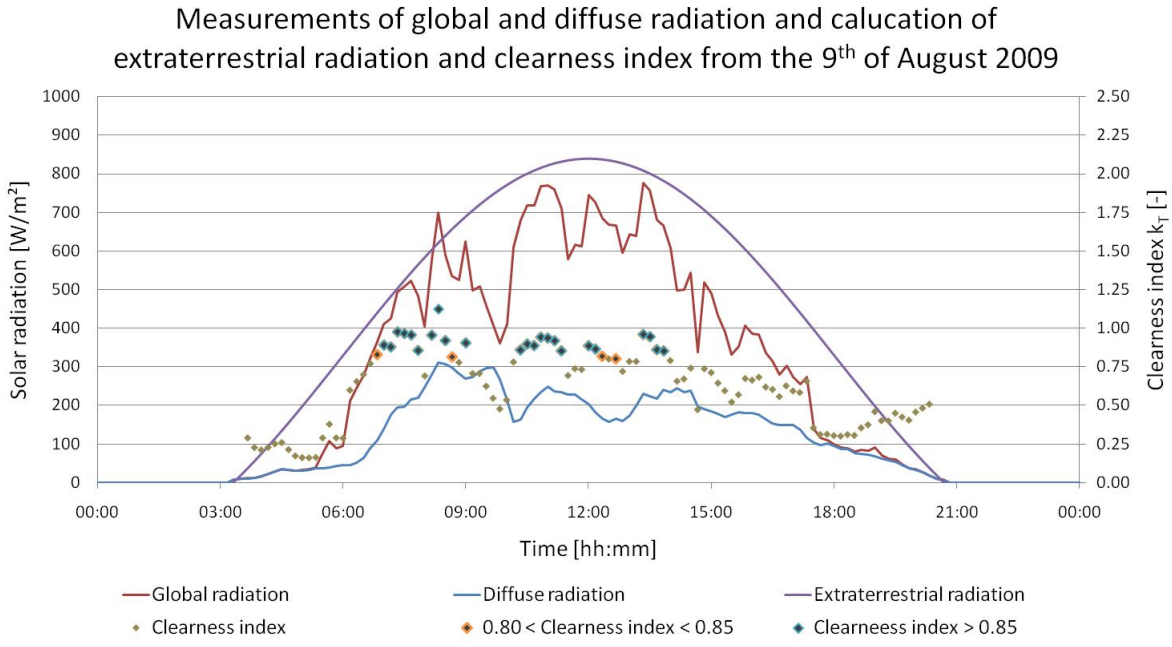

Figure 2.18 The measurements of the global and diffuse radiation and calculated values of the extraterrestrial radiation and clearness index from the 9th of August 2009.

The measurement of the global and diffuse radiation on horizontal indicates that on this day there was drifting clouds, resulting in a variation of the clearness index. The orange dots indicate a clearness index higher than 0.80, and the blue dots a clearness index higher than 0.85. It can be seen that a clearness index higher than 0.80 occurs several times during the day, because of the drifting clouds and the added inter-reflection. In the morning at 8:30 it can be seen that the measured global radiation exceeds the calculated extraterrestrial radiation, again because of the inter-reflection from the drifting clouds.

In Figure 2.19 the weighted hourly values based on the measurements is compared to the correlations of 'Orgill and Hollands' and 'Erbs et al.'. It is here seen that there is a good agreement between the measurements and both 'Orgill and Hollands' and 'Erbs et al.' in the interval between 0 and 0.30 of the clearness index and again from 0.60 to 0.80. But for values between 0.30 and 0.60 of the clearness index, the weighted values based on the measurements shows a higher value for the diffuse radiation than the calculations with the two correlations. For values of the clearness index higher than 0.80 both 'Orgill and Hollands' and 'Erbs et al.' suggests a constant value of either 0.177 ('Orgill and Hollands') or 0.165 ('Erbs et al.'). The weighted values based on the measurements suggests an increase in the diffuse fraction, which is also seen in Figure 2.18, due to the increase in global and diffuse radiation on the horizontal plane because of inter-reflection and drifting clouds.

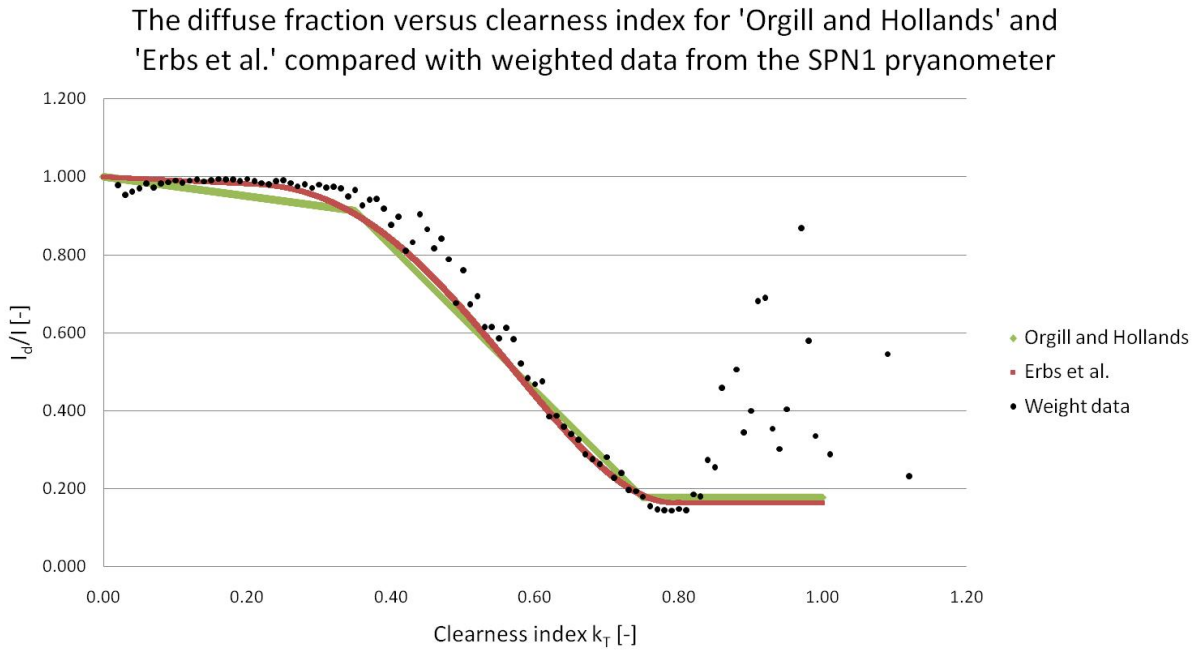

Figure 2.19 The diffuse fraction versus clearness index based on the hourly weighted data from the SPN1 compared with the correlations from 'Orgill and Hollands' and 'Erbs et al.'.

Accuracy of the 2 correlations on a daily, monthly and yearly basis

The accuracy of the 2 correlations is investigated on 6 different days with different sky conditions; see Figure 2.20 to Figure 2.22. The figures show the measured and calculated solar radiation on the horizontal plane, for both a summer and a winter situation.

The measured and calculated solar radiation with the correlations on clear sky days are seen in Figure 2.20, where both a summer day (19th of July 2009), and winter day (17th of March 2010), are shown. On both occasions the correlations (green and orange curve) overestimates the diffuse radiation compared to the measured diffuse radiation (blue curve). The correlation from 'Orgill and Hollands' gives slightly higher values than 'Erbs et al.'. The overestimation of the diffuse radiation on the 19th of July 2009 results in an average decrease of beam radiation of 7 % during the day. On the 17th of March 2010 the average decrease in the beam radiation is 5 % during the day.

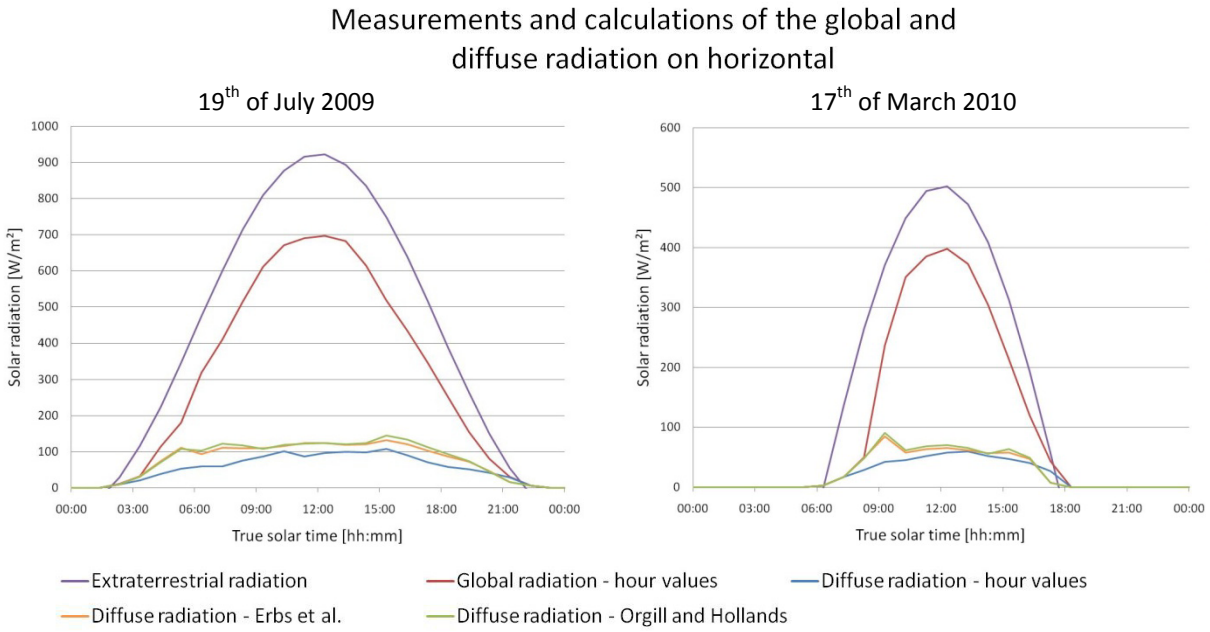

Figure 2.20 Measured and calculated values on horizontal for two different clear sky days: 19th of July 2009 and the 17th of March 2010.

Figure 2.21 shows the correlations on a mixed day with drifting clouds. On the 6th of July 2009 there were clouds around midday causing a decrease in the global radiation and an increase in the diffuse radiation. Both correlations calculate the increase in diffuse radiation, but not to the same extent as the measured diffuse radiation. The 27th of March 2010 was a day with clouds in the morning and afternoon. Here it can be seen that around noon when the sun was free of clouds and the measured global radiation increased, both correlations calculated a steep decrease in the diffuse radiation, where the measurements only shows a slight decrease in the diffuse radiation. This is due to the inter-reflection of the snow and the inter-reflection from the clouds. On both days the correlations underestimates the diffuse radiation which is in good agreement with the results seen in Figure 2.19.

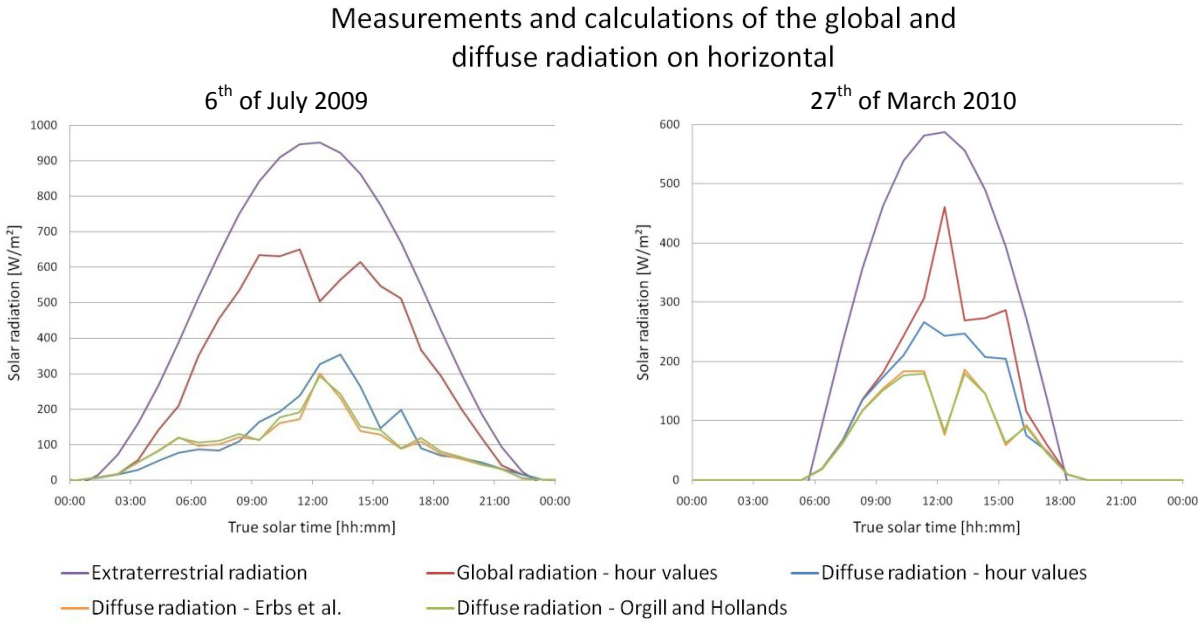

Figure 2.21 Measured and calculated values on horizontal for two different mixed sky days; the 6th of July 2009 and the 27th of March 2010.

On overcast sky days both correlations shows a good agreement with the measured values, see Figure 2.22, for both the summer and winter situation. This is because the difference between the measured global radiation and the calculated value of the extraterrestrial radiation is high. This results in a small clearness index, thereby assuming the global and diffuse radiation is the same.

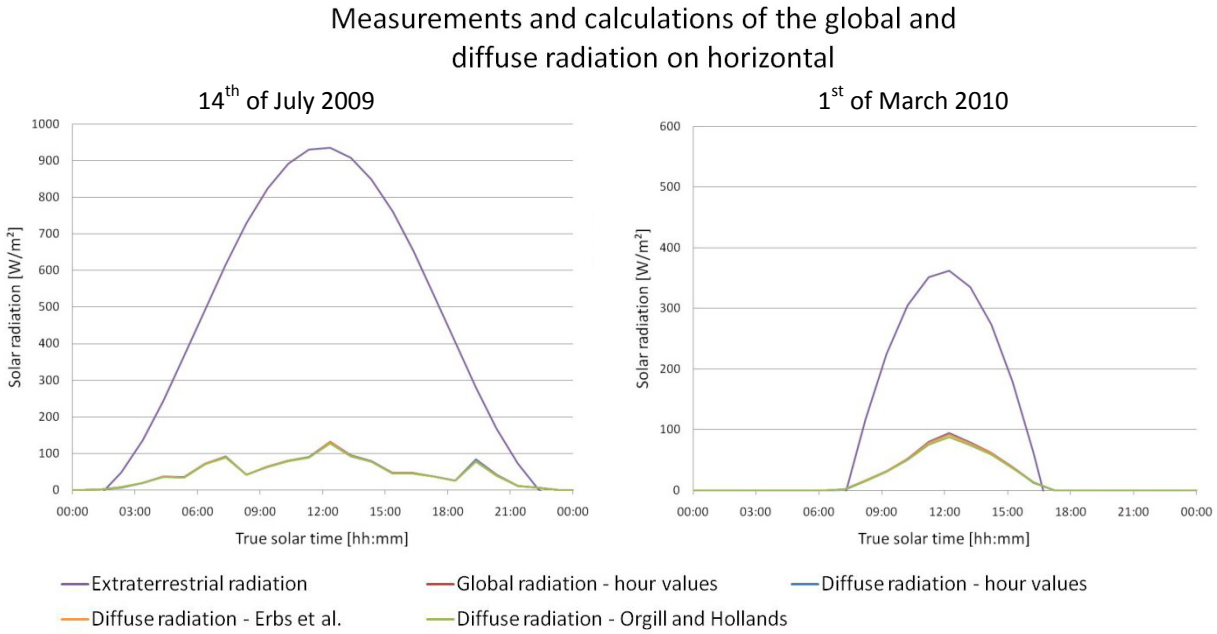

Figure 2.22 Measured and calculated values on horizontal for two different overcast sky days; the 14th of July 2009 and the 1st of March 2010.

On a monthly basis the correlations both overestimate and underestimate the diffuse radiation on the horizontal plane, see Figure 2.23. The figure shows the beam radiation on the horizontal plane, derived

from the measurements, with the clear blue bars. The calculated beam radiation with the correlations is shown with the clear green for 'Orgill and Hollands' and clear red bars for 'Erbs et al.'. The hazy blue, green and reds bars are the measured diffuse radiation and the calculated diffuse radiation with the correlations.

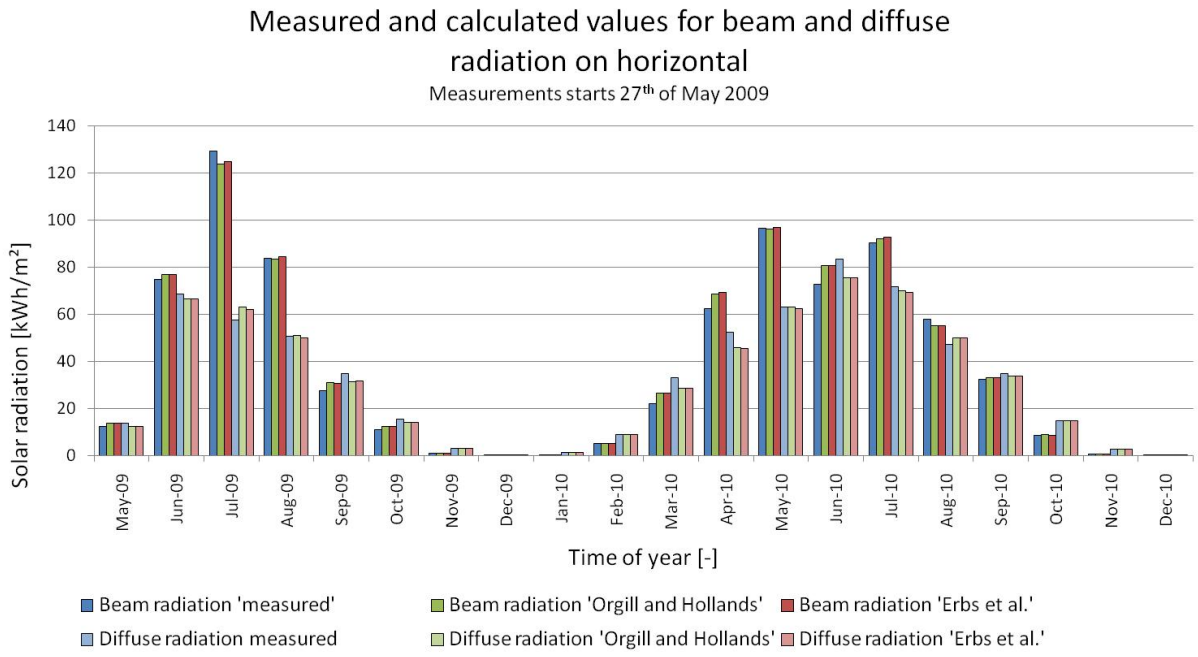

Figure 2.23 Measured and calculated direct and diffuse radiation on horizontal for 2009 and 2010.

Table 2.4 shows the total values of both the measurements and the calculations of the beam and diffuse radiation on the horizontal plane summarised over the whole measuring period of little over 16 months. Both correlations underestimate the diffuse radiation and are thereby overestimating the beam radiation. The 'Erbs et al.' correlation underestimates the diffuse radiation with 3.7 % and overestimates the beam radiation with 3.0 %. The 'Orgill and Hollands' correlation underestimates the diffuse radiation with 3.3 % and overestimates the beam radiation with 2.7 %.

Table 2.4 The comparison between measured and calculated values from 2009 and 2010 of beam and diffuse radiation.

	Measured		**'Orgill and Hollands'**		**'Erbs et al.'**	
	Beam	**Diffuse**	**Beam**	**Diffuse**	**Beam**	**Diffuse**
	[kWh/m²]	**[kWh/m²]**	**[kWh/m²]**	**[kWh/m²]**	**[kWh/m²]**	**[kWh/m²]**
2009/2010	789	657	810	636	813	633
Deviation [%]	-	-	2.7	-3.2	3.0	-3.7

Analyses of the two correlations show that at times there is a good agreement between the measured values of diffuse radiation and the calculations with the correlations of 'Orgill and Hollands' and 'Erbs et al.'. But it also shows that at specific values for the clearness index there is a need for improvement of the correlations. This is especially true for values of the clearness index higher than 0.80. The overall effect of the inaccuracy of the correlations is an overestimation of the beam radiation, because the diffuse radiation is underestimated.

2.2.2 Evaluation of the radiation models suitability for Greenland

Once the measured global radiation has been divided into beam and diffuse radiation on the horizontal plane it is necessary to calculate the radiation onto a given surface in terms of tilt and orientation. For this application several radiation models have been developed, and the most commonly referred to are Liu and Jordan, Hay and Davies, HDKR and Perez. These models are here investigated for their suitability at high latitudes and Greenlandic conditions.

Each of the radiation models divides the contribution onto a given surface into 3 contributions: beam radiation, I_b, diffuse radiation, I_d and ground reflected radiation, where the ground reflected radiation is defined as the global radiation, I, multiplied with the albedo, ρ, for the ground.

The investigation here is carried out using measured values of the global radiation to calculate the total radiation on vertical surfaces facing North, South, East and West. These results are then compared with measured values of the total radiation also on vertical surfaces facing North, South, East and West.

The ground reflected radiation onto the surfaces is here determined based on measurements thereby eliminating the uncertainty attached with calculating of the ground reflected radiation based on a fixed value for the albedo.

The 'Liu and Jordan' model

The 'Liu and Jordan' model assumes that the diffuse radiation from the sky is uniformly distributed across the sky, and therefore is often referred to as the isotropic model. The total radiation onto a tilted surface, I_T, [Liu and Jordan 1963] is given as:

$$I_T = I_b \cdot R_b + I_d \cdot \left(\frac{1 + cos\beta}{2}\right) + I \cdot \rho \cdot \left(\frac{1 - cos\beta}{2}\right) \qquad (2\text{-}4)$$

Where R_b is the view factor for the beam radiation between the measured surface and the calculated surface, and β is the tilt of the surface.

The 'Hay and Davies' model

The Hay and Davies model is an anisotropic model and assumes that the diffuse radiation from the sky is not uniformly distributed across the sky. Part of the diffuse radiation is concentrated around the beam

radiation, and called circumsolar diffuse radiation [Hay and Davies 1978]. The Hay and Davies model derives the circumsolar diffuse radiation through an anisotropy index, A_i, which is given as:

$$A_i = \frac{I_{bn}}{I_{on}} = \frac{I_b}{I_o} \qquad (2\text{-}5)$$

where I_{bn} and I_b is the beam normal radiation and the beam radiation on the horizontal plane, and I_{on} and I_o is the extraterrestrial normal radiation and the extraterrestrial radiation on the horizontal plane. Therefore the anisotropy index gives the ratio of beam radiation to that of the extraterrestrial radiation. Since the circumsolar diffuse radiation is concentrated around the beam and has the same direction as the beam radiation it is multiplied with R_b instead of the view factor for isotropic diffuse radiation. The Hay and Davies model gives the total radiation on a tilted surface as:

$$I_T = (I_b + I_d \cdot A_i) \cdot R_b + I_d \cdot (1 - A_i) \cdot \left(\frac{1 + cos\beta}{2}\right) + I \cdot \rho \cdot \left(\frac{1 - cos\beta}{2}\right) \qquad (2\text{-}6)$$

The 'HDKR' model

The HDKR model is a continuation of the Hay and Davies model, but has added a term to the isotropic diffuse radiation in order to account for horizontal brightening. The term is originally from Temps and Coulson [Temps and Coulson 1976], but was derived only for clear sky days. Klucher modified the term so it would be suitable for cloudy skies as well [Klucher 1978].

The diffuse radiation on a tilted surface is therefore in the HDKR model given as:

$$I_{d,T} = I_d \cdot A_i \cdot R_b + I_d \cdot (1 - A_i) \cdot \left(\frac{1 + cos\beta}{2}\right) + I_d \cdot \left(f \cdot sin^3 \cdot \left(\frac{\beta}{2}\right)\right) \qquad (2\text{-}7)$$

Where f is the modulating factor from Klucher. The first term in the equation of the diffuse radiation on a tilted surface accounts for the circumsolar radiation, the second term is the isotropic diffuse radiation and the last term is the horizontal brightening.

Radiation on a tilted surface according to the HDKR model is therefore:

$$I_T = (I_b + I_d \cdot A_i) \cdot R_b + I_d \cdot (1 - A_i) \cdot \left(\frac{1 + cos\beta}{2}\right) \cdot \left(1 + f \cdot sin^3 \cdot \left(\frac{\beta}{2}\right)\right) + I \cdot \rho \cdot \left(\frac{1 - cos\beta}{2}\right) \qquad (2\text{-}8)$$

The 'Perez' model

The Perez model is a more detailed analyse of the diffuse radiation on a tilted surface [Perez et al. 1987].

The diffuse radiation on at tilted surface according to the Perez model, where both the circumsolar diffuse radiation and horizontal brightening diffuse radiation is taken into account, is given as:

$$I_{d,T} = I_d \cdot \left((1 - F_1) \cdot \left(\frac{1 + cos\beta}{2} \right) + F_1 \cdot \frac{a}{b} + F_2 \cdot sin\beta \right) \qquad (2\text{-}9)$$

where F_1 and F_2 are circumsolar and horizontal brightening coefficients and a and b are terms that accounts for the angles of incident of the circumsolar diffuse radiation on the tilted and horizontal surfaces.

The radiation on a titled surface according to the Perez models is given as:

$$I_T = I_b \cdot R_b + I_d \cdot (1 - F_1) \cdot \left(\frac{1 + cos\beta}{2} \right) + I_d \cdot F_1 \cdot \frac{a}{b} + I_d \cdot F_2 \cdot sin\beta + I \cdot \rho \cdot \left(\frac{1 - cos\beta}{2} \right) \qquad (2\text{-}10)$$

In order to evaluated the accuracy of the four radiation models the total radiation on vertical surfaces facing North, South, East and West is calculated and compared to measurements. The measured data were collected in Sisimiut from the middle of July 2003 to the end of September 2007 with a measuring device called the Solarhat.

Measurements from the Solarhat in Sisimiut

The purpose of the Solarhat was to map and analyse the reflection from the ground by measuring the total and reflected radiation on vertical surfaces facing North, South, East and West. For the purpose of assessing the accuracy of the four radiation models the measurements are here used to compare the calculated values of the total radiation. The ground reflected radiation is here, in all four models, disregarded when calculating the values for the total radiation and is subtracted from the measurements of the total radiation. This is to eliminate further inaccuracy because of the ground reflected radiation.

The Solarhat was installed in the fall of 2003 at Asiaq's climate station on Teleisland in Sisimiut, see Figure 2.24.

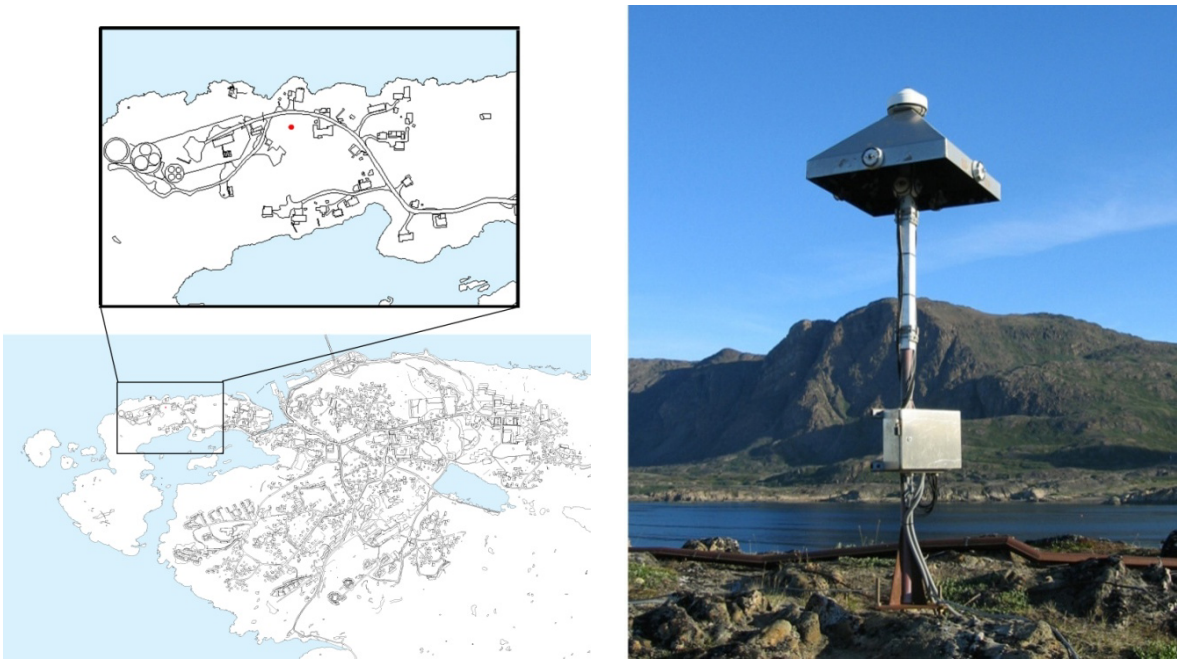

Figure 2.24 The Solarhat at ASIAQ's climate station on Teleisland in Sisimiut. The location is marked with red on the map on the left.

The Solarhat is equipped with 9 pyranometers which continuously measure irradiance with a time step of 5 minutes, see Figure 2.25. The measured data is: The global radiation measured with a pyranometer, type CM 11 from Kipp & Zonen, the total radiation on vertical surfaces facing north, south, east and west measured with CM 3 pyranometers also from Kipp & Zonen and the reflected radiation on vertical surfaces again facing north, south, east and west measured with CM 3 pyranometers from Kipp & Zonen.

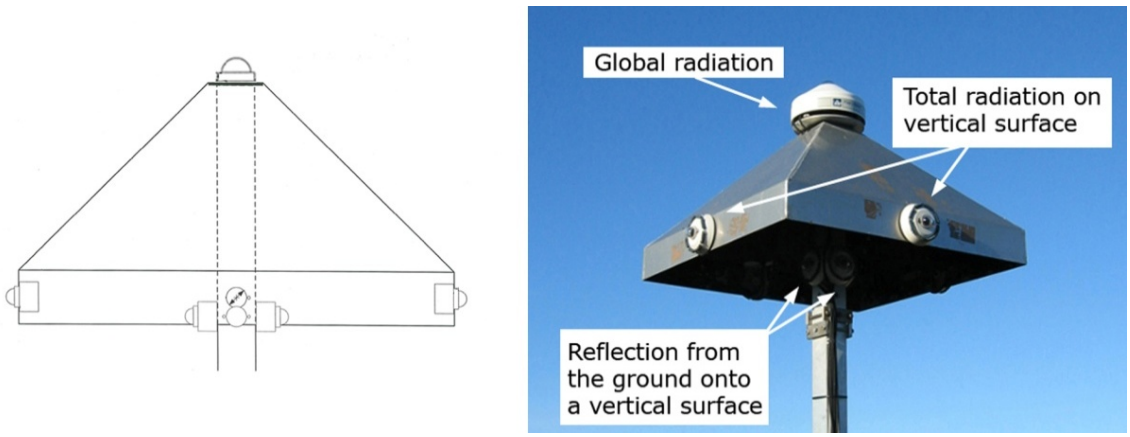

Figure 2.25 Left: A principle sketch of the Solarhat. Right: Measurements from the Solarhat.

In Figure 2.26 a 360° view around the Solarhat is shown. The mountains are seen in the north and east direction, and water in the north, south and west direction. In the area surrounding the Solarhat there are no buildings or major obstructions. Only minor obstructions are seen, such as poles from other measuring equipment.

Figure 2.26 A 360° angle around the Solarhat; north, east, south and west.

The mountains seen in the north and east direction on Figure 2.26 influences the measurements, in such a way that the registration of sunrise is delayed because the sun has to rise free of the mountains in the morning before direct solar radiation is measured. In the same way the day is cut short by the mountains in the north, because the sun sets behind the mountains. In the summer where midnight sun occurs for a period of 5 days, the period is cut short again because of the mountains in the north. The solar altitude is here higher than 0°, but the sun will stay behind the mountains.

The measurements used here to analyse the radiation models are the data from 2004, 2005 and 2006. In order to avoid faulty measurements from electrical disturbances, only radiation measurements obtained when the calculated solar altitude angle is positive are used.

Accuracy of the 4 radiation models on a daily, monthly and yearly basis

Since the radiation models are based on information of the beam and diffuse radiation, the initial division of the global radiation is carried out using the 'Erbs et al.' correlation. Again the evaluation is based on 3 different sky conditions for both the summer and winter situation.

Figure 2.27 shows the measured and calculated values for the 3rd of July 2006 which was a clear sky day. On the north facing surface the 'Hay and Davies' model (green curve) is the most accurate model, with the 'HDKR' model (purple curve) following. The 'Liu and Jordan' (red curve) and 'Perez' model (turquoise curve) are the least accurate models in the north facing direction. In the south facing direction the picture is reversed with the 'Liu and Jordan' model as the most accurate, while the other three models all overestimate the total radiation onto the surface.

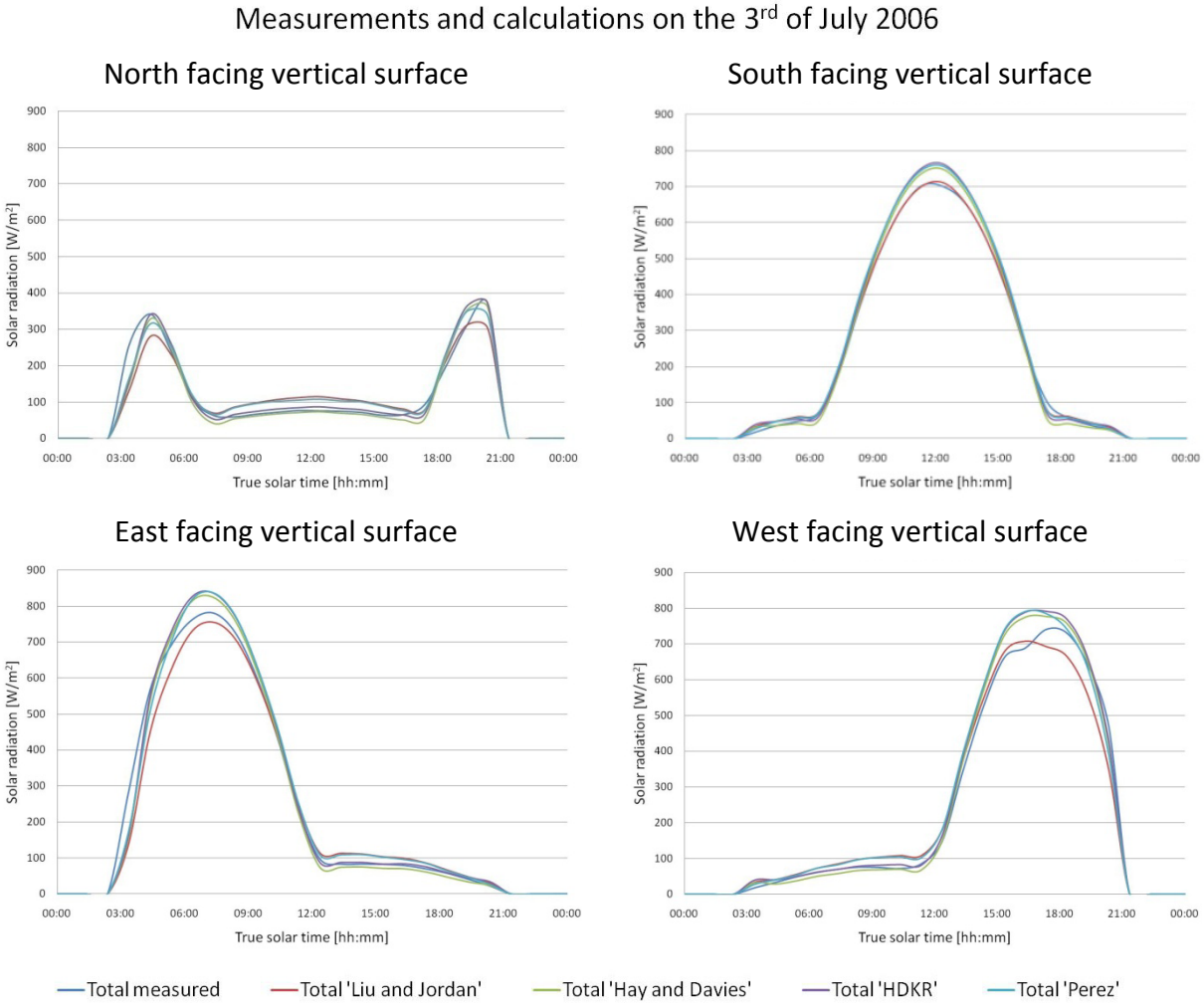

Figure 2.27 Measured and calculated values on the 3rd of July 2006, clear sky summer day.

On an east and west facing surface the picture is the same as on the south facing surface. The 'Liu and Jordan' model is the most accurate, while the three other models are overestimating the total radiation.

The conditions on a winter day with clear sky is shown with measurements from the 15th of March 2006, see Figure 2.28. In the north facing direction The 'Isotropic' and 'Perez' models slightly overestimate the total radiation while the 'Hay and Davies' and 'HDKR' models both underestimate the total radiation. In the south facing direction all four model overestimate the radiation, with the 'Liu and Jordan' model as the most accurate and the 'Perez' model next.

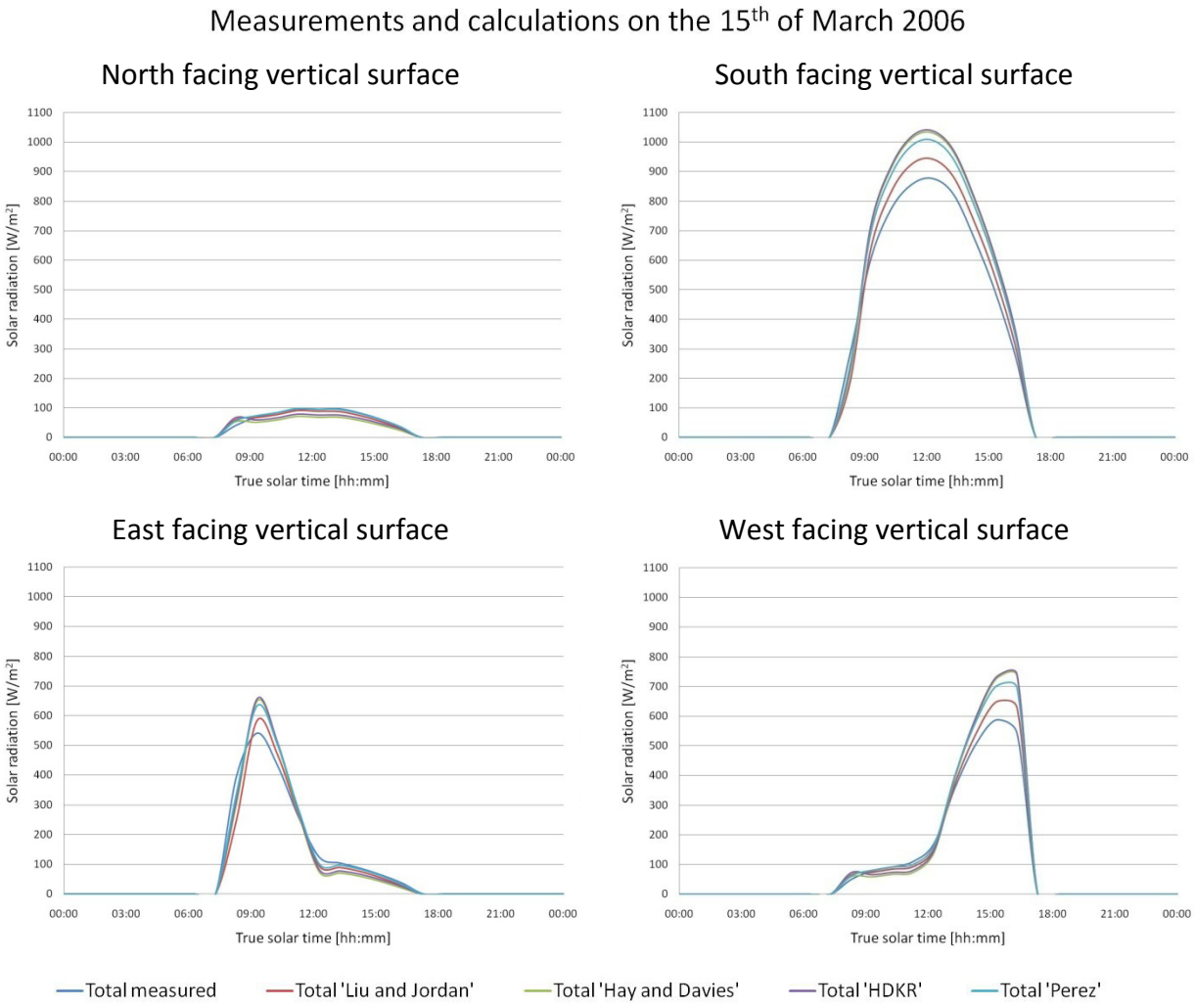

Figure 2.28 Measured and calculated values on the 15th of March 2006, clear sky day winter.

In the east and west facing directions the picture is the same as on the south facing surface. The 'Liu and Jordan' and the 'Perez' models calculated values are closest to the measurements.

Figure 2.29 shows the values from the four models on a mixed sky day during the summer. On this day the models have difficulties following the measured values of the total radiation. In the north facing direction the 'Liu and Jordan' model has the least deviation throughout the day, but is not following the measurements very well. In the south facing direction the models follow the measurements in a better way throughout the day. The 'Liu and Jordan' model is the most accurate, but still overestimates the total radiation.

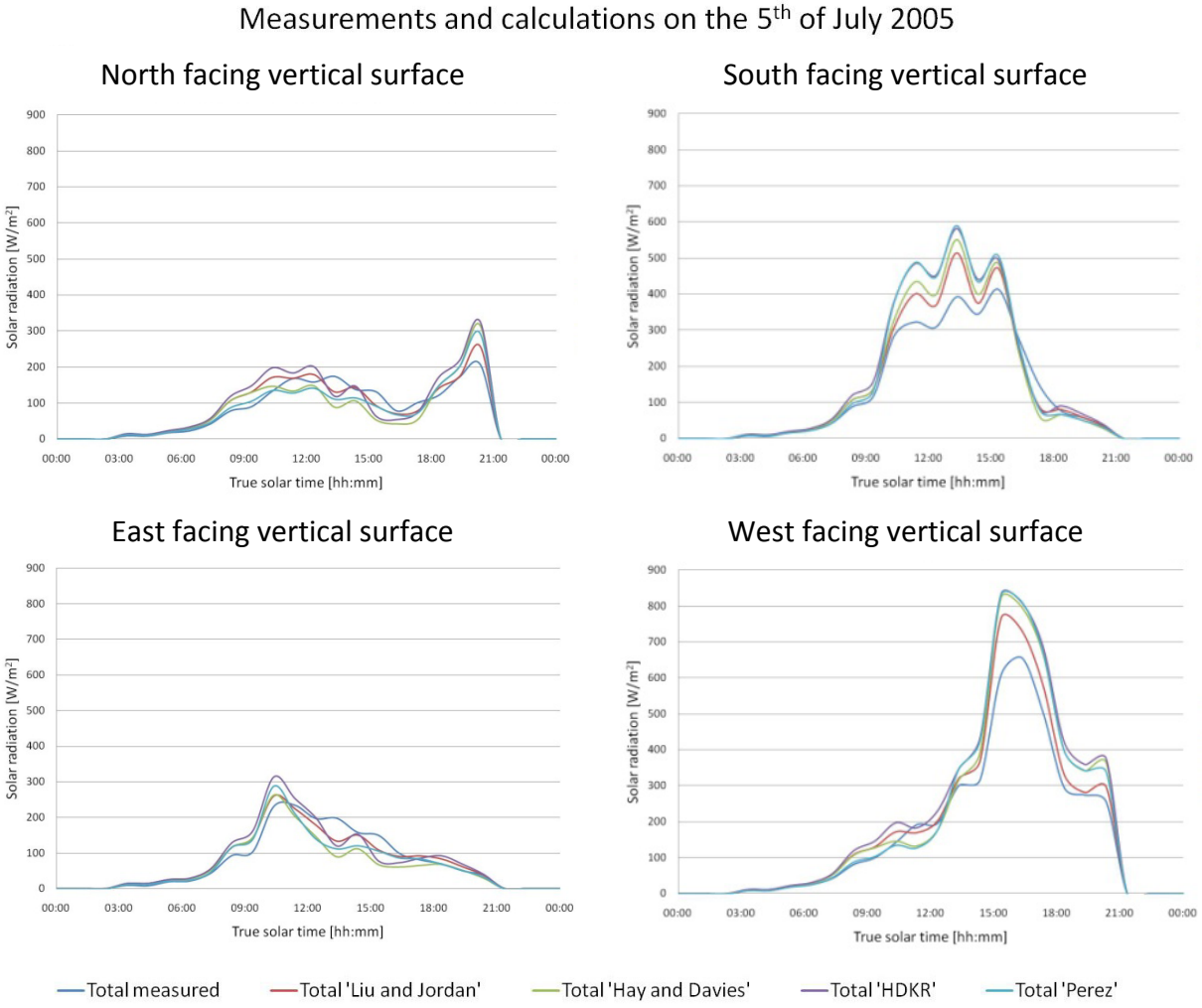

Figure 2.29 Measured and calculated values on the 5th of July 2005, a mixed sky summer day.

On the east facing surface, all four models are more successful in following the measurements. The 'Liu and Jordan model' is again the most accurate. On the west facing surface the 'Liu and Jordan' model is the most accurate, but all four models are overestimating the total radiation compared to the measurements.

The measurements from the 7th of March 2005 show the results on a mixed sky day in the winter see Figure 2.30. The situation is the same as was seen on a mixed sky summer day. In the north and east direction, all four models underestimate the total radiation compared to the measured values and have difficulties following the measurements. In the south and west facing direction the 'Liu and Jordan' model is the most accurate, but all four models are overestimating the total radiation.

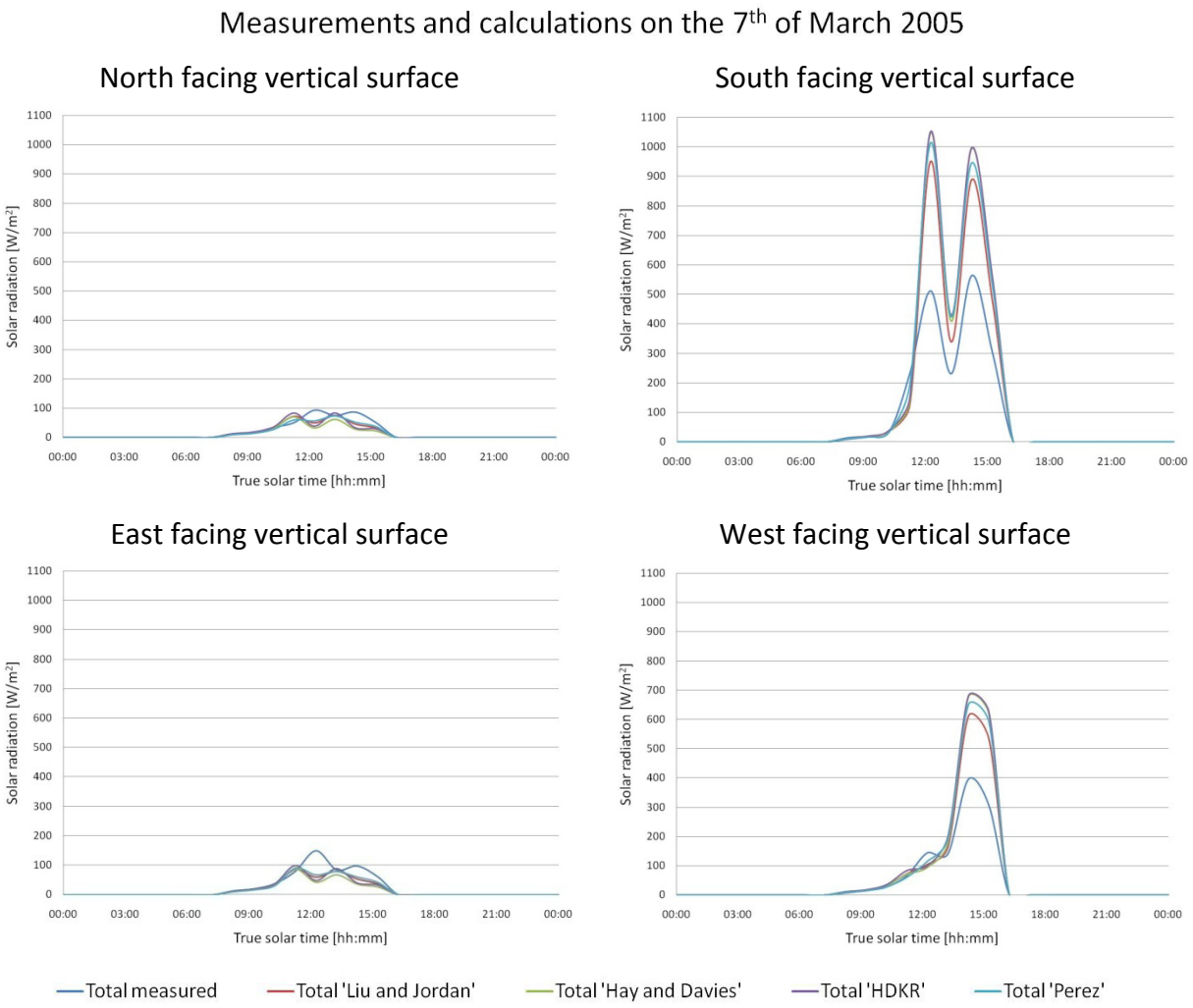

Figure 2.30 Measured and calculated values on the 7th of March 2005, mixed sky day winter.

On overcast days the picture changes again, see Figure 2.31. The 23rd of July 2005 shows an overcast summer day. It can be seen on the figure that the 'Perez' model for all four directions is the most accurate model.

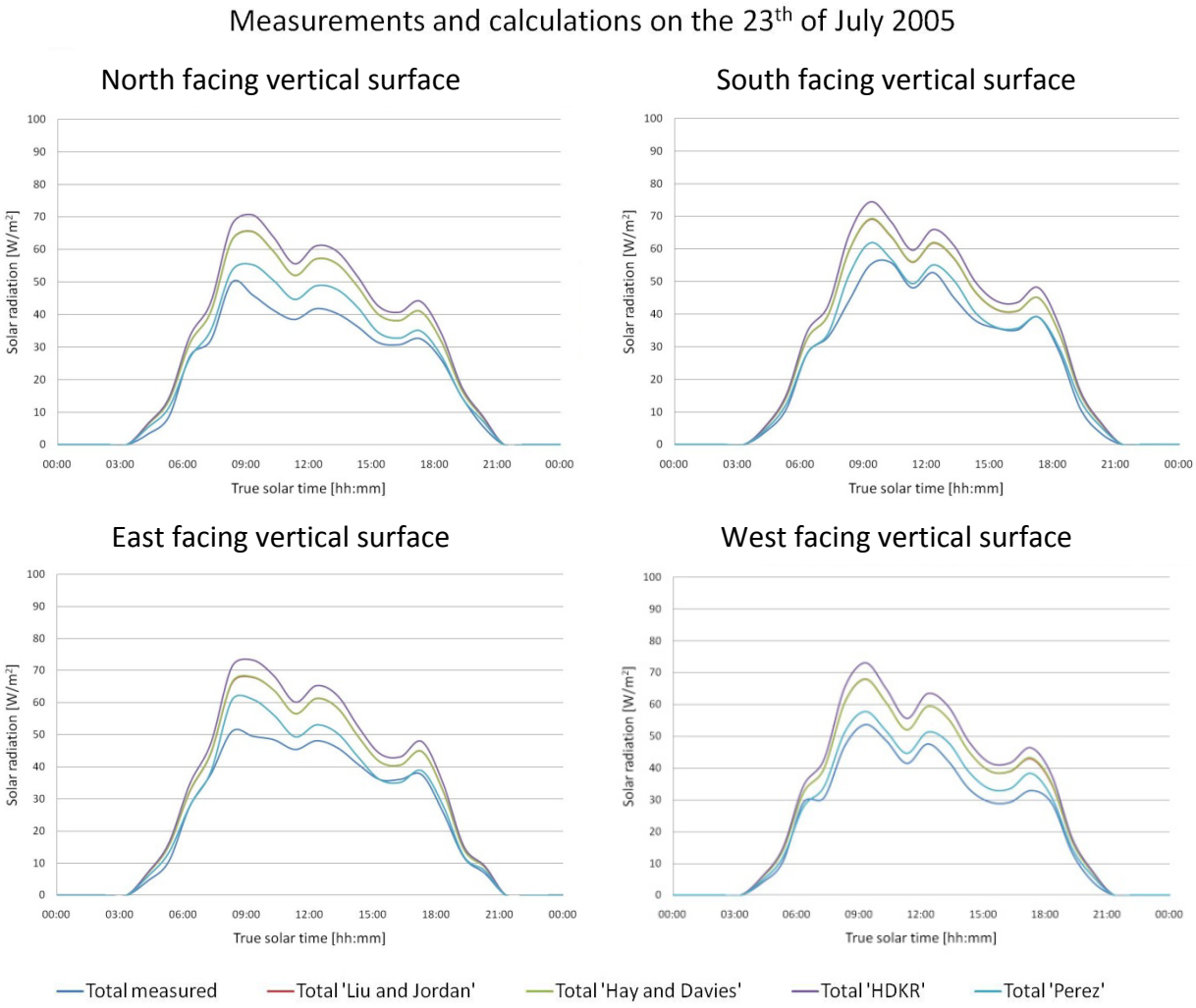

Figure 2.31 Measured and calculated values on the 23rd of July 2005, an overcast sky summer day.

The 26th of March 2004 was a winter day with an overcast sky. The models are slightly overestimating the total radiation on the south facing surface. In the other directions the models are slightly underestimating the total radiation, see Figure 2.32.

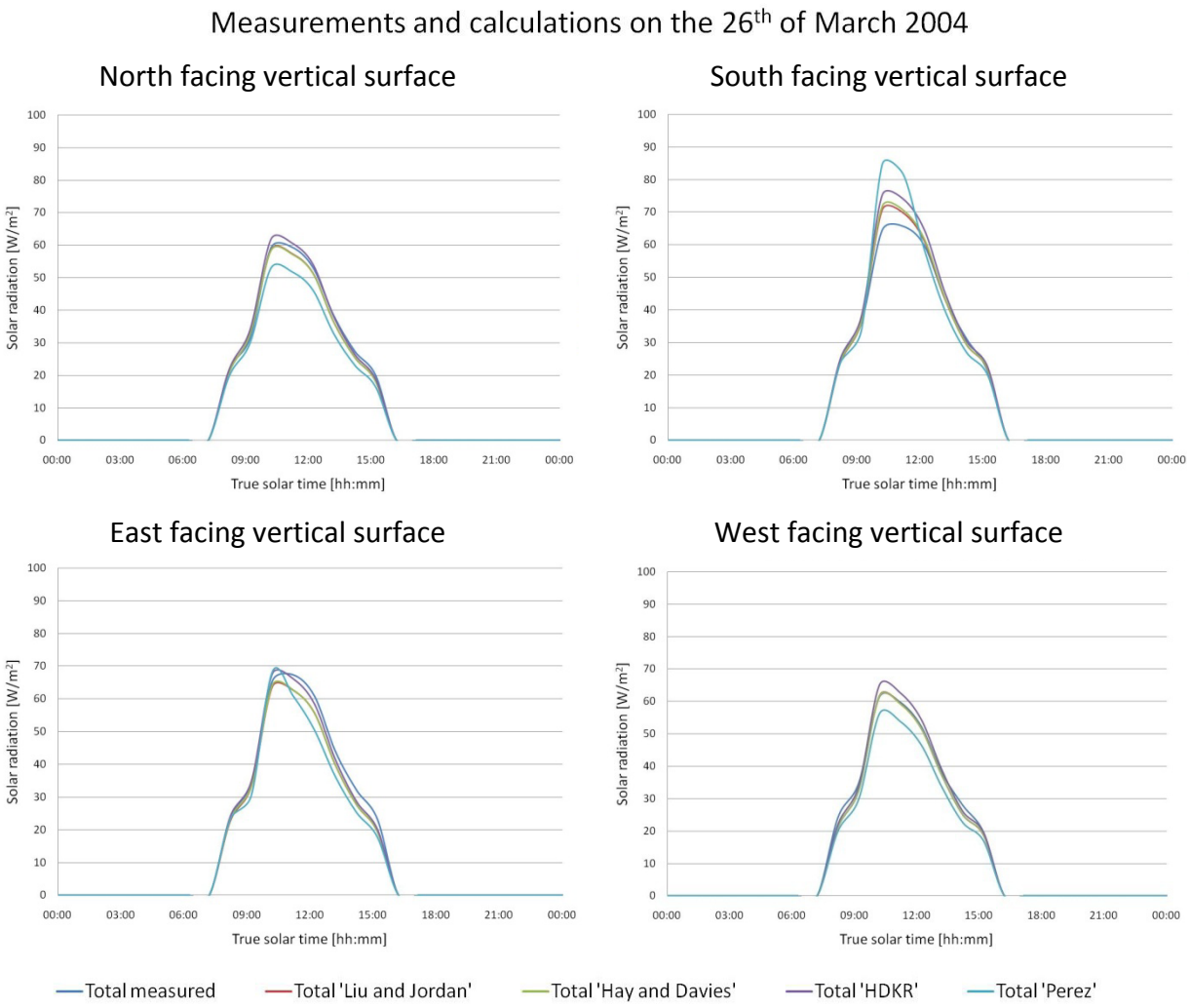

Figure 2.32 Measured and calculated values on the 26th of March 2004, an overcast sky day winter.

The analysis on a daily basis shows, that the 'Liu and Jordan' is the most accurate of the four models, but all four models have difficulties depicting the measurements under the different sky conditions. On clear days the models all overestimate the total radiation in the four directions. The same thing happens on overcast days in both the winter and summer situation. On mixed days the models have slightly more difficulty calculating the total radiation and again they all overestimate the total radiation. In conclusion the analyses of the four models show that the results are not in good agreement with the measurements, especially when there are clouds in the sky.

In Figure 2.33 thru Figure 2.35 the monthly average values are shown for the four directions. The average is based on measurements from 2004, 2005 and 2006.

The results from the north facing surface can be seen in Figure 2.33. The models underestimate the total radiation in the winter months. From April to September the 'Liu and Jordan', 'HDKR' and 'Perez' models all overestimate the radiation. The 'Hay and Davies' model continues to underestimate the radiation in the spring months, and does not start to overestimate the radiation until June. The 'HDKR' model is the model with the biggest deviation from the measurements on a north facing vertical surface. In the summer months it suggests the highest amount of radiation.

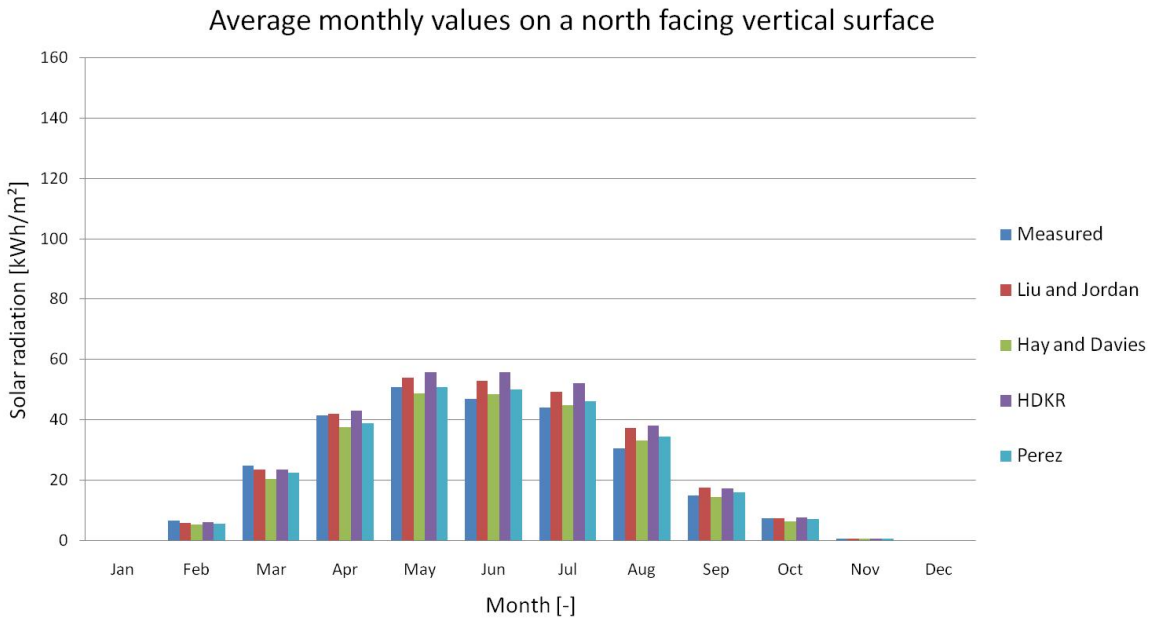

Figure 2.33 Average monthly values on a north facing vertical surface.

In the south facing direction it is again the 'HDKR' model which has the biggest deviation from the measurements, followed by the 'Perez' model. In general all four models are overestimating the total radiation on a south facing vertical surface, except the 'Liu and Jordan' model in April. The deviation from the measurements is biggest in the south facing direction.

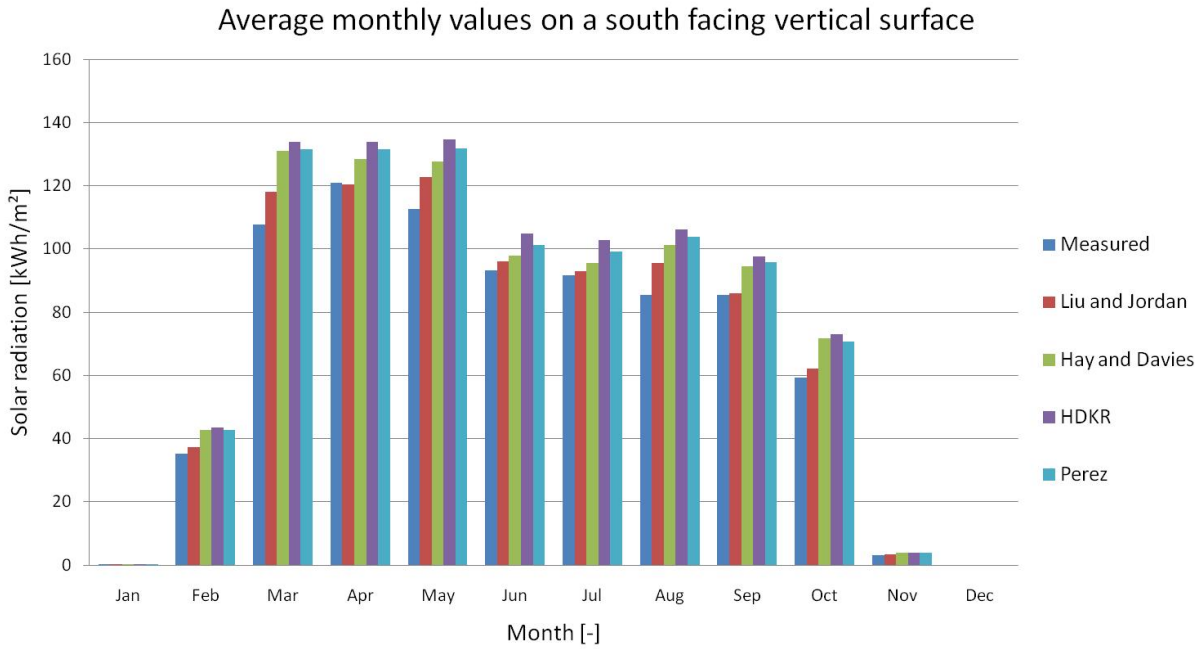

Figure 2.34 Average monthly values on a south facing vertical surface.

In the east facing direction, the models, as a general rule, no longer overestimate the total radiation, Figure 2.35. In the months of February, March and April, both the 'Liu and Jordan', 'Hay and Davies' and the 'Perez' model underestimate the total radiation. The 'HDKR' model overestimates throughout the year, and has the biggest deviation from the measured radiation.

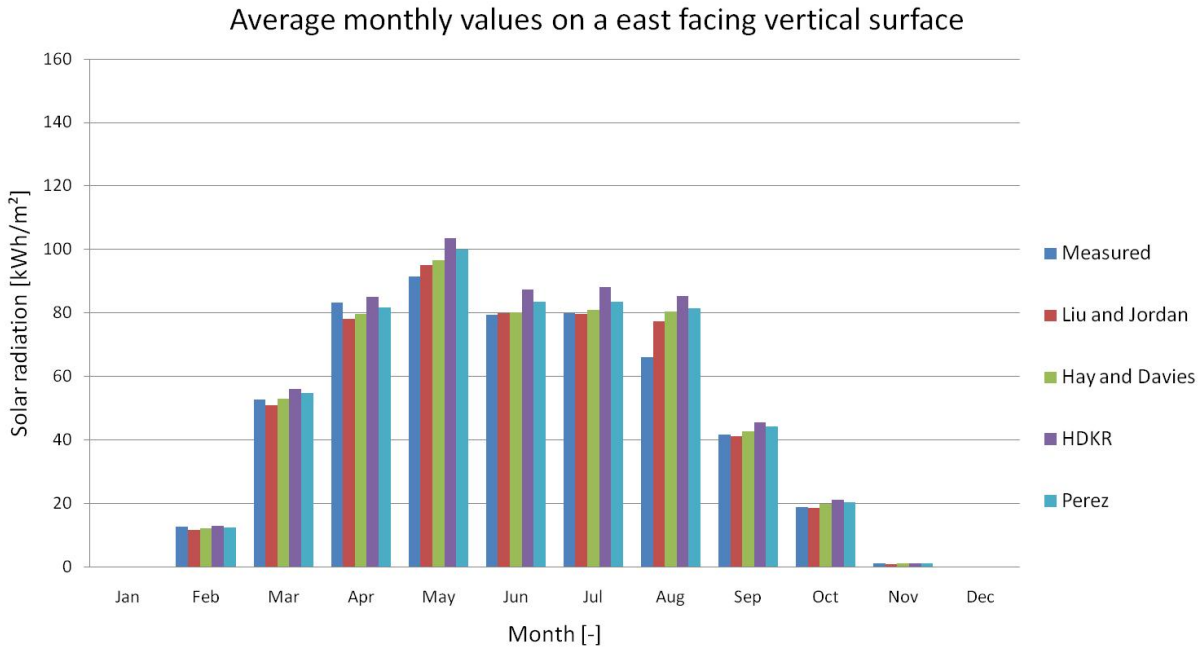

Figure 2.35 Average monthly values on an east facing vertical surface.

On the west facing vertical surface all four models overestimate the total radiation compared to the measurements throughout the year, see Figure 2.36. The 'HDKR' model again shows the biggest deviations, followed by the 'Perez' model. The 'Liu and Jordan' model is the most accurate on a west facing vertical surface.

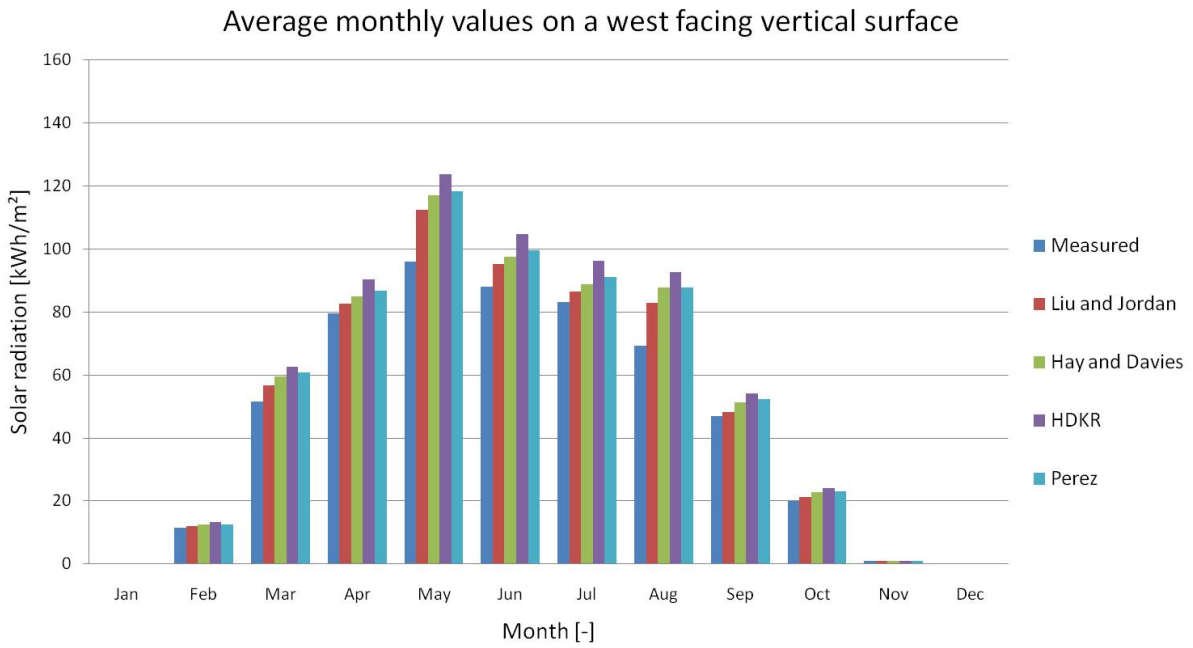

Figure 2.36 Average monthly values on a west facing vertical surface.

The calculated values with the four different models on a yearly basis can be seen in Table 2.5, which shows that the most accurate model is different for the different directions. In the north facing direction the 'Perez' model is the most accurate, followed by the 'Hay and Davies' model. In the south, east and west facing direction the 'Liu and Jordan model' is the most accurate, overestimating the total radiation with 5 % towards south, 1 % towards east and 9 % towards west, see Table 2.6.

Table 2.5 The average yearly calculated values for vertical surfaces facing North, South, East and West, with 4 different radiation models.

	North	South	East	West
	[kWh/m²]	[kWh/m²]	[kWh/m²]	[kWh/m²]
Measured	269	795	527	547
Liu and Jordan	291	835	534	599
Hay and Davies	261	895	547	623
HDKR	300	935	586	662
Perez	273	913	563	633

Table 2.6 The percentage deviation from the average yearly values of the measured and the calculated values for vertical surfaces facing North, South, East and West, with 4 different radiation models.

	North	South	East	West
	[%]	[%]	[%]	[%]
Liu and Jordan	8	5	1	9
Hay and Davies	-3	13	4	14
HDKR	12	18	11	21
Perez	2	15	7	16

Whether looking on individual days, a monthly or a yearly basis, the 'Liu and Jordan' model is the most accurate. The attempts to take into account the circumsolar diffuse radiation and the horizontal brightening, does not result in improvements compared to the measured values. It should be noted that since the models are based on diffuse fraction correlation which also contains inaccuracies, this will influence the results from the individual model, as will inaccuracies associated with measurements in general.

2.3 Discussion

The results from the investigations of the two diffuse correlations, 'Erbs et al.' and 'Orgill and Hollands', show that both correlations underestimates the diffuse radiation and thereby overestimate the beam radiation. Of the two correlations 'Orgill and Hollands' is the most accurate.

The results also show that there is a need for an improved correlation which will take the special conditions at high latitudes into account. Unfortunately the amount of available data relating to diffuse radiation is not sufficient to calculate a new correlation.

The evaluation of the four radiation models is dependent on the calculations from the correlation, and any inaccuracy in the correlation will have an influence on the result of the analysis of the radiation models. Nevertheless the investigation carried out shows that the different attempts to take into account both circumsolar diffuse radiation and horizontal brightening diffuse radiation are not suitable for the conditions in Greenland. Of the four models investigated in this thesis the 'Liu and Jordan' model – the isotropic model - is the most accurate radiation model.

It is therefore recommended to install either the SPN1 pyranometer or a similar pyranometer able to obtain diffuse radiation measurements at more locations in Greenland, in order to increase the data pool from which a new correlation can be calculated.

The evaluation of the radiation models indicates a need for a specific radiation model for Greenland which takes the coastal location, the mountains and the conditions of inter-reflection into account. It is therefore recommended to measure the total and reflected radiation in different directions at different locations, to provide input for radiation models, so that the solar radiation on different tilted and oriented surfaces in Greenland can be determined with improved accuracy.

Chapter 3 Reflection from the ground

In evaluations of the climate system and the energy balance of the earth, the reflection from the ground plays an important role especially when the ground is covered with snow. The reflection from the ground is also important in the planning or optimizing of a solar heating system or the energy efficiency of a building. The reflection from the ground is described by the albedo, given as the ratio between the solar radiation received by a surface and the radiation which is reflected back. The reflection from snow is high and often found to be between 75 % and 90 % [Wiscomb and Warren 1980, Warren 1982, Koenderink and Richards 1992], depending on whether it is new snow or old snow [Pirazzini 2004]. When the ground is not covered with snow the albedo depends on the soil and vegetation types [Wang et al. 2005].

It is important to have a correct representation of the solar radiation both from the sky, and reflected from the ground [Psiloglou et al. 1997], especially at high latitudes where the ground is covered with snow [Dragsted et al. 2008]. Previous studies on the albedo of snow, suggests a dependency of the solar zenith angle on the albedo, since the angle of incident has a large impact on whether or not the radiation is absorbed or reflected [Choudhury and Chang 1981, Yamanouchi 1983, Pirazzini 2004, Wang and Zender 2010]. The dependency of the albedo for snow on the incident angle is reported as strongly influenced by the grain size of the snow. [Yamanouchi 1983] reported that new snow has a weak dependency and more eroded snow had a stronger dependency of the solar zenith angle. In the study from [Choudhury and Chang 1981] the dependency of the solar altitude angle is shown to account for a variation in the albedo by up to 8 %. In [Wang and Zender 2010] the dependency of the zenith angle accounts for a variation of around 4 %. This investigation of accurate representation of ground reflected radiation does not dispute this connection between the albedo and the solar zenith angle. But the measurements are unable to confirm this connection because of the strong directional dependence in the measurements and influence from the surroundings.

This investigation focuses on how the reflected radiation from the ground is calculated and will map the directionality of the reflected radiation. The effective albedo for the ground is presented as a function of the difference between the orientation of the surface and the location of the sun. Calculating the effective albedo in this way will increase accuracy of the calculated reflected radiation from the ground onto a tilted surface. The intention is to replace the often used method of uniform values for the albedo of 0.2 when the ground is not covered with snow and 0.7 when the ground is covered with snow as seen in [Shah and Furbo 2005].

3.1 The basis for the analysis

As mentioned in chapter 2 the Solarhat was constructed as part of a research project running from 2003 to 2006. The purpose of the Solarhat was to map and analyse the reflection from the ground, by measuring the total and reflected radiation on vertical surfaces in 4 different directions, along with the global radiation, see Figure 3.1. With these measurements it is possible to investigate the directional dependency of the reflection.

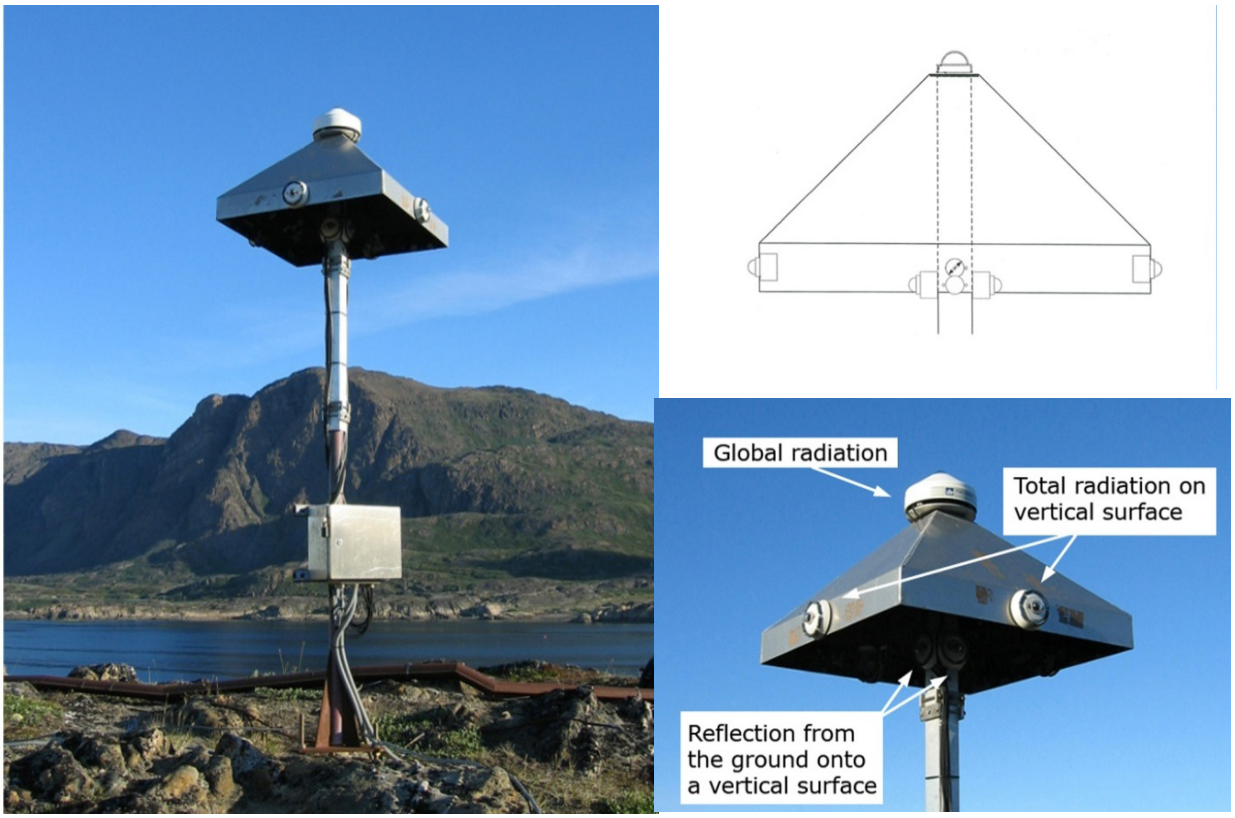

Figure 3.1 The Solarhat installed at Teleisland in Sisimiut. Right top: Sketch of the Solarhat. Right bottom: Description of the measurements from the Solarhat.

In order to obtain a reasonable accuracy for the calculated effective albedo, several assumptions and limitations must be fulfilled for the measurements.

For the solar altitude the limit is set for 10°, to increase measuring accuracy. Measurement of the global radiation must be higher than 150 W/m^2 and for the reflected radiation the limit is 5 W/m^2. These limits are set to insure a high accuracy, and avoid measurements with inaccuracies attached. An additional limit is incorporated stating that the global radiation must be lower than the calculated extraterrestrial radiation on a horizontal surface at the earth surface. This will eliminate faulty measurements caused by electrical disturbances, but unfortunately also situations where the global radiation is rightfully higher than the extraterrestrial radiation, caused by inter-reflection from drifting clouds as seen in chapter 2.

Measurements from the period where the sun is placed with an azimuth between 75° and 85° are also disregarded, because of shadows cast on the Solarhat by a nearby pole, see Figure 3.2.

Figure 3.2 A 360° angle around the Solarhat; North, East, South and West. Showing the obstruction from a nearby pole in red circle.

Based on the measured data the effective albedo is calculated using an equation assuming a diffuse reflection from the ground. The equation is described in Solar Engineering of Thermal processes by Duffie and Beckman [Duffie and Beckmann 1991]:

$$I_R = I \cdot \rho \cdot \left((1 - cos\beta)/2\right) \quad (3\text{-}1)$$

Where $\left((1 - cos\beta)/2\right)$ is the view factor from a surface to the ground for the surface tilted with an angle β. The angle is here set to 90°, assuming a horizontal terrain where the Solarhat is placed and a vertical surface of the pyranometer measuring the reflected radiation. Although the terrain is not completely horizontal a previous study by Jensen and Lauritsen [Jensen and Lauritsen 2006] has proven this assumption to be acceptable. I is the global radiation and I_R is the reflected radiation measured with pyranometers on vertical surfaces facing North, South, East and West. This results in the following equation for the effective albedo:

$$\rho = (2 \cdot I_R)/I \quad (3\text{-}2)$$

The effective albedo can then be determined for each of the directions: North, South, East and West, which means the directional dependency of the reflection, can be analyzed.

The attached inaccuracy of the calculated effective albedo is found by:

$$S_\rho = \sqrt{\left(\frac{2}{I} \cdot S_{I_R}\right)^2 + \left(\frac{-2 \cdot I_R}{I^2} \cdot S_I\right)^2} \quad (3\text{-}3)$$

Where S_ρ is the uncertainty of the albedo determined by equation (3-3). S_{I_R} and S_I is the uncertainty of the pyranometers which for the CM 11 is 2 % and for the CM 3 is 5%. This results in an inaccuracy of less than 6 % for the calculated effective albedo.

In Figure 3.3 the uncertainty is shown for the effective albedo on March 18th 2004. The uncertainty is shown as a band around the individual effective albedo in each of the directions. It can be seen that the higher the effective albedo the higher the uncertainty. It is assessed that this method of calculating the effective albedo based on the measurements is not attached with high uncertainty due to inaccuracies in the measurements.

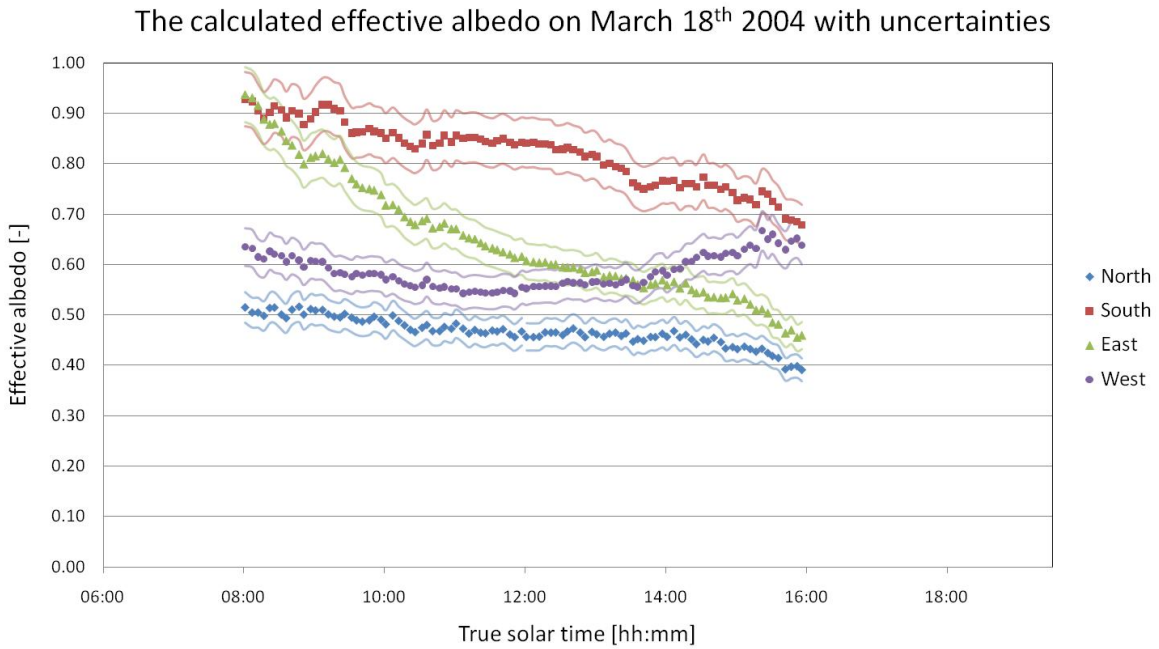

Figure 3.3 The uncertainty for the effective albedo for March 18th 2004.

3.2 Analysis of measurements

The analyzed data from the Solarhat is measured from the 16th of July 2003 until 30th of September 2007. In Figure 3.4 the yearly global radiation measured with the Solarhat is shown along with the yearly global radiation from the reference year for Sisimiut. The figure shows that there is a good correspondence between the measured values and the reference year, as the measured values are just slightly lower than the values from the reference years.

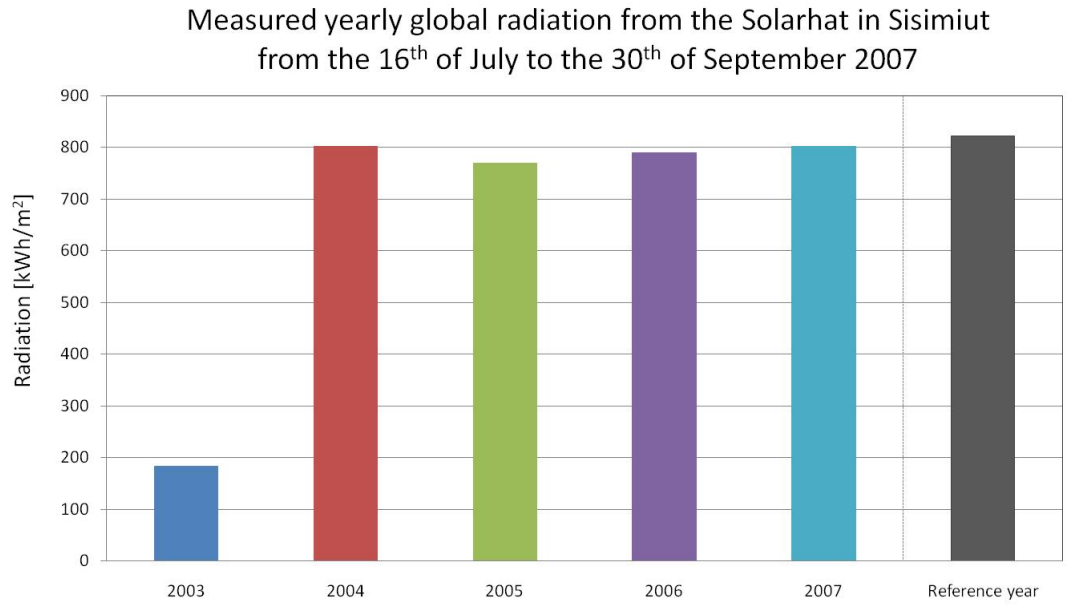

Figure 3.4 The yearly global radiation measured with the Solarhat from the 16th of July 2003 until the 30th of September 2007.

The measured total radiation with the Solarhat on the four vertical surfaces facing North, South, East and West can be seen in Figure 3.5. The measurements are started in the middle of 2003, which accounts for the much lower values from this year. The figure shows only a small variation in the measurement during the four years the Solarhat was in operation.

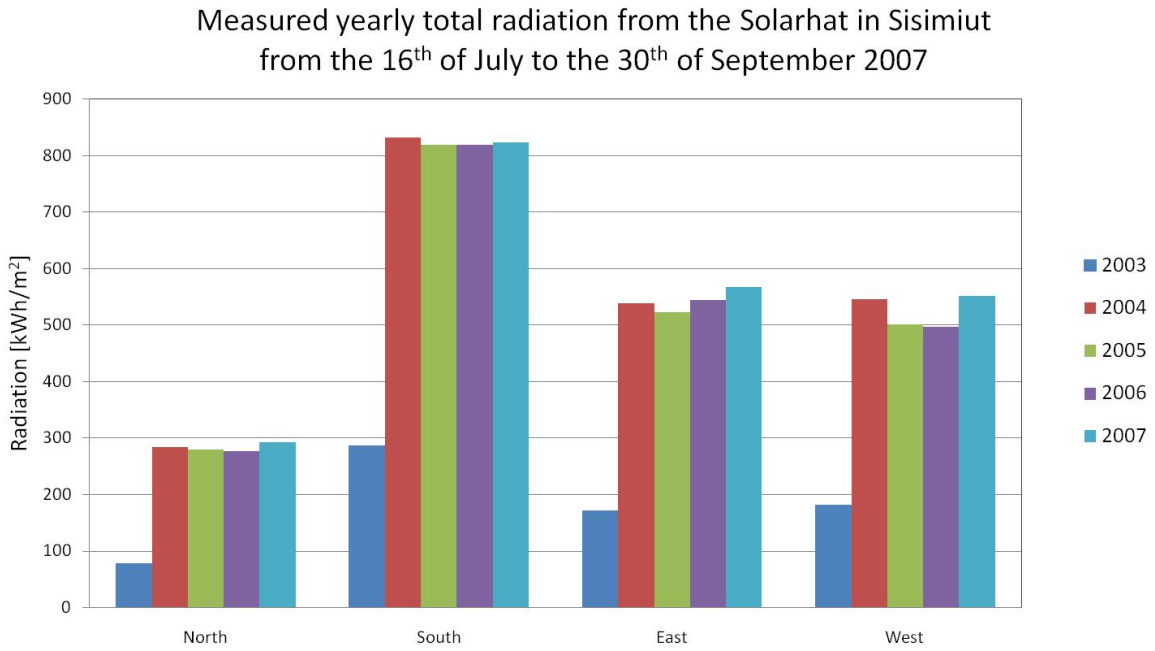

Figure 3.5 The measured total radiation from the Solarhat on four vertical surfaces facing North, South, East and West.

The reflected radiation measured with the Solarhat is shown in Figure 3.6. Again the low values for 2003 are because the measurements are only from the last half of the year. This is also the reason why there is no variation in the measured reflected radiation on the fours surfaces facing the different directions as seen in the measurements form the other years. The measurements of the reflected radiation also indicate that 2007 was sunnier than the previous years.

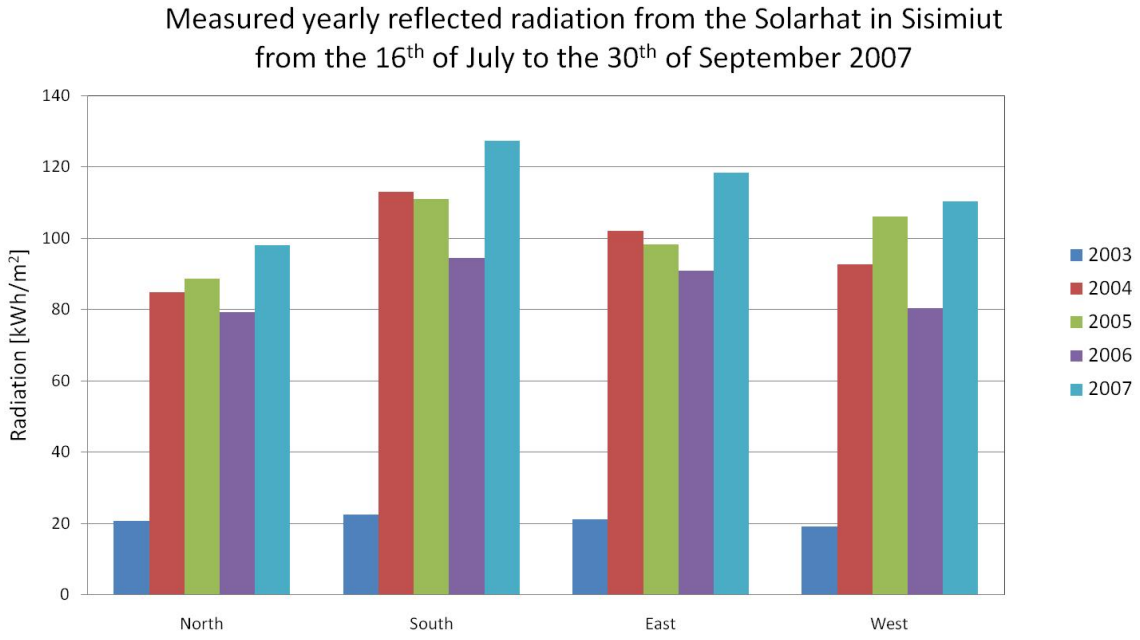

Figure 3.6 The measured reflected radiation from the Solarhat on four vertical surfaces facing North, South, East and West.

The average values of the yearly total and reflected radiation from 2004, 2005 and 2006 in the four directions are shown in Table 3.1. It can here be seen that although the reflected radiation on a North facing vertical surface accounts for 30 % it only amount to 84 kWh/m². The reflected radiation on the South facing surface is 106 kWh/m², which account for 13 % of the total radiation on a South facing vertical surface. The reflected radiation is 97 kWh/m² for East, and 93 kWh/m² for the West facing surface.

Table 3.1 The total and reflected radiation onto vertical surfaces facing North, South, East and West.

Average of 2004, 2005 and 2006	North	South	East	West
	[kWh/m²]	[kWh/m²]	[kWh/m²]	[kWh/m²]
Total radiation	280	823	535	515
Reflected radiation	84	106	97	93
Percentage of reflected radiation of total radiation	30	13	18	18

3.2.1 Yearly variation of the albedo

The yearly variation of the effective albedo is shown in Figure 3.7 thru Figure 3.11 for 2003 to 2007. Each point represents a calculated value of the effective albedo with a time step of 5 minutes. The blue dots are the effective albedo with the reflection measured with the North facing pyranometer. The red dots are the calculations with the South facing pyranometer, the green dots are with the East facing pyranometer and the purple dots are with the West facing pyranometer.

Because of the earlier mentioned limitations of the measurement criteria, there are no adequate measurements from November, December and January. The limits in terms of the solar altitude, which states that the solar altitude must be above 10° for measurements, are not met from the 27th of October until 14th of February.

The figures show that the effective albedo is largest in the winter months when the ground is covered with snow, compared with the summer months when the ground is not covered with snow. In the winter months values higher than 1 for the effective albedo appear. This is due to the fact that the equation presented by Duffie and Beckman assumes that the reflected radiation from the ground is distributed isotropically, when it is in fact directionally dependent. The strong directional dependency is especially seen when the ground is covered with snow. Here the effective albedo based on the measurements from the South facing pyranometer, the red dots, are noticeably higher than the effective albedo based on the measurements from the pyranometer facing North, the blue dots, see Figure 3.8.

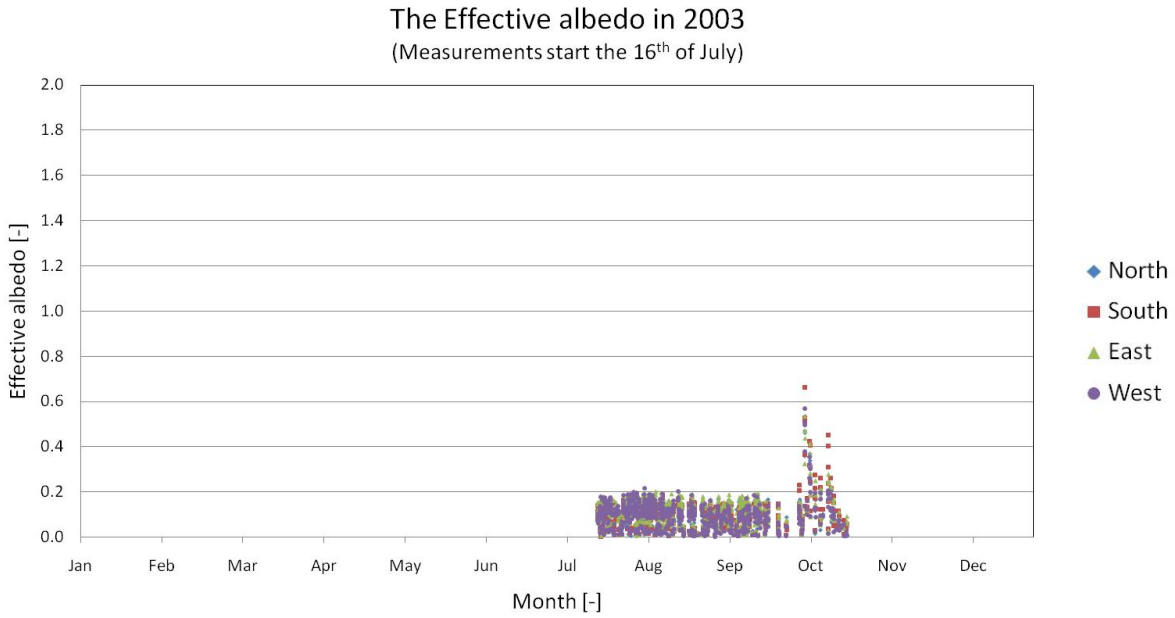

Figure 3.7 The effective albedo in 2003, (measurements starts the 16th of July).

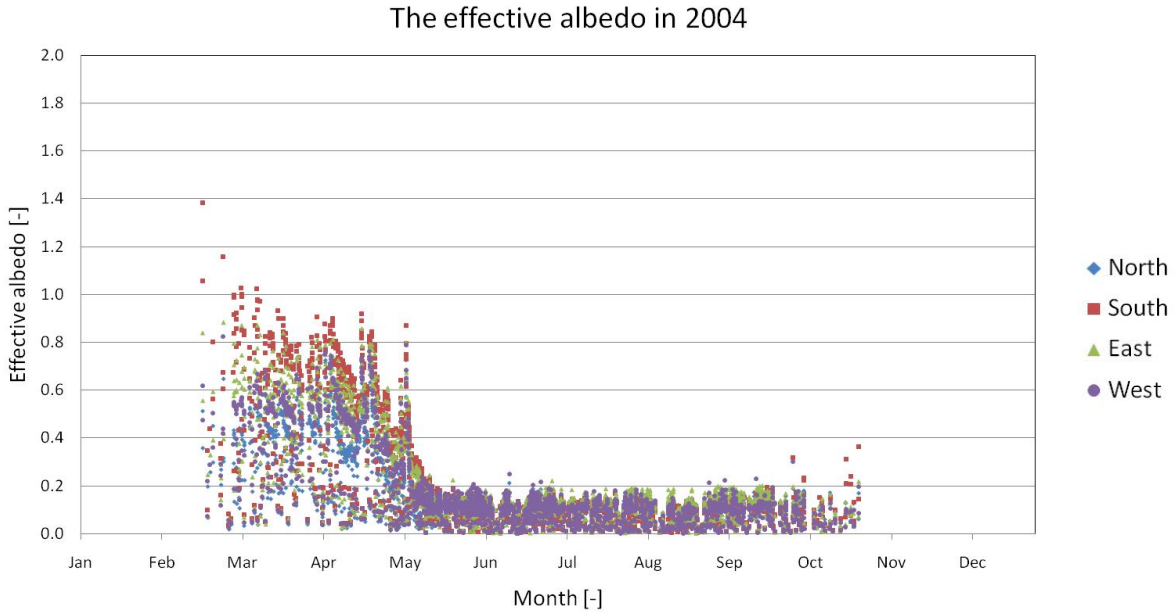

Figure 3.8 The effective albedo in 2004.

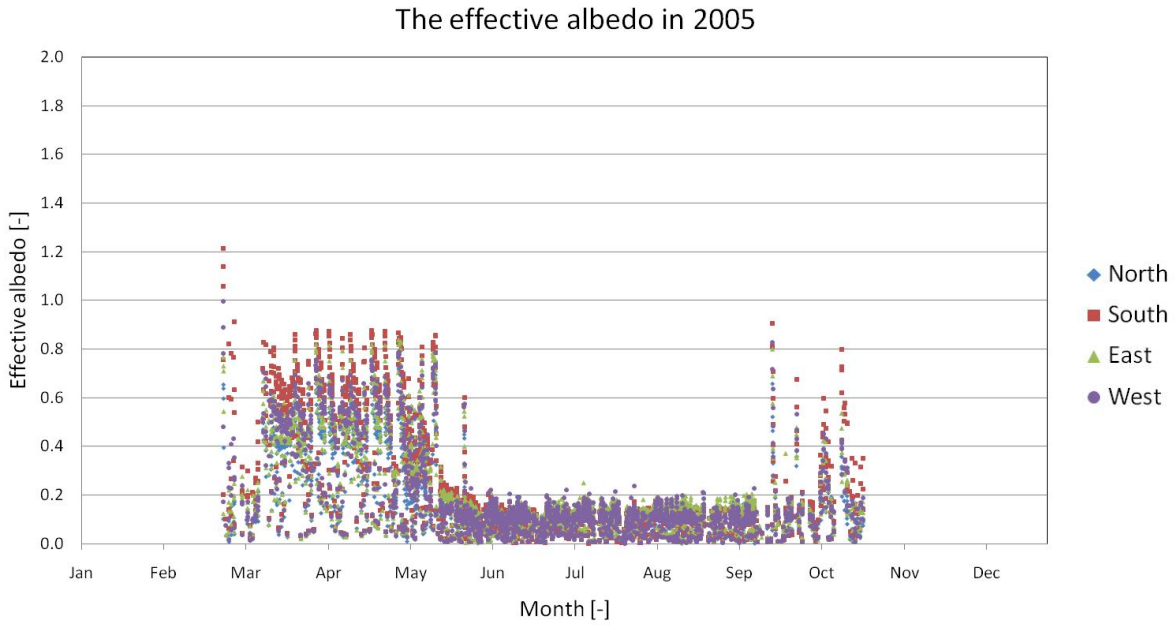

Figure 3.9 The effective albedo in 2005.

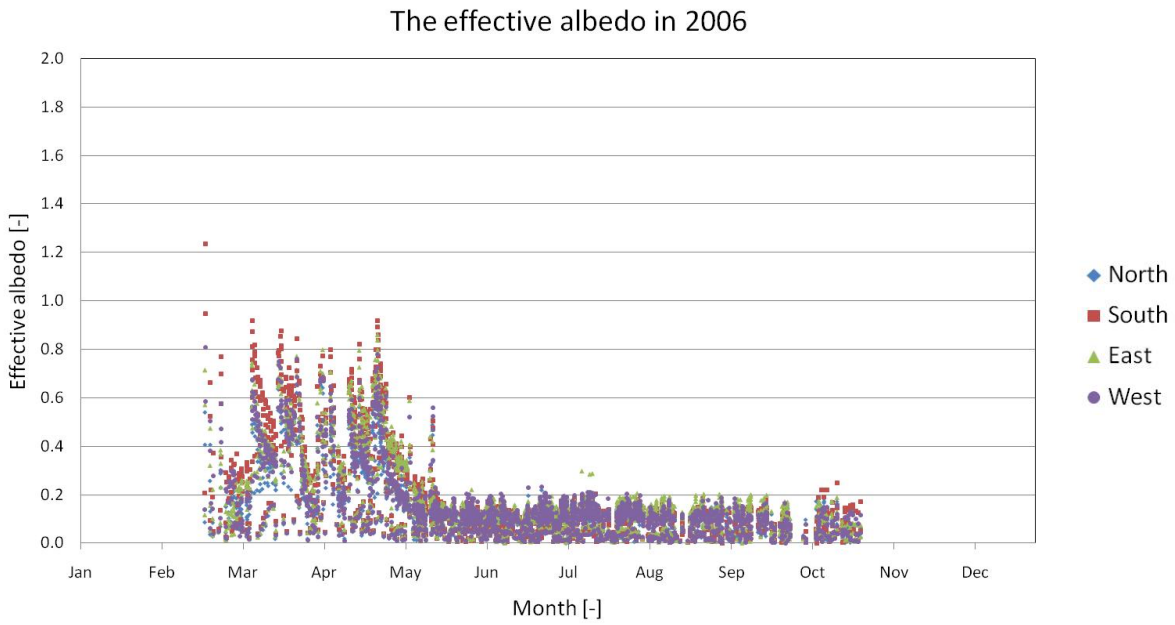

Figure 3.10 The effective albedo in 2006.

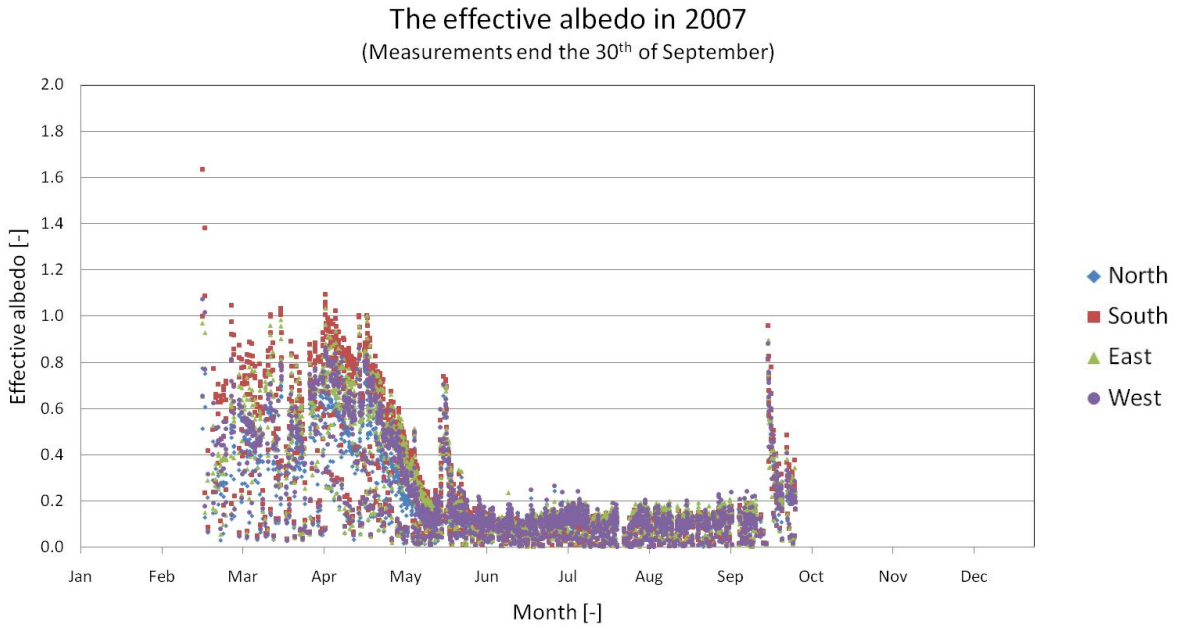

Figure 3.11 The effective albedo in 2007, (measurements end the 30th of September).

3.2.2 Daily variation of the effective albedo

In the following the daily variation of the effective albedo is investigated on four different occasions;

when the ground is covered with snow and the sky is clear

when the ground is covered with snow, and the sky is overcast

when the ground is not covered with snow and the sky is clear

when the ground is not covered with snow, and the sky is overcast

In Figure 3.12 the measured values from all 9 pyranometers are shown for the 18th of March 2004, which was a clear sky day where the ground was covered with snow. On this day the global radiation reaches values just above 400 W/m². The total radiation measured on the South facing vertical surface reaches values over 1000 W/m². The asymmetric curve for the total radiation on vertical surfaces in the East and West facing direction is due to the mountains seen in Figure 3.2.

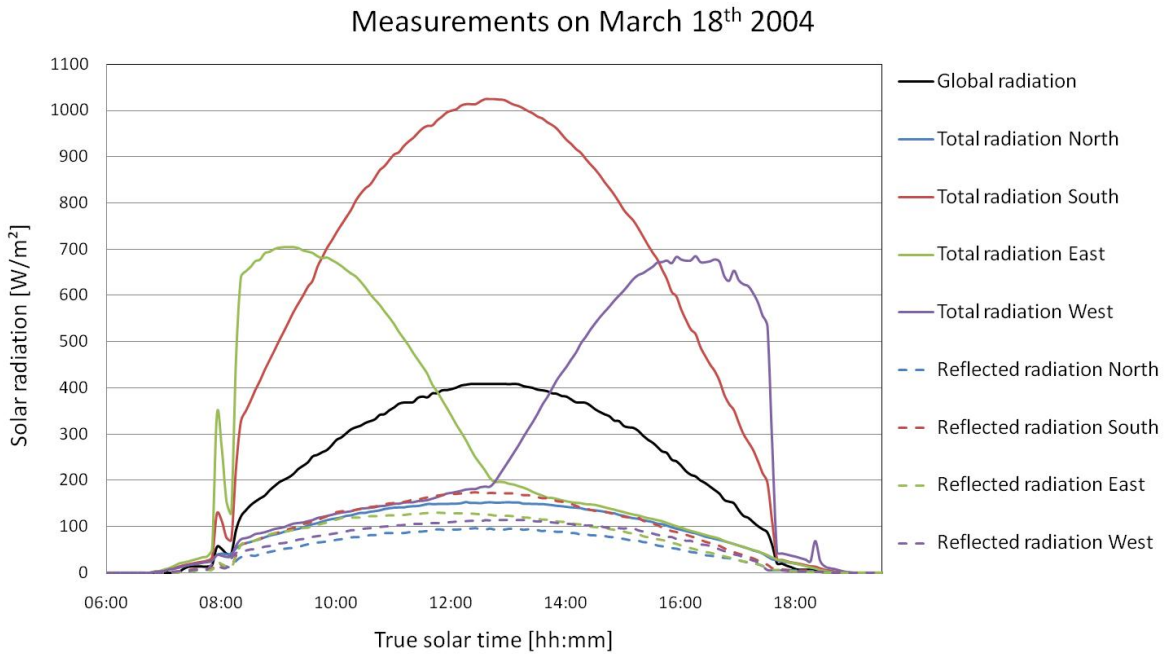

Figure 3.12 Measured radiation on the 18th of March 2004.

The effective albedo on the 18th of March 2004 is shown in Figure 3.13. The highest values of the effective albedo are mostly seen in the South facing direction, except for a short time in the morning. The lowest values for the effective albedo are in the North facing direction. For the East and West facing directions, the values from the East are highest in the morning of the two whilst the values from West are highest in the afternoon of the two.

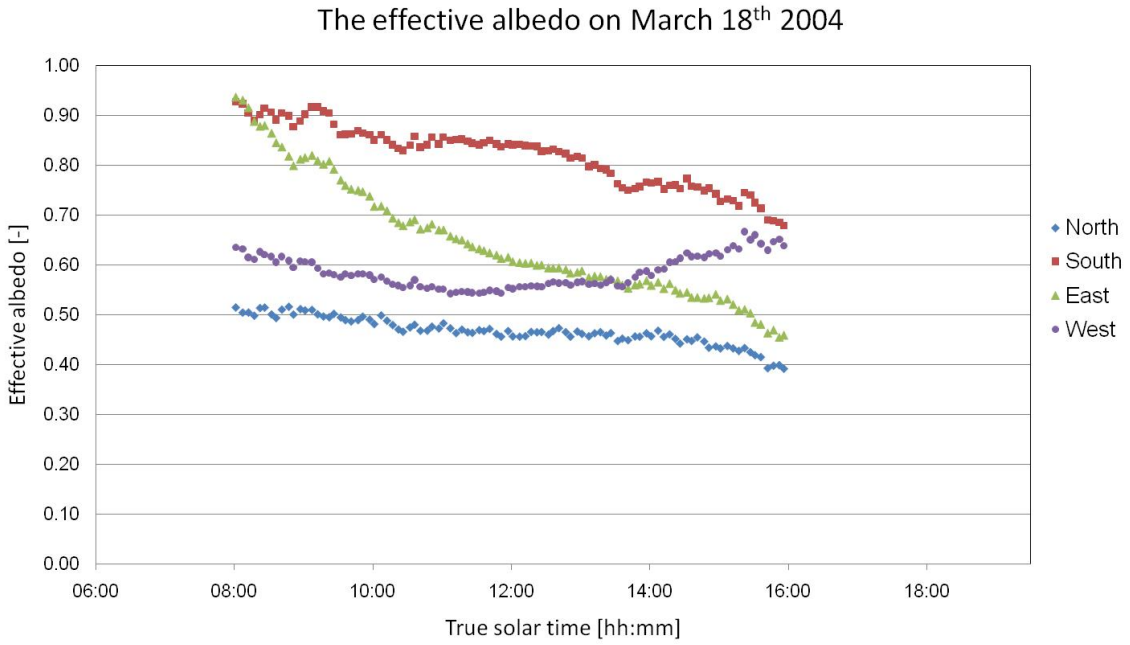

Figure 3.13 The effective albedo on the 18th of March 2004.

In Figure 3.14 the effective albedo on the 18th of March 2004 is shown as a function of the difference between solar azimuth and the surface azimuth. When the ground is covered with snow and there is beam radiation, the reflection of radiation is very specular, with most of the radiation being reflected forward as seen in the figure.

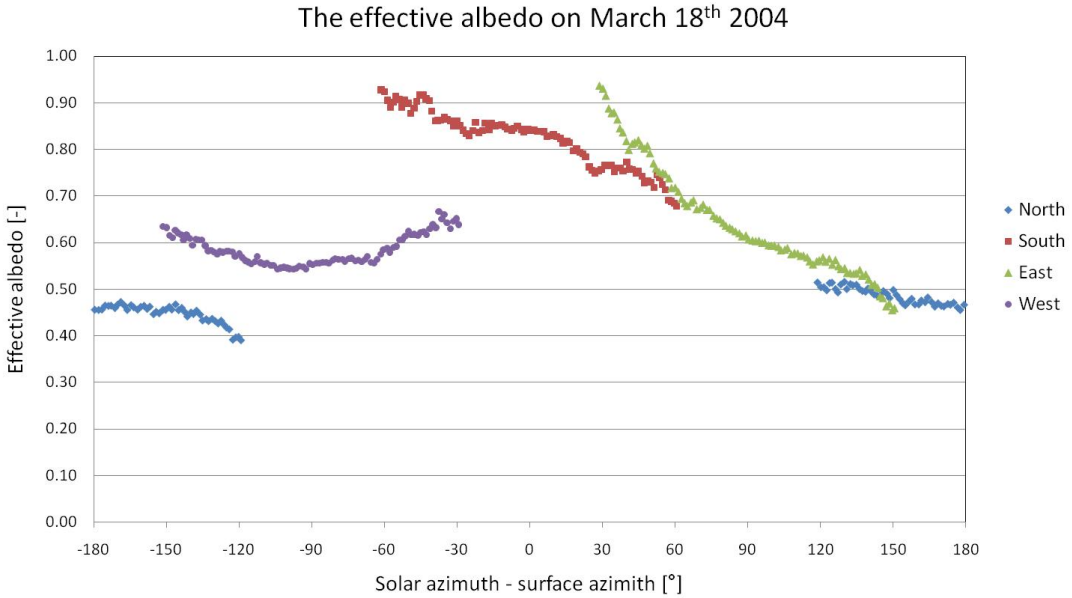

Figure 3.14 The effective albedo on the 18th of March 2004 as a function of the difference between solar azimuth and surface azimuth.

The measurements on the 17th of March 2006 are shown in Figure 3.15. On this day the ground was covered with snow and the sky was overcast. The maximum values for the global radiation stays beneath 250 W/m², and there is not much variation in the total values measured in the 4 different directions. The same is true for the reflected radiation.

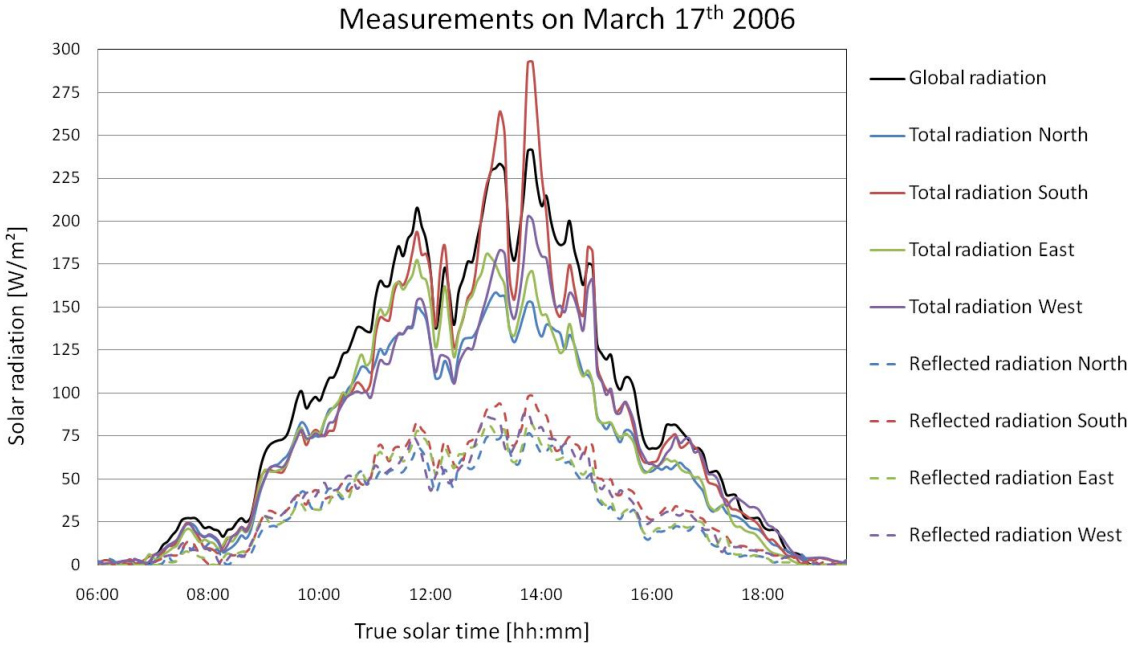

Figure 3.15 Measured radiation on the 17th of March 2006.

Figure 3.16 shows the calculation of the effective albedo on March 17th 2006. There are fewer values than on a clear sky day. This is due to the limitation of the global radiation, which states that it must be higher than 150 W/m². The figure shows that there is less variation in the effective albedo in the different directions compared to a clear day.

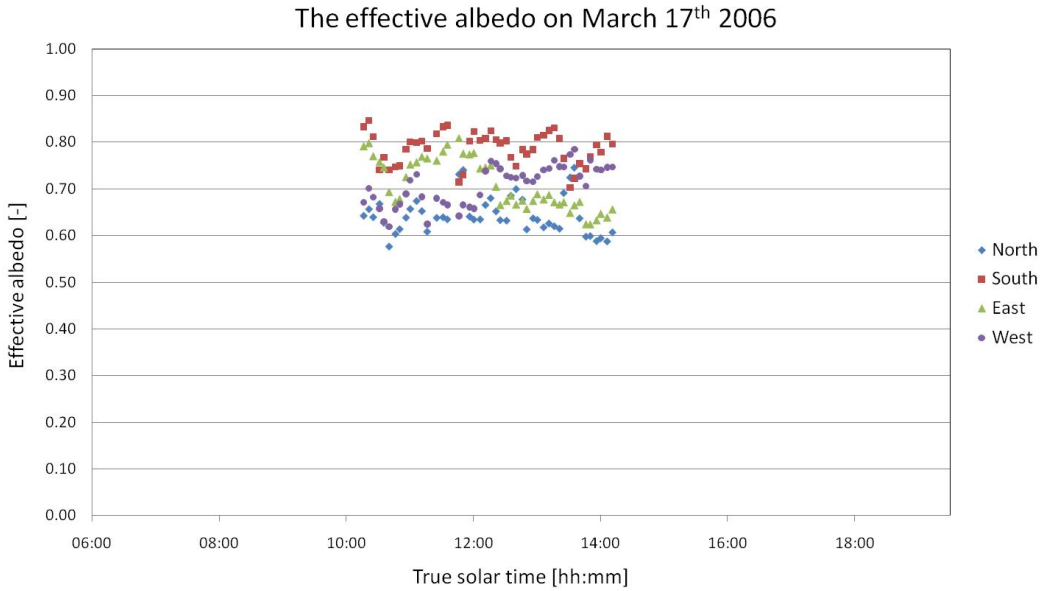

Figure 3.16 The effective albedo on the 17th of March 2006.

The effective albedo as a function of the difference between the solar azimuth and the surface azimuth on the 17th of March 2006 is shown in Figure 3.17. It can be seen that considerably less radiation is reflected than on clear sky days. The reflection is more diffuse when it is cloudy, which is also reported by Choudhury and Chang [Choudhurry and Chang 1981].

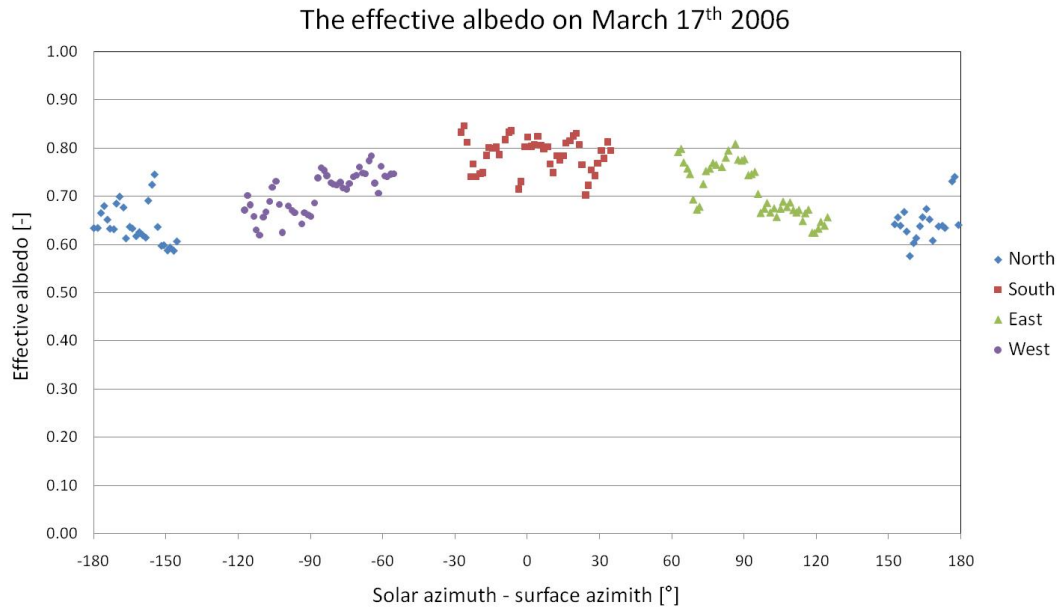

Figure 3.17 Effective albedo on the 17th of March 2006 as a function of the difference between solar azimuth and surface azimuth.

Following are the results on the 3rd of July 2006 which was a clear sky day where the ground was not covered with snow. The measurements of the solar radiation are shown in Figure 3.18. Here it can be seen that the global radiation reaches values of about 750 W/m², and the total radiation measured on the South facing pyranometer is less than the radiation measured in the East and West directions.

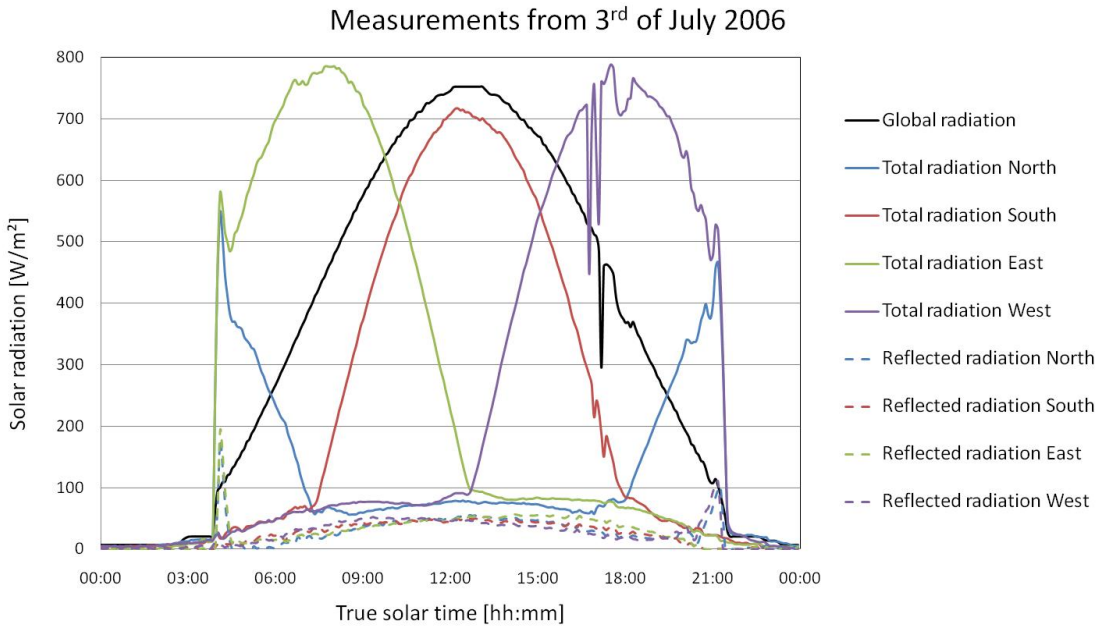

Figure 3.18 Measured radiation on the 3rd of July 2006.

This is a result of the increase in the solar altitude from winter to summer. In the summer months the pyranometers - which are placed vertically - facing East and West are more favourably placed, in terms of angle between the sun and the surface, than the South facing pyranometer. The effects of the mountains are seen by the abrupt start in radiation in the East facing direction in the morning, and also in the West facing direction by the abrupt stop in the afternoon.

In Figure 3.19 the calculation of the effective albedo is shown for the 3rd of July 2006. It can here be seen that there is little variation in the albedo in the different directions. The gap seen in the measurements in the late afternoon is due to the elimination caused by shadows cast by a nearby pole (see Figure 3.2).

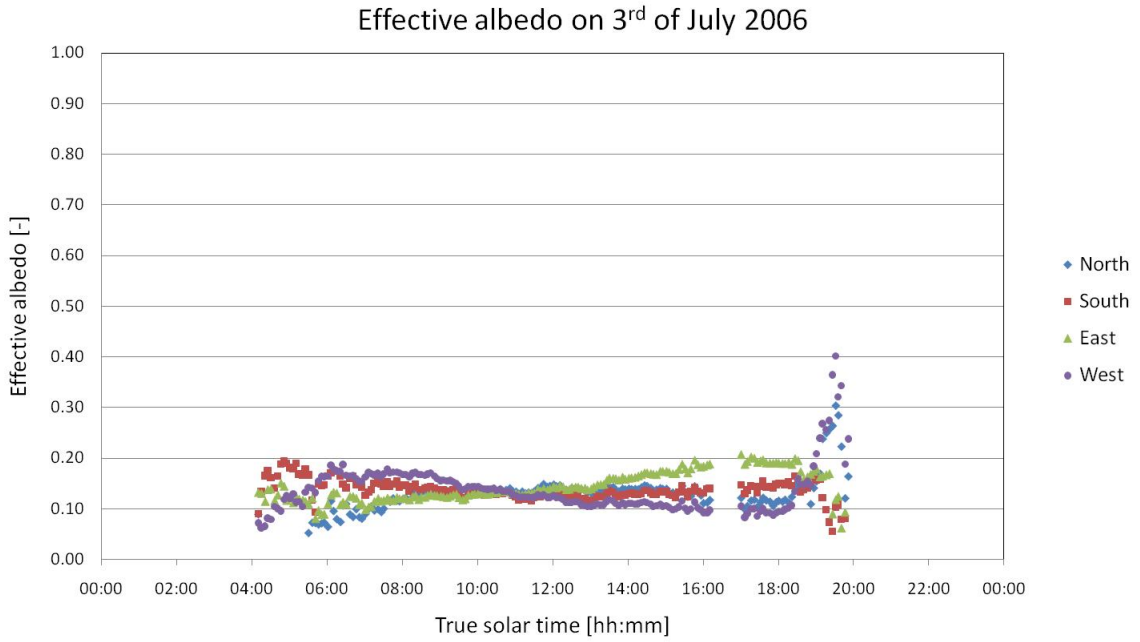

Figure 3.19 Effective albedo on the 3rd of July 2006.

Figure 3.20 shows the effective albedo as a function of the difference between the solar azimuth and the surface azimuth. The curve has a local minimum where the difference between the solar azimuth and the surface azimuth is 0°. This means that slightly more radiation is reflected backwards than forward, opposite of what is seen for snow covered ground. Also it is no longer possible to detect the strong specular dependency.

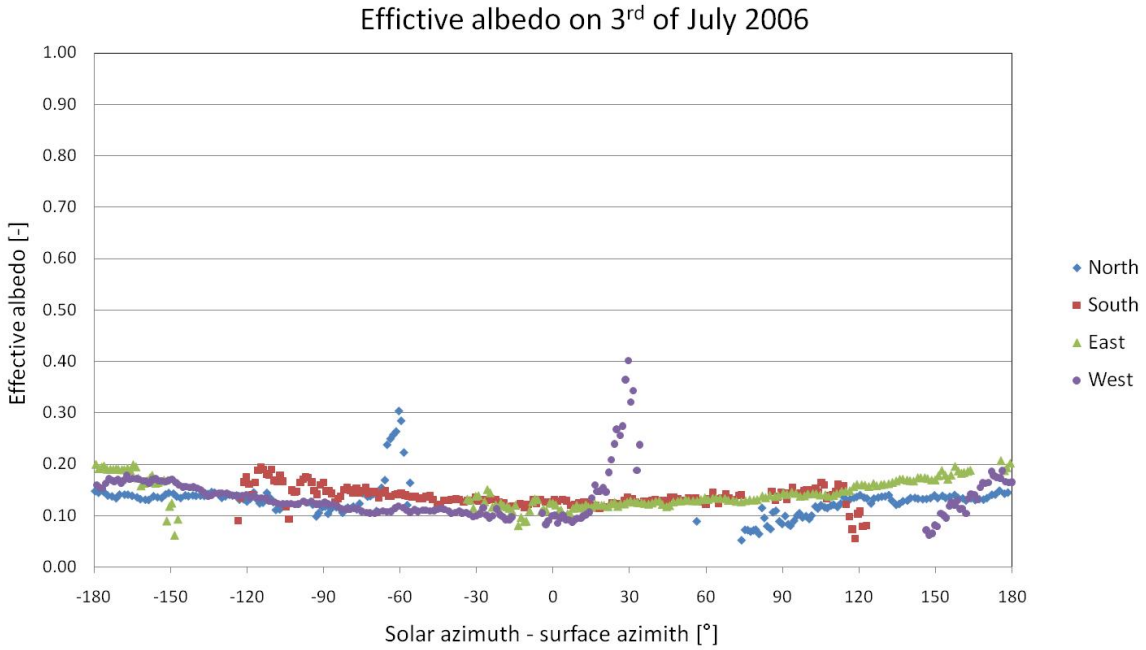

Figure 3.20 Effective albedo on the 3rd of July 2006 as a function of the difference between the solar azimuth and the surface azimuth.

The two peaks seen for the North and West albedo is caused by an increase in reflected radiation, which happens when the sun is setting and therefore comes close to the horizon. As mentioned earlier, the sun is setting behind the mountains to the North during the summer. As it comes closer to the horizon the increase in reflected radiation is due to the reflection from the water. This happens at solar azimuth between 100° and 125°, see Figure 3.21.

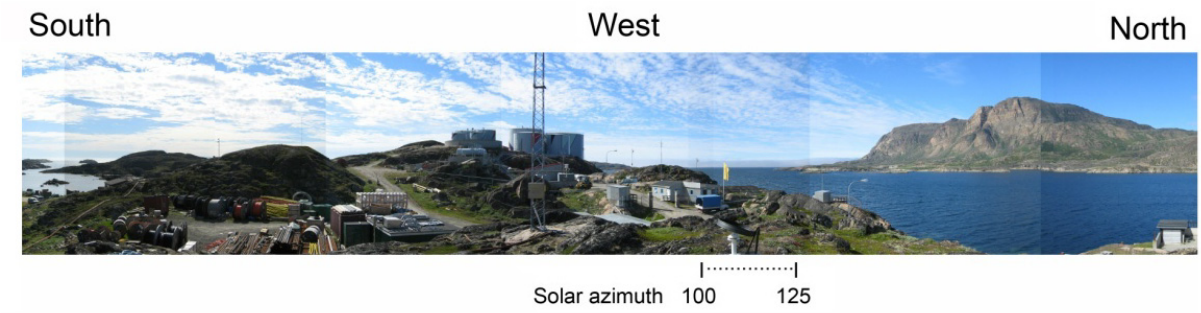

Figure 3.21 View from the Solarhat towards West.

The measurements on the 24th of July 2005 are shown in Figure 3.22. This day was an overcast day with no snow on the ground. The figure shows that there is little variation in the measured values in both the total and the reflected radiation in the different directions.

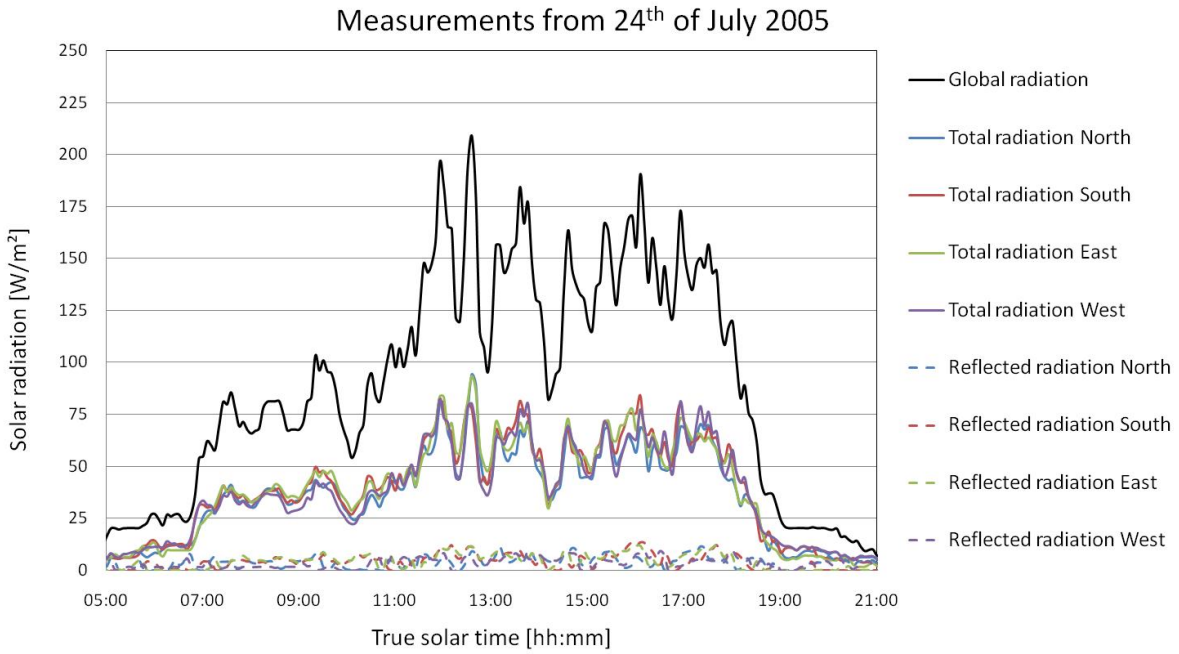

Figure 3.22 Measured radiation on the 24th of July 2005.

The calculated effective albedo on the 24th of July 2005 can be seen in Figure 3.23. Again only few values are seen due to the low global radiation, and no variation is detected.

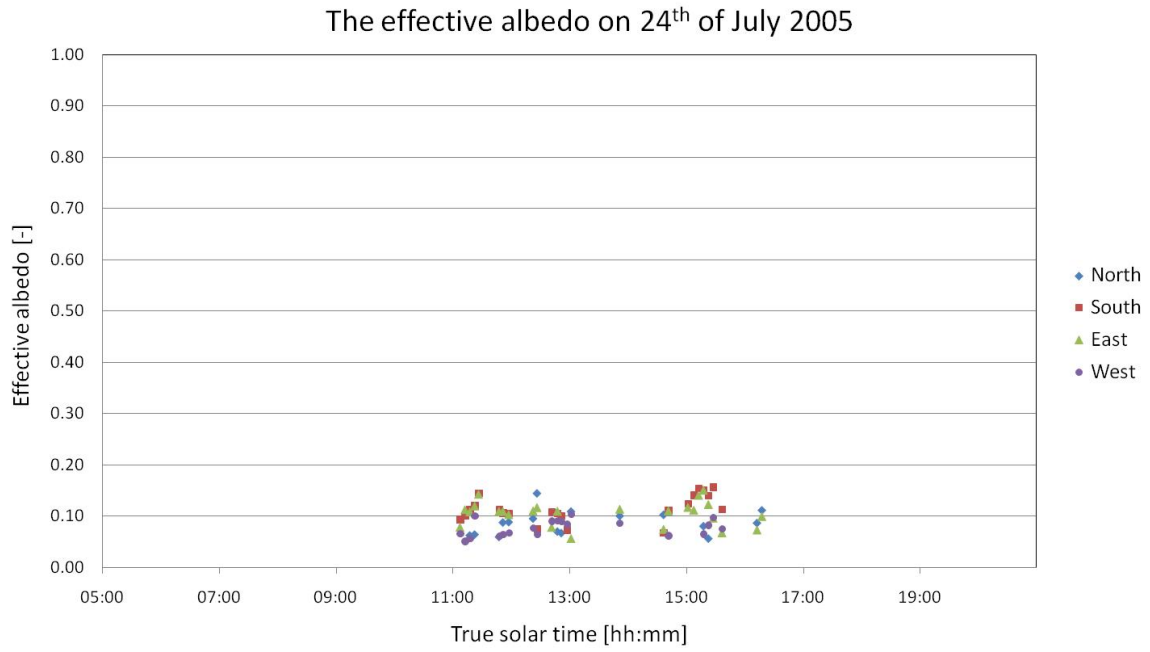

Figure 3.23 Effective albedo on the24th of July 2005.

The effective albedo is shown as a function of the difference between the solar azimuth and the surface azimuth on the 24th of July 2005 can be seen in Figure 3.24. Again the reflection becomes more diffuse on overcast days, as seen for the winter day when the ground was covered with snow (Figure 3.17).

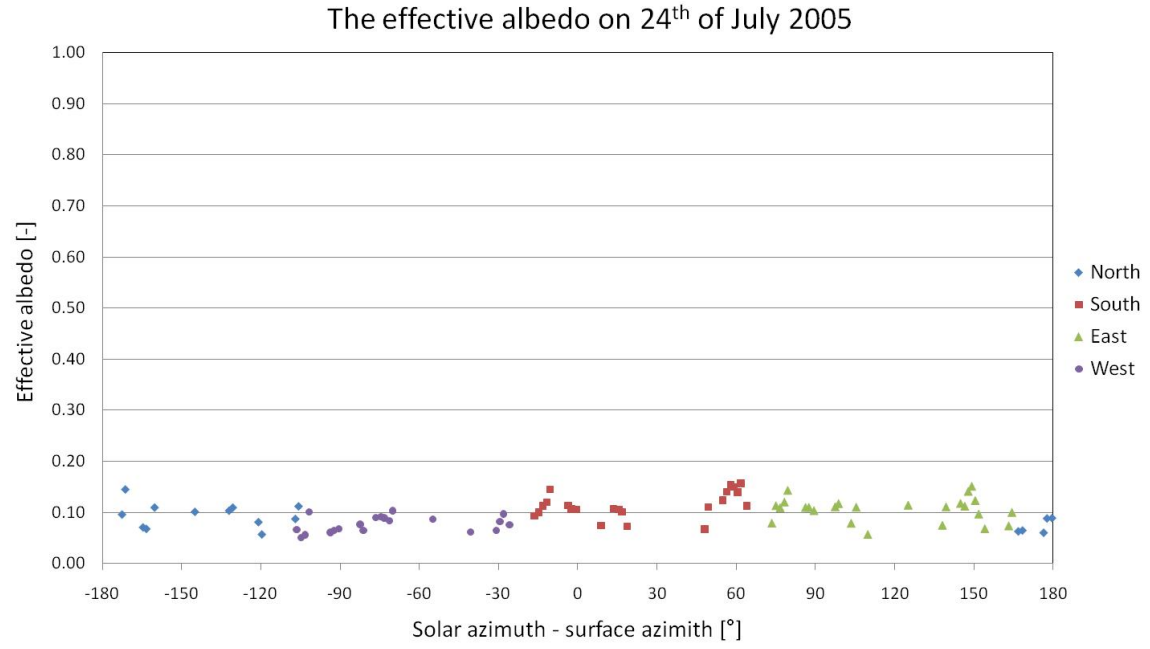

Figure 3.24 Effective albedo on the 24th of July 2005 as a function of the difference between the solar azimuth and the surface azimuth.

A principle sketch showing the two different situations of reflection from the ground is in Figure 3.25. On the left the winter situation is seen, where the snow is acting as a mirror, reflecting most of the radiation forward. On the right the summer situation is shown. When the ground is not covered with snow the vegetation and gravel will obstruct the radiation from the sun and reflect most radiation backwards.

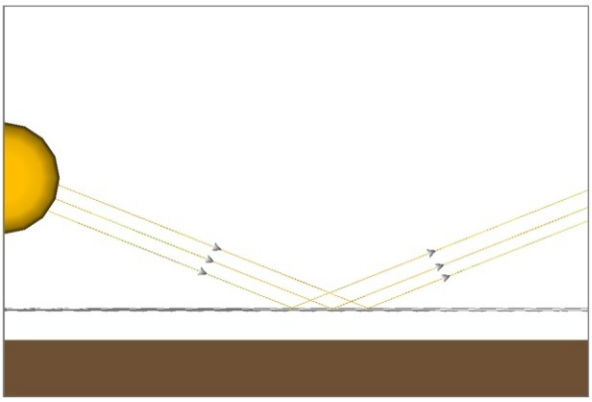

Figure 3.25 Left: Reflection from snow-covered ground

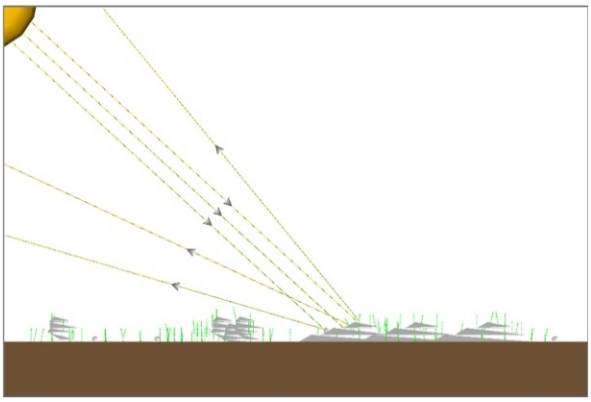

Right: Reflection when the ground is not covered with snow.

3.2.3 Monthly variation in the effective albedo

In the following, equations of the albedo on a monthly basis are presented as functions of the difference between the solar azimuth and the surface azimuth. Because of the limitations mentioned earlier there are no equations for the months of November, December and January. Since the solar radiation in the months of November, December and January is low, the reflected radiation will be equally low. It is therefore reasonably to state that an accurate calculation for these three months is not of vital importance. The effective albedo can either be a constant value of 0.7 in all directions, or it can be determined based on equations for October and February.

The values of the calculated effective albedo based on data from the 4 years of measurements are individually weighted against the global radiation in order to achieve a fair representation of the albedo, which can be used in calculations. The weighted effective albedo is given as:

$$\rho_g = \frac{\sum(\rho \cdot I)}{\sum I} \tag{3-4}$$

The equations are found by regression analysis, and can be seen in Table 3.2.

Table 3.2 The effective albedo as a function of x, which is the difference between the solar azimuth and the surface azimuth, (°).

Jan	
Feb	$\rho(x) = -1 \cdot 10^{-5} \cdot x^2 - 5 \cdot 10^{-5} \cdot x + 0.7031$
Mar	$\rho(x) = -7 \cdot 10^{-6} \cdot x^2 - 0.0001 \cdot x + 0.6031$
Apr	$\rho(x) = -5 \cdot 10^{-6} \cdot x^2 - 0.0002 \cdot x + 0.6083$
May	$\rho(x) = -1 \cdot 10^{-6} \cdot x^2 - 5 \cdot 10^{-5} \cdot x + 0.2392$
Jun	$\rho(x) = 6 \cdot 10^{-8} \cdot x^2 - 1 \cdot 10^{-5} \cdot x + 0.1294$
Jul	$\rho(x) = 1 \cdot 10^{-7} \cdot x^2 - 1 \cdot 10^{-5} \cdot x + 0.133$
Aug	$\rho(x) = 1 \cdot 10^{-7} \cdot x^2 + 1 \cdot 10^{-5} \cdot x + 0.1324$
Sep	$\rho(x) = -1 \cdot 10^{-7} \cdot x^2 - 1 \cdot 10^{-5} \cdot x + 0.1776$
Oct	$\rho(x) = -2 \cdot 10^{-6} \cdot x^2 - 3 \cdot 10^{-5} \cdot x + 0.2276$
Nov	
Dec	

In the following the equations are presented graphically. In Figure 3.26 the months from February until May can be seen, showing the spring months. The directional dependency is seen for the months where the ground is covered with snow: February, March and April, where the reflection is forward.

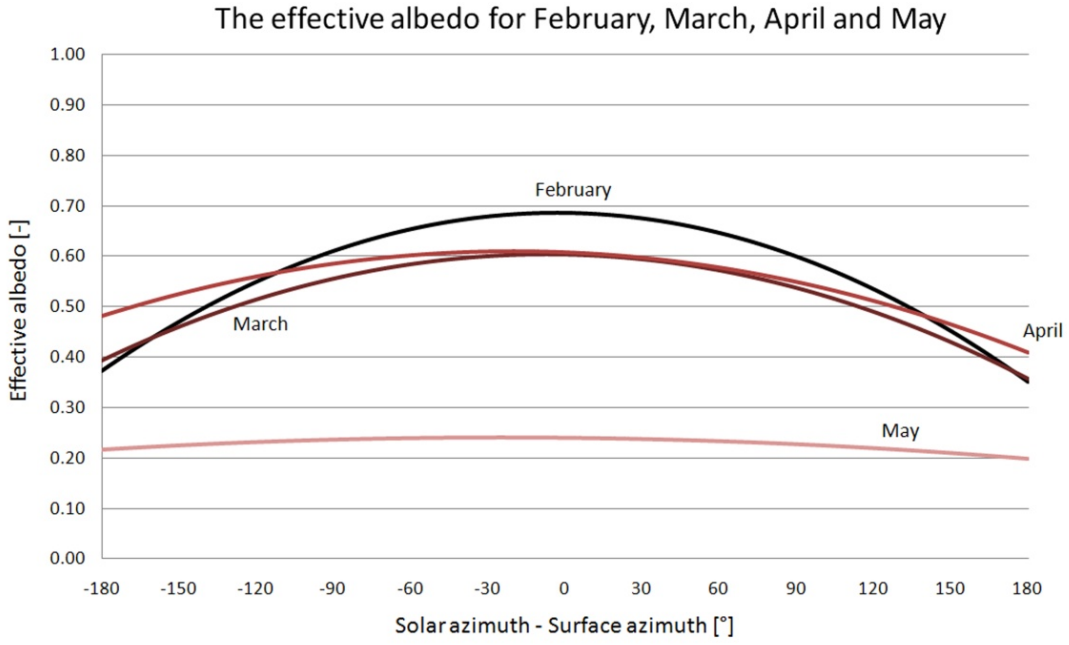

Figure 3.26 The effective albedo for the spring months; February, March, April and May.

Figure 3.26 also shows that the function of the effective albedo for April is higher than the function for March. This is due to the increase in temperature and the increase in solar altitude, which causes the snow to start melting. The top layer of snow then thaws and refreezes leaving an ice-like surface with a higher effective albedo.

In Figure 3.27 the functions of the effective albedo for the summer and fall months are shown. It can be seen that there is very little variation in the albedo over the summer, where the effective albedo stays between 0.1 and 0.2 and most radiation is reflected backwards. As the weather changes in the beginning of the fall the albedo increases and changes from favoring backwards reflection to favoring forwards reflection seen in October.

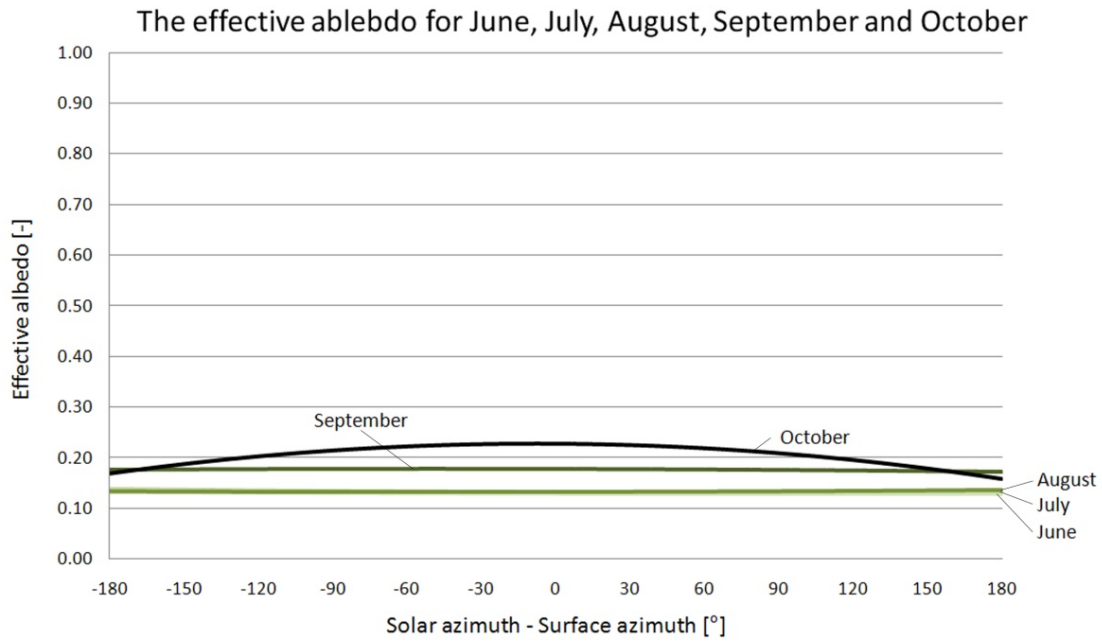

Figure 3.27 The effective albedo in the summer and fall months; June, July, August, September and October.

The accuracy of the equations is evaluated by comparing the calculated reflected radiation in the four directions with the average values from the Solarhat from 2004 to 2006. For the months of November, December and January, the equation for February is used to calculate the reflected radiation.

The method of using constant values for the albedo is also compared with the measurements from the Solarhat. Here 0.7 is used for snow covered ground and 0.2 is used when the ground is not covered with snow. The ground is assumed to be covered with snow is from the middle of September to the end of April, which is in good agreement with the results seen in Figure 3.7 thru to Figure 3.11.

The calculated and measured values can be seen in Table 3.3, and the deviation in Table 3.4. Here it can be seen that both methods of calculating the reflected radiation are attached with levels of error compared to the measured values. The method using equations has a good agreement in the South and East directions, where the deviation is around 3 %, but in the North and West directions the deviation is

around 13 %. The equations overestimate the reflected radiation in the North and West direction, but underestimate the reflected radiation in the South and East direction. The results using two constant values for the summer and winter albedo, gives a uniform reflected radiation in all four directions. The level of error compared to the measurements is highest in the North facing direction with 65 % higher reflected radiation than measured. In the South facing direction the deviation was 28 %.

Table 3.3 The measured and calculated reflected radiation on vertical surfaces facing North, South, East and West using the equations and using a uniform albedo of 0.2 without snow and 0.7 with snow.

Average of 2004, 2005 and 2006	North	South	East	West
	[kWh/m²]	[kWh/m²]	[kWh/m²]	[kWh/m²]
Measured reflected radiation	78	100	94	85
Equations	87	98	92	95
Albedo = 0.7 / 0.2	129	129	129	129

Table 3.4 The deviation of the calculated values from the measured values of the reflected radiation on vertical surfaces facing North, South, East and West.

Deviation from the measured reflected radiation	North	South	East	West
	[%]	[%]	[%]	[%]
Equations	12	-3	-2	13
Albedo = 0.7 / 0.2	65	28	38	52

3.3 Discussion

The investigation showed that snow reflects solar radiation like a mirror. The effective albedo is therefore a function of the difference between the solar azimuth and the surface azimuth. Equations for the effective albedo were determined for each month of the year based on measurements. The equations are suited as input for simulation models.

In order to improve the accuracy of the reflected radiation on tilted surfaces, it is recommended to carry out detailed measurements, so that the reflection from direct radiation from the sun and the reflection from the diffuse radiation can be separated. In this way, equations for the reflection of both direct and diffuse radiation as functions of difference between the solar azimuth and the surface azimuth can be derived. Also it is recommended to carry out albedo measurements for other locations than Sisimiut.

Chapter 4 Thermal performance of a solar heating system in Greenland

This chapter will present an analysis of the yearly thermal performance of a solar heating system at four different locations; Uummannaq, Sisimiut, Nuuk and Copenhagen, in order to evaluate the potential of a solar domestic hot water system in Greenland. The analysis is based on simulations with the simulation tool MantlSim, which calculates the thermal performance of a solar domestic hot water system, where the storage tank is a mantle tank.

4.1 Simulation program MantlSim

MantlSim is a simulation tool developed to calculate the thermal performance of a solar domestic hot water system, and was developed by Furbo and Berg in 1990 [Furbo and Berg 1990]. The program has been modified and improved throughout the years, first in 1996 by Shah and Furbo [Shah and Furbo 1996], then in 1999 and 2000 by Shah alone [Shah 1999, Shah 2000] and the latest and most extensive modification was carried out in a PhD study by Knudsen in 2004 [Knudsen 2004].

Furbo and Shah introduced in 1996 changes to the heat transfer coefficients in the mantle based on an experimental investigation with 3 different designs of mantle tanks. The changes Shah introduced in 1999 and 2000 are also focused on improvements of the heat transfer correlations in the program. The latest changes by Knudsen further improves the calculations of the heat transfer between mantle fluid and inner and outer mantle wall, and between the tank wall and the domestic hot water. Also the calculations of the thermal stratification both above and where the mantle is placed were improved. The most significant changes by Knudsen, were: to introduce the possibility of changing the placement of the inlet to the mantle and to take mixing of the solar collector fluid in the mantle into account.

Changes to MantlSim according to Greenlandic conditions

The program was developed to calculate the thermal performance of a system placed in Copenhagen. It was therefore necessary to modify the source-code and create new program-files for the locations of Uummannaq, Sisimiut and Nuuk. The changes to the program consisted of changing the location in terms of longitude and latitude, the temperature of the cold water inlet and introducing periods with snow and give an albedo for to the snow, to take the Arctic conditions into account.

The latitude and longitude of the four locations used in the program can be seen in Table 4.1

Table 4.1 Latitude and longitude for the locations simulated in MantlSim.

	Latitude [°]	Longitude [°]
Uummannaq	52.12 W	70.67 N
Sisimiut	53.67 W	66.92 N
Nuuk	51.75 W	64.17 N
Copenhagen	12.57 E	55.68 N

The cold water temperature is given as a constant temperature throughout the year and is lowered in the program files from 10 °C to 2 °C for the locations in Greenland.

The albedo for the ground is given in the program file for Copenhagen as 0.2 throughout the year. In the program files for the new locations in Greenland snow covered ground is introduced.

The albedo for snow-covered ground is defined as 0.7 and for ground not covered with snow as 0.2. The periods when the ground is assumed to be covered with snow for the three locations in Greenland can be seen in Table 4.2.

Table 4.2 The periods for each location when the ground is assumed covered with snow.

Uummannaq	*From*	1/9	*To*	1/5
Sisimiut	*From*	15/9	*To*	15/4
Nuuk	*From*	1/10	*To*	1/4

Weather data

The weather data used as input for the program is the reference year for each of the four locations presented in chapter 2. MantlSim uses the isotropic model to calculate solar radiation on tilted surfaces.

Reference system

The solar heating system analysed is a typical domestic hot water system for a single family house.

The solar collector chosen for this analysis is a solar collector called BA22 from Batec A/S, with a transparent area of 2.19 m². The collector has inlet in the bottom, connected to a manifold with vertical strips leading to a manifold at the top which is connected to the outlet. This design insures a good emptying behaviour during stagnation, which is especially important for conditions in Greenland. The efficiency expression for the collector is:

$$\eta = 0{,}767 \cdot k_\theta - 3{,}867\frac{(T_m - T_a)}{G} - 0{,}010\frac{(T_m - T_a)^2}{G} \qquad (4\text{-}1)$$

where η is the collector efficiency

T_m is the mean solar collector fluid temperature in the solar collector [°C]

T_a is the ambient air temperature [°C]

G is the solar irradiance on the collector [W/m²]

k_θ is the incidence angle modifier [-]

$$k_\theta = 1 - tan^{3.43}\left(\frac{\theta}{2}\right) \qquad (4\text{-}2)$$

where θ is the incidence angle for beam radiation on the collector [°]

The storage tank is a mantle tank from Solvarmebeholderen.dk, and has a volume of 165 l. The auxiliary volume is 53 l and the volume heated by the mantle is 159 l. The diameter of the tank is 0.400 m and the height is 1.313 m. The outer diameter of the mantle is 0.449 m and the volume of the mantle is 22 l. The in- and outlets to the tank are all through the bottom of the tank reducing the heat loss from the tank. The mantle tank was chosen because of its advantages compared with spiral tanks systems [Furbo 2004].

The flow rate in the solar collector loop is based on the recommendation from an investigation carried out at the Technical University of Denmark in the period from 1987 to 1990, where three systems were tested side-by-side in order to investigate significance of the flow rate [Furbo 2004]. The investigation recommended the flow rate to be between 0.1-0.2 l/min per m² solar collector. For this investigation the flow rate in the solar collector loop is 0.2 l/min per m² solar collector, which results in a flow rate of 0.438 l/min.

The draw off from the system is assumed to be 150 l a day, with 50 l in the morning, 25 l at noon and 75 l in the evening over the course of two hours.

4.2 Parametric analysis

The thermal performance of the system will be calculated as the yearly thermal performance and will be evaluated based on the system performance, the system solar fraction and the relative performance.

The system performance describes the proportion of the hot water consumption that is provided by energy from the sun:

System performance = Tapped energy – Auxiliary energy – Pump energy – Control system energy *(4-3)*

where the tapped energy describes the hot water consumption and the auxiliary energy describes the need for additional energy besides the solar heat to maintain enough hot water in periods where there is insufficient solar radiation. For the location of Copenhagen it is assumed that the auxiliary energy is supplied by an electric heating element in the summer months from April to September, and by an oil burner in the winter months. For the Greenlandic locations it as assumed that the auxiliary energy is supplied by an oil burner all year.

The pump energy describes the energy used by the circulation pump and is given as an output from the programme. The energy for the control system is not given as an output, but is calculated separately by using the information of the hours the pump is in operation. Using the assumption that the control system uses 2 W when the pump is in operation and 1 W when it is not in operation, it is possible to calculate the energy for the control system.

The system solar fraction offers the same information but seen as the percentage of the total hot water consumption that is covered by energy from the sun:

System solar fraction = System performance / Tapped energy ·100 *(4-4)*

The relative performance gives the effects of the parametric analysis compared with the chosen reference. The relative performance is defined as:

$$\text{Relative performance} = \frac{\text{Net. utilized solar energy of the system in question}}{\text{Net. utilized solar energy of the reference system}} \cdot 100 \qquad (4\text{-}5)$$

where the Net. utilized solar energy gives the energy supplied by the solar heating system to the domestic hot water consumption. The Net. utilized solar energy is given as:

Net. utilized solar energy = Tapped energy – Auxiliary energy *(4-6)*

4.2.1 Solar collector

The analysis of the collector can be divided into two parts: the physical placement of the solar collector and parameters describing the solar collector efficiency.

The physical placement of the solar collector is determined by the tilt and the orientation of the solar collector. The initial investigation of the tilt is carried out with the solar collector facing due South.

Tilt

The parametric analysis carried out for the tilt of the solar collector can be seen in Figure 4.1. The optimum tilts for the four locations are: 60° for Uummannaq, 57° for Sisimiut, 55° for Nuuk and 46° for Copenhagen. The results shows as expected an increasing optimum tilt with an increase in the latitude. A change to the tilt of the solar collector of ±10° will result in a decrease in thermal performance of less than 2 % for all four locations.

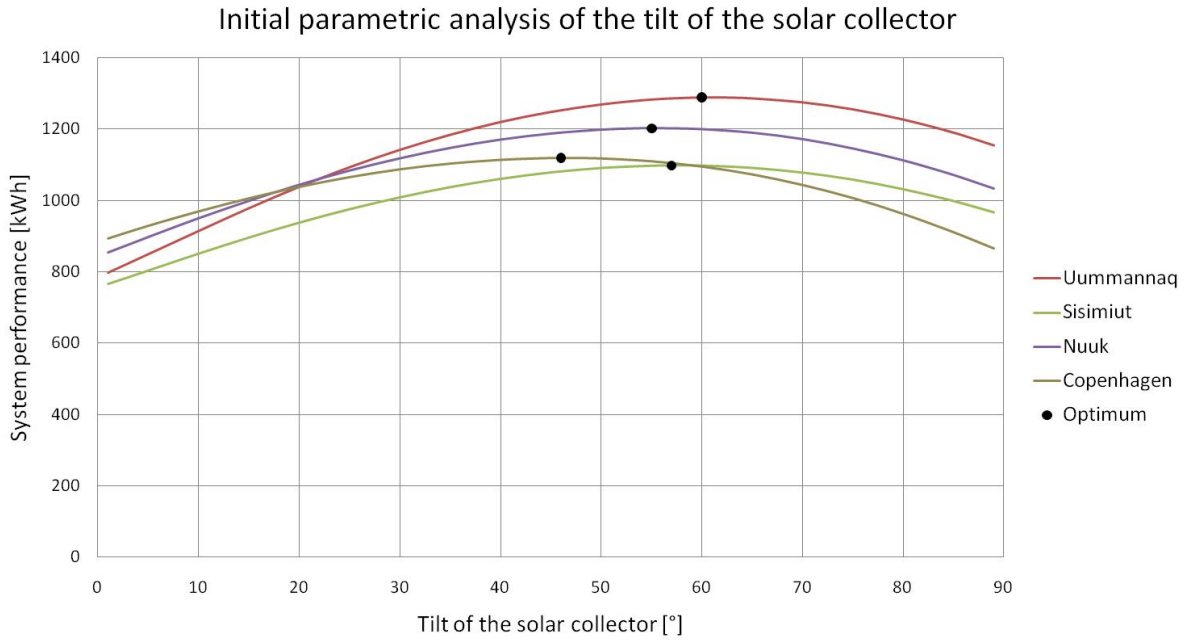

Figure 4.1 The yearly system performance as a function of the solar collector tilt with an orientation directly towards south.

In Figure 4.2 the relative performance is shown as a function of the initial investigation of the tilt. Here the influence of the latitude can be seen more clearly. The figure shows that a system located at high latitude will have a larger decrease in the yearly performance if the solar collector is placed with a low tilt, compared to at system placed at lower latitudes and with the same tilt. A system with a vertically placed solar collector will have a larger relative yearly performance at high latitudes than at lower latitudes, which also was seen in section 2.1.3.

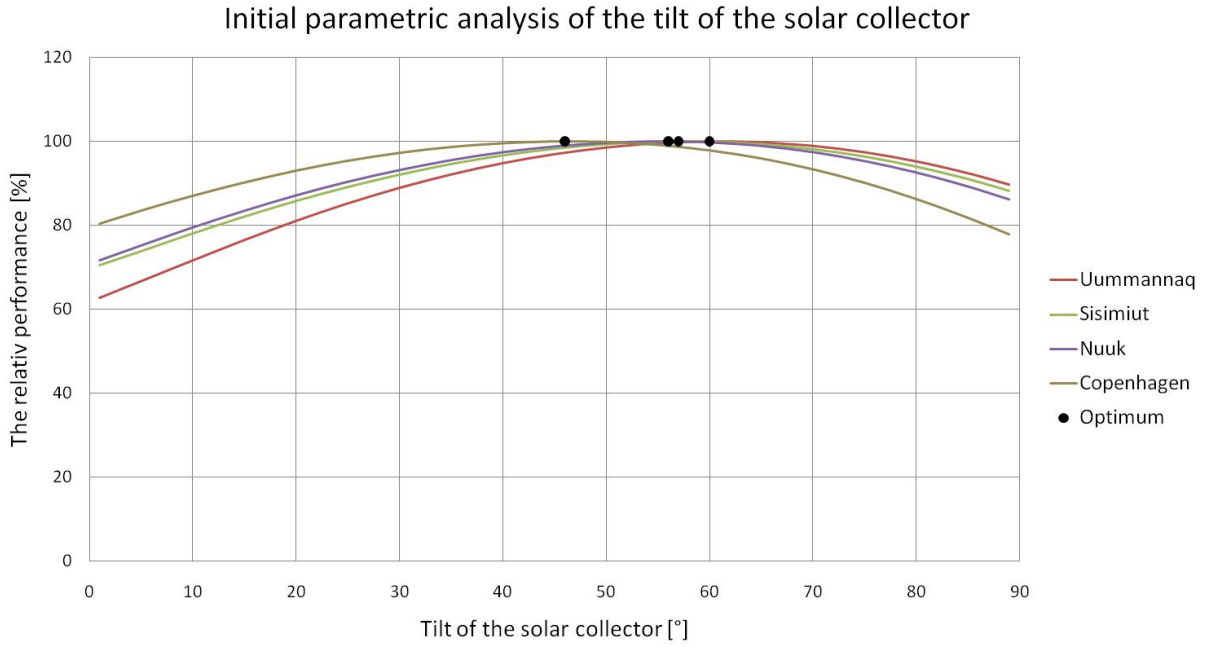

Figure 4.2 The relative performance as a function of the solar collector tilt with an orientation directly towards south.

Orientation

Using the optimum tilt for each location, the optimum orientation of the solar collector is found. Since the weather data used in the program is the reference years for each of the locations and these are based on measurements, the influence of shadows from mountains and of the reflection from the sea will be taken into account for the locations in Greenland.

The results from the parametric analysis can be seen in Figure 4.3 showing the system performance as a function of the orientation of the solar collector (-90° is directly east and +90° is directly west). The optimum orientation is 5° towards west for Uummannaq, 13° towards west for Sisimiut, 10° towards west for Nuuk and 5° towards east for Copenhagen. The optimum orientation for a collector placed in either of the Greenlandic locations is turned towards west, due to the location of the mountains to the east and the sea to west. The results of the optimum orientation are also influenced by the hot water consumption and the tapping profile. The reason for only a slight turning of the collector in Uummannaq is because Uummannaq is placed off the mainland and thereby the shadows from the mountains are reduced. The figure also shows that the performance is more influenced by the orientation in Greenland compared to

Copenhagen, since the decrease in performance happens more rapidly in Greenland when turning away from the optimum.

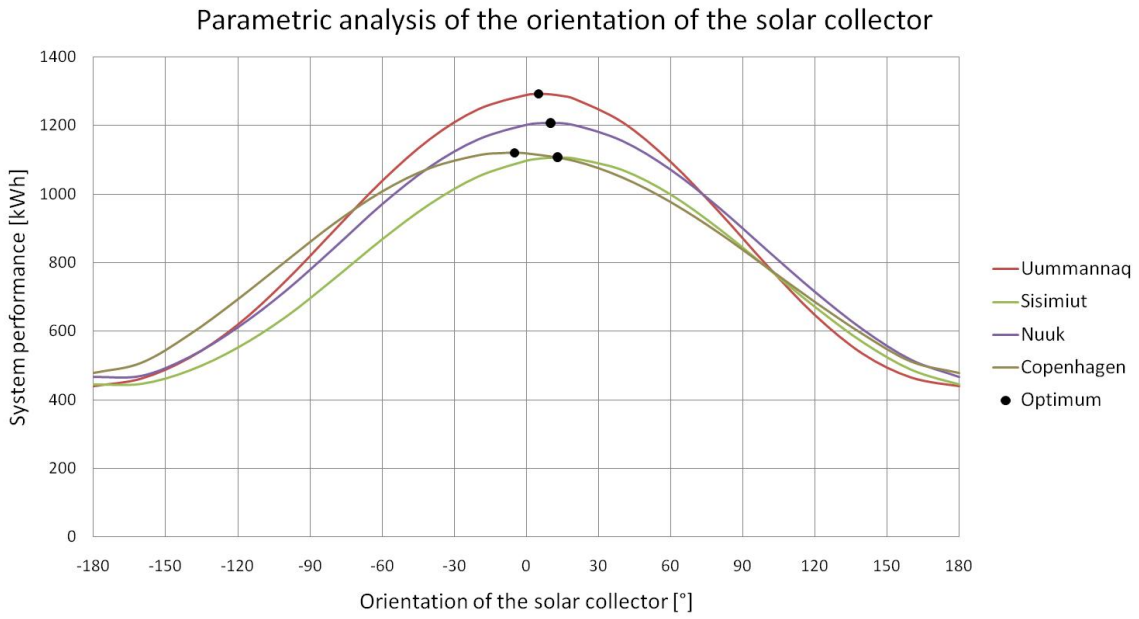

Figure 4.3 The system performance as a function of the orientation of the solar collector using the optimum tilts for each location.

Figure 4.4 shows the relative performance as a function of the orientation of the solar collector. Here it can be seen that there is good symmetry for Copenhagen (brown curve). For the Greenlandic locations it can be seen that they are all slightly influenced by mountains in the east, and for the location of Uummannaq the mountains also effect the result in the west and northern direction.

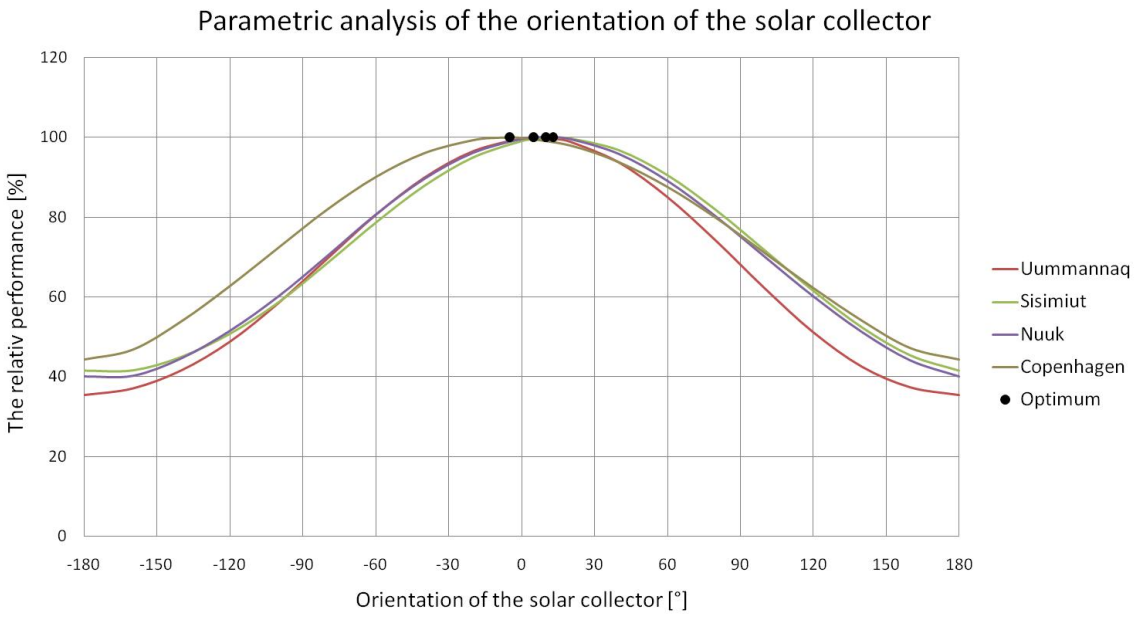

Figure 4.4 The system performance as a function of the orientation of the solar collector using the optimum tilts for each location.

After finding the optimum orientation, the optimum tilt must be checked to see if the new orientation has influenced the optimum tilt, which was the case for Nuuk, changing the optimum tilt from 55° to 56°. In Table 4.3 an overview for the optimum orientation and tilt of the solar collector for these particular systems can be seen for each of the locations.

Table 4.3 The optimum orientation and tilt for the solar collector for these particular systems. A negative value for the orientation indicates the direction towards east.

		Uummannaq	Sisimiut	Nuuk	Copenhagen
Orientation	**[°]**	5	13	10	-5
Tilt	**[°]**	60	57	56	46

The following parametric analysis uses the tilts and orientations which were found to be the optimum for each location.

The yearly thermal performance of the reference system in each of the locations before any changes are suggested is seen in Table 4.4. The highest thermal performance is seen for the system in Uummannaq with a system performance of 1292 kWh followed by the system in Nuuk with 1208 kWh, then Copenhagen with 1120 kWh and at last Sisimiut with 1107 kWh. When viewing the system solar fraction it can be seen that the system in Copenhagen covers the largest part of the hot water consumption with 45 % followed by Uummannaq with 43 %. Sisimiut has the lowest system solar fraction with 37 % and Nuuk the second lowest with 40 %.

Table 4.4 The yearly thermal performance of the reference system in Uummannaq, Sisimiut, Nuuk and Copenhagen.

		Uummannaq	Sisimiut	Nuuk	Copenhagen
System performance	**[kWh]**	1292	1107	1208	1120
System solar fraction	**[%]**	43	37	40	45

The solar collector is described in the program with the max efficiency, heat loss, thermal capacity and the power of *a* in the calculation of the incidence angle modifier. The analysis of the collector will here focus on the max efficiency, heat loss coefficient and the power of *a* for the solar collector.

Maximum efficiency

The parametric analysis of the maximum efficiency can be seen in Figure 4.5, where the maximum efficiency is varied from 0.50 to 0.99. The results show that the performance increases if the maximum efficiency is increased. Increasing the max efficiency has a slightly higher effect in Uummannaq than the

other locations, which is due to the higher amount of beam radiation. The maximum efficiency could be improved by increasing the transmittance of the glass and decreasing the reflectance. The maximum efficiency could also be improved by increasing the absorptance of the absorber. The current max efficiency for the collector used for the simulations, the BA22 collector from Batec A/S is shown on the figure with the black dots. The collector is not fitted with anti reflection treated glass which would improve the collector's maximum efficiency by 5 % as described by [Furbo and Shah 2003].

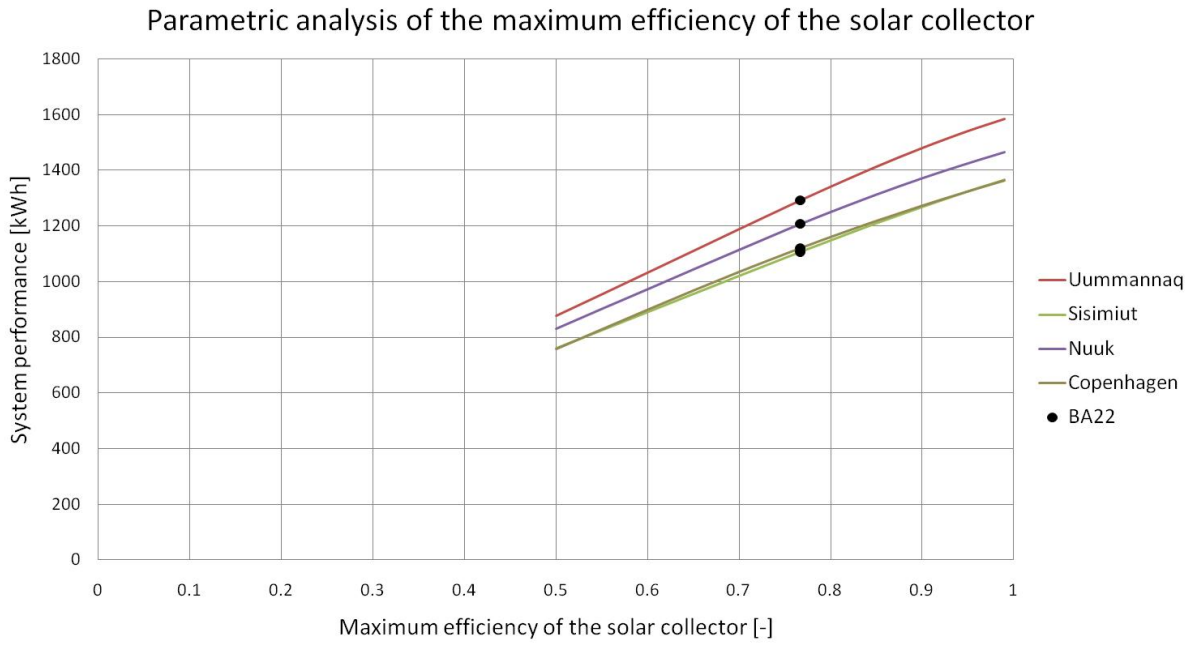

Figure 4.5 The system performance as a function of the maximum efficiency of the solar collector.

Heat loss

The heat loss from the solar collector is described as one coherent heat loss coefficient, covering both the standard heat loss and the temperature dependent heat loss. The variation of the heat loss can be seen in Table 4.5, where the heat loss is varied from -20 % to +20 %

Table 4.5 The variation of the heat loss coefficient for the solar collector in the parametric analysis.

		-20 %	-15 %	-10 %	-5 %	0	+5 %	+10 %	+15 %	+20 %
Heat loss coefficient	**[W/m²K]**	3.494	3.712	3.930	4.149	4.367	4.585	4.804	5.022	5.240

The results from the parametric analysis can be seen in Figure 4.6, showing that the reduction in heat loss coefficient has a slightly stronger impact for the systems in Greenland compared to the results from Copenhagen, which is due the lower ambient temperature in Greenland. If the heat loss is reduced by 10 % this will result in an increase in the performance of 3 % in Greenland and 2 % in Copenhagen.

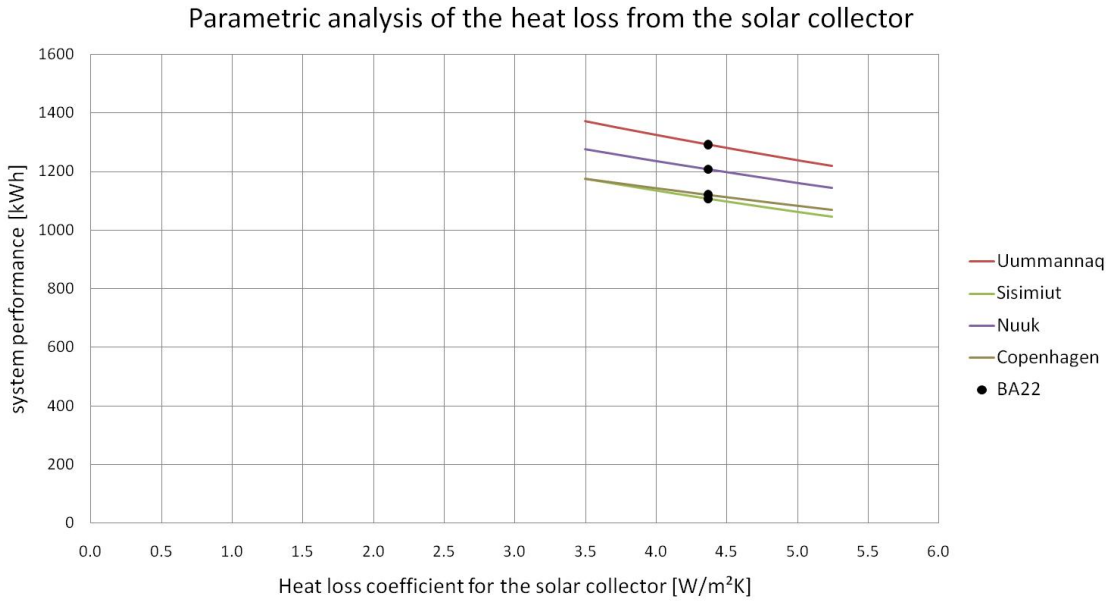

Figure 4.6 The system performance as a function of the heat loss coefficient from the solar collector.

The relative performance shows that the performance, in regards to the heat loss coefficient, is influenced by the location, see Figure 4.7. Uummannaq and Sisimiut are the locations with the lowest yearly average ambient temperature with -5.5 °C in Uummannaq and -3.4 °C in Sisimiut, which is why these locations are more influenced by the heat loss coefficient.

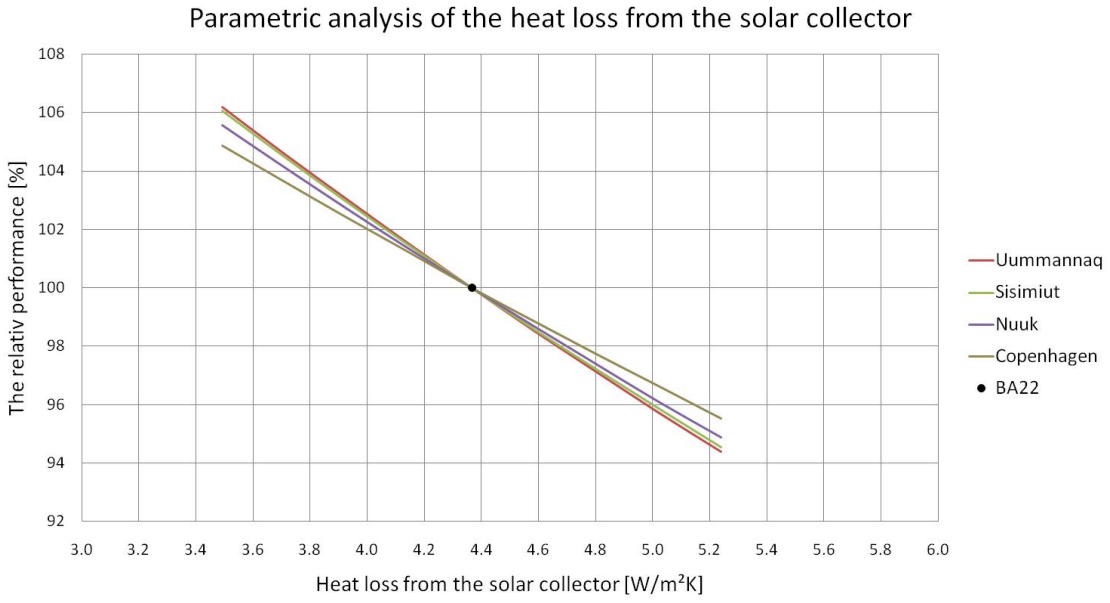

Figure 4.7 The relative performance as a function of the heat loss coefficient from the solar collector.

The heat loss from the solar collector can be decreased by increasing the insulation on the sides and back of the collector and inserting teflon foil between the absorber and glass cover. Both options would increase the price of the collector.

Power of a in the calculation of the incidence angle modifier

The incidence angle modifier k_θ is calculated by:

$$k_\theta = 1 - tan^a\left(\frac{\theta}{2}\right) \qquad (4\text{-}7)$$

Where k_θ is the incidence angle for beam radiation on the collector and *a* is the power to which the tan equation is lifted.

In Figure 4.8 it can be seen that the higher *a* is, the higher the yearly thermal performance will be. Inserting teflon foil in the solar collector will have a positive effect on *a*, and therefore increase the overall performance.

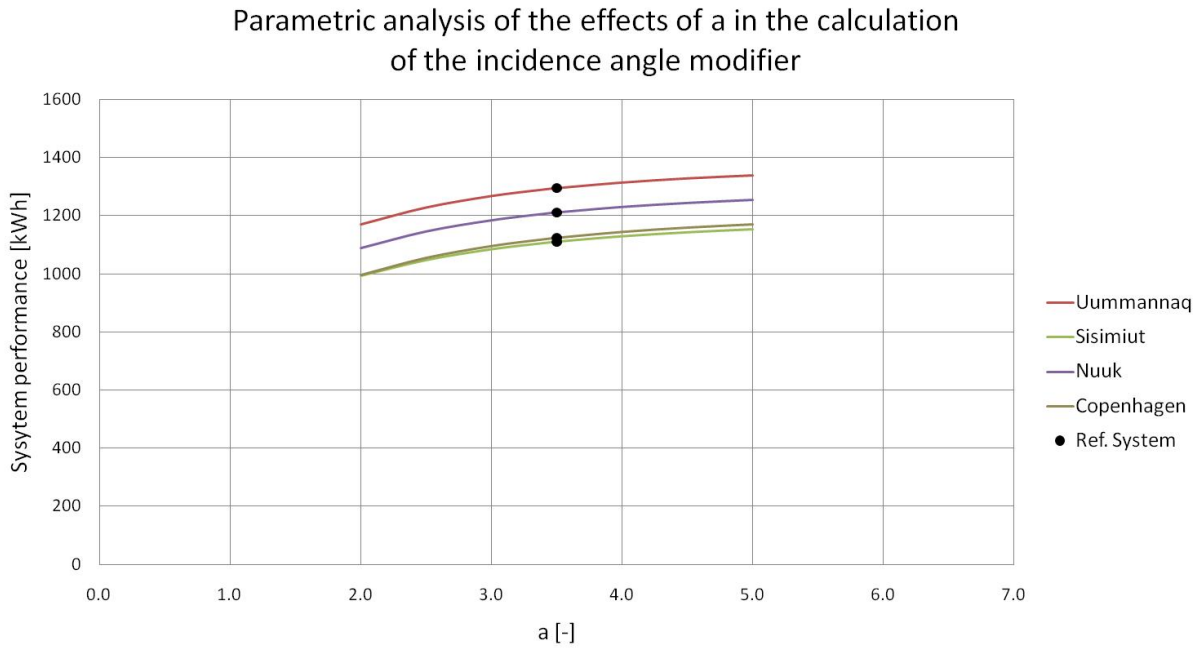

Figure 4.8 The system performance as a function of a.

Collector area

It is important to have a good inter-action between the solar collector area and the storage tank. A rule of thumb says that the size of the storage tank should be around 50 l per m² solar collector area, which means that for a storage tank of 165 l an appropriate area of the solar collector would be 3 m². The size of the solar collector area chosen in the reference system is 2.19 m², which is small compared with the rule of thumb. In Figure 4.9 the parametric analysis for the solar collector area can be seen, and as expected the area equal to the BA22 shows that increasing the area would give a significant improvement in the performance of the whole system.

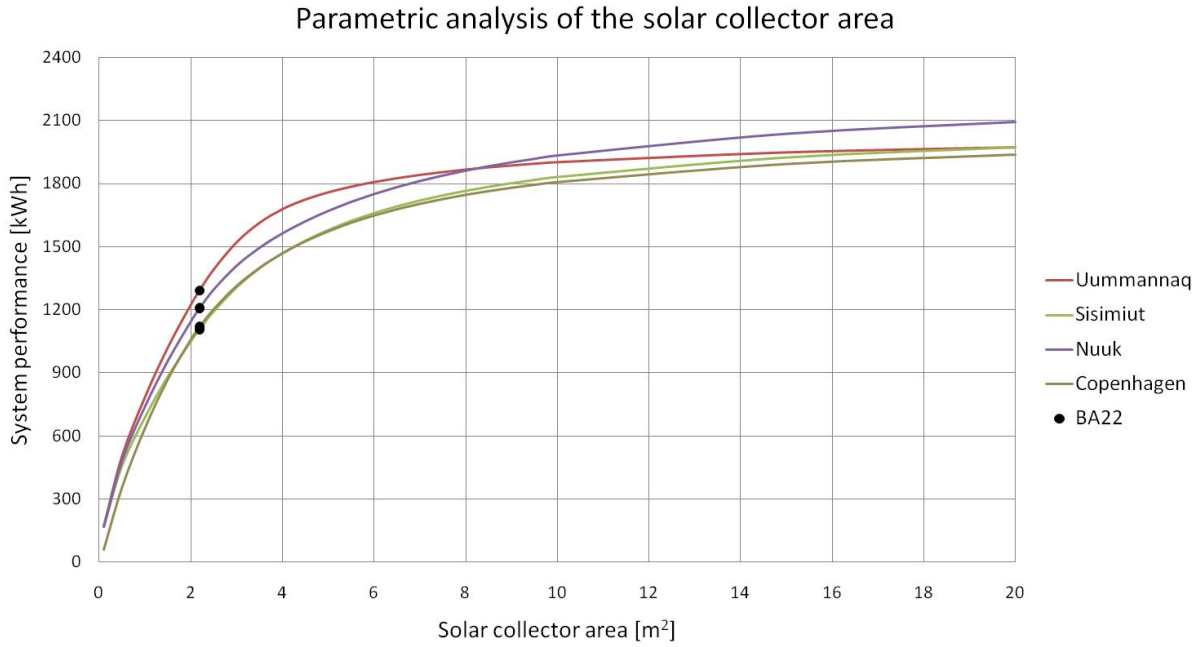

Figure 4.9 The system performance as a function of the solar collector area.

The figure also shows that increasing the solar collector area from 2 m² to 3 m² gives a higher increase in thermal performance, than increasing the area from 6 m² to 7 m². The results from Uummannaq shows that once the 'optimum' area is reached around 4.5 m², a further increase in the area will give less relative increase in performance compared to the other locations. This is due to the higher amount of beam radiation in Uummannaq, which means the tank will be fully loaded when the weather conditions allow it, and having a larger solar collector area will not result in more energy transferred to the tank.

In Figure 4.10 the relative performance is shown, and here it becomes even more evident that once the optimum area is reached for Uummannaq additional collector area gives little increase in the yearly performance. Continuing to increase the collector area in Sisimiut will result in a continuing increase in performance which is due to the higher amount of diffuse radiation in Sisimiut.

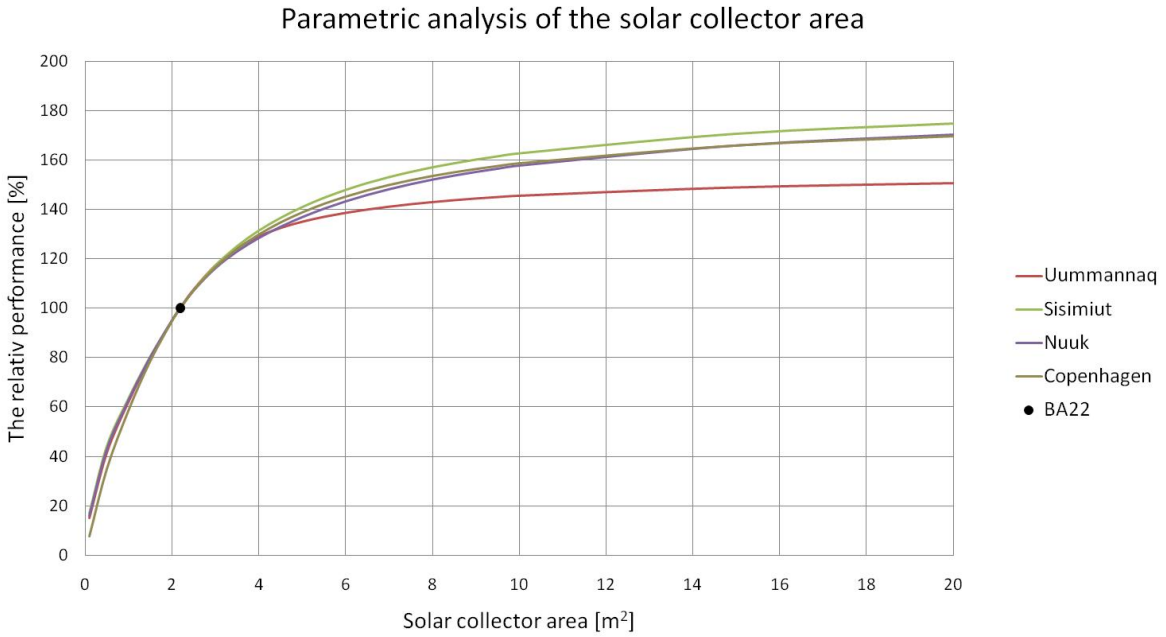

Figure 4.10 The relative performance as a function of the solar collector area.

It should be noted that the flow in the solar collector loop was changed when the solar collector area was changed according to the assumption that the flow rate is 0.2 l/min per m² solar collector.

4.2.2 Solar collector loop

The parameters which are investigated in the solar collector loop are: the flow rate in the solar collector loop, the controls of the pump, the pipe lengths and the insulation on the pipes.

Flow

The recommendations in [Furbo 2004] states that the flow rate in the solar collector loop in a low-flow mantle tank system should be between 0.1 – 0.2 l/min per m² solar collector area. This is investigated varying the flow from 0.05 l/min per m² solar collector area to 1.00 l/min per m² solar collector area, which corresponds to 0.11 l/min to 2.19 l/min, seeTable 4.6.

Table 4.6 The variation in the flow rate.

x l/min per m² solar collector	0.05	0.10	0.15	**0.20**	0.25	0.30	0.35	0.40	0.60	0.80	1.00
Flow rate [l/min]	0.110	0.219	0.329	**0.438**	0.548	0.657	0.767	0.876	1.314	1.752	2.190

The result can be seen in Figure 4.11 with the system performance as a function of the flow rate. On the figure it can be seen that the chosen flow rate in the reference system gives the best performance.

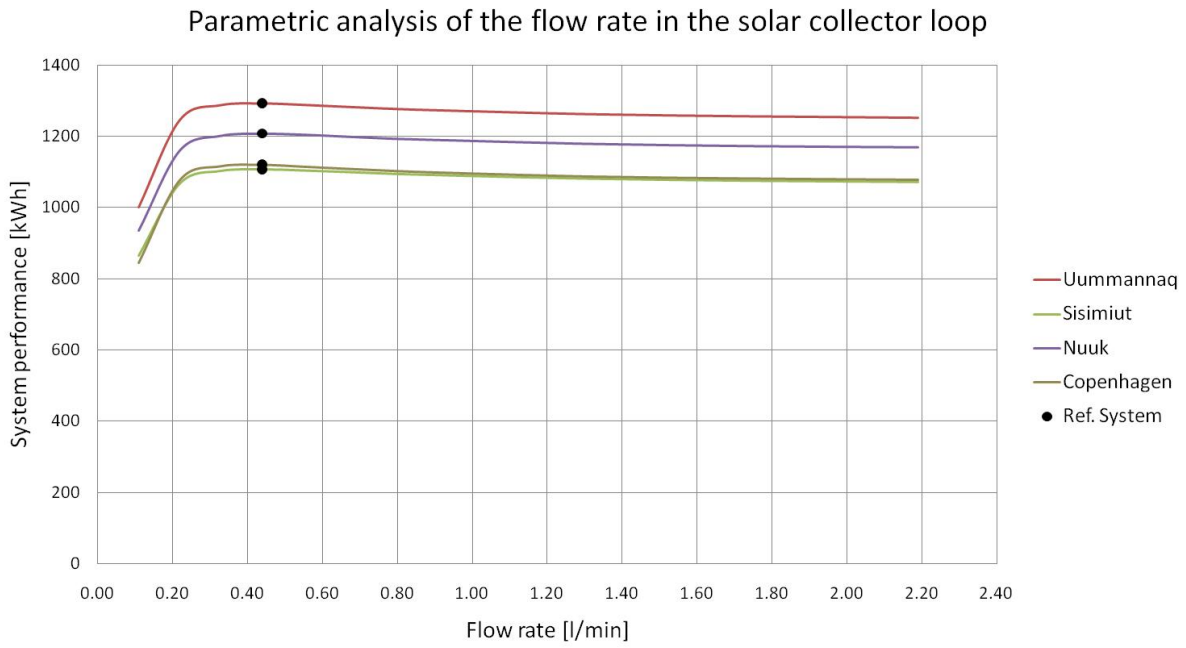

Figure 4.11 The system performance as a function of the flow rate in the solar collector loop.

The effect of the flow rate on the relative performance can be seen in Figure 4.12. It reveals quite surprisingly that the location and difference in climate does not influence the flow rate.

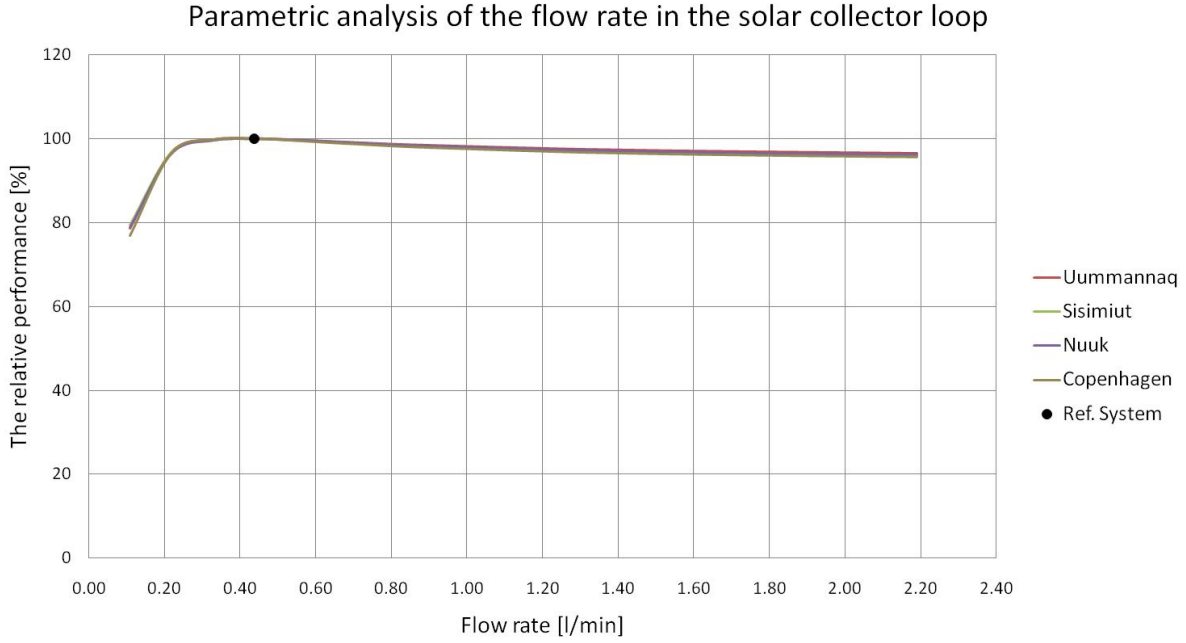

Figure 4.12 The relative performance as a function of the flow rate in the solar collector loop.

Temperature difference for when the pump should start operating

The operation of the pump in the solar collector loop is controlled by temperature differences between the temperature in the solar collector and the temperature in the bottom of the mantle. In the reference system the pump will start operating when the temperature difference is 10 °C or higher.

In Figure 4.13 the effects of the starting temperature difference is shown. The results shows that this temperature setting has very little effect and that the 10 °C chosen for the reference system is a reasonable setting for all four locations.

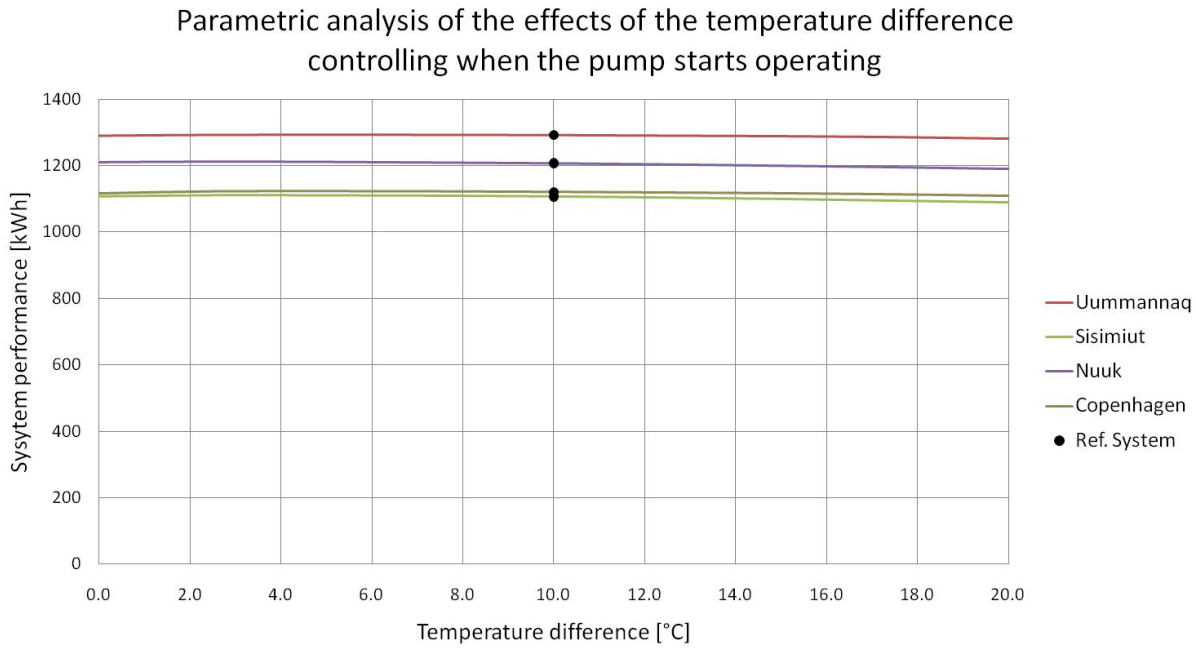

Figure 4.13 The system performance as a function of the temperature difference for when the pump should stop start operating.

Temperature difference for when the pump should stop operating

The stopping of the pump in the solar collector loop is also controlled by the temperature difference between the solar collector and bottom of the mantle. In the reference system the pump will stop operating when the temperature difference reaches 2 °C or less.

The effect of the stopping temperature difference on the yearly thermal performance is seen in Figure 4.14. Again little effect is detected. The chosen 2 °C in the reference system is a reasonable setting for all four locations.

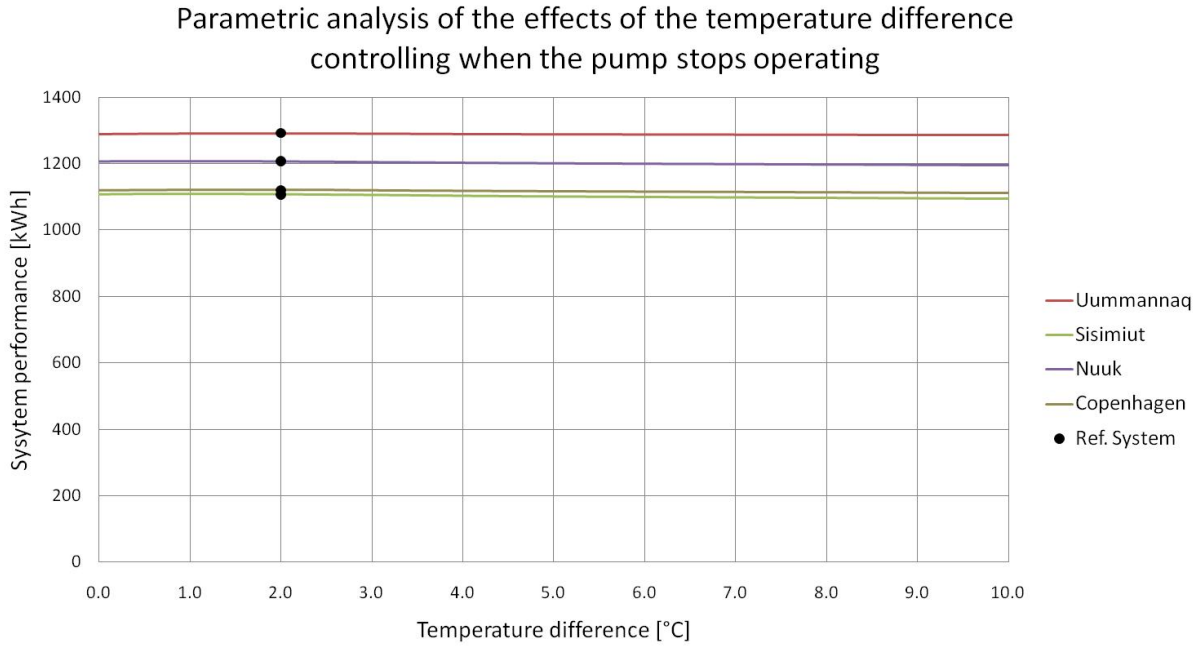

Figure 4.14 The system performance as a function of the temperature difference for when the pump should stop operating.

Pipe length

In MantlSim the solar collector loop is spilt in to 4 different sections, each describing a specific part of the solar collector loop. In Figure 4.15 the different sections are shown: the dotted red line gives the pipe section going from the collector outside to the roof and the full red line is the continuation of the same pipe section but from the roof inside to the storage tank. The full blue line is the pipe section going from the storage tank on the inside to the roof, and the continuation of the pipe section is the dotted blue line giving the section outside from the roof to the collector. In the reference system the collector is assumed to be placed on the roof with the outlet connected to 0.5 m of pipe outside, and 3.5 m inside before reaching the storage tank. The same lengths are assumed going back to the collector from the storage tank: 3.5 m inside and 0.5 m outside.

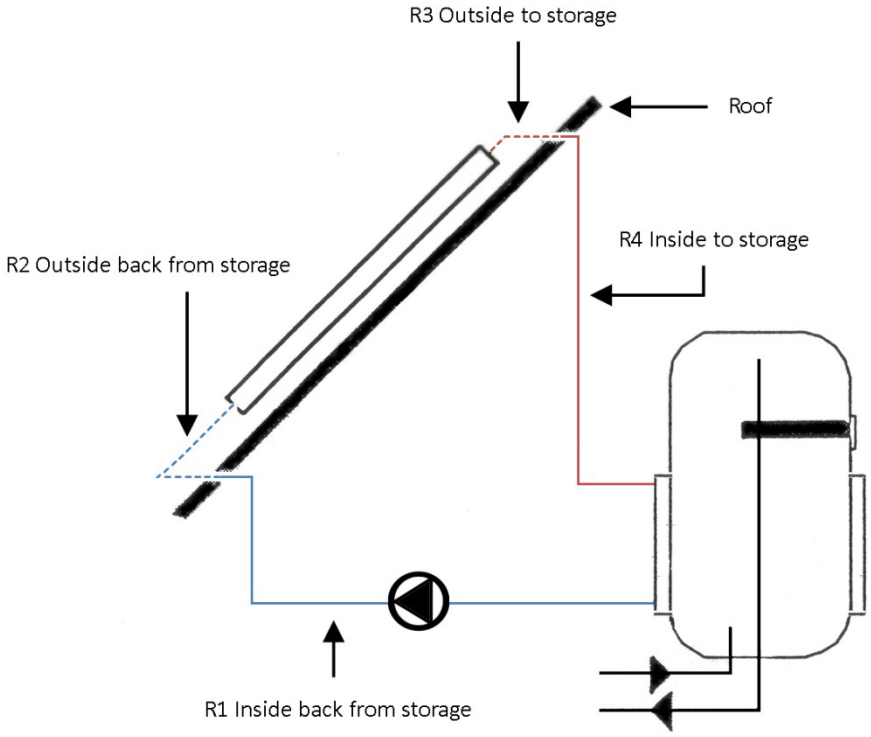

Figure 4.15 Schematic showing the definition of the different pipe sections in MantlSim.

The results from Uummannaq of the parametric analysis with the effects of the pipe lengths on the performance can be seen in Figure 4.16. It is clear that the pipe lengths carrying the hot solar collector fluid have the greatest effect on the performance of the whole system, see the red full and dotted curve in Figure 4.16. Of the two hot sections it is naturally the section outside which has most impact. Of the sections with the cold solar collector fluid it is again the pipe length outside which has most impact.

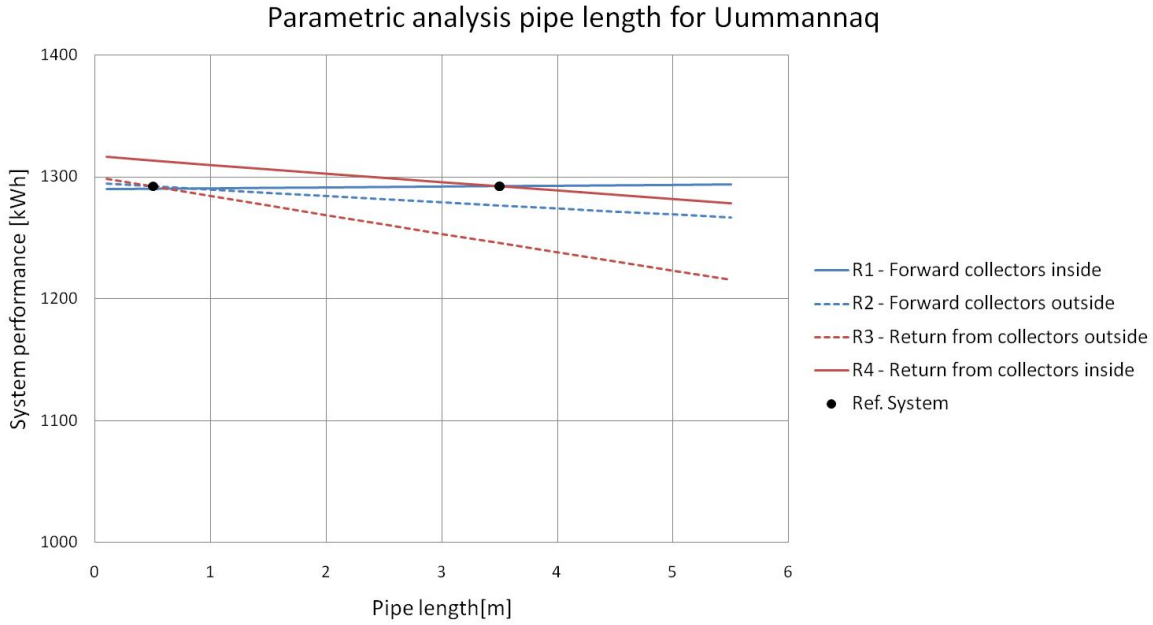

Figure 4.16 The system performance as a function of the pipe length in the solar collector loop for a system in Uummannaq.

The results are the same for Sisimiut and Nuuk.

For Copenhagen the results shows the same tendency, but not with as big an impact as in Uummannaq which is because of the higher ambient temperature in Denmark compared to Greenland. Nevertheless it is also important in Denmark to reduce the pipe lengths, especially on the hot side of the solar collector loop on the inside as well as the outside.

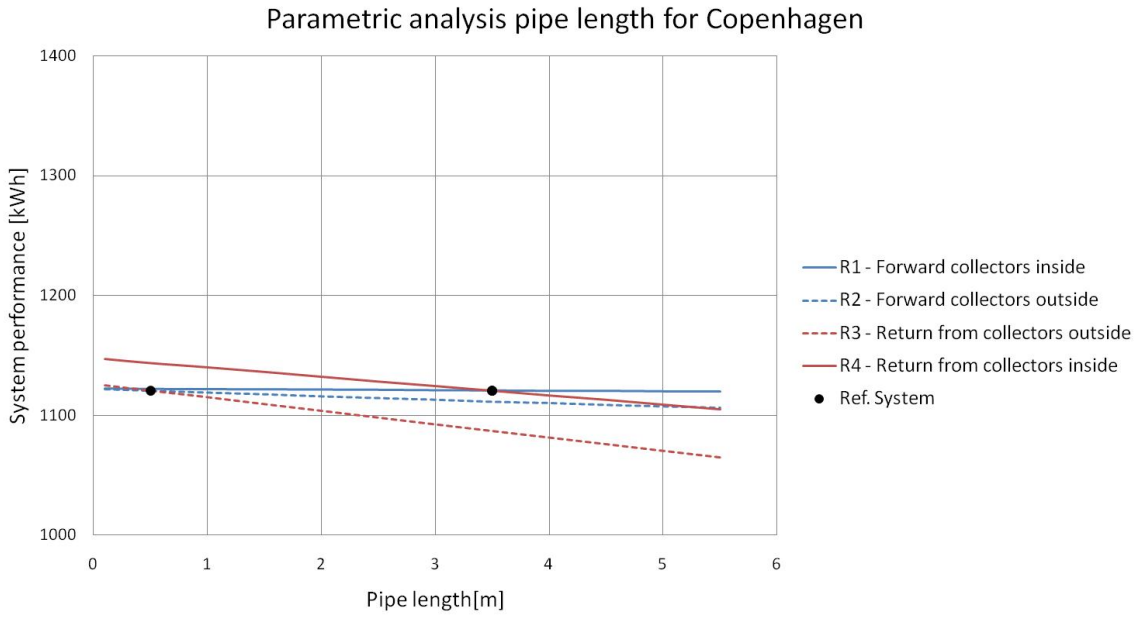

Figure 4.17 The system performance as a function of the pipe length in the solar collector loop for a system in Copenhagen.

Having short pipe lengths in the solar collector loop is of importance, but especially in the sections from the solar collector loop to the storage tank. The pipe should be lead through the roof as soon as possible reducing the pipe length outside the building envelope. From the storage tank back to the collector it is also important to reduce the pipe length outside the building envelope.

Pipe insulation

The influence of the pipe insulation is investigated individually for each pipe section, and the results for Uummannaq can be seen in Figure 4.18. An increase of the pipe insulation on the return from the collectors inside the building will increase the performance of the system. Increasing the insulation on the return from the collector outside will also increase the performance, but not as strongly because the pipe length influences the results. In the reference system the pipe length on the sections from the collector are 0.5 m outside and 3.5 m inside, therefore the influence of the pipe section inside is higher than the influence of the pipe section outside. The figure shows that the cold pipe sections are well insulated with 1 cm of mineral wool. In fact the results show that decreasing the insulation on the pipe section forward to the collector inside will increase the performance. This is due to the low cold water inlet temperature, which will influence the temperature of the solar collector fluid running back to the collector, where it then will benefit positively by running un-insulated through the house to the roof where the collector is placed.

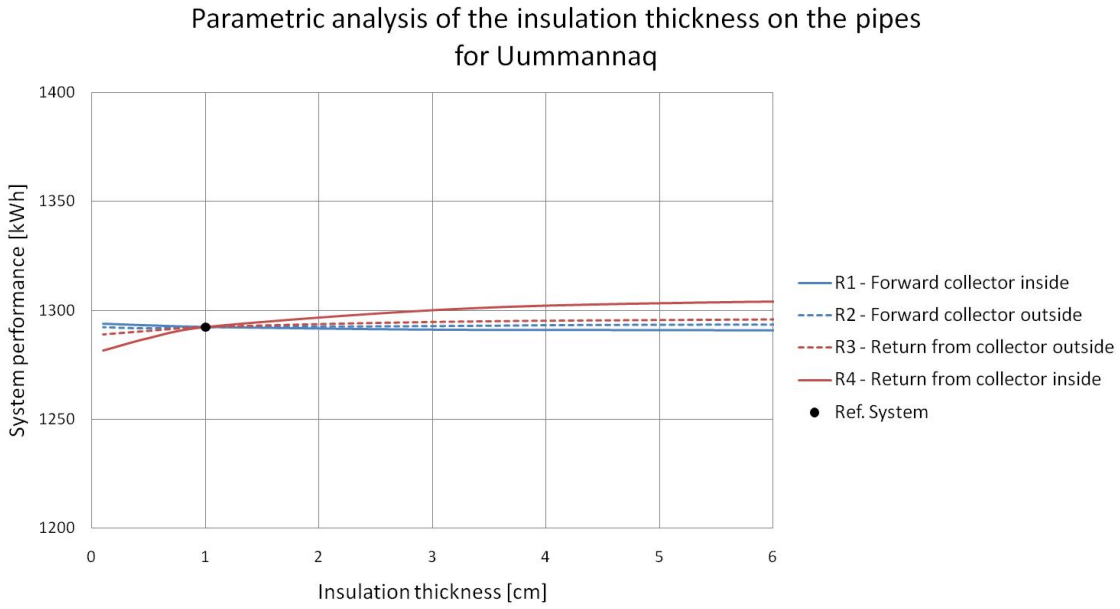

Figure 4.18 The system performance as a function of the insulation on the pipes in the solar collector loop in the system in Uummannaq.

The same results are seen for Sisimiut and Nuuk.

The investigation for Copenhagen can be seen in Figure 4.19. The results are the same for the pipe section carrying the hot solar collector fluid: more insulation will increase the performance of the system. But for a system in Copenhagen there are no benefits from running the cold solar collector fluid through the house un-insulated to the collector, which is because of the higher cold water inlet temperature in Copenhagen compared to the locations in Greenland.

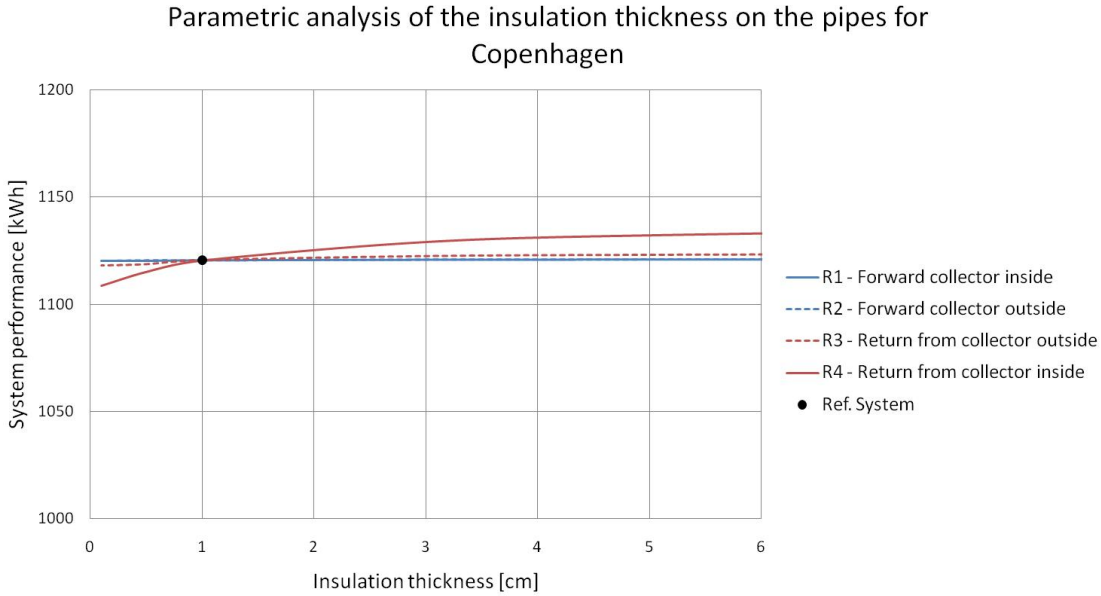

Figure 4.19 The system performance as a function of the insulation on the pipes in the solar collector loop in the system in Copenhagen.

PUR foam

If the insulation material on the pipes is changed from mineral wool to PUR-foam and the thickness of the insulation material is kept the same the system performance will only result in a minor improvement, which can be seen in Figure 4.20. The overall improvement is less than 1 % for all 4 locations.

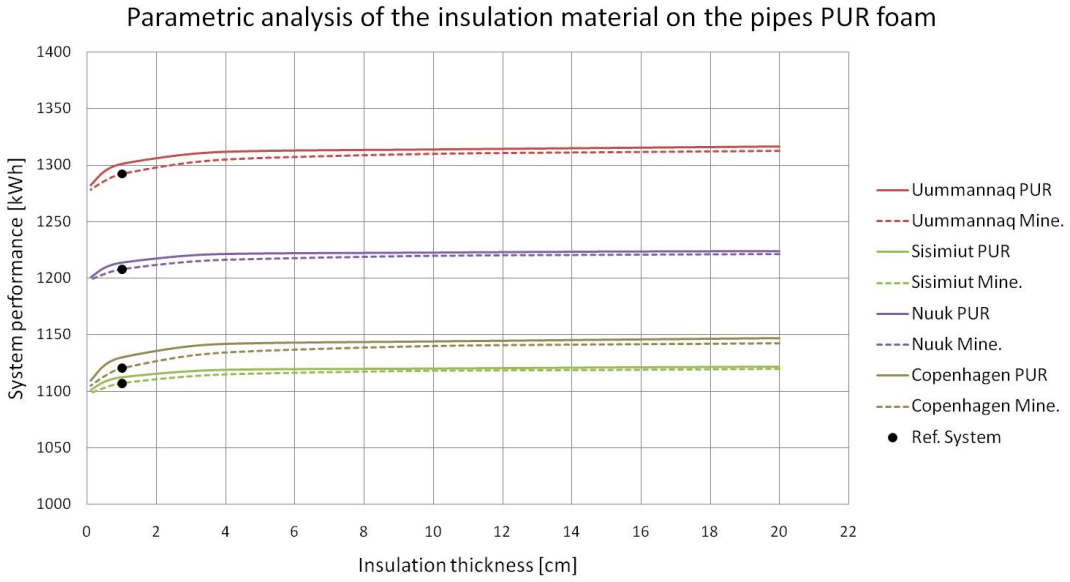

Figure 4.20 The system performance as a function of the insulation material on the pipes.

4.2.3 Storage tank

The storage tank is investigated in terms of the insulation thickness, thermal bridges, height and diameter ratio, height of the mantle and the inlet to the mantle.

Insulation of the tank is investigated individually for the top of the tank, the sides with and without the mantle and for the bottom of the tank.

Insulation thickness top

Insulation on the top of the tank is important since this part of the tank is always heated to a least 50 °C. For this specific storage tank it is sufficient to insulate the top with 6 cm of PUR foam, see Figure 4.21. The mantle tank from solvarmebeholderen.dk is insulated with 31 cm which is more than enough. An increase in insulation thickness from 6 cm to 31 cm, results in an increase in system performance of 1.5 %.

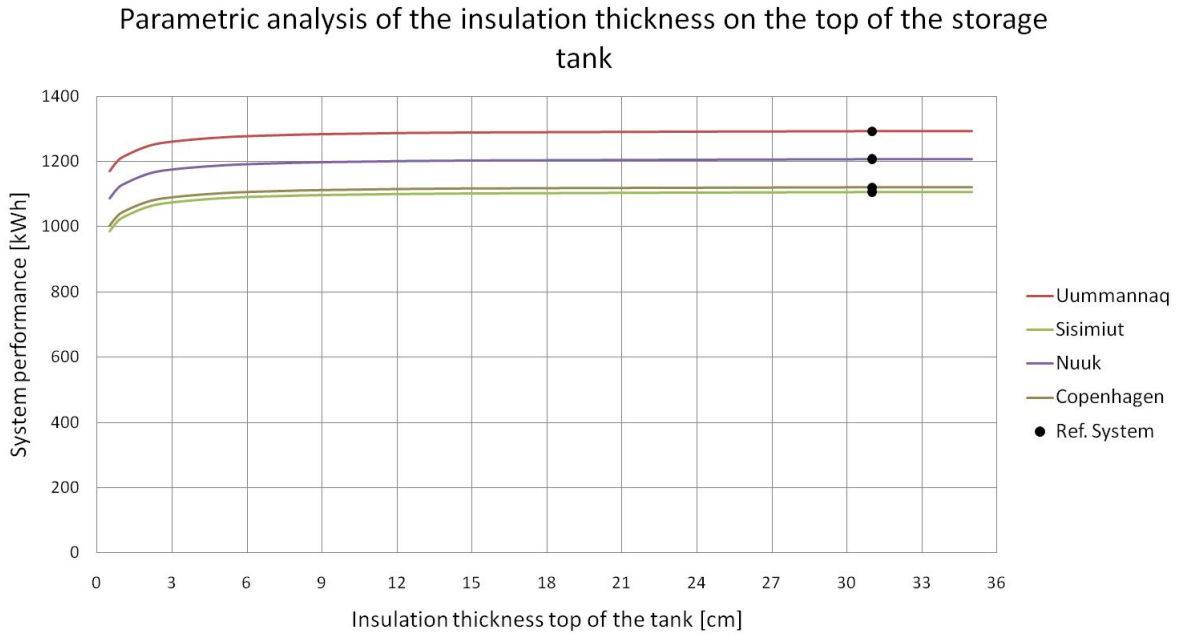

Figure 4.21 The system performance as a function of the insulation thickness in the top of the tank.

Insulation thickness sides without mantle

The insulation thickness on the side of the tank above the mantle is also important since most of this area is also always heated to at least 50 °C. In Figure 4.22 the effects of the insulation thickness can be seen. Compared to the results from the top insulation it can be seen that the thermal performance of the system is strongly influenced by the side insulation above the mantle, which is because the surface area of this part of the tank is large compared to the top of the tank. The reference system is insulated with 9.6 cm PUR-foam, which is sufficient.

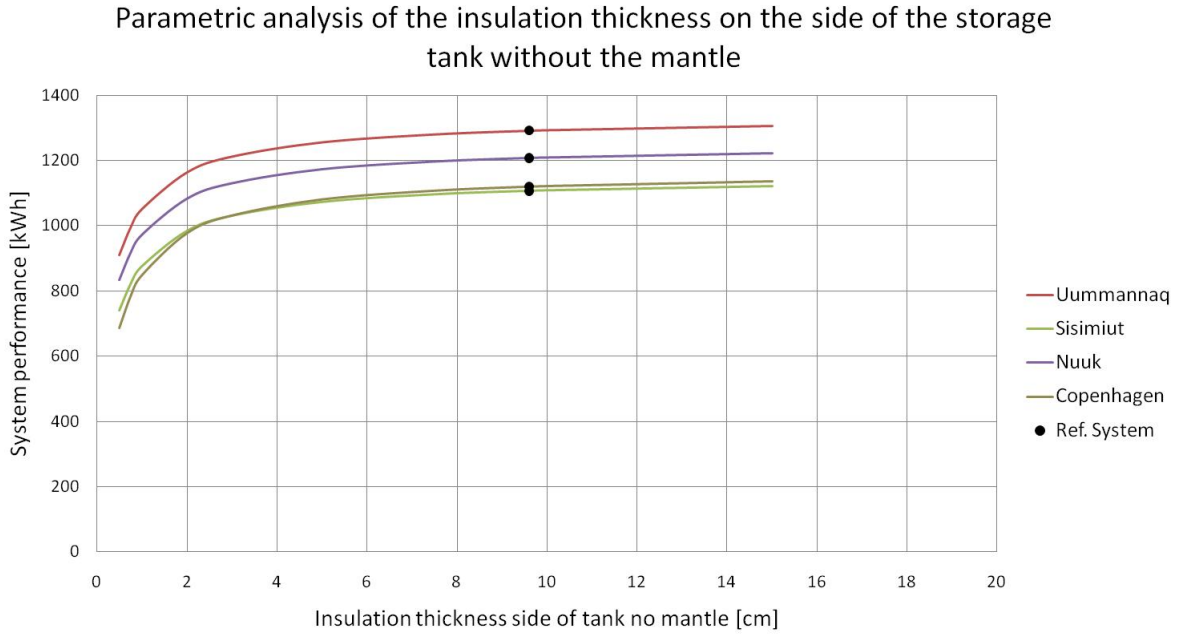

Figure 4.22 The System performance as a function of the insulation thickness on the side of the storage tank without the mantle.

Insulation thickness sides with mantle

The results from the investigations of the insulation on the sides of the storage tank where the mantle is placed shows unexpected results, see Figure 4.23. Decreasing the side insulation around the mantle in a system in Greenland will increase the system performance, which is opposite of what is seen for Copenhagen where a decrease in insulation results in a decrease in performance.

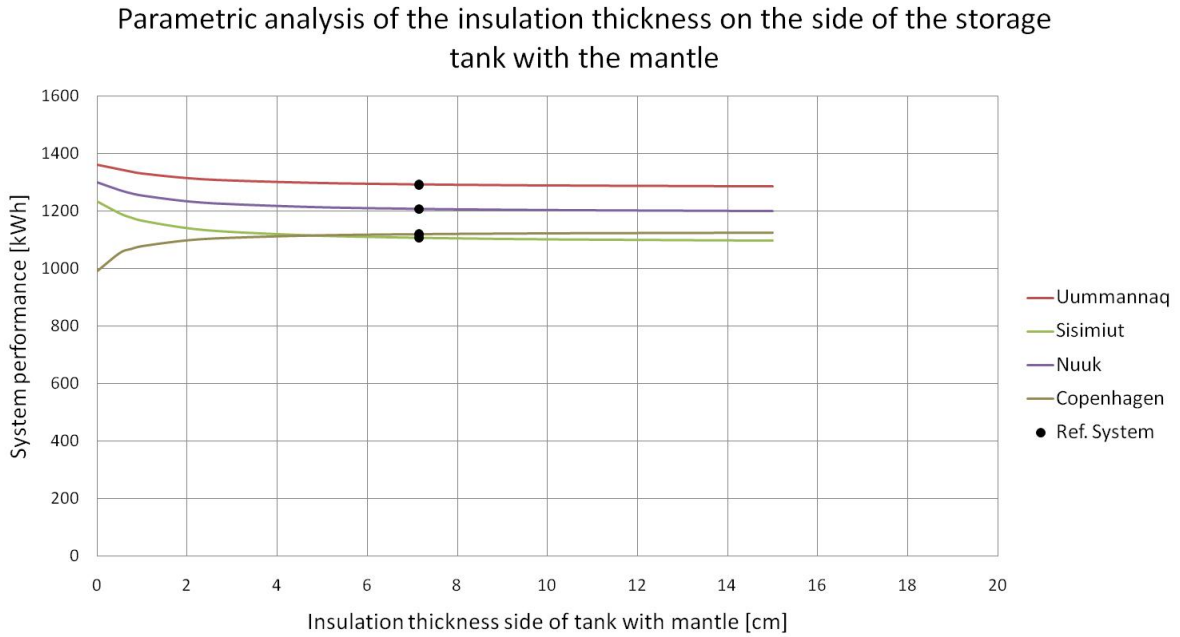

Figure 4.23 The system performance as a function of the insulation thickness on the side of the storage tank where the mantle is located.

The reason for this is the cold water inlet temperature to the system and the fact that the system is placed inside at room temperature. This results in an average mantle fluid temperature which is lower than the room temperature. Therefore heat is transferred from the room to the fluid in the mantle.

Insulation thickness bottom

No insulation on the bottom gives the best performance in the locations in Greenland as well as in Copenhagen, see Figure 4.24. The bottom of the tank has a lower temperature than the room temperature and therefore heat is transferred from the room to the water placed at the bottom of the tank, as seen in the situation with the insulation at level with the mantle for the Greenlandic locations.

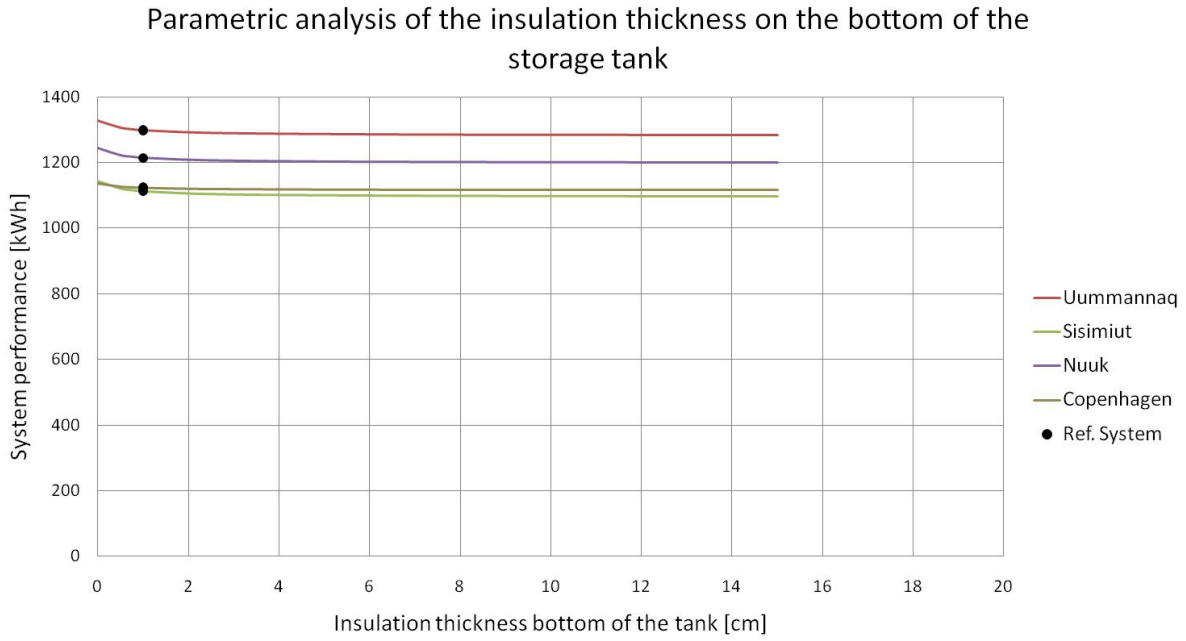

Figure 4.24 The system performance as a function of the insulation thickness at the bottom of the storage tank

Thermal bridges

Heat lost through thermal bridges occurs when the insulation is perforated by pipe leading to or away from the storage tank, for instance when drawing hot water from the tank and introducing cold water. Thermal bridges at the top of a storage tank can have a large negative influence on the thermal performance of a solar heating system [Furbo 1982]. Here the effects of thermal bridges are investigated both for the top and bottom of the tank.

The decrease in system performance because of thermal bridges at the top of the tank can be seen in Figure 4.25. If the systems investigated here have an extra heat loss coefficient of 1 W/K because of thermal bridges at the top of the tank, this will result in a reduction of system performance of up to 23 %. If the heat loss coefficient from thermal bridges at the top is 2 W/K the reduction will be as high as 45 %. In the reference system the thermal bridges is assumed to be 0 W/K since there are no connections or perforation at the top of the tank, thereby insuring the highest performance of the system.

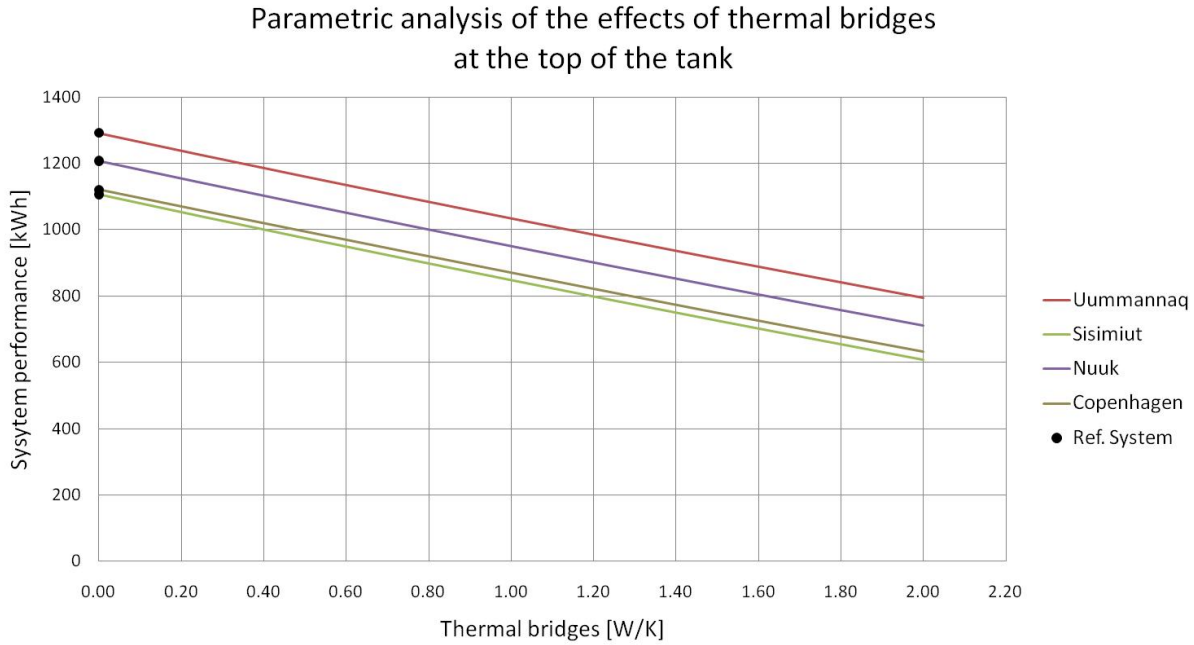

Figure 4.25 The system performance as a function of thermal bridges at the top of the tank.

The influence of thermal bridges in the top of the tank on the relative performance is seen in Figure 4.26. Here it can be seen that thermal bridges have a stronger influence in Sisimiut and Copenhagen than in Nuuk and Uummannaq.

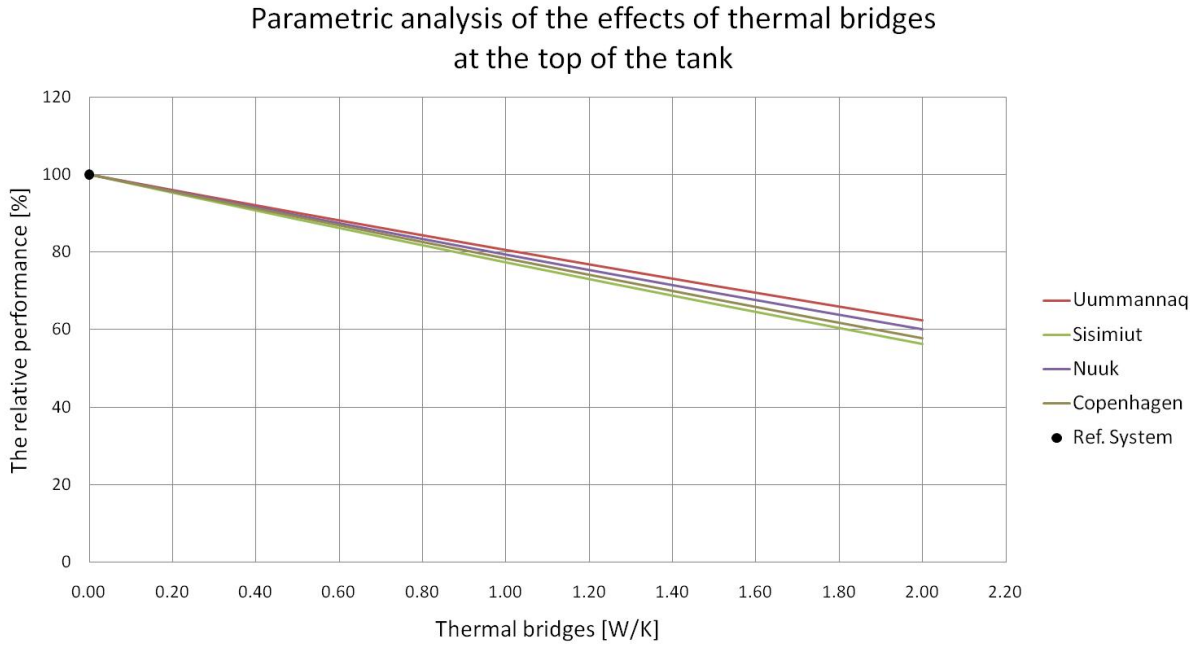

Figure 4.26 The relative performance as a function of thermal bridges at the top of the tank.

Thermal bridges at the bottom of the tank can increase the performance of the solar heating system see Figure 4.27. The reason for this is the same as for the insulation at the bottom of the storage tank: the heat transfer will be in the direction towards the tank and not away from it. The reference system is assumed to have a heat loss coefficient of 1 W/K due to the connections at the bottom of the tank.

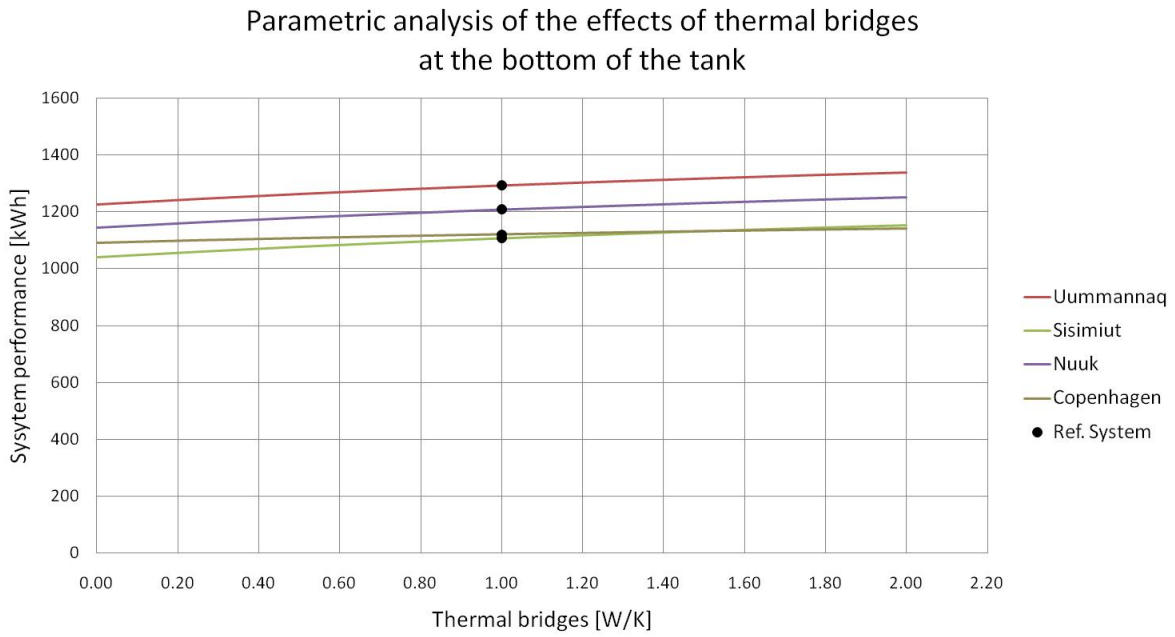

Figure 4.27 The system performance as a function of thermal bridges at the bottom of the tank.

In Figure 4.28 the effects of the thermal bridges in the bottom of the tank on the relative performance can be seen. The results show that having thermal bridges in the bottom of the tank will increase the yearly thermal performance of the system in both the Greenlandic locations and Copenhagen.

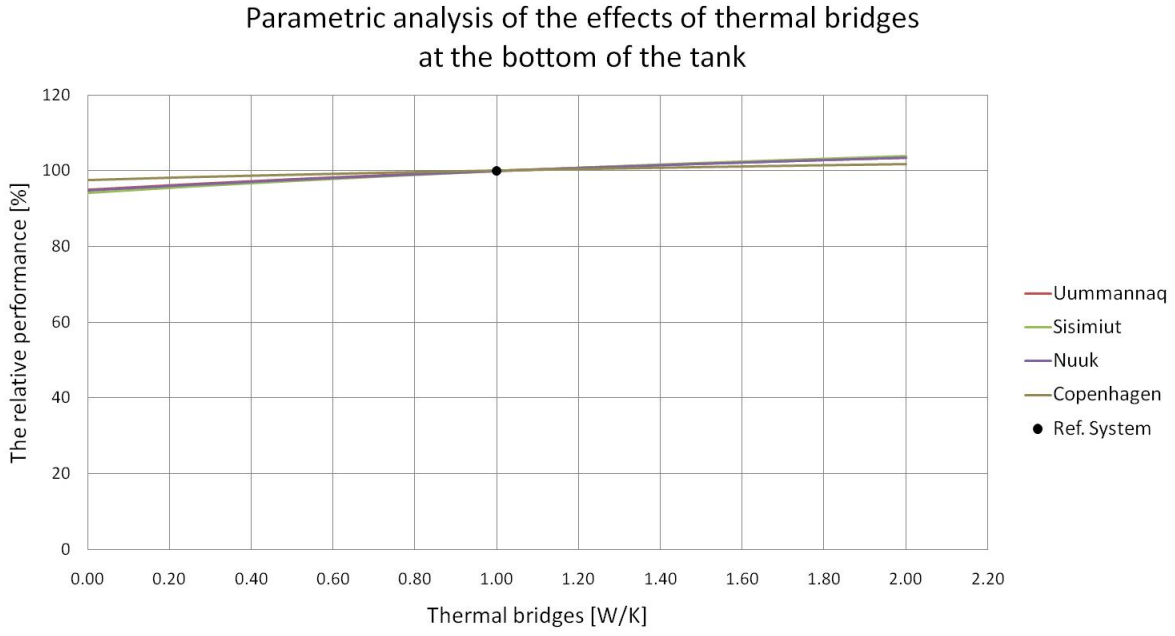

Figure 4.28 The relative performance as a function of thermal bridges at the bottom of the tank.

H/D ratio

The H/D ratio describes the relationship between the height and diameter of the storage tank. The volume of both the tank and the mantle are kept constant as well as the ratio between of the height of the mantle and the height of the tank, see Figure 4.29. Also the auxiliary volume is kept constant.

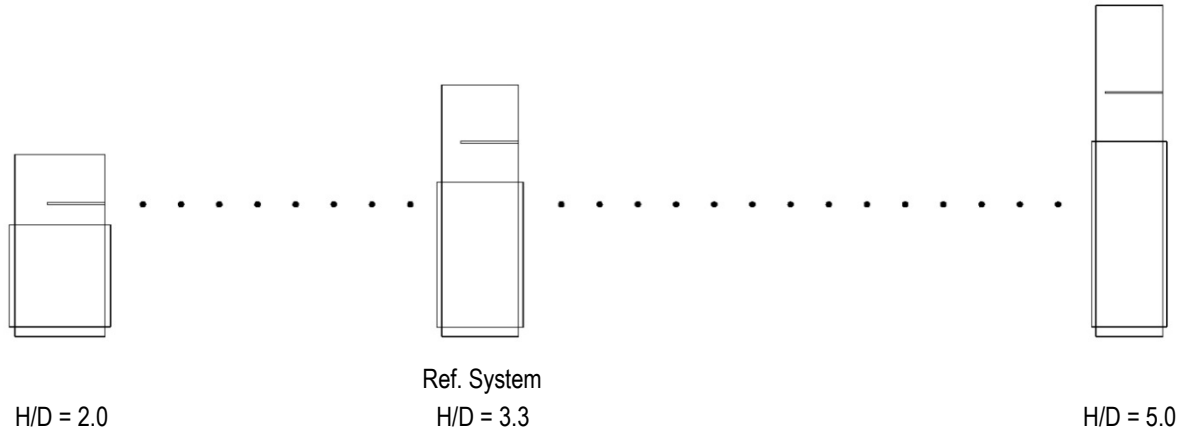

Figure 4.29 Schematic showing the change in the shape of the tank when analysing the H/D ratio.

The H/D ratio is varied from 2.0 to 5.0, see Figure 4.30. Here it can be seen that increasing the H/D ratio to 4.8 slightly will increase the performance. If the H/D is higher than 4.8 the performance will decrease. The increase from a H/D ratio of 2.0 to 4.8 will for this system result in an maximum increase in system performance of 1.5 %. The increase is slightly higher for the Greenlandic locations compared to Copenhagen where the increase in performance is 0.8 %.

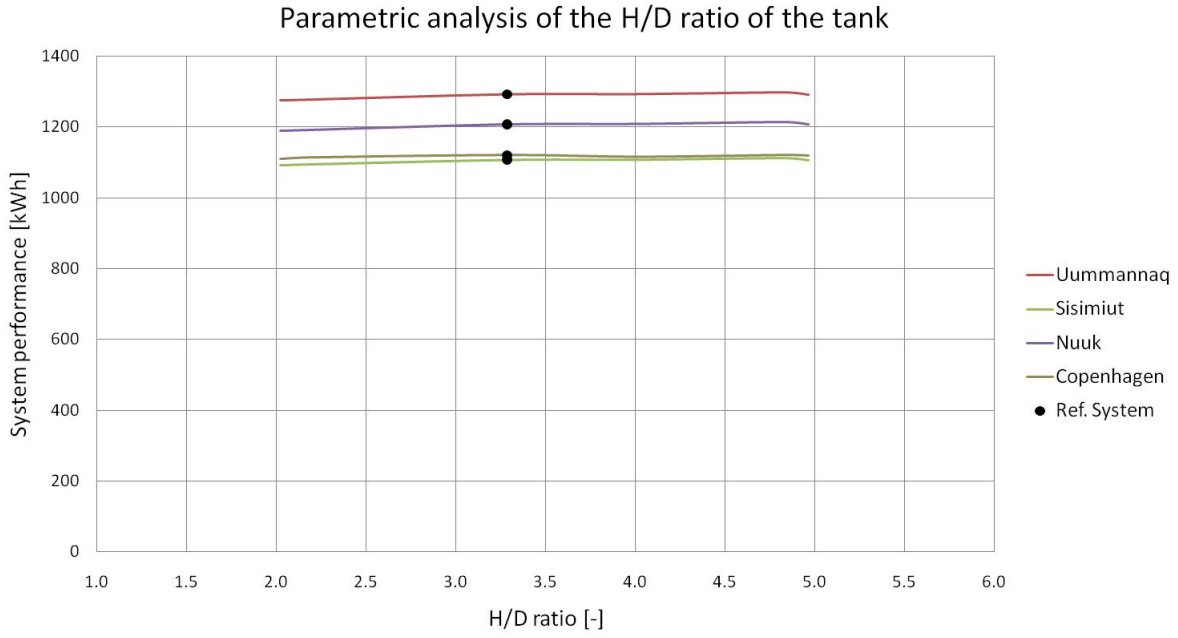

Figure 4.30 The system performance as a function of the height / diameter ratio, H/D.

Height of the mantle

The investigation is carried out maintaining the same diameter of the mantle and only changing the height of the mantle, which means that volume in the mantle, will change with the height. The height of the mantle does not exceed the placement of the electric heating element. The results of the investigation can be seen in Figure 4.31. Increasing the height of the mantle and thereby also the volume in the mantle will slightly increase the performance of the system. It can be seen that the reference system could be improved by changing the design, and increasing the height of the mantle to just beneath the electric heating element.

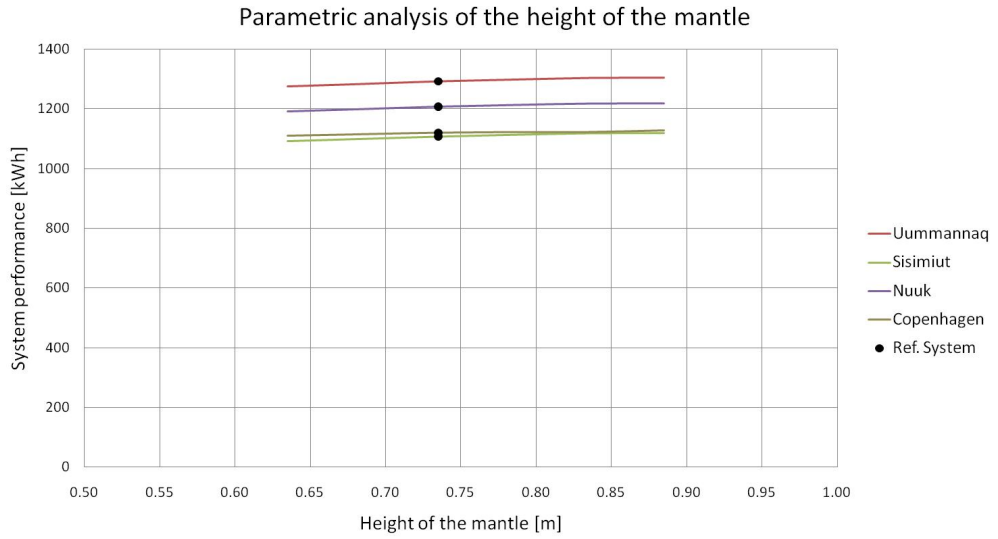

Figure 4.31 The system performance as a function of the height of the mantle.

Inlet to the mantle

Investigations of the placement of the inlet to the mantle show that the inlet should be in the top of the mantle, see Figure 4.32. If the inlet is placed in the middle of the mantle or the bottom, it will destroy the stratification in the tank, and thereby decrease the performance of the system.

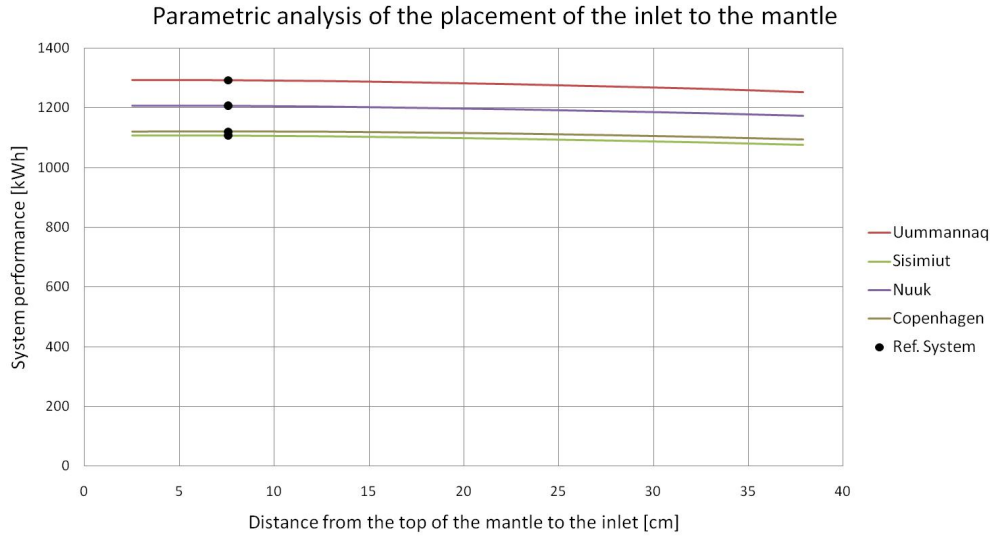

Figure 4.32 The system performance as a function of the placement of the inlet to the mantle

4.2.4 Draw off volume and profile

Hot water consumption

The hot water consumption of the reference system is assumed to be 150 l/day. This is a higher consumption than normally assumed for a normal family in Denmark, but it is regarded as an accurate assumption based on the measurement from the Low energy house in Sisimiut, where the average hot water consumption is128 l/day for two people. The effects of the hot water consumption can be seen in Figure 4.33, where it is evident that that the higher the consumption the more energy can be drawn from the system, which is seen for all 4 locations.

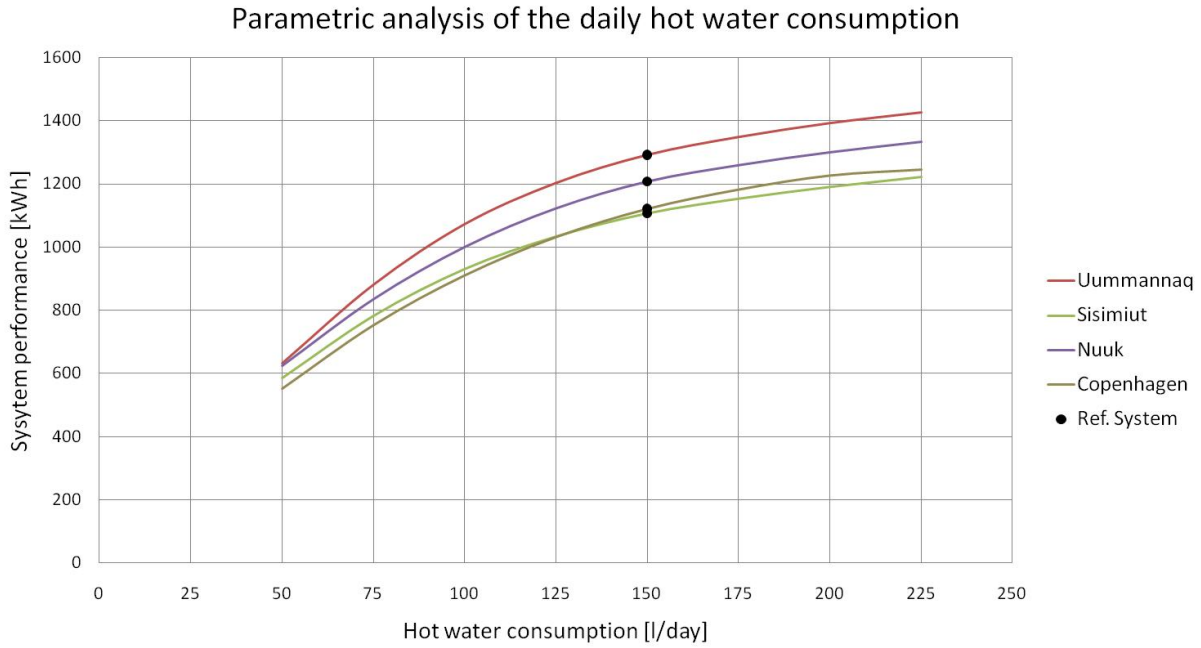

Figure 4.33 The system performance as a function of the hot water consumption.

Although a higher performance of the system is the result of higher hot water consumption, on a yearly basis, the share which is covered with energy from the system decreases with increasing hot water consumption, see Figure 4.34. This means that the auxiliary energy will have to supply more energy to maintain the family's need for hot water. With a hot water consumption of 150 l/day the system solar fraction will be 43 % for Uummannaq, 37 % for Sisimiut, 40 % for Nuuk and 45 % for Copenhagen.

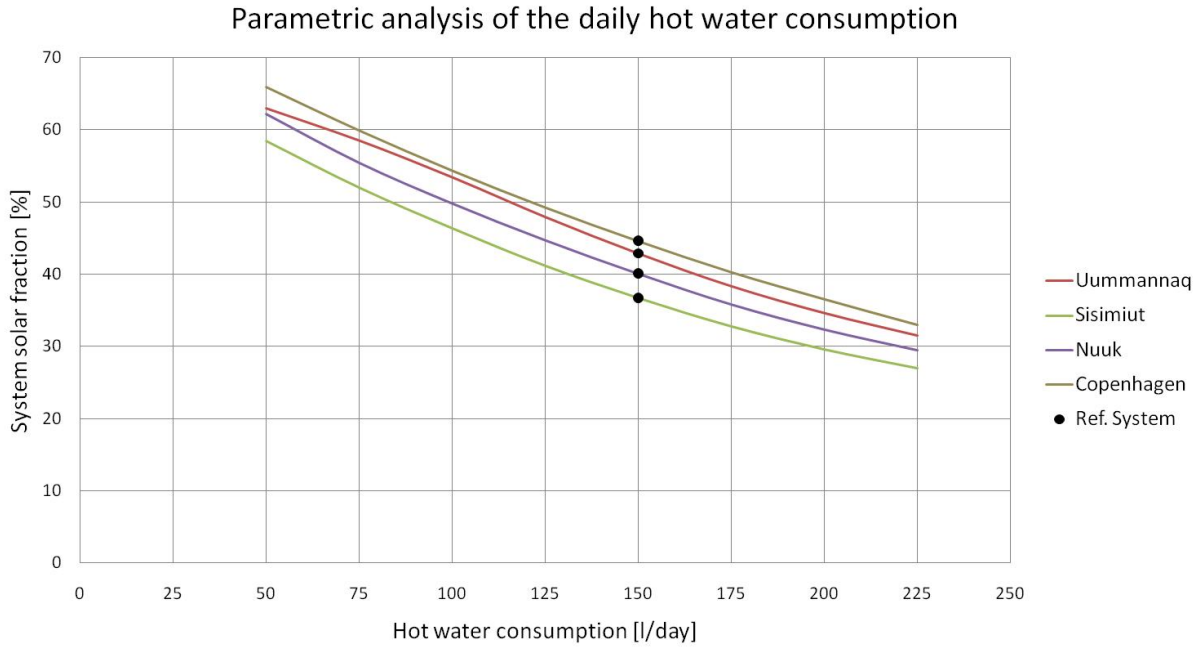

Figure 4.34 The system solar fraction as a function of the hot water consumption.

Draw off profile

The influence of the draw off profile is investigated, and several profiles are setup, see Table 4.7, all maintaining a daily hot water consumption of 150 litres. The draw off profile used in the reference system assumes tapping of 50 litres in morning, 25 litres just after noon and 75 litres in the evening, which is regarded to be a normal draw off profile. The other profiles investigated are where all 150 litres are tapped either in the morning, at noon or in the evening, and then 3 profiles where 100 litres are tapped either in the morning, noon or evening with additional tapping twice a day of 25 litres. See Table 4.7 for an overview of the profiles.

Table 4.7 Draw off profiles to investigate their influence on the performance of a system.

	Morning	**Noon/afternoon**	**Evening**
Ref. System	50 liters from 08:00-10:00	25 liters from 13:00-14:00	75 liters from 20:00-23:00
Primarily morning	100 liter from 06:00-10:00	25 liters from 13:00-14:00	25 liters from 20:00-21:00
Morning	150 liters from 06:00-10:00	-	-
Primarily noon	25 liters from 08:00-09:00	100 liter from 12:00-16:00	25 liters from 20:00-21:00
Noon	-	150 liters from 12:00-16:00	-
Primarily evening	25 liters from 08:00-09:00	25 liters from 13:00-14:00	100 liter from 19:00-23:00
Evening	-	-	150 liters from 19:00-23:00

The result of the simulations with the different profiles can be seen in Figure 4.35, showing that the highest performance is obtained with the profiles where the majority of the tapping takes place at noon. The reason for this is that the energy supplied by the sun is utilized right away, eliminating heat losses from being stored in the tank and then used at a later time. The poorest performance is when the tapping takes place in the morning, which is because the sun has no chance to supply the tank with energy, and the energy in the tank from the sun is at least a day 'old'.

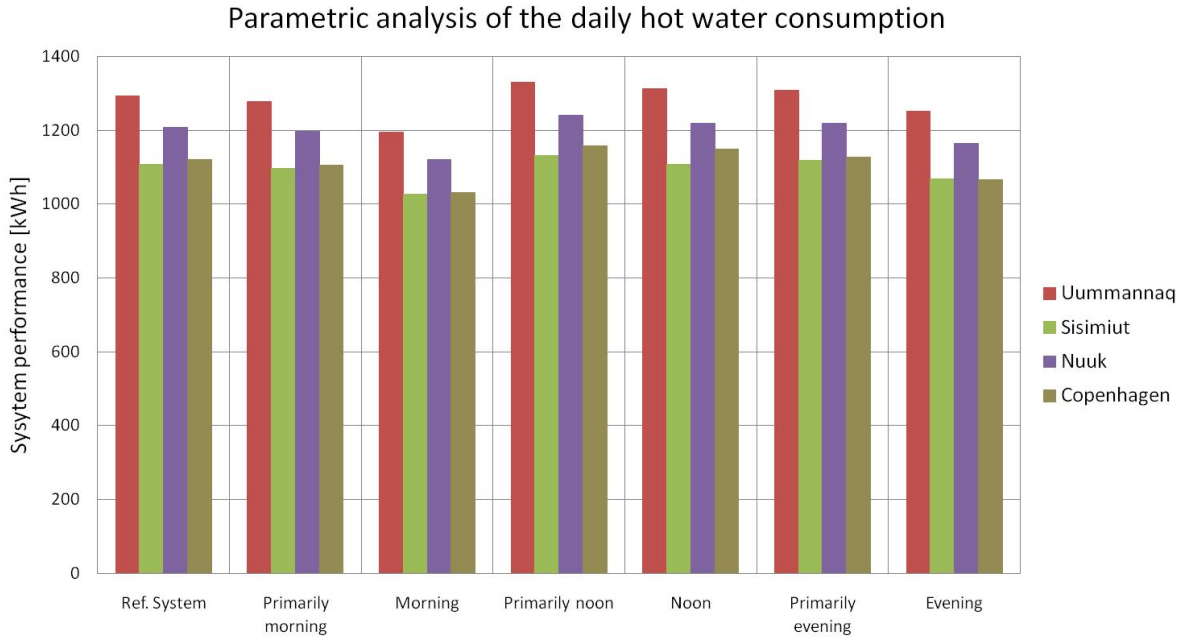

Figure 4.35 The system performance as a function of the hot water tapping profile.

4.3 Discussion

The yearly thermal performance of the solar heating system investigated here shows that a system solar fraction of up to 50 % can be obtained with a collector area between 3.0 - 4.5 m² depending on whether the location is Uummannaq, Sisimiut or Nuuk, assuming a daily hot water consumption of 150 l. This means that up to 50 % of the hot water demand of a single family house can be covered by energy from the sun. For a system in Copenhagen with a collector area of 3.0 m² the yearly thermal system solar fraction will be 55 %.

The placement of the solar collectors is important and the orientation should not deviate more than ± 30° from the optimum orientation for each of the locations. The tilt should not deviate more than 15° from the optimum. The optimum tilt at the 4 locations are: Uummannaq 60°, Sisimiut 57°, Nuuk 56° and Copenhagen 46°. The optimum orientations are: Uummannaq 5° towards west, Sisimiut 13° towards west, Nuuk 10° towards west and Copenhagen 5° towards east. A suitable collector for the Arctic conditions must have a low heat loss coefficient since the effects of the cold climate will decrease the

performance rapidly. Choosing a collector with anti reflection treated glass which results in a higher maximum efficiency will also improve the performance. The size of the collector area is dependent on the hot water consumption and the storage tank. In Denmark a rule of thumb says 1 m² per 50 l hot water consumption. In Greenland the collector area should be around 1 m² per 40 l hot water consumption. For a family of four with a hot water consumption between 150 l – 200 l, the collector area should be between 3.75 – 5.00 m².

The following recommendations can be given for the solar collector loop. The flow rate should be between 0.15- 0.20 l/min per m² collector area for low flow mantle systems. The pipes leading from the collector to the storage tank outside the building envelope should be as short as possible, and well insulated. The same is true for the pipe leading to the storage tank inside the building envelope.

The storage tank investigated here is a mantle tank and chosen for its advantages both in terms of performance, but also in terms of durability. For any storage tank chosen for a solar heating system sufficient insulation on the top and sides of the tank is important, and it is especially important to avoid pipes leading away from the tank through the top of the tank.

User habits influence the thermal performance of a solar heating system, and the recommendations is to have most of the hot water drawn in the afternoon and evening and limit the use in the morning, where the hot water most often is supplied by the auxiliary energy. Information of the volume of hot water consumption for the typical Greenlandic family is sparse, but based on the measurement from the Low energy house it can be assumed to be slightly higher than in Denmark. For dimensioning purposes it is therefore estimated to be a reasonable assumption that the hot water consumption in Greenland is 50-70 l per person in the house.

Chapter 5 Low Energy House in Sisimiut

In 2004 the building of a Low Energy House in Sisimiut, Greenland, began and the house was finished in April 2005, see Figure 5.1. The focus of the project was to minimise the energy consumption required for heating by using the latest technology within building methods, insulation, windows, ventilation and solar heating. The aim was to reduce the energy consumption for heating permitted in the new Greenlandic building code of 2006 by 50 %, which would result in a reduction from 160kWh/m² to 80 kWh/m² [Rode et al. 2009].

Figure 5.1. Low Energy House in Sisimiut, Greenland.

The house was built with increased insulation in the walls, floor and ceiling, and extra attention to the seal around the windows and doors. A ventilation unit with heat exchange was installed, along with 3-layered glass windows with a low emission coating and vacuum between the inner glasses. The house was also equipped with a solar heating system for heating the domestic hot water. The performance and experiences from the first 5 years is analysed and described in the following. It was of major importance that the house and its equipment, notably the solar heating system, was built and installed by local workers, thereby increasing their knowledge. By having local workers building and installing the equipment, the idea was that if and when problems did occur, the local workers had the skills to solve the problems in situ, with long distance support from the Technical University of Denmark.

The Low Energy House was designed as a double-house for two families, sharing an entrance hall and a boiler room, with a total floor area of 197 m², see the floor plan in Figure 5.2. During the first 5 years the number of occupants has varied, from fully occupied to periods with no habitants. At the present time only one side of the house, apartment 1, is occupied fulltime by a family of two. Apartment 2 is used as an exhibition and as guest house for visitors.

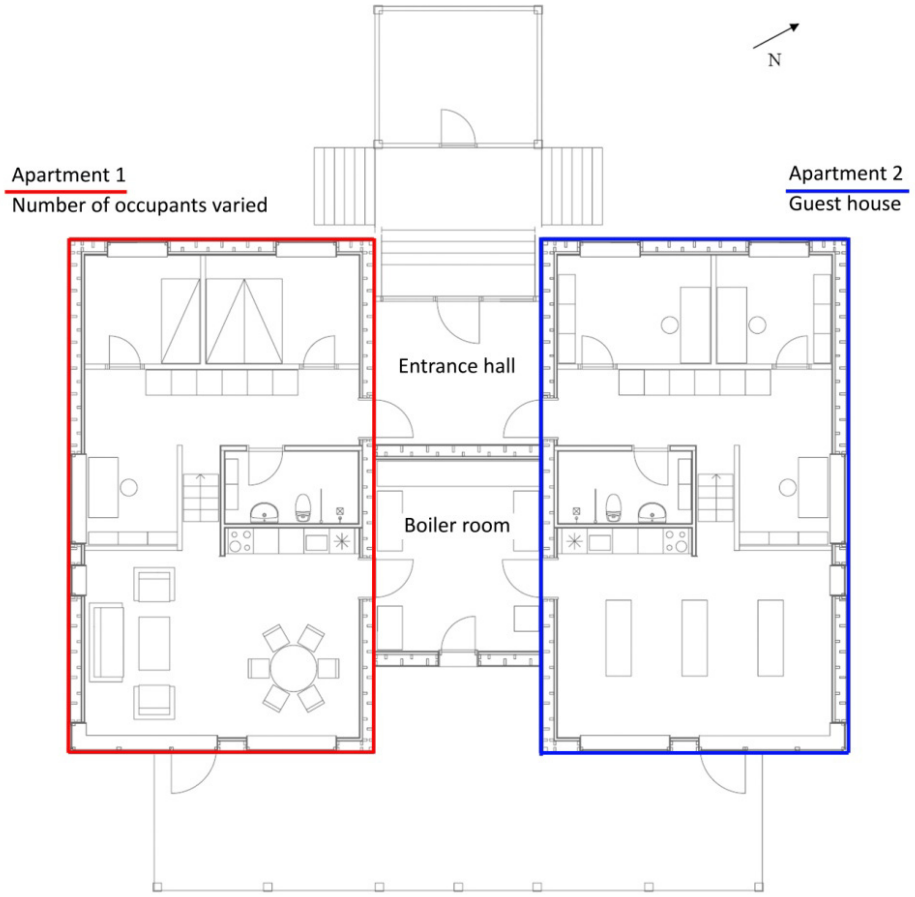

Figure 5.2. Floor plan of the Low Energy House in Sisimiut, Greenland.

5.1 System design

The solar heating system installed in the Low Energy House is an over dimensioned system for heating the domestic hot water, with an additional option for sending heat to a radiator in the entrance hall during very sunny periods [Furbo and Shah 2002]. The system consists of 6 flat-plate solar collectors from Velsun (now Velux) type S08, see Figure 5.3 left. The collectors are installed with a tilt of 70° and are oriented 56° towards east from south. The transparent area of the collectors is 8.31 m², and the collectors have a max efficiency of 0.79 and a heat loss coefficient of 4.121 W/m²K.

The efficiency of the solar collector is:

$$\eta = 0{,}79 \cdot k_\theta - 3.756\frac{(T_m - T_a)}{G} - 0.0073\frac{(T_m - T_a)^2}{G} \qquad (5\text{-}1)$$

where the incidence angle modifier k_θ is:

$$k_\theta = 1 - tan^{4.04}\left(\frac{\theta}{2}\right) \qquad (5\text{-}2)$$

Figure 5.3. Flat-plate solar collectors on the Low Energy House and the installations in the boiler room.

The storage tank installed is a 265 l steel mantle tank from Nilan A/S, type Danlager 2000, see Figure 5.3 right. The storage tank is equipped with both a top spiral and an electric heating element for heating the auxiliary volume of 74-85 l. In- and outlets for the domestic water are situated at the bottom of the tank, which reduces the heat loss through thermal bridges. The storage tank is insulated sufficiently with 65 mm PUR foam at the top, 50 mm at the sides and 30 mm at the bottom.

An expansion vessel is installed in the solar collector loop, and has a volume of 18 l which is sufficient for the collector area. A rule of thumb for dimensioning the expansion vessel recommends that the volume of the expansion vessel be 3 times the volume of the fluid content in the solar collectors for systems, where

boiling is allowed in the solar collectors, by turning off the circulation pump during sunny periods with high system temperatures [Peres et al. 2003, Dragsted et al. 2009]. Since the solar collectors each has a volume of 0.9 l the expansion vessel should therefore have a minimum volume of 16.2 l.

The system is designed with a radiator installed in the solar collector loop, with a 3-way valve and a control unit, so that in sunny periods, when the storage tank is fully heated, the 3-way valve will open and supply heat for the entrance hall. It is connected directly on the return line from the solar collectors, so the storage tank can be by-passed, see Figure 5.4.

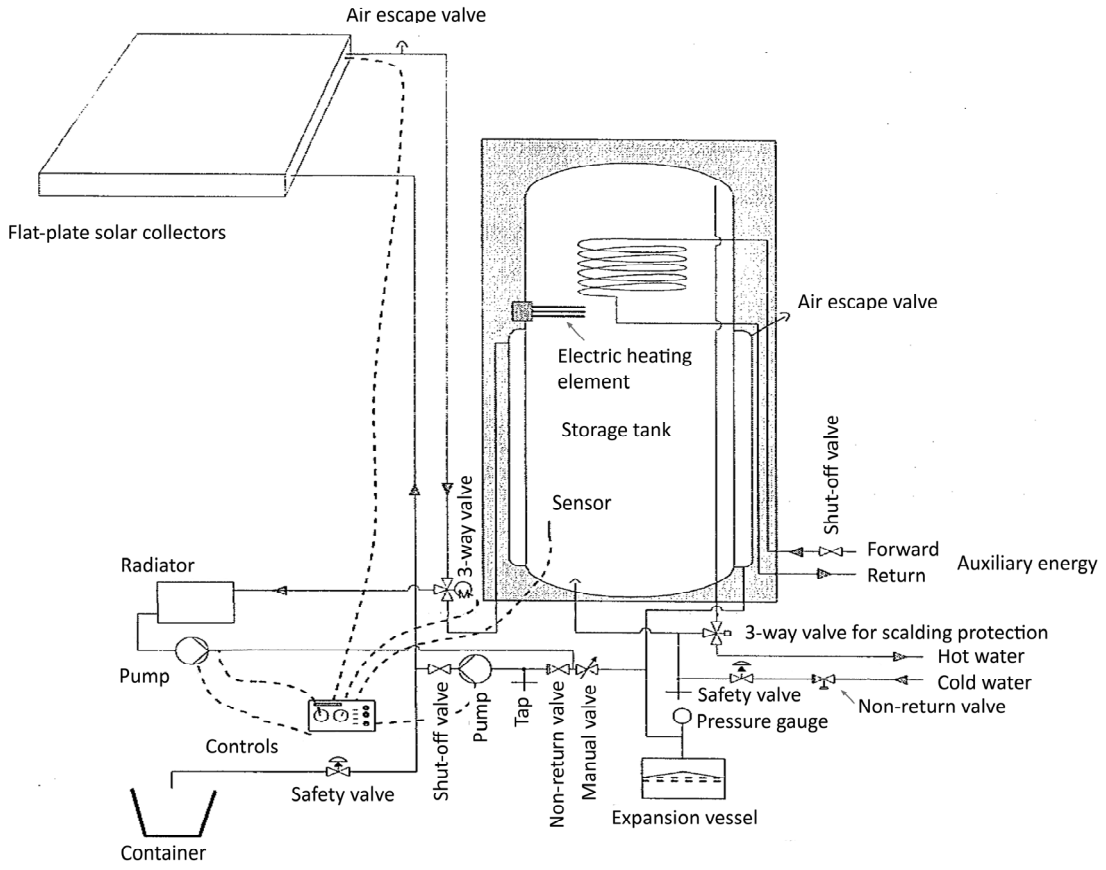

Figure 5.4. Schematic of the system design of the solar heating system in the Low Energy House in Sisimiut.

5.2 Thermal performance of the solar heating system

The house was equipped with numerous sensors to monitor the performance of the individual systems and monitor comfort levels in the house. It is evaluated on a yearly basis by the Department of Civil Engineering at Technical University of Denmark [Rode 2006, Rode 2007, Rode 2008, Vladykova 2009, Kotol et al.].

The monitoring system for the solar heating system consists of 4 energy meters, measuring the energy transferred from the solar panels, the domestic hot water consumption, the auxiliary energy supply to the

hot water tank and the solar heat sent to the radiator in the entrance hall, all in kWh. The measuring period which is analysed here is from July 2005 until December 2010. In order to analyse the performance of the solar collectors and the system, the global radiation is evaluated alongside the measurements from the system. The global radiation over the period is obtained from different measuring stations located in Sisimiut, since there is no pyranometer installed on the Low Energy House. Figure 5.5 shows the locations, from which the global radiation is measured and used in this analysis.

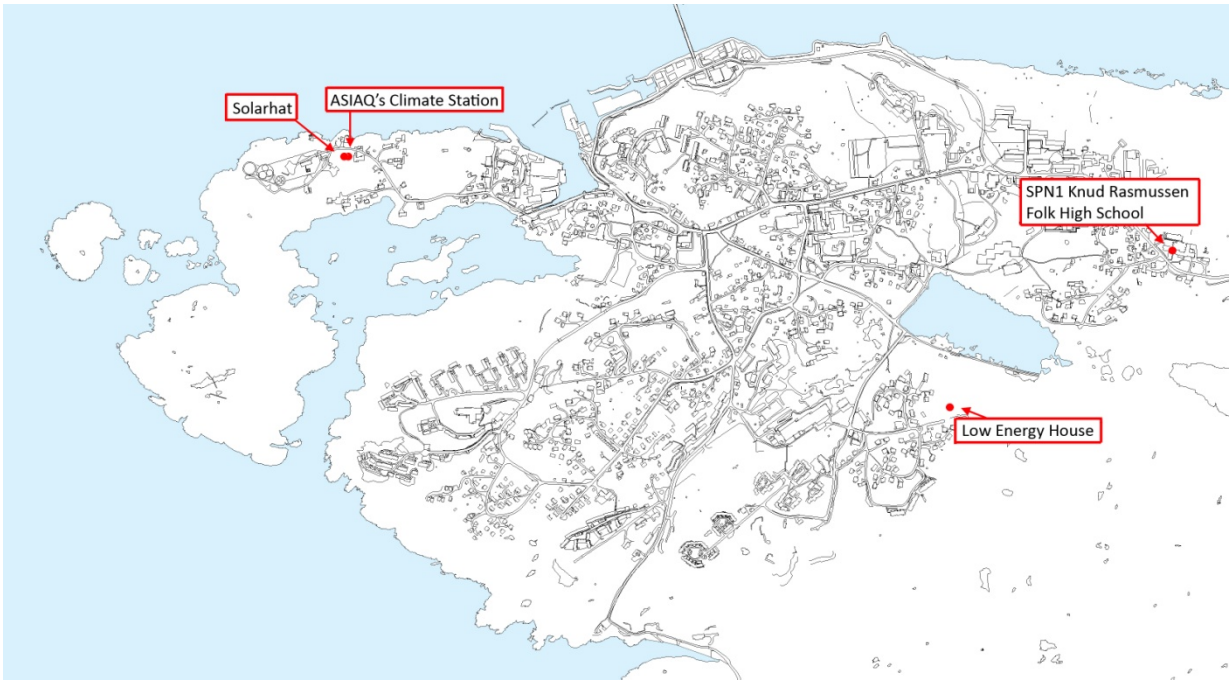

Figure 5.5. Locations where the global radiation is measured in Sisimiut.

Even though the global radiation is taken from different locations, it is assessed that the influence from shadows on the individual locations in terms of the mountains is a matter of a time shift and is so small that it can be disregarded.

5.2.1 Yearly summary of the measurements

The measurements from the solar heating system in the period from July 2005 until December 2010 can be seen in Table 5.1. The energy from the solar collectors to the hot water tank varies throughout the years with the difference in received radiation, but is also very dependent on the control setting and hot water consumption. The measurements of the energy from the solar collectors are also attached, unfortunately with errors, since it was discovered that thermosyphoning occurs in the system in cold periods without sunshine. In this way large energy quantities are lost from the hot water tank. Thermosyphoning is registered by the energy meter as energy production by the solar collectors, and thereby indicates too high an energy production.

The measurements of the hot water consumption show the variation in numbers of occupants in the house. For a period of 9 months, from July 2007 to March 2008, there were no inhabitants in the house

which is seen in the measurements from both 2007 and 2008. The average hot water consumption is 113 l/day which in connection with the varied number of occupants is a normal consumption. Measurements from 2010 show the yearly average consumption to be 128 l/day which is higher than normally would be expected from a family of two compared to Danish standards.

The energy consumption transferred from the auxiliary energy source to the hot water tank is an average of 2047 kWh a year. It can be seen in Table 5.1 that the measured energy for auxiliary energy is higher in 2006 compared to the average. This can be explained by an increase in hot water consumption especially in the winter months, where the consumption is around 20 % higher than the average.

The excess solar energy describes the solar heat sent to the radiator in the entrance hall, and the measurements shows that for the first 3½ years no energy was sent to the radiator. This was due to faulty equipment and an installation error which will be described later. In 2009 and 2010 the measurements shows that the radiator finally received energy, 823 kWh in 2009 and 684 kWh in 2010.

The global radiation varies throughout the years, with an average of 852 kWh/m² a year.

Table 5.1 The yearly measurements form the Low Energy House from 2005 to 2010.

	Solar heat to tank	**Dom. hot water consumption**	**Aux. energy to tank**	**Solar heat to radiator**	**Global radiation**	**Calculated total solar radiation on a surface tilted 70° and oriented 56° East******
	[kWh]	[kWh]	[kWh]	[kWh]	[kWh/m²]	[kWh/m²]
2005 (July –December)	690	1200	1279	0	330*	286
2006	1793	2591	2574	0	827*	720
2007	2351	1200	1091	0	833**	690
2008	4226	1553	1228	0	895**	713
2009	3058	2370	1828	823	941**	780
2010	2576	2747	1859	684	862***	711

* Global radiation measurements from the Solarhat at Teleisland in Sisimiut.

** Global radiation measurements from ASIAQ's measuring station at Teleisland in Sisimiut.

*** Global radiation measurements from SPN1 at Knud Rasmussen Folk High School in Sisimiut.

**** Calculated using the Erbs. correlation and the isotropic model on an hourly basis with the reflection from the ground calculated using the equations from chapter 3.

5.2.2 Changes to the system

After the installation of the system it was noticed that the delivered pipes, from Velux type ZFM and ZFR, for the forward and return line to the collectors were installed without reducing the length according to the distance between the solar collectors and the storage tank. This resulted in several meters of pipe laid curled up in the attic of the Low Energy House. This was due to lack of experience of the installers, because they did not know that they should reduce the pipe length as much as possible. The pipes were refitted and the length reduced in the summer 2007.

Thermosyphoning turned out to be a problem in the system, and was observed at night time on several occasions, especially during the winter months where the driving force in terms of temperature difference between the ambient temperature and the temperature in the storage tank was highest. It was first noticed in December 2006, and then again in 2007 and 2008 in a much stronger way, see Figure 5.6. The reason why the thermosyphoning increased in 2007 and 2008 was due to the former mentioned reduction of pipe length to and from the collectors, which reduced the pressure drop in the pipes and therefore improved the conditions for thermosyphoning. In December 2009 a magnetic valve was installed on the forward line to the solar collectors to prevent thermosyphoning. The valve is controlled with a signal from the pump, so that it will close if the pump is not in operation. The effects of the valve can be seen in the beginning of 2010, but unfortunately the problem with thermosyphoning seems to be returning in the end of 2010, which could be due to debris in the pipes, which block the valve and prevents it from closing, see Figure 5.6.

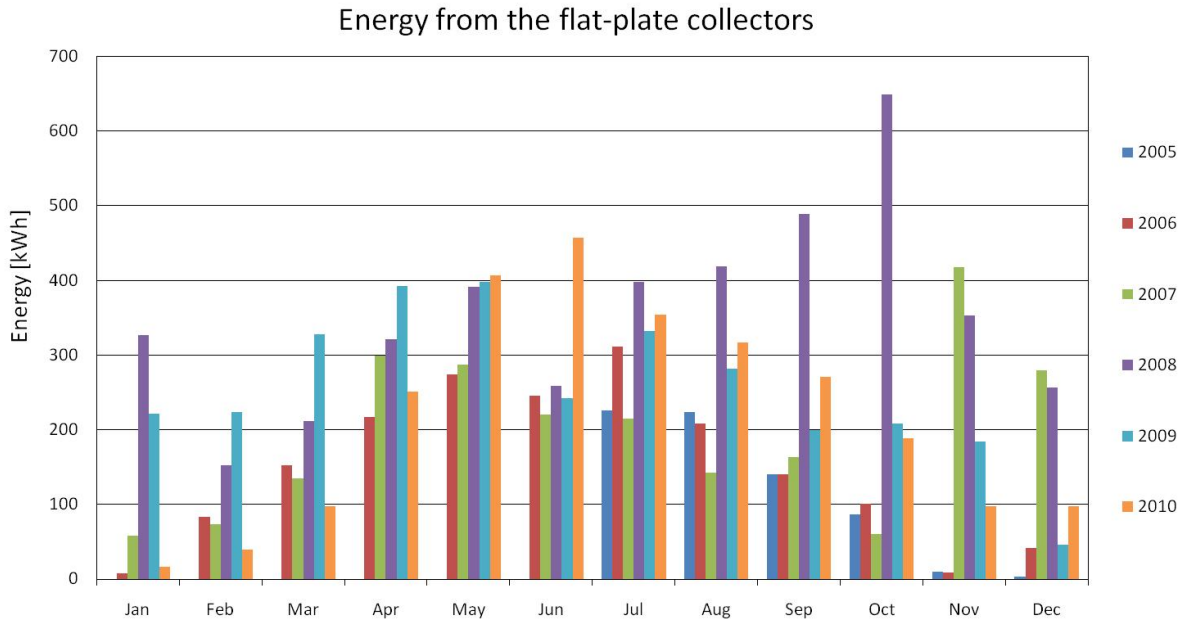

Figure 5.6 The performance of the flat-plate collectors from July 2005 to December 2010.

The measurements show that using the radiator as a bypass for the system in sunny periods did not work as planned. A valve was supposed to open when the storage tank was completely loaded and send the

solar collector fluid through the radiator in the entrance hall and from there back to the collectors. It was therefore decided to replace both the valve and the control unit sending the signal to the valve, from March of 2009, to ensure that the problem was fixed. During the installation it was noticed that the valve was blocked by debris from the installation like pieces of wood, metal shaving and such, so it might not have been the equipment failing but rather human errors during installation.

Because of these findings in 2009 it is reasonable to believe, that since the thermosyphoning seems to be returning in the end of 2010 it is again leftover debris which prevents the magnetic valve from fully closing to prevent the thermosyphoning.

An unfortunate result of the repair to the system is that the temperature in the entrance hall reaches very high levels. The intention of the radiator was to allow the system also to produce heat to the entrance hall in very sunny periods. Since the number of habitants has been reduced the storage tank is more often fully loaded because the energy withdrawn is reduced. More energy than intended is therefore sent to the radiator. Also the entrance hall has large window areas and receives large amounts of solar radiation when the sun is shining, reducing the need for addition heat. The radiation should have been placed in a room where direct solar radiation is not available through windows. To correct this, the radiator was temporarily moved outside in May 2010, awaiting a major renovation of the system which will be undertaken in the summer of 2011.

A full investigation of the system in the spring of 2010 revealed the most critical system installation error to date. The forward and return line from the collectors had been reversed, so that the hot return from the collectors were connected to the bottom of the mantle and the cold forward line to the collectors was connected to the top of the mantle. This of course had a strong influence on the performance, as it destroyed the stratification in the storage tank. The pipes were swapped to the correct position in May 2010.

In the summer of 2010 3 students were given the task of analyzing and investigating the system by applying temperature sensors on the outside of the pipes in the boiler room in the Low Energy House [Ørbæk et al. 2010]. They found that the 3-way valve connected to the radiator would open when the top of the hot water tank reached 65 °C and the bottom reached 60 °C, which means that the hot water tank is not fully loaded when heat is sent to the radiator. The 3-way valve should open when the top of the tank reaches 95 °C and the bottom 80 °C. This has yet to be changed in the system controls.

5.2.3 Yearly thermal performance of the system

Based on measurements from the first 5 years of operation the performance of the solar heating system was evaluated. The net utilized solar energy is defined as the tapped energy minus the energy supplied by the auxiliary energy to the tank, see equation (5-3). The calculated net utilized solar energy is therefore very dependent on the hot water consumption both in terms of volume and time of year when the tapping takes place. The solar fraction is defined as the net utilized solar energy divided by the tapped energy, see equation (5-4), which makes the solar fraction equally dependent on the hot water consumption, in terms of how much and when.

Net utilized solar energy = Tapped energy + Radiator energy – Auxiliary energy *(5-3)*

Solar fraction = Net utilized solar energy / (Tapped energy + Radiator energy) *(5-4)*

Including the energy sent to the radiator is not the conventional way of calculating the net utilized solar energy and solar fraction, but is assed here to give a more accurate picture of the performance of the system.

Both the net utilized solar energy and the solar fraction are calculated for the Low Energy House from 2005 until 2010, see Table 5.2. It can be seen that both the net utilized solar energy and the solar fraction vary from year to year, because of the variation in hot water consumption, see Figure 5.7. Also the initial setup of the system has had an influence on the performance of the system along with the changes to the system throughout the years. The highest values are reached in 2010 for the system, but this performance is unfortunately 7.5 % lower than expected in the preliminary investigation carried out by Simon Furbo and Louise Shah [Furbo and Shah 2002].

The utilized solar radiation is the net utilized solar energy divided by the solar radiation received by the surface, see equation (5-5).

Utilized solar radiation = Net utilized solar energy / Radiation received by the collectors *(5-5)*

The low utilization of the solar radiation from the collectors is connected with both the varying consumption but also the faulty setting in the controls of the system.

Table 5.2 The yearly performance of the solar heating system at the Low Energy House from 2005 to 2010.

	Hot water consumption	Net utilized solar energy	Solar fraction	Calculated total solar radiation on a surface tilted 70° and oriented 56° East *	Utilized %age of the solar radiation
	[kWh]	[kWh]	[%]	[kWh/m²]	[%]
2005 (July –December)	1200	-79	-7	286	-3.3
2006	2591	17	1	720	0.3
2007	1200	109	9	690	1.9
2008	1553	325	21	713	5.5
2009	2370	1365	43	780	21.1
2010	2747	1572	46	711	26.6

* Calculated using the Erbs. correlation and the isotropic model on an hourly basis with the reflection from the ground calculated using the equations from chapter 3.

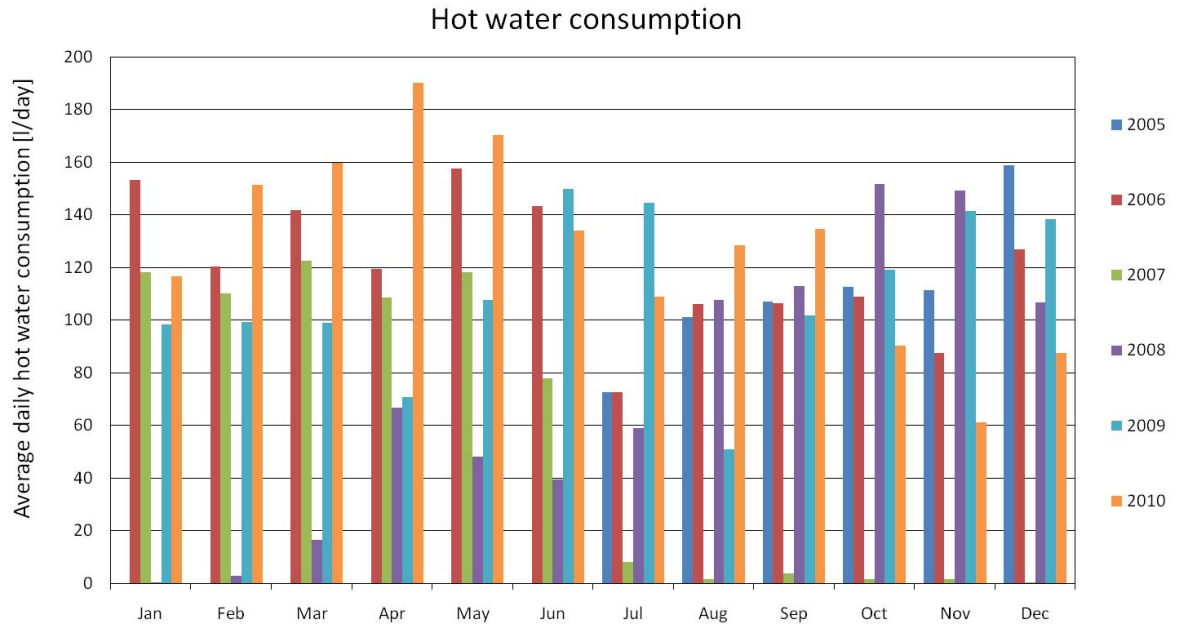

Figure 5.7 The average daily hot water consumption from July 2005 to December 2010.

5.3 Discussion

The Low Energy House in Sisimiut has through the years provided data and important experience on solar heating systems in an Arctic climate.

Installation

Proper training of the installers is of major importance, both in connection with installation of a new system but also in connection with repairs of the system. Errors with debris and not fitted pipes in the solar collector loop are easy to avoid, if the installers are made aware that this can cause problems later on in the system. Errors with incorrect connection of the pipes from the solar collector could be solved using colour-codes. By using red and blue tape and marking both ends of the pipes before installation, it would be possible to have a 'cold' and 'warm' pipe which could help insure that similar errors does not happen again.

Design

An important experience gained from the system at the Low Energy House is an awareness of the effects of thermosyphoning, which can be a large problem under Arctic conditions. The large difference between the ambient temperature and the temperature in the storage tank during the winter months gives a potential driving force for thermosyphoning, which will take heat from the storage tank and cool it in the solar collectors before returning it to the storage tank. Installing a magnetic valve controlled by the operation of the pump in the solar collector loop will solve the problem, so the valve closes when the pump is not in operation.

It is also important to have correct control settings, which is not specific for Greenland but true for any solar heating system. When the temperature setting for the heating of the tank is too low, the performance of the system is very poor.

Another important experience from the system at the Low Energy House is the confirmation that a pressurized system with an expansion vessel is suitable for Arctic conditions. Greenland is more frequently affected by power-outages than Denmark, which is why it is important to take into account that power for the circulation pump may be cut during sunny periods causing the solar collector fluid to boil and expand, requiring an expansion vessel to handle the overflow.. In the 5 years the system has been in operation there has been no problem with the solar collector fluid escaping from the loop and it has not been necessary to refill the system.

Thermal performance

Over the years the thermal performance of the solar heating system has been improved by correcting the errors found. The solar fraction reached 46 % in 2010, which must be considered a good performance of

the system, when hot water consumption is taken into account, although it still is 7.5 % lower than estimated performance.

There are still things that could help optimize the system. First of all it is expected that the performance of the system would improve, if the house was fully occupied by two families as originally planned. If that is not possible, the alternative solution with a bypass-radiator, which is now temporarily placed outside, should be improved by moving the radiator to a room without big window areas or connect the by-pass to the existing space heating system of the house. Since the thermosyphoning seems to have happened again in 2010 it is important in the future to secure that the magnetic valve always is working well. If these problems could be solved, it is not unrealistic to expect that the solar fraction could exceed at least 50 %.

It is recommended to educate installers and use pre-fabricated components of solar heating systems in Greenland. By using such components the risk of installation errors are reduced.

Chapter 6 Knud Rasmussen Folk High School in Sisimiut

The Knud Rasmussen Folk High School (KRH) was established in 1962 as the first Folk High School in Greenland. The school is located in Sisimiut, see Figure 6.1, and through the years the school has played an important role in maintaining the cultural heritage in Greenland.

Figure 6.1. Map showing the location of the Knud Rasmussen Folk High School in Sisimiut.

In the summer of 2008 a large solar heating system was installed on the school. The system is based on flat plate collectors and evacuated tubular collectors see Figure 6.2. It is the first system in Greenland, where evacuated tubular solar collectors are installed vertically on the roof in such a way, that solar radiation from all directions can be utilized. It was also, at the time of installation, the largest system in Greenland, with a collector area of 62.4 m². The system supplies energy for both the domestic hot water loop and for the space heating loop.

Figure 6.2. Knud Rasmussen Folk High School in Sisimiut, Greenland.

The KRH contains both classrooms and dormitories for the students. During summer the school is open for tourists to stay in the otherwise vacant dormitories.

6.1 System design

The solar heating system at the KRH is a combined domestic hot water and space heating system designed and installed by the Swedish company ExoHeat (now ExoTech). The system consists of both flat plate and evacuated solar collectors and has a transparent area of 62.4 m², where the transparent area of the flat plate collectors is 20.7 m² and the transparent area of the evacuated tubular collectors is 41.7 m². The placement of the collectors can be seen in Figure 6.3.

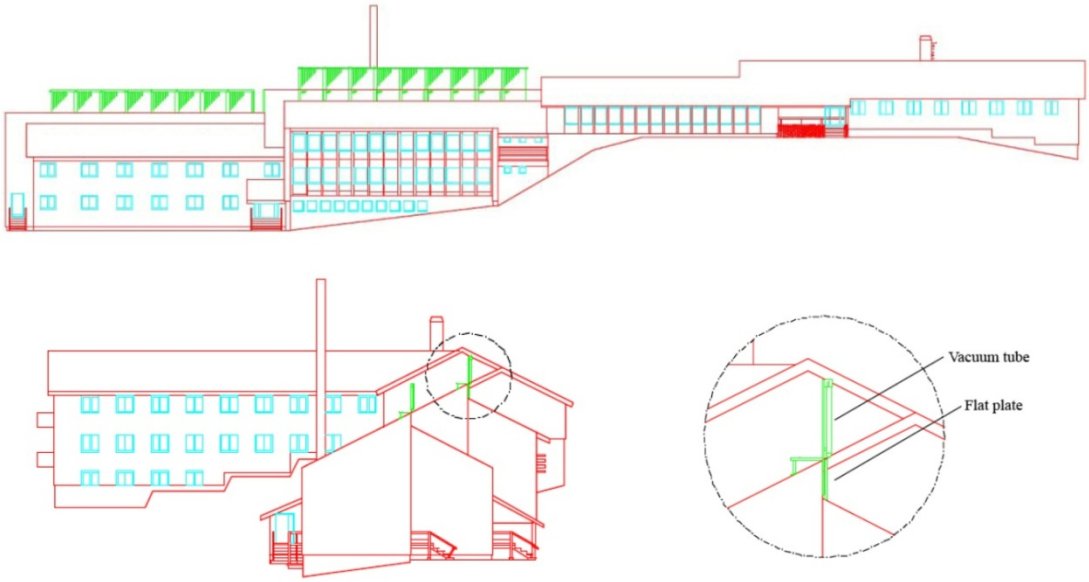

Figure 6.3. Schematic drawing of the placement of the solar collectors on the KRH.

The 9 flat plate collectors are from Sonnenkraft type SK500L, with an absorber area of 2.21 m² per collector. The collectors are placed vertically on the rise between the two sides of the roof. The in- and outlet to the collectors is at the top of the collectors, which potentially can cause problems during stagnation in the collectors. The two manifolds in each of the collectors are placed vertically with horizontal strips going between them.

The efficiency of the flat plate solar collectors is:

$$\eta = 0.778 \cdot k_\theta - 3.384\frac{(T_m - T_a)}{G} - 0.016\frac{(T_m - T_a)^2}{G} \qquad (6\text{-}1)$$

Where the incidence angle modifier k_θ is:

$$k_\theta = 1 - tan^{3.93}\left(\frac{\theta}{2}\right) \qquad (6\text{-}2)$$

The 17 evacuated tubular collectors are from Exoheat (now ExoTech) type VA 1585 Arctic, with an transparent area of 4.9 m² and a gross area of 4 m² per collector. The evacuated tubular collectors are also placed vertically, but at the highest point of roof, so the collectors are not shielded by the building in any direction. The collectors use the heat-pipe principle, where the solar collector fluid in the solar collector loop passes by the condenser in the manifold collecting the heat from the heat-pipe.

The connection to the collectors from the boiler room is by 3 separate strings, one for the flat plate collectors and two for the evacuated tubular collectors. The flat plate collectors are installed in two series with 4 in one series and 5 in the other series, see Figure 6.4.

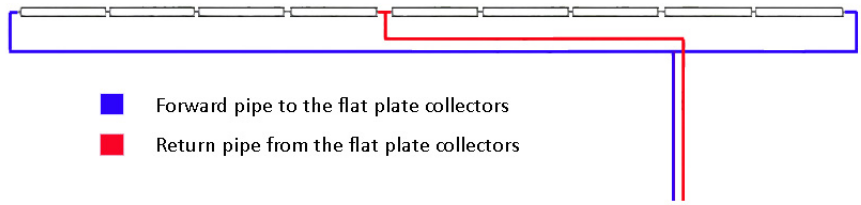

Figure 6.4 Schematic of the pipes going to and from the flat plate collectors.

The evacuated tubular collectors are also connected in series, divided into two, so the first string has 9 collectors and the second has 8 collectors, see Figure 6.5 and Figure 6.6.

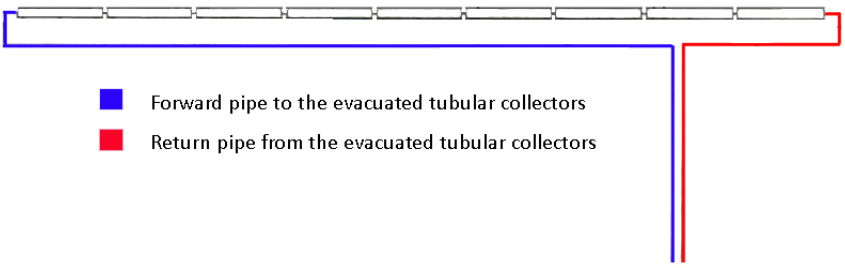

Figure 6.5 Schematic of the pipes going to and from the first string of evacuated tubular collectors.

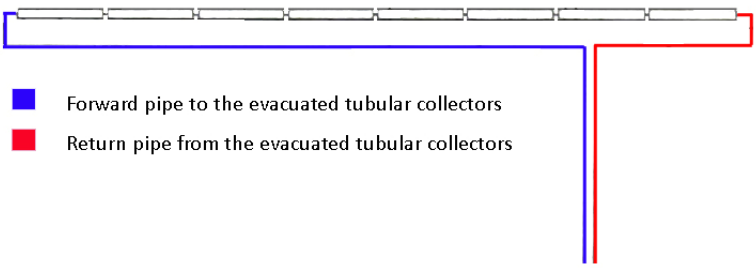

Figure 6.6 Schematic of the pipes going to and from the second string of evacuated tubular collectors

The control of the solar collectors is designed in such a way that the pump driving the solar collector fluid to the flat plate collectors will start when there is a positive gain in difference of temperature between the temperature in the bottom of the tank and the temperature in the flat plate collectors. In this way the flat plate collectors is used to pre-heat the solar collector fluid before solar collector fluid enters the

evacuated tubular collectors. In periods where there is no sun on the flat plate collectors, the pump driving the solar collector fluid to the flat plate collectors will be turned off, since the temperature gain will be negative, because the temperature difference between the bottom of the tank and the temperature in the flat plate collectors is negative. This control setting utilizes the advantages in terms of a smaller heat loss coefficient of the evacuated tubular collectors compared with the flat plate collectors.

The storage tank installed in the boiler room is also from Sonnenkraft type PS2000, with a volume of 2000 l. The tank is designed as a preheating storage tank, with external heat exchangers both for charge and discharge of the storage tank. The energy from the solar collectors is transferred by an external heat exchanger of the type SLM50, which also holds the controls for the solar collector loop, see Figure 6.7.

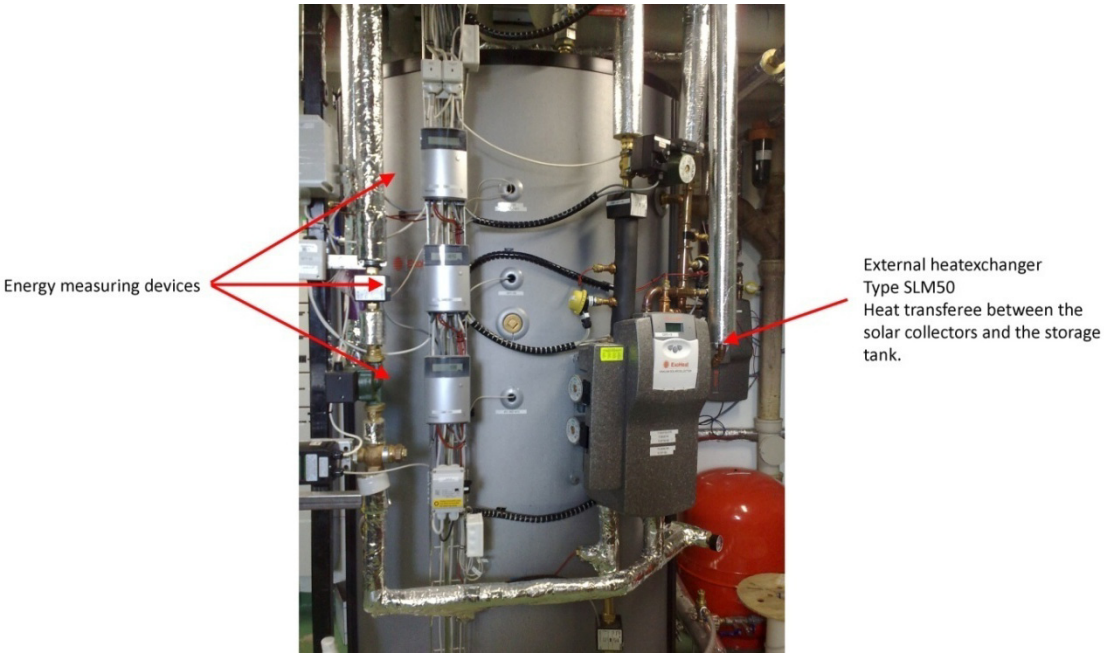

Figure 6.7 Picture of the storage tank with the external heat exchanger and energy measuring devices

The SLM50 is designed to induce and maintain stratification in the storage tank. It is connected to the tank in two levels; at the top of the tank and at the middle of the tank, see Figure 6.8.

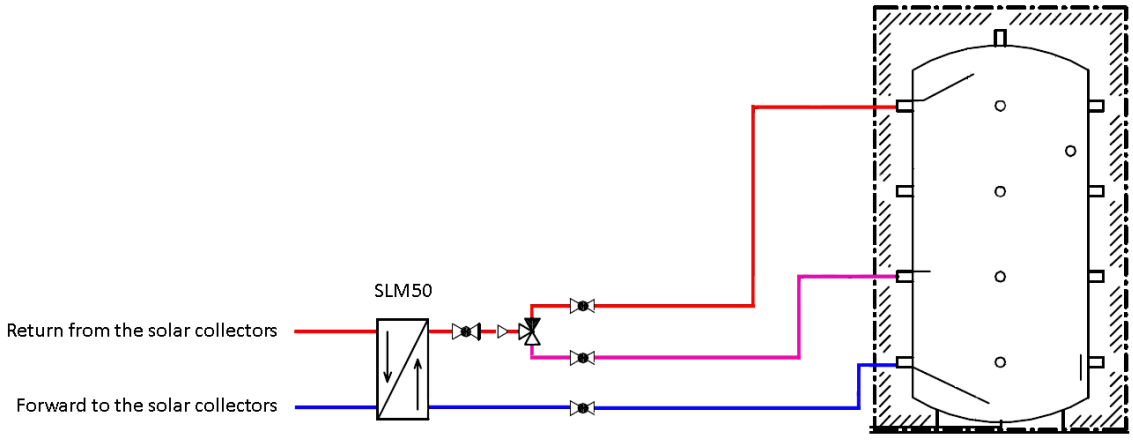

Figure 6.8 Schematic figure of the connection from the SLM50 to the storage tank.

The SLM50 will, based on the temperature that is delivered from the solar collectors, open the appropriate valve and send the heat into the storage tank at the right level.

The storage tank delivers hot water to the domestic hot water loop and the space heating loop both to the old and new part of the school. The division of the school into new part and old part is shown in Figure 6.9. The priority of the system is first to deliverer energy for the domestic hot water consumption in the new part of the school. The secondary priority is to deliver energy to the space heating loop of both the new and the old part of the school along with the domestic hot water for the old part of the school.

Figure 6.9 A schematic showing the division of the school into to old part and new part.

The domestic hot water loop for the new part of the school is connected to two heat exchangers where the first will raise the temperature of the cold water inlet by means of solar energy, and the second will further raise the temperature if needed with energy from the oil burner, see Figure 6.10.

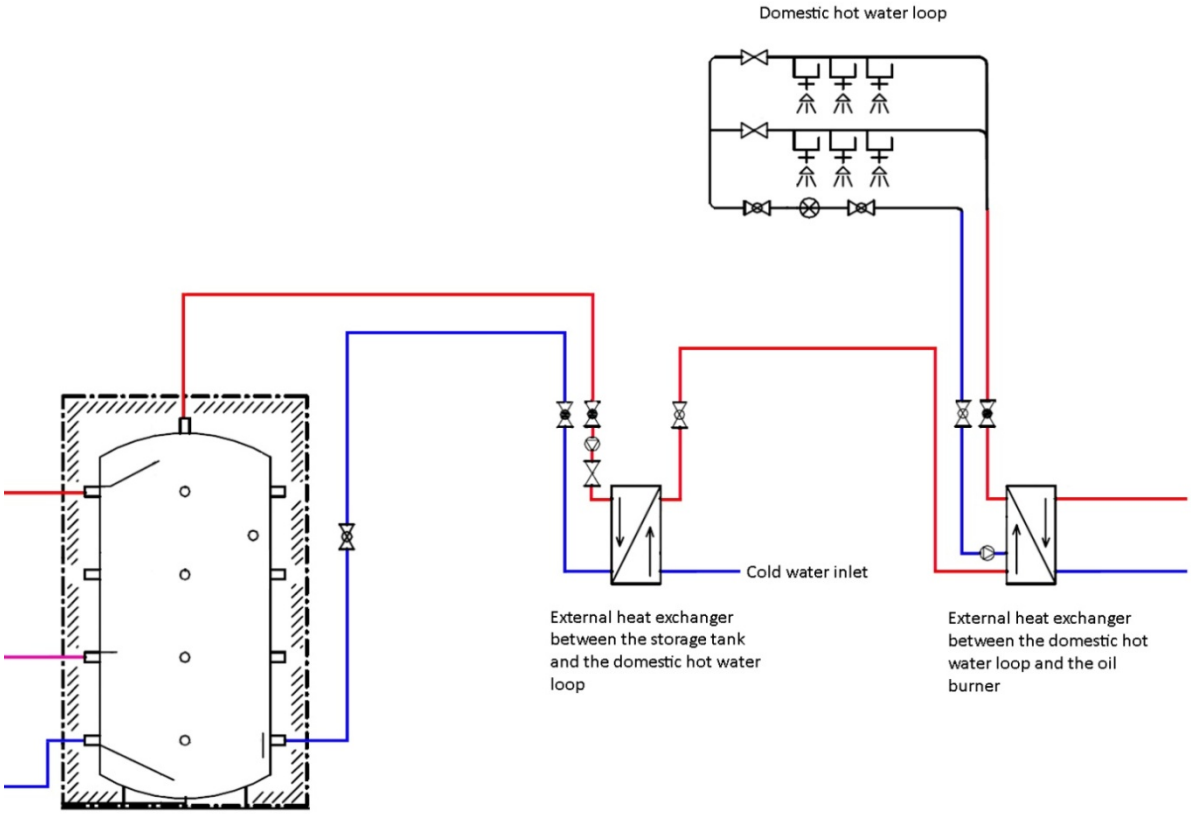

Figure 6.10 Schematic figure of the domestic hot water loop with the two heat exchangers.

The connection to the space heating loop is shown in Figure 6.11. Here it can be seen that hot water is taken from the storage tank just above the middle of the tank. The return from the space heating loop is connected to the lower inlet of the two leading back from the heat exchanger from the solar collector loop. The aim of the connection to the space heating loop is to raise the return temperature to the oil burner, thereby decreasing the energy needed to reheat the water before sending it back to the space heating loop. The figure also shows how the old part of the school is connected both for domestic hot water and space heating. The return from the domestic hot water for the old part of the school is connected to the forward line to the space heating also for the old part of the building.

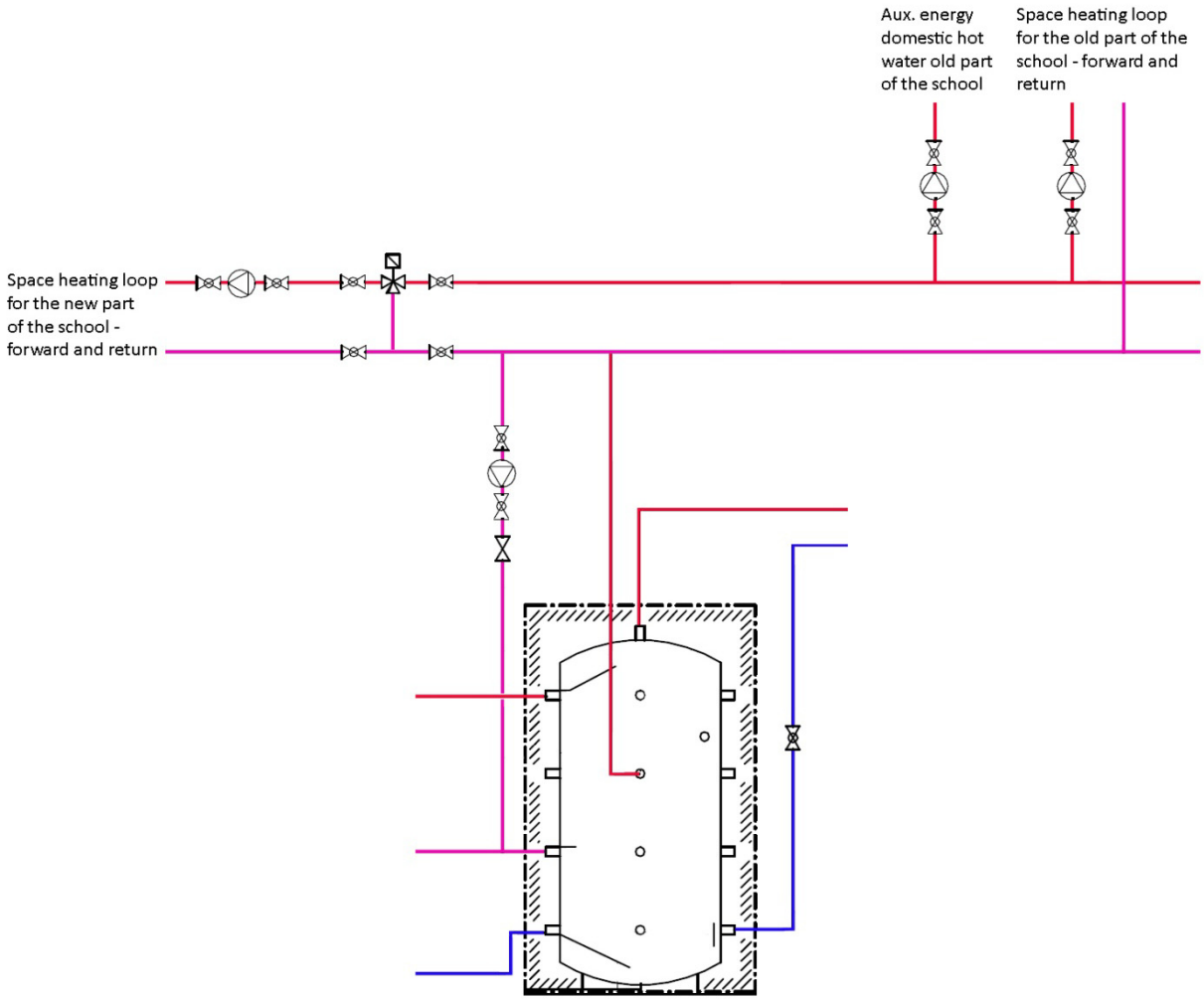

Figure 6.11 Schematic figure of the connection to the space heating loop in the new part of the school and the further connection to the old part of the school.

The estimate from Exoheat regarding the yearly thermal performance of the system states that the solar gain will be 46 MWh and the useful energy will be the same, corresponding to 737 kWh per m² collector per year.

6.2 Thermal performance of the solar heating system

The system at KRH is equipped with numerous measuring devices monitoring the temperatures, energy quantities and solar radiation.

The energy measurements are:

1. Energy supplied from the solar collectors to the external heat exchanger, on the glycol side of the external heat exchanger.
2. Energy supplied by the external heat exchanger - from the solar collectors to the storage tank, on the water side of the external heat exchanger.
3. Energy consumption for the domestic hot water loop in the new part of the school.
4. Energy supplied to the domestic hot water for the new part of the school from the storage tank.
5. Energy supplied from the oil burner to the domestic hot water for the new part of the school.
6. Energy consumption for space heating in the new part of the school.
7. Energy supplied to the space heating loop in the new part of the school from the storage tank.

Besides the energy consumptions measured, temperature measurements are made including the ambient temperature. The global and diffuse radiation is also measured, with a SPN1 pyranometer as mentioned in chapter 2.

6.2.1 Yearly summary of the measurements

The system was installed in the summer of 2008 and taken into operation in August of 2008. Unfortunately several errors and wrongful connections were made during the installation of the monitoring system. These were corrected in the late spring of 2009. This means that even though the system has been in operation since August 2008, the evaluation period here is from the 27th of May 2009 to the 31st of December 2010, see Table 6.1 and Table 6.2. Initially viewing the measurements reveal a fault in the system in the months of April, May, June and July of 2010, see Table 6.2. An electronic device in the controls for the heat exchanger delivering heat from the storage tank to the domestic hot water was defective. Therefore no solar energy was transferred to the domestic hot water from the storage tank in these months.

Table 6.1 Measurement from the system at KRH from 2009.

2009

	Solar heat to tank (Glycol)	Solar heat to tank (Water)	Dom. hot water consumption new part	Energy from tank to dom. hot water new part	Aux. to dom. hot water new part	Energy space heating new part	Energy from tank to space heating new part
	[kWh]	[kWh]	[kWh]	[kWh]	[kWh]	[kWh]	[kWh]
May	376	294	293	212	153	1065	194
Jun	1931	1573	1084	917	573	6076	567
Jul	2796	2196	689	696	365	3776	1686
Aug	2685	2393	1132	1121	383	3711	1233
Sep	1726	1615	1518	1221	720	7759	194
Oct	1144	1078	1953	1026	1365	12661	26
Nov	212	209	1775	267	1944	17765	5
Dec	2	2	510	28	918	1542	2
Total [MWh]	10.9	9.4	9.0	5.5	6.4	68.2	3.9

Table 6.2 Measurement from the system at KRH from 2010.

2010

	Solar heat to tank (Glycol)	Solar heat to tank (Water)	Dom. hot water consumption new part	Energy from tank to dom. hot water new part	Aux. to dom. hot water new part	Energy space heating new part	Energy from tank to space heating new part
	[kWh]	[kWh]	[kWh]	[kWh]	[kWh]	[kWh]	[kWh]
Jan	2	3	1073	116	6911	1422	1
Feb	897	861	1737	779	6058	1342	4
Mar	1670	1611	1743	697	6672	1465	479
Apr	1154	1079	1360	0	4804	1710	773
May	591	557	898	1	2309	1027	208
Jun	914	889	252	1	1353	273	630
Jul	773	715	834	1	862	861	420
Aug	579	524	770	393	798	382	73
Sep	550	900	1482	552	2248	932	0
Oct	388	707	1665	455	4642	1261	0
Nov	40	66	1936	185	5531	1794	0
Dec	0	0	595	67	2272	547	0
Total [MWh]	7.6	7.9	14.3	3.2	44.5	13.0	2.6

In the following each of the measurements is presented graphically, where the starting point of the measurement from 2009 is raised to that of 2010 at the same time, in order to visualise the difference in the development throughout the year.

Energy supplied from the solar collectors to the storage tank, both glycol and water

The measured energy from the solar collectors to the storage tank is shown in Figure 6.12. Here it is evident that the energy produced by the solar collectors in 2010 is significantly lower than in 2009. The reason for this is unclear, but could be an effect of the defective electronic component decreasing the energy taken from the tank and thereby the energy delivered to the tank. This will increase the temperatures in the collectors and increase the periods with stagnation, and in the worse case cause the solar collector fluid to leave the solar collector loop through the safety valves because of the build up of pressure in the solar collector loop.

Also the figure shows the heat loss from the heat exchanger where the heat from the solar collector fluid (glycol) is transferred to the water medium in the storage tank. This is of course higher for 2009 where more energy is transferred compared to 2010, where less energy is transferred to the tank.

The reason why the transferred energy to the tank increases to levels above what has been delivered from the solar collectors towards the end of 2010 is due to the positive gain from the temperature in the boiler room.

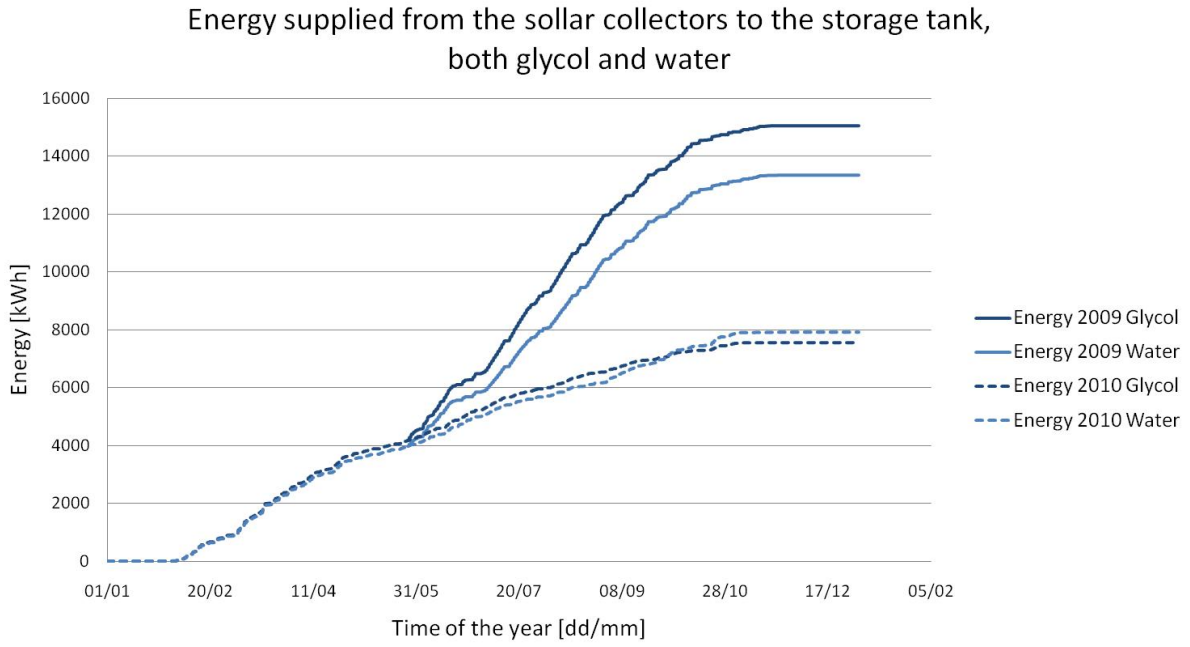

Figure 6.12 The supplied energy from the solar collectors to the storage tank in kWh.

Energy consumption for the domestic hot water in the new part of the school

The energy consumption for the domestic hot water for the new part of the school is shown in Figure 6.13. The consumption from 2009 seems to slow down for two weeks in the end of June, most likely due to the end of a semester and students leaving the school. The same occur in December where it is reasonable to assume that the students again will leave the school to go home.

The measurements from 2010 shows the same trends, with the only differences that the semester ends for summer holiday in the middle of May, and the Christmas holiday starts a little later.

The hot water consumption in the 7 months of operation in 2009 was 9.0 MWh. The consumption in the same 7 months of 2010 was 7.5 MWh, slightly lower compared to 2009. The yearly consumption in 2010 was 14.3 MWh.

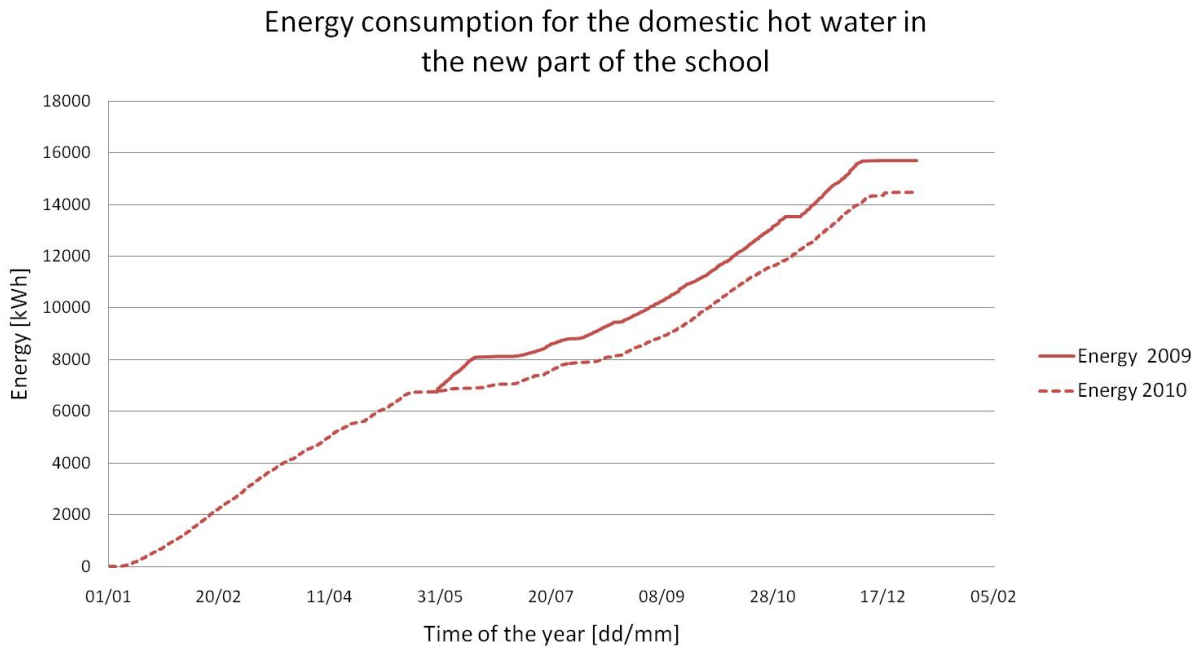

Figure 6.13 The hot water consumption in kWh for the new part of the school.

Energy supplied from the storage tank to the domestic hot water for the new part of the school

As mentioned earlier control system electronics problems meant that no energy was sent from the storage tank to the domestic hot water in the period from April to July in 2010, which is seen clearly in Figure 6.14.

The measurements from 2009 show that there is a two week period from the middle of June to the end of June where there is either no available hot water in the storage tank, no need for hot water in the new part of the school or an fault in the system. A reasonable explanation for this is that the semester has ended and therefore the students have left the school. As there is a two week gap until summer students

arrive, there is no need for hot water. At the end of 2009 it can be seen that the same occurs and no energy is transferred from the storage tank to the domestic hot water. The reason here is that there is no energy in the storage tank to transfer, since there is very little solar radiation at this time.

From the measurements from 2010 it can be seen that the supply of energy to the domestic hot water from the storage tank begins in February, and delivery of energy continues until the time when the fault occurs. After the fault has been corrected the energy delivered from the storage tank to the domestic hot water is lower than at the same time in 2009. The reason for this is, evaporation of solar collector fluid causing less energy to be transferred from the collectors to the storage tank and therefore less energy can be transferred from the tank to the domestic hot water.

The total amount of energy transferred from the storage tank to the domestic hot water for the 7 months of 2009 was 5.5 MWh which means that more than half of the energy consumption for the hot water in the new part of the school was covered with energy from the solar heating system. In all 12 months of 2010 only 3.2 MWh was transferred, due to the electrical fault during the spring and summer.

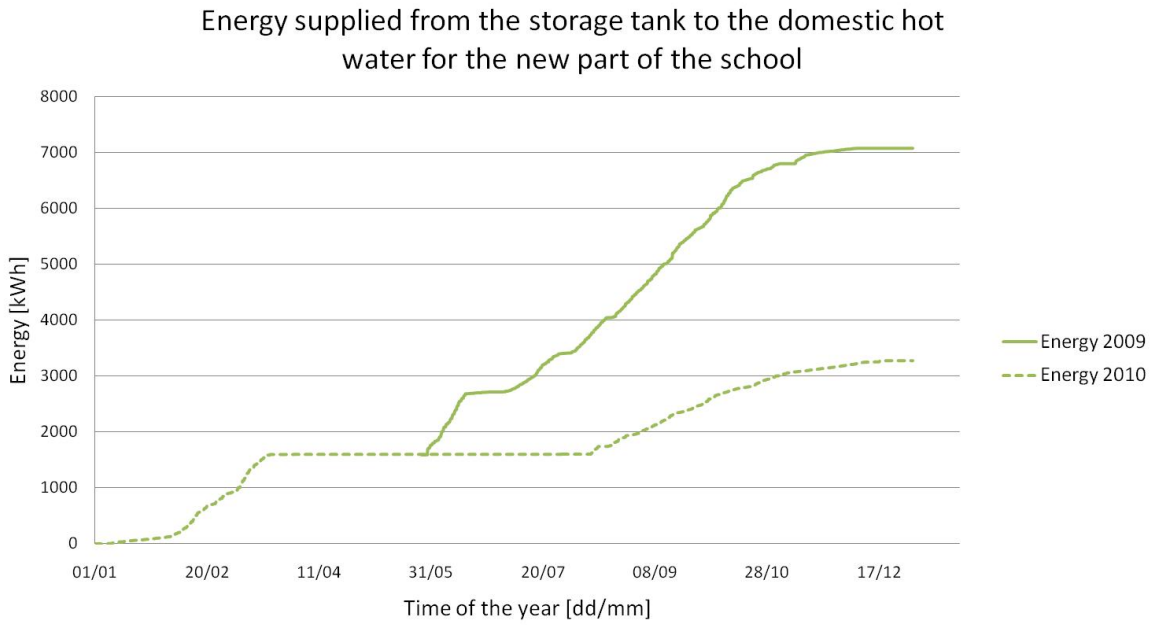

Figure 6.14 The energy from the storage tank used to heat the domestic hot water for the new part of the school in kWh.

Energy supplied from the oil burner to the domestic hot water for the new part of the school

The energy supplied from the auxiliary energy system to the domestic hot water for the new part of the school can be seen for both 2009 and 2010 in Figure 6.15. Although there was an control system fault during the summer of 2010, this has not caused an increase in the energy needed from the auxiliary system. This is connected to the decrease in demand of hot water during the summer months, which means the effect will be less noticeable.

The figures from both 2009 and 2010 follow the same trends as seen for the hot water consumption with a steady consumption in the spring, fall and winter time. During the summer where it is assumed there are few students in the school the consumption decreases.

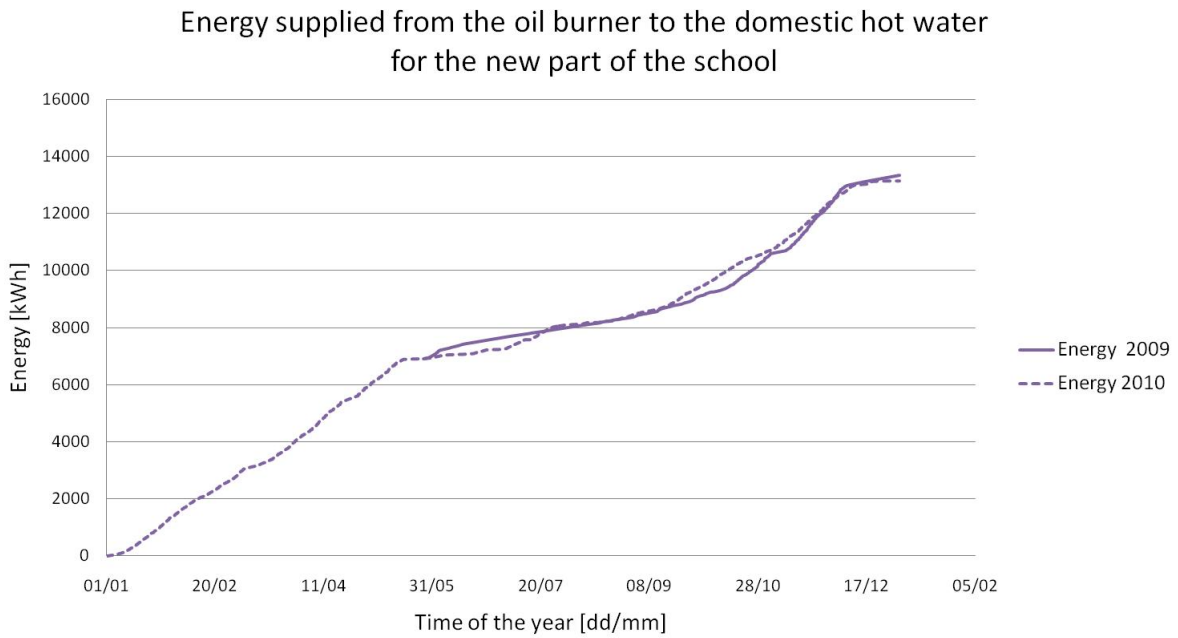

Figure 6.15 Auxiliary energy for the domestic hot water consumption for the new part of the school in kWh.

The supplied energy from the auxiliary system for the 7 months of 2009 was 6.4 MWh. During the same months in 2010 the energy from the auxiliary system was 6.1 MWh, which is a slightly lower compared to 2009 because of the decrease in hot water consumption. The total amount of auxiliary energy needed for the domestic hot water in 2010 was 13.0 MWh.

Energy consumption for space heating in the new part of the school

The energy used for space heating in the new part of the school can be seen in Figure 6.16. As expected the need for space heating is highest in the fall, winter and spring months because of the Arctic climate. On the figure it can be seen that there also is a need for space heating during the summer, which is due to the low ambient temperature. Again the consumption in 2009 is slightly higher than in 2010. The energy needed for space heating in the 7 months where the measuring system was in operation in 2009 was 68.2 MWh. The total demand in 2010 was 113.1 MWh.

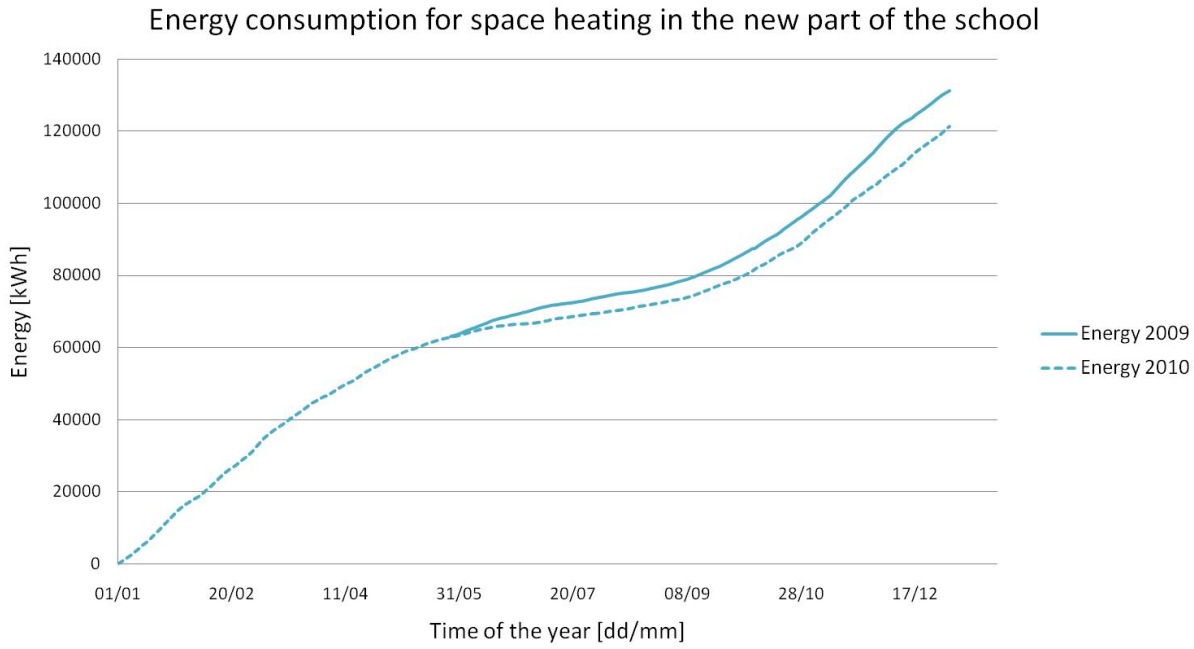

Figure 6.16 The space heating demand for the new part of the school in kWh.

Energy supplied from the storage tank to the space heating loop for the new part of the school

In Figure 6.17 the energy transferred from the storage tank to the space heating loop is shown. Here it can be seen that the energy transferred in 2009 is much larger than in 2010. The control system fault preventing the system from transferring energy to the domestic hot water loop, should have allowed for more energy to be transferred to the space heating loop.

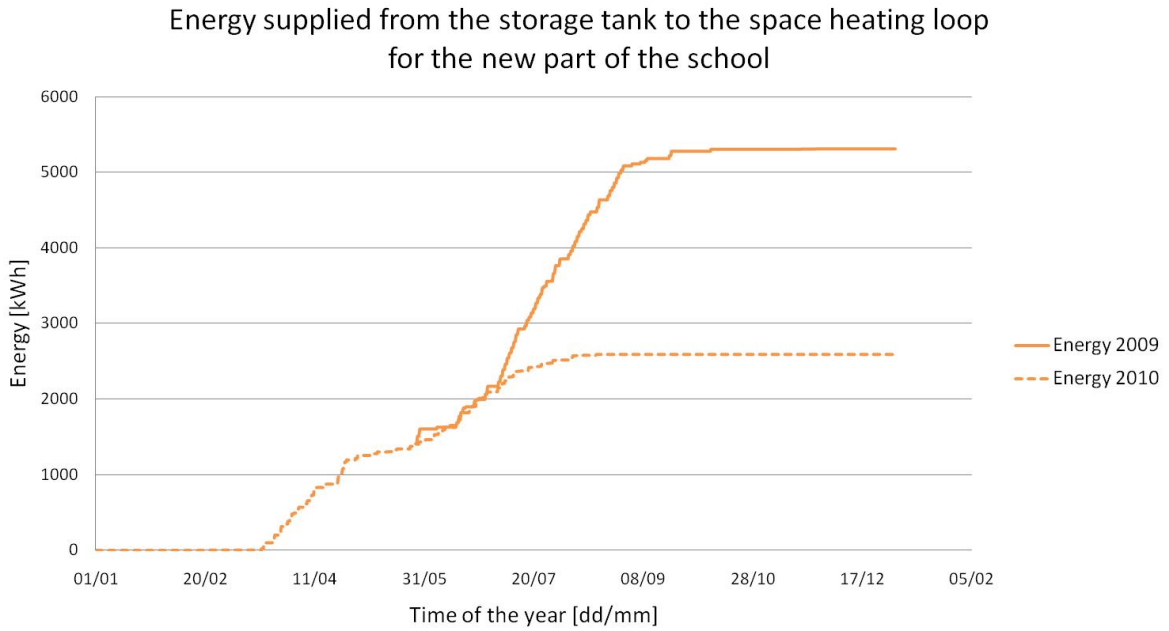

Figure 6.17 The energy from the storage tank used in the space heating loop for the new part of the school in kWh.

The energy supplied from the storage tank to the space heating loop was in 2009 3.9 MWh. In the same months in 2010 only 1.1 MWh was transferred from the tank to the space heating loop, meaning a reduction of more than 70 % compared to the measured value from 2009. The total amount transferred from the tank to the space heating loop in 2010 was 2.6 MWh.

The reason for this decrease in transferred energy is unclear, but suggests that there may be a fault in the control of the system and on the priority between transferring heat for hot water consumption and space heating. When the tank is fully loaded, or the bottom of the tank reaches 60 °C, then energy should be transferred to the space heating loop if of course there is a need for space heating. In June 2010, when the system was unable to supply energy to the hot water loop, the consumption for space heating was 3142 kWh, but only 630 kWh was transferred from the storage tank.

6.2.2 Changes to the system

As mentioned earlier the system was thoroughly checked in the spring of 2009, by both an electrician from DTU and a craftsman from OV-Consult. The measuring system was corrected for faulty connections and misplaced sensors. In the design and installation of the system OV-Consult found several things which needed attention.

The system was set in operation in August 2008 and during the first months the solar collector fluid left the system numerous times. There were two reasons for this:

1. One of the tools used for the pipe connections was faulty, causing the solar collector fluid to leak out at every other pipe connection.
2. The circulation pump in the solar collector loop was not strong enough. When boiling occurred in the solar collectors the pump was unable to empty the collectors sufficiently, thereby causing the remaining fluid to continue boiling and the pressure to increase causing the connections between the collectors to come apart.

These two faults were corrected and a new and stronger pump was installed.

Another problem was located in the air escape valve on the roof, causing the solar collector fluid to leave the system. A small paper ring inside the valve responsible for opening the valve allowing air in the solar collector loop to escape, had been ‘eaten’ by the glycol in the solar collector fluid. The valves were therefore removed, under the assumption that the new stronger pump will be able to push air out of the collector. There is still the possibility to release air in the solar collector loop through manual valves on the roof. This change in the system may have induced the problem of solar collector fluid leaving the solar collector loop, since the air cannot escape from the loop through the valve, and therefore it is not removed until someone manually releases the air on the roof.

In the forward line from the storage tank to the space heating loop risk of thermosyphoning was noticed in the design of the system, therefore a non-return valve was installed to insure that thermosyphoning does not occur.

6.2.3 Yearly thermal performance of the system

Determination of the yearly thermal performance in terms of net utilized solar energy and solar fraction is not possible because the total energy supplied from the auxiliary energy system is not measured. Therefore the thermal performance of the system will be evaluated in terms of available solar radiation and utilization of the energy provided by solar collectors and how well the system supplied energy to the hot water loop and the space heating loop.

The amount of available solar radiation is based on the measurements of global and diffuse radiation from the roof of the building, measured with a SPN1 pyranometer. Using the isotropic radiation model it is estimated how much solar radiation is received by both the flat plate collectors and the evacuated tubular solar collectors. The evacuated tubular solar collectors are made up of round tubes with a receiving backside, making it difficult to calculate the received solar radiation because of the determination of area and orientation. They are here assumed to consist of two flat surfaces, one facing in the same direction as the flat plate collectors and one facing the opposite direction. The area used for the evacuated tubular collectors facing either direction is the transparent area: the width of the glass multiplied with the length of the tube.

Using the isotropic radiation model and the measurements of the global and diffuse radiation from the SPN1, the received radiation can be calculated, see Figure 6.18. The measurements from 2009 are again from the 27th of May to the 31st of December. The measurements from 2010 are for the whole year.

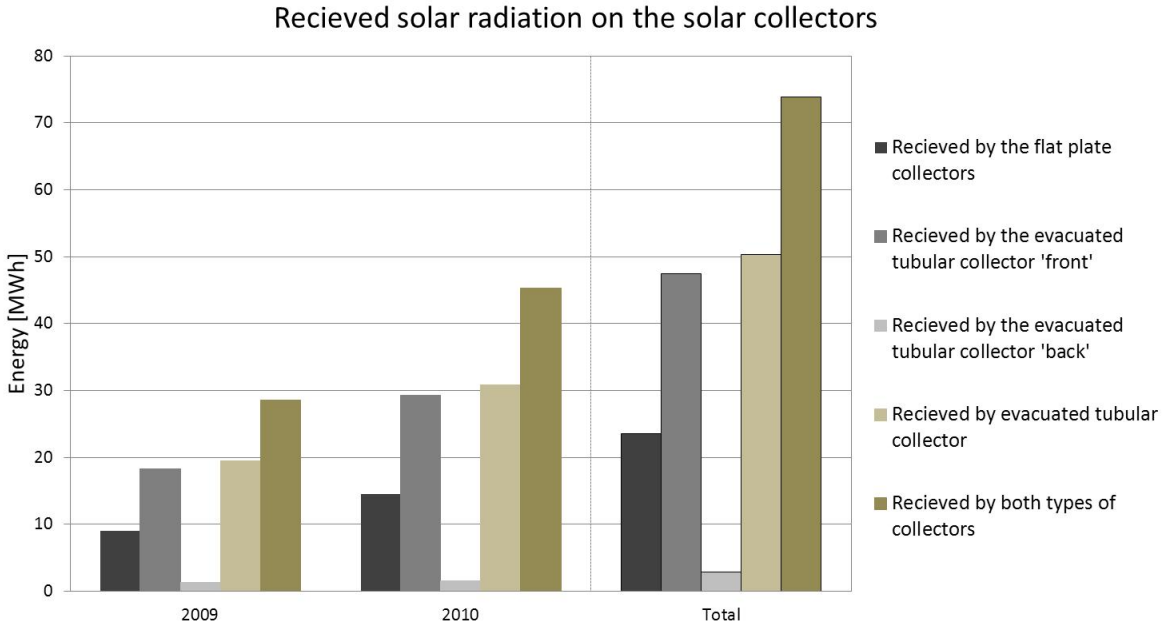

Figure 6.18 The received radiation by the flat plate collectors and the evacuated tubular collectors.
As the transparent area of the evacuated tubular collectors is twice that of the flat plate collectors, the received radiation on the 'front' is also twice as high. The radiation received on the back of the evacuated tubular collectors is almost as high as that received by the flat plate collectors.

In Figure 6.19 the thermal performance of the solar collectors can be seen. The figure shows that even though the amount of solar radiation received in 7 months of 2009 was lower than the radiation received in the whole of 2010, the produced energy was higher in the 7 months of 2009 compared to the values from 2010. This could again be explained by the loss of fluid in the solar collector loop. The ratio of solar radiation which was turned into energy sent to the storage tank for the 7 months of 2009 was 24 %, and only 12 % for 2010.

The total amount of energy produced by the solar collectors form 27th of May 2009 to the 31st of December 2010, was 17 MWh, which is considerably less than the 46 MWh a year that was the estimate by Exoheat.

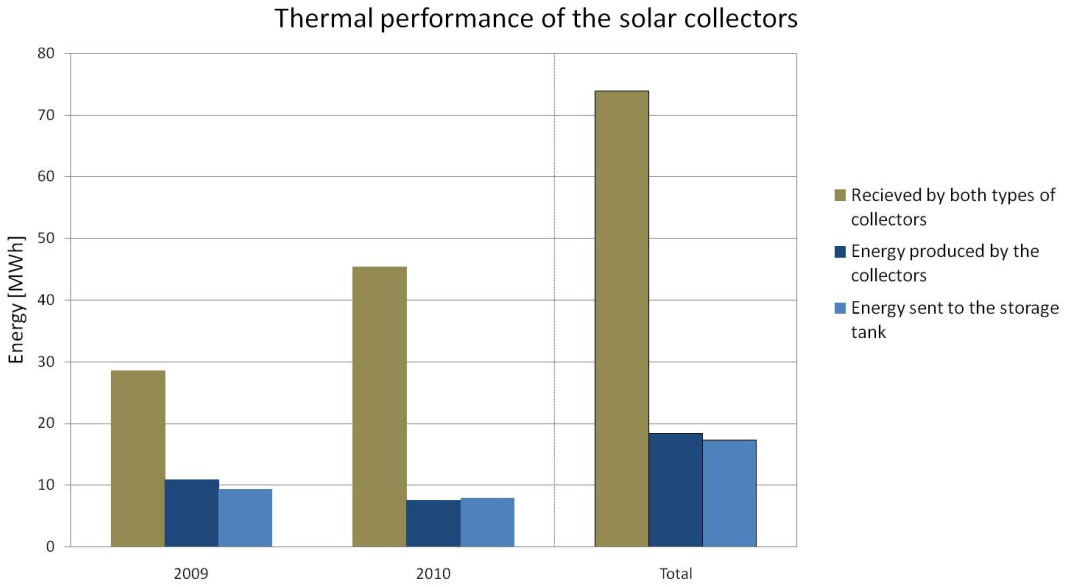

Figure 6.19 The thermal performance of the solar collectors.

As mentioned earlier, the priority of the system is first to supply the domestic hot water loop and then the space heating loop. In Figure 6.20 the amount of energy transferred to the domestic hot water consumption and the space heating loop can be seen. In the 7 months of 2009, 5.5 MWh was transferred to the domestic hot water loop and 3.9 MWh for the space heating loop. In 2010 3.2 MWh was transferred to the domestic hot water loop and 2.6 MWh to the space heating loop. With four months during the spring and summer of 2010, where no energy was transferred to the domestic hot water loop, the total amount transferred from the tank to the domestic hot water loop in 2010 was as expected, less than what was transferred in the 7 months of 2009. It would be expected that in 2010 the energy transferred to the space heating loop would be equally higher, because of the 4 four months where no

energy was transferred to the domestic hot water consumption, thereby leaving more energy available for the space heating loop. The figures shows that this is not the case, and supports the conclusion that the solar collector fluid has evaporated out of the system and therefore less energy is produced in the solar collectors.

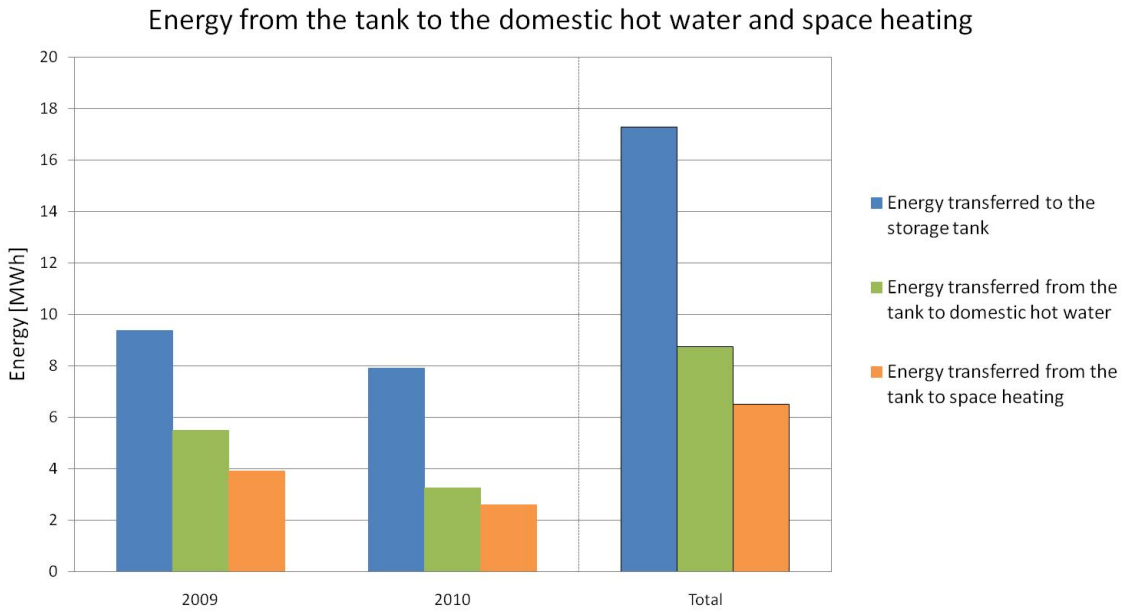

Figure 6.20 Energy sent from the storage tank to the domestic hot water and space heating.

In Figure 6.21 the monthly energy consumption for the new part of the school is shown, along with the energy transferred from the storage tank and from the oil burner to the domestic hot water. It can be seen on the figure that the hot water consumption (red columns) decreases in July and December, due to the students leaving the school. The figure also shows that during the summer months the solar heating system covers most of the demand for hot water. As the amount of sun decreases so does the transferred energy from the storage tank whilst the energy provided from the oil burner increases.

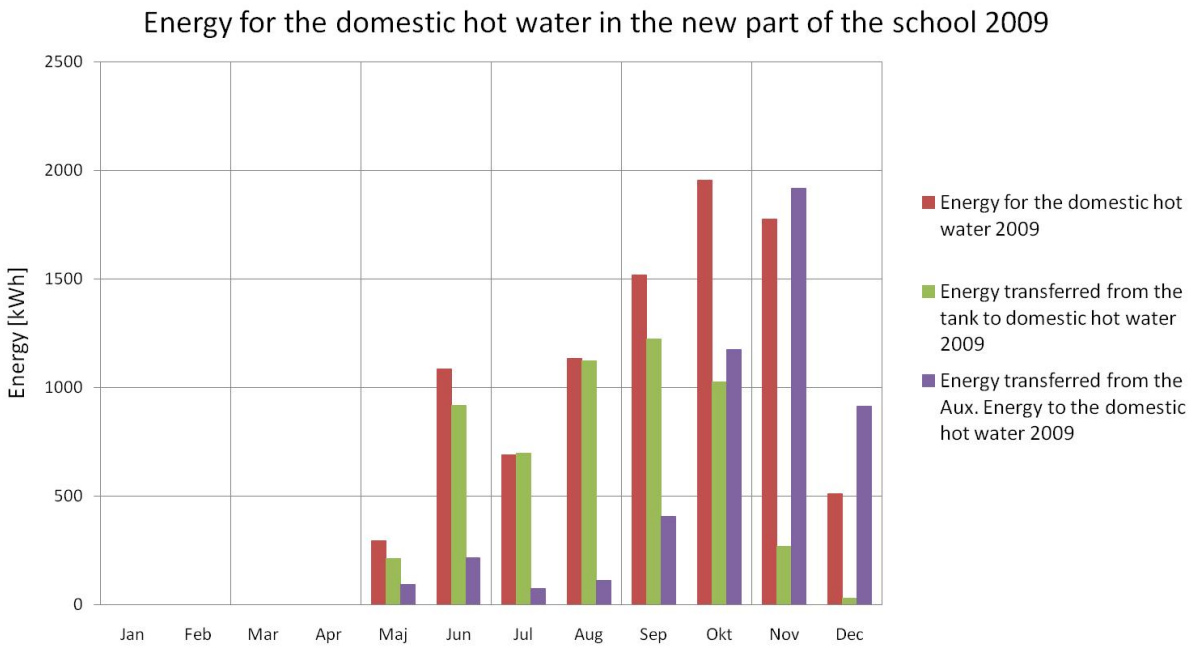

Figure 6.21 Energy for the domestic hot water in the new part of the school in 2009.

The same trends are seen in Figure 6.22 for 2010, but with exception of the 4 months where no energy was transferred from the storage tank to the domestic hot water. The figure also shows that the amount of energy transferred in the fall from the storage to the domestic hot water is much less than the energy transferred in 2009.

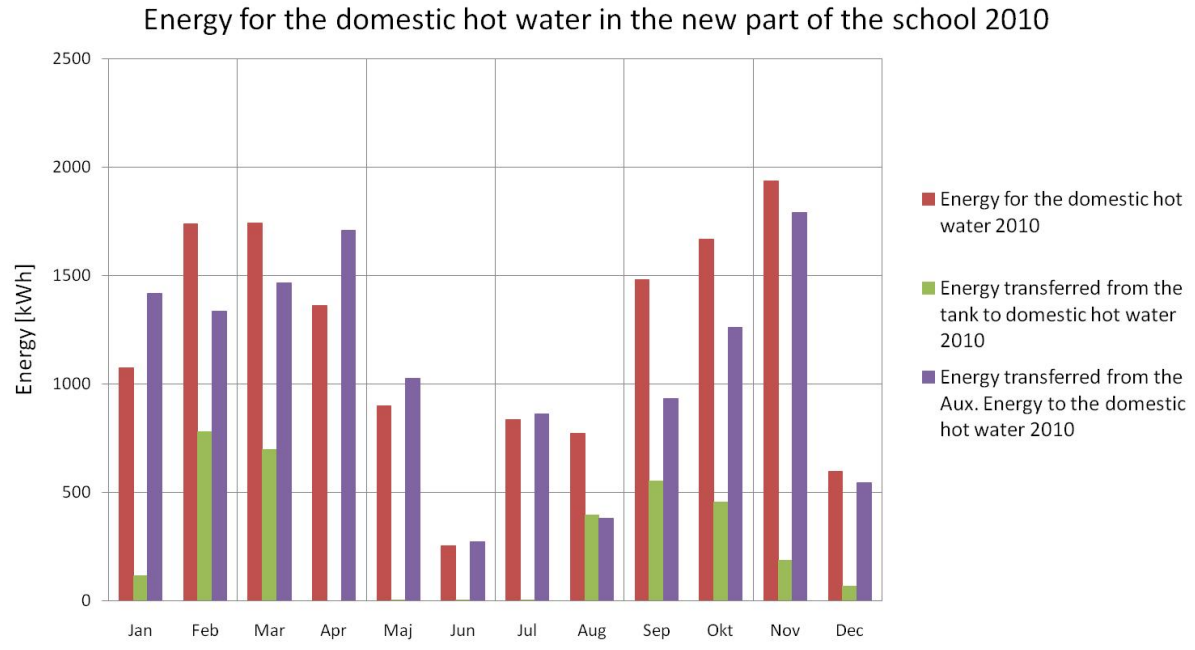

Figure 6.22 Energy for the domestic hot water in the new part of the school in 2010.

In Figure 6.23 the energy transferred on a monthly basis from the storage tank to the space heating loop for the new school is shown. The figure shows that the solar heating system does supply energy to the space heating loop, and if it is possible to change the controls, has the potential to cover a larger part of the space heating than it does at present.

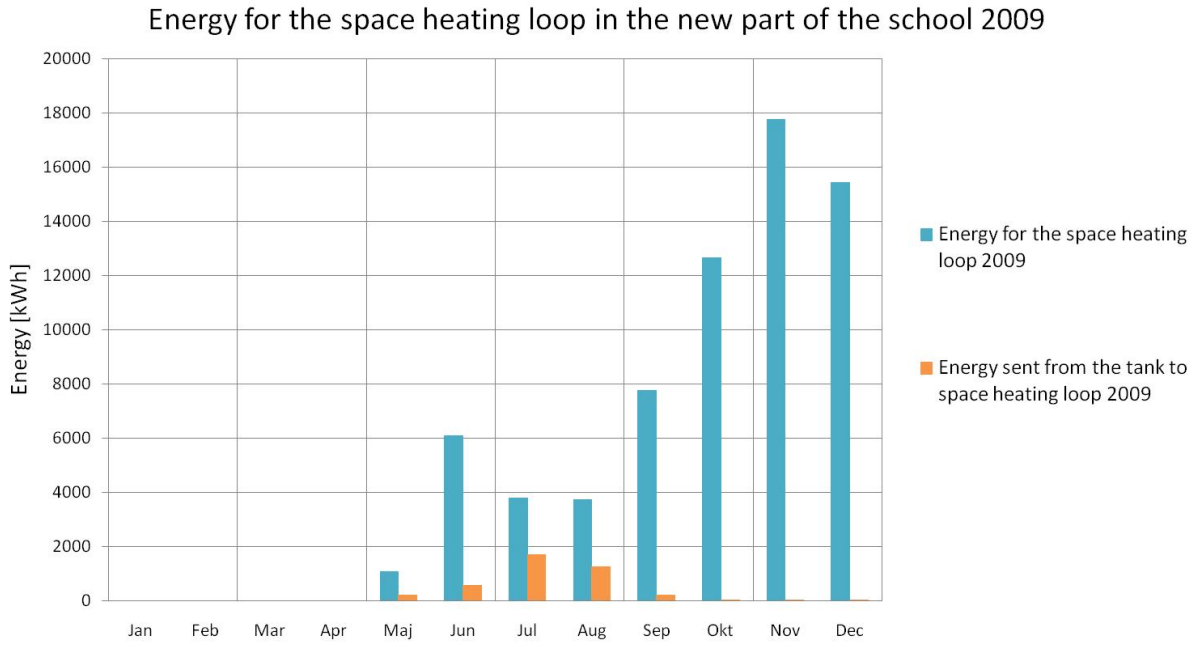

Figure 6.23 Energy for the space heating loop in the new part of the school in 2009.

For 2010 the picture is the same, see Figure 6.24. Again if it is possible to increase the amount of energy transferred from the tank to the space heating, there is a need for it in the school.

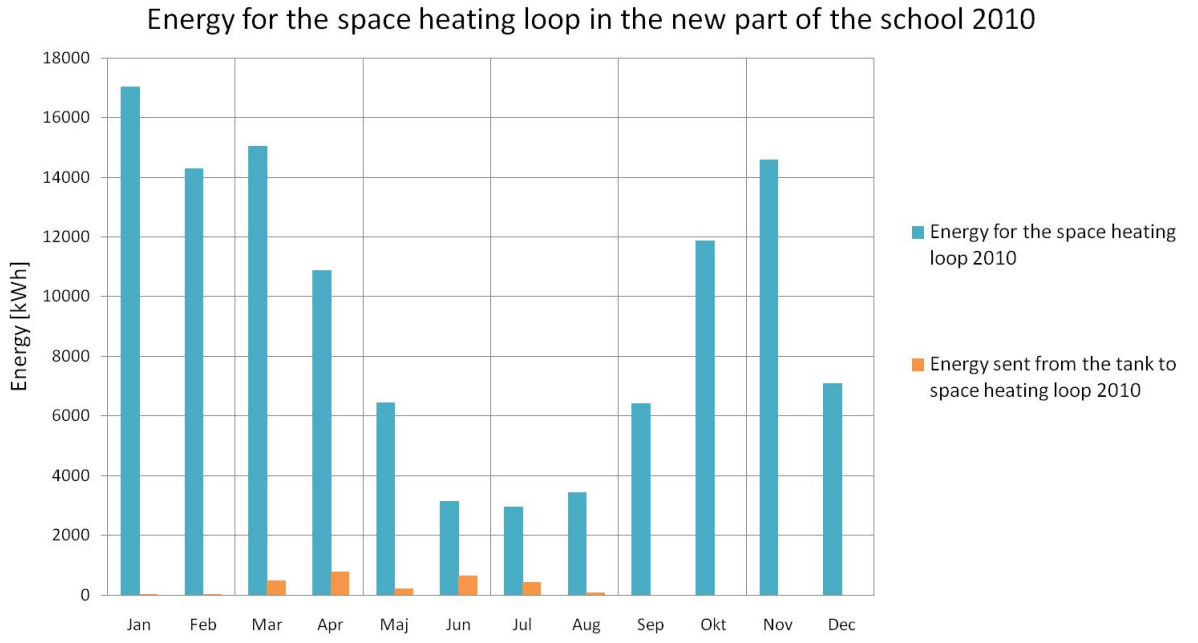

Figure 6.24 Energy for the space heating loop in the new part of the school in 2010.

6.3 Discussion

The solar heating system at the High School has since 2008 supplied energy for both the domestic hot water loop and the space heating loop. Experience from the installation of the system with both flat plate collectors and evacuated tubular collectors, along with measurements and analyses of the systems performance over 17 months has provided useful knowledge of the obstacles and possibilities for similar systems under Arctic conditions.

Installation

The installation of the system was carried out with help from professional installers from ExoTech. This was intended to improve the knowledge of the local installers. Although the language barrier from Swedish to Danish was an obstacle, faulty equipment resulted in much larger problems, since the solar collector fluid leaked out of the system.

Design

The design of the system with a transparent area of 62.4 m² and a 2000 l storage tank is not ideal, especially when the small heat exchanger between the collectors and the tank is taken into account. A storage tank of 3000 l would be better along with a larger external heat exchanger.

The hot water consumption of the school goes down during the summer in periods, when there are no students. For this reason it is important that the solar heating system is designed to cover the loss of demand from both the domestic hot water loop in the new school, and the consumption from the large kitchen, to maintain a discharge from the system.

Thermal performance

The analysis of the thermal performance shows that the system, when it is operating as intended, is able to cover most of the hot water consumption in the new part of the school during June, July, August and September. The system also provides energy to the space heating loop from May through to September and the measurements show that there is a potential to cover a larger amount of the space heating.

The coverage seen in 2010 is strongly affected by the control system fault, combined with the removing of the air escape valves without installing new valves. The measurements show that the stronger pump has not been able to push the air trapped in the collectors out of the system. It is therefore recommended that air is manually removed from the system by the valve placed on the roof as soon as possible, and that new air escape valves are inserted again where the old valves were removed in order to prevent the problem recurring.

The combination of faults described above has made evaluation of the potential of the system very difficult.

During the 17 months which were investigated, 9.4 MWh was sent to the domestic hot water loop, and 5.8 MWh was sent to the space heating loop. This is far below the estimated potential from ExoTech stating that the yearly useful energy from the system would be 46.0 MWh. This can to some extend be explained by the control system electronics fault and air trapped in the collectors, but it is also necessary to investigate the inter-play between the temperatures in the system and the control settings used to optimise the system.

Chapter 7 Pressure and temperature development in a solar heating system during stagnation

Most solar domestic hot water systems in Denmark are installed with a pressurized solar collector loop and an expansion vessel. The same is true for the systems installed in Greenland, and both the system in the Low energy house and at Knud Rasmussen Folk High School have pressurized solar collector loops and expansion vessels.

In 2009 a research project was carried out in order to investigate the pressure and temperature development in a solar heating system during stagnation. It was a part of an Energy Research Project "Quality insurance of solar heating systems" and carried out in cooperation with Batec Solvarme A/S.

The aim of the project was to elucidate how stagnation in the solar collectors affects the solar collector loop, the solar collector fluid and the expansion vessel [Dragsted et al. 2009]. As part of the project a dimensioning tool for Danish conditions was developed to determine the size of a pressurized expansion vessel for a solar collector loop in a solar heating system, which in sunny periods is protected from critical high temperatures by turning off the circulation pump if the temperatures are higher than a certain level.

The systems installed in Greenland are subject to more frequent periods with stagnation, since the power supply is less stable in Greenland compared to Denmark. If there is a power outage during a sunny period, the solar collector fluid will stand still in the solar collectors and eventually start to boil and thereby increase the pressure in the solar collector loop.

7.1 Experimental setup

The experimental setup consisted of three flat plate solar collectors which were installed in the collector loop along with a pressurized expansion vessel, see Figure 7.1 top left and right. The collector loop was designed in a way which made it possible to test different inlet connections to the collectors and different numbers of collectors, see Figure 7.1, bottom left.

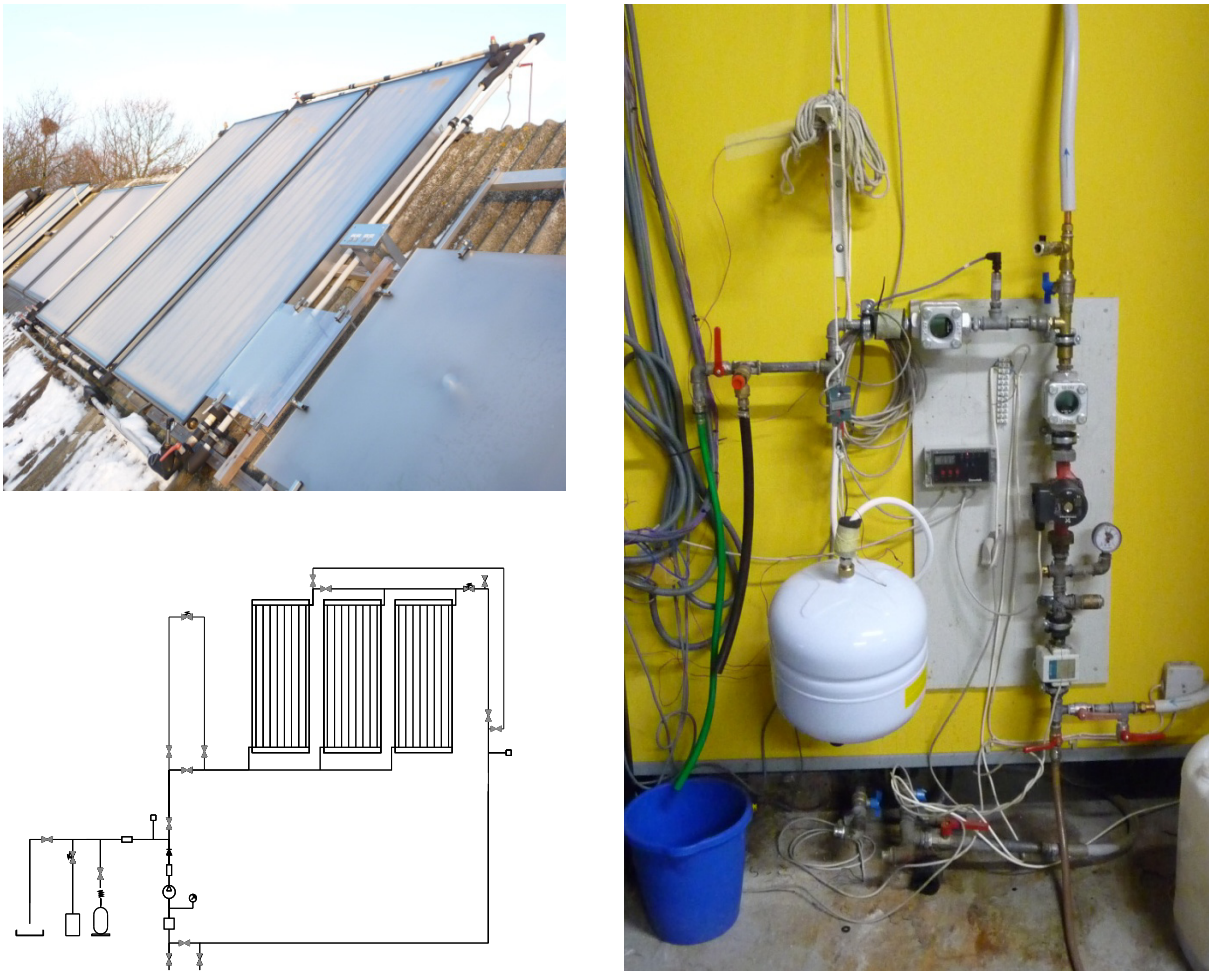

Figure 7.1 Pictures of the setup at the experimental test stand at the Technical University of Denmark and sketch of the solar collector loop.

The three flat plate solar collectors were BA30 from the Danish company Batec Solvarme A/S, with manifolds at the top and at the bottom and with 8 parallel strips between the manifolds. It was the same type of collector as the one used in the investigation in chapter 4 but with a larger absorber area. The collectors had a good emptying behaviour [Hausner and Fink 2000, Perers et al. 2003]. The absorber area of each collector was 3.0 m². The fluid content of each collector is 2.26 l. The efficiency expression for the collectors was:

$$\eta = 0{,}767 \cdot k_\theta - 3{,}867\frac{(T_m - T_a)}{G} - 0{,}010\frac{(T_m - T_a)^2}{G} \qquad (7\text{-}1)$$

Where the incidence angle modifier k_θ is:

$$k_\theta = 1 - tan^{3.43}\left(\frac{\theta}{2}\right) \qquad \text{With } k(60°) \qquad (7\text{-}2)$$

In the experimental setup the collectors were placed with a tilt of 45° and an orientation of 10° towards west from south. The pressurized expansion vessel, which was from the company Elbi, had a volume of 24 l and a pre-pressure of 3.0 bar. The solar collector fluid was a 32 % mixture of propylene glycol and water without inhibitors.

7.2 Equipment

The measuring period was from the 15th of July 2009 until the 31st of March 2010, during which measurements were collected both electronically and manually.

The measurements collected electronically: Total and diffuse radiation on the collector surface, pressure in the top and bottom of the solar collector loop, the weight of the expansion vessel and temperature measurements both inside the solar collectors and in the solar collector loop. Manually the PH-value and propylene glycol % of the solar collector fluid was recorded throughout the experiment.

The solar radiation was measured with pyranometers from Kipp and Zonen. The total radiation was measured with a CM 11 and diffuse radiation with a CM 5 pyranometer.

The pressure was measured in the solar collector loop at the level of the bottom of the collectors and at the inlet to the expansion vessel. The pressure was measured with pressure sensors from Sensor Technics. Type CTE8010GQ0.

The expansion vessel was installed in such a way that the increase in weight of the vessel was monitored by a transducer from Celesco, see Figure 7.1.

During the measuring period different setups were investigated, see Figure 7.2, along with variations of the pre-pressure of the expansion vessel and the system filling pressure, to test different conditions for stagnation.

The different setups investigated:

One collector with direct inlet (A)

One collector with U-inlet (B)

Three collectors with direct inlet (C)

Three collectors with U-inlet (D)

The strategy for the experiment was to control the pump in the collector loop in such a way that it was turned off when the temperatures in the collectors reach 90 °C. This induced stagnation in the collectors.

During the entire measuring period 97 stagnation periods were registered. The continuous measurements of the PH-value and propylene glycol percentage showed no change in either. PH-value maintained a value of 7 and the propylene glycol percentage stayed at 32 %.

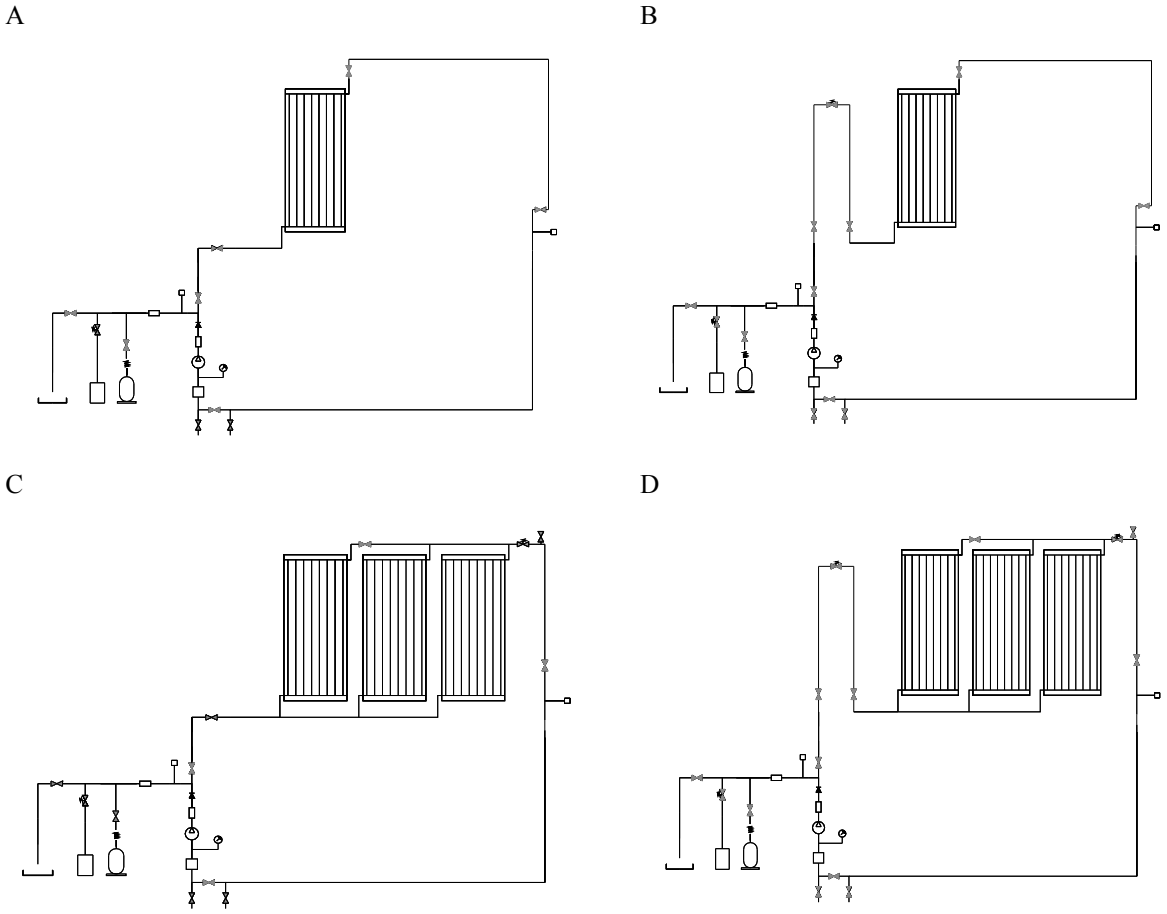

Figure 7.2 Sketches of the different setups investigated.

7.3 Measurements

The measurements from the investigations are shown for two sunny days: the 21st of July 2009 and the 1st of September 2009. The setup on the 21st of July was with one collector and direct inlet to the collector. The setup on the 1st of September was with three solar collectors and direct inlet to the collectors. The pre-pressure of the expansion vessel was set at 1.0 bar, and the system filling pressure was also 1.0 bar during both days.

7.3.1 One collector and direct inlet (a)

The measured solar radiation and ambient temperature is shown in Figure 7.3, and it can be seen that the 21st of July 2009 was a day with drifting thin clouds and a high ambient temperature.

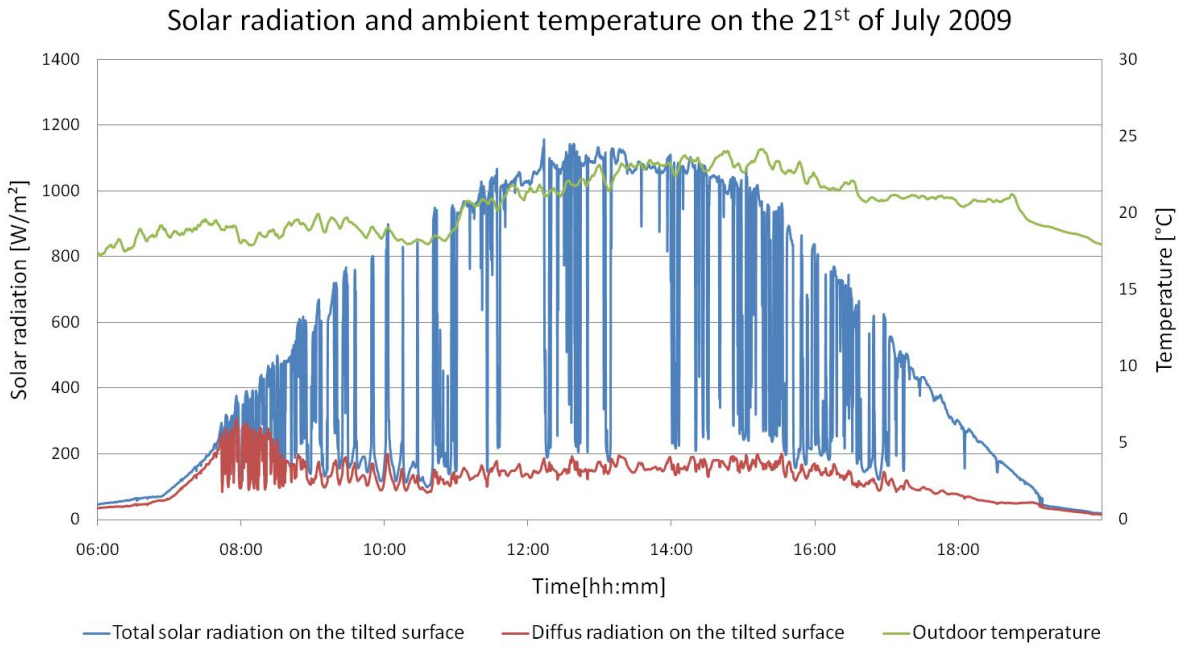

Figure 7.3 Solar radiation and ambient temperature on the 21st of July 2009.

In Figure 7.4 the increase in the weight of the expansion vessel is shown along with the pressure measured in the system on the 21st of July 2009. It can here be seen that the collectors reach stagnation just after 11:30 am, and that this state is more or less maintained until the afternoon around 15:30 pm.

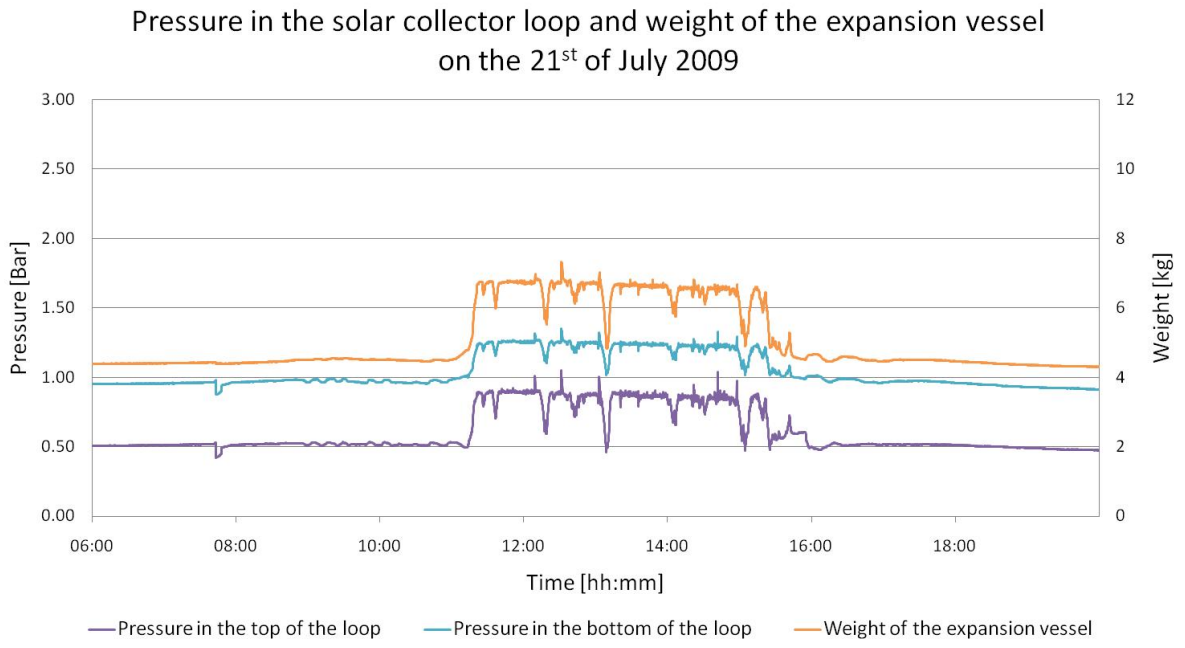

Figure 7.4 Pressure in the collector loop and weight of the expansion vessel on the 21st of July 2009.

The weight of the fluid pushed into the expansion vessel can be seen in Figure 7.5 along with the pressure difference between the top and the bottom of the collector loop. The figure shows that 2.3 kg is pushed into the expansion vessel during stagnation, which corresponds to 98 % of the total fluid volume in the solar collectors.

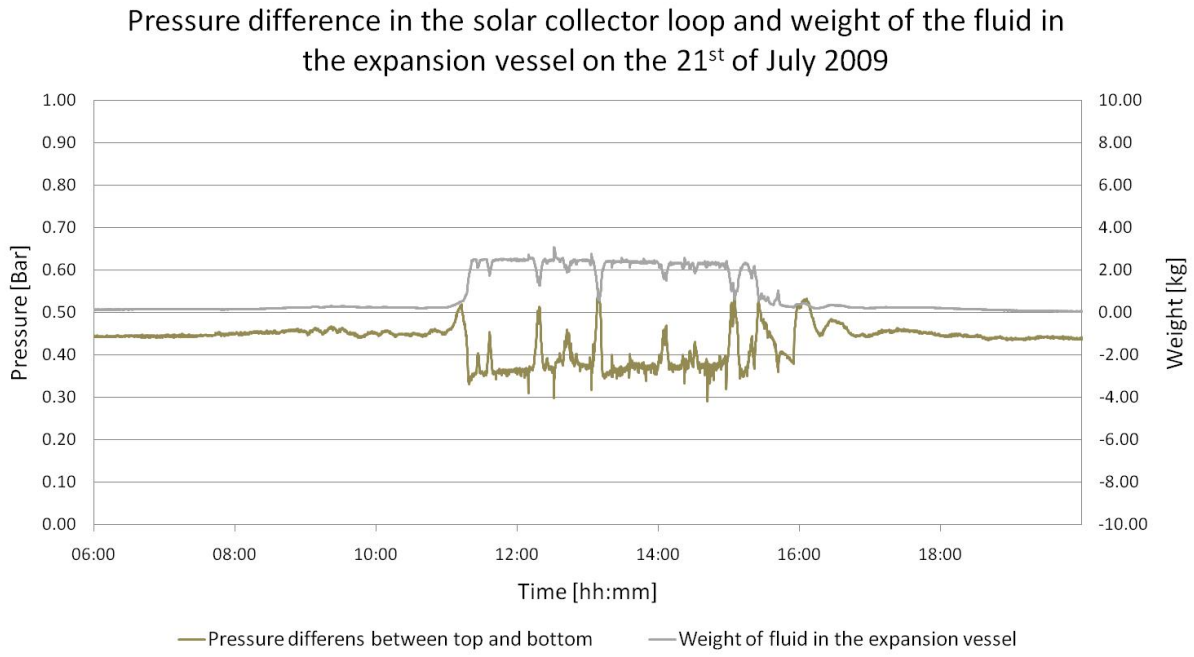

Figure 7.5 Weight of fluid in the expansion vessel and pressure difference between top and bottom in the collector loop on the 21st of July 2009.

In the investigations of the other setups, the measurements shows that the volume pushed into the expansion vessel during stagnation varies from 90% to 109% of the total volume of fluid in the collectors. When the volume in the expansion vessel exceeds that of the total fluid volume in the collectors, it is because the steam production in the collectors is pushed into the pipe leading away from the collector through the top outlet of the collector, thereby pushing more fluid into the expansion vessel. The interface between gas and fluid is at the bottom level of the collectors, both in the pipe and in the collector.

Figure 7.6 shows the temperatures in the collector loop, from the expansion vessel to the inlet to the collector. As soon as the pump is turned off, high temperatures in the solar collectors are prevented from reaching any vital components of the collector loop. It can be seen that during the day the stagnation in the collector is affected by the drifting clouds, where the temperature drops and the pump starts up again until the temperatures in the collector again reaches 90 °C and the pump is turned off.

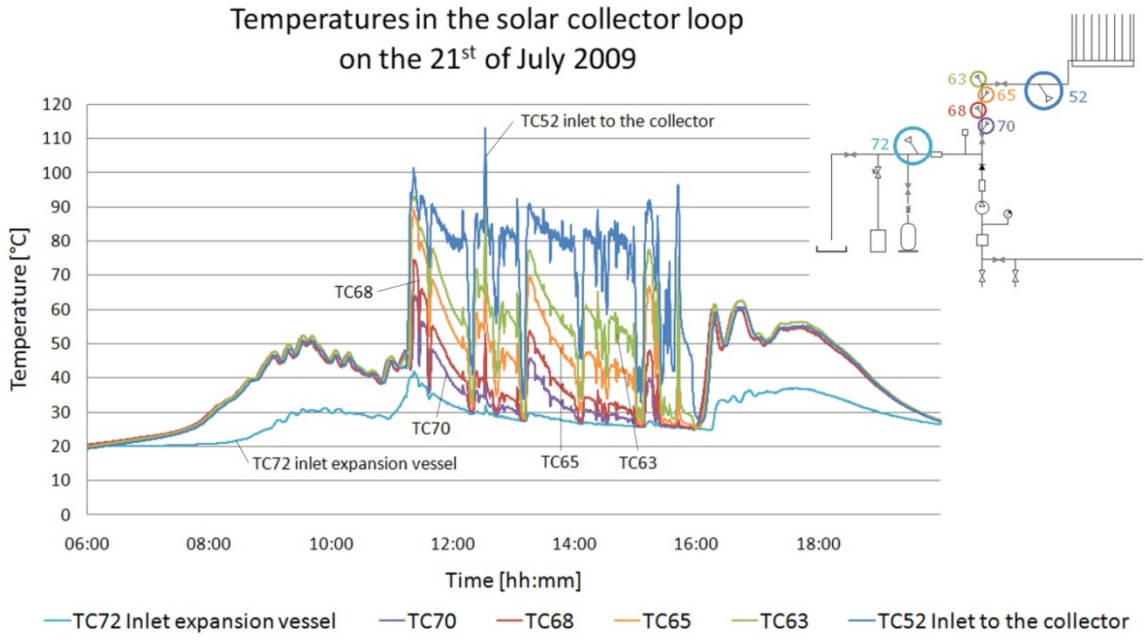

Figure 7.6 Temperatures in the collector loop from the expansion vessel to the inlet to the collectors on the 21st of July 2009.

The temperatures in the collector loop from the outlet from the collector to the expansion vessel can be seen in Figure 7.7. The same tendency can be seen here as in Figure 7.6, as soon as the pump is turned off the transfer of high temperatures stops.

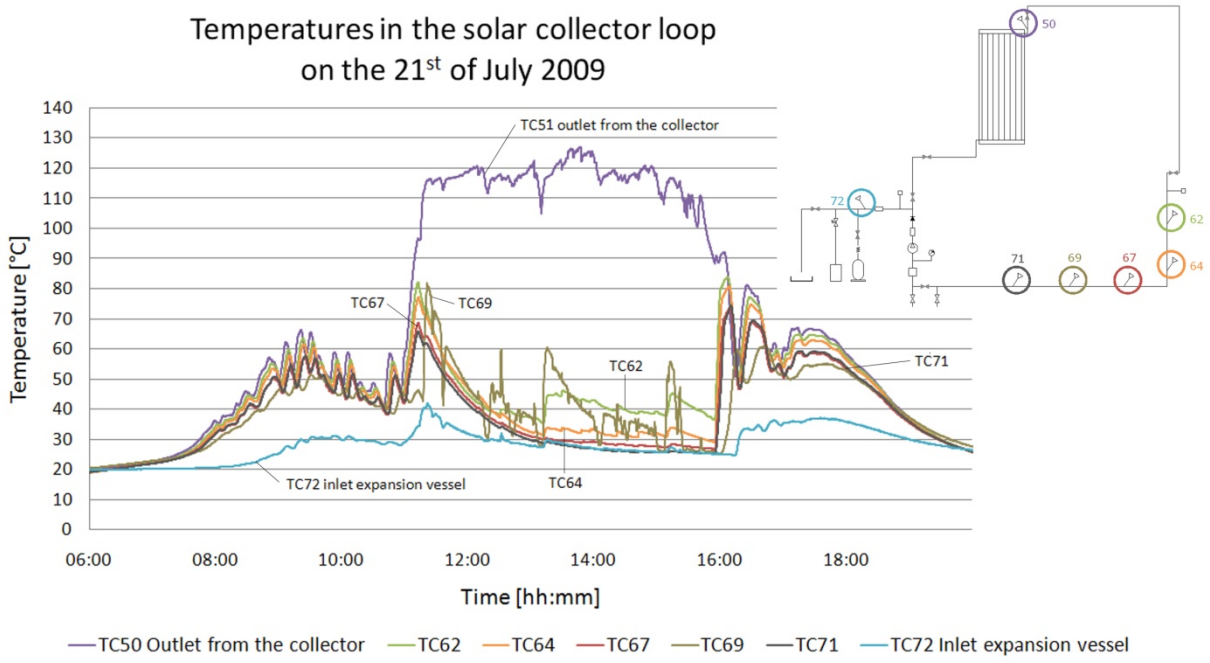

Figure 7.7 Temperatures in the collector loop from outlet of the collectors to the expansion vessel on the 21st of July 2009.

The investigations with the U-connection before the inlet to the collectors shows that this has little effect on the temperature development, pressure, and mass of fluid pushed into the expansion vessel. This means that having a non-ideal connection to the collectors is of no vital importance as long as the solar collectors have a good emptying behaviour.

7.3.2 Three collectors and direct inlet (c)

The measurements from the setup with three collectors and direct inlet are shown in the following. The solar radiation and ambient temperature is shown in Figure 7.8. It can be seen that the 1st of September 2009 was a day with very few clouds and high ambient temperature. The diffuse radiation increases in the afternoon because of occurrence of clouds.

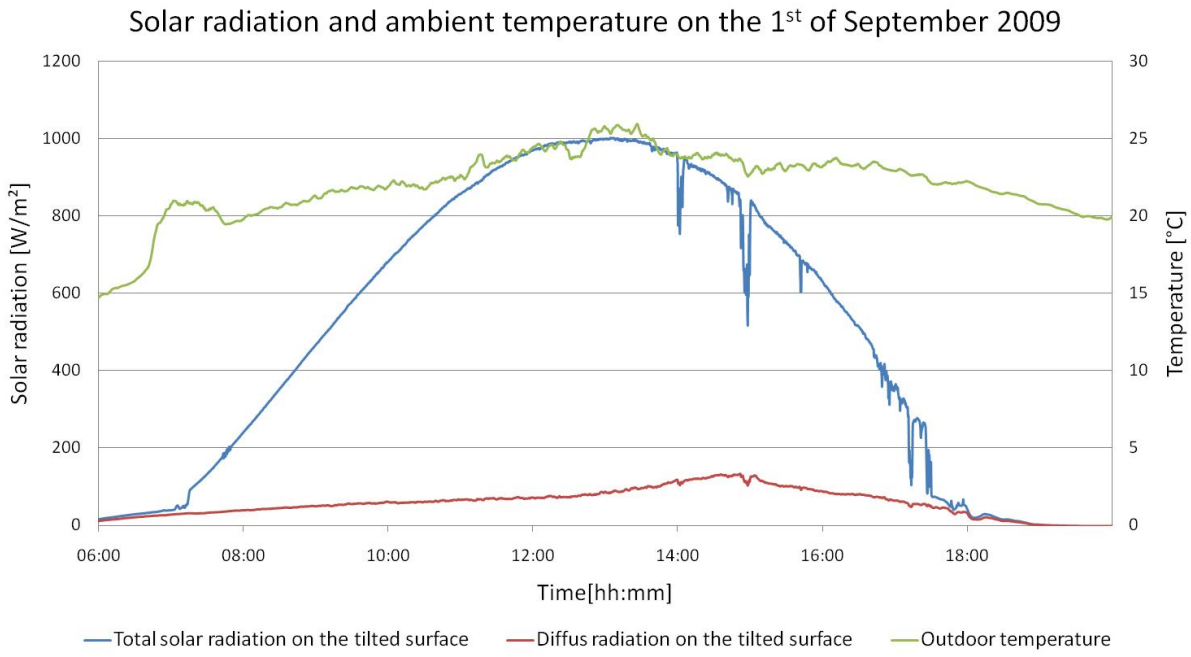

Figure 7.8 Solar radiation and ambient temperature on the 1st of September 2009.

The weight of the expansion vessel and the pressure in the system is shown in Figure 7.9. It can here be seen that the collectors reach stagnation just after 10:00 am, and this state is maintained until the afternoon around 15:30 pm.

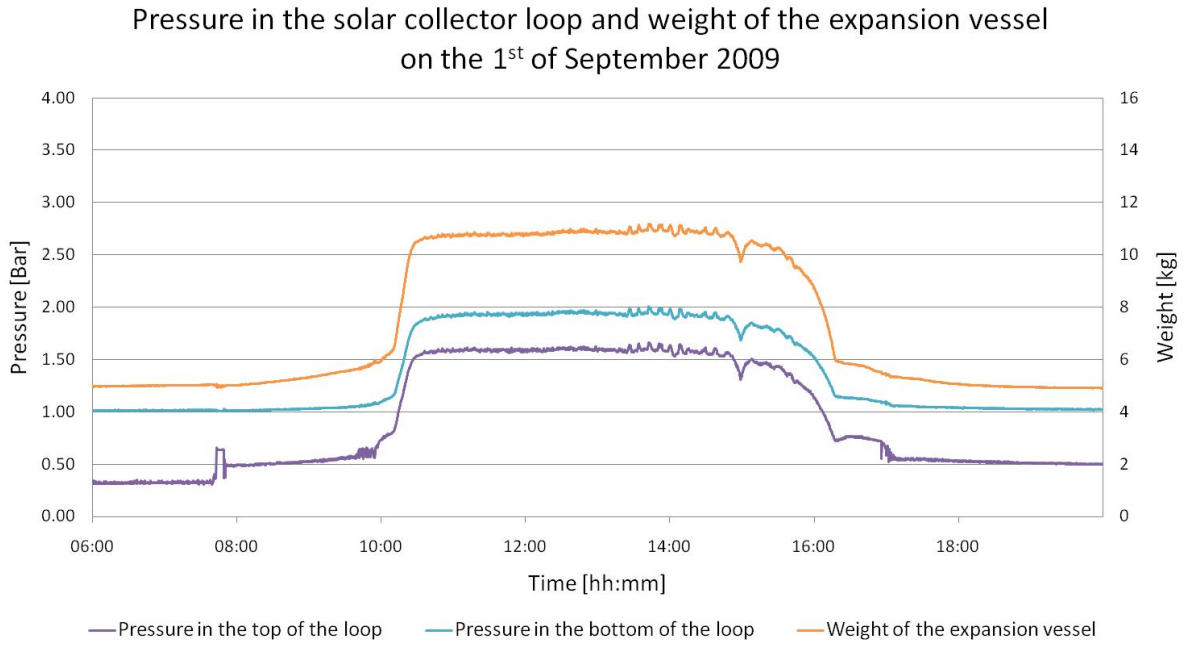

Figure 7.9 Pressure in the collector loop and weight of the expansion vessel on the 1st of September 2009.

The weight of the fluid pushed into the expansion vessel and the pressure difference between the top and the bottom of the collector loop can be seen in Figure 7.10. The figure shows that 6.5 kg is pushed into the expansion vessel during stagnation, which corresponds to 95% of the total fluid volume in the solar collectors.

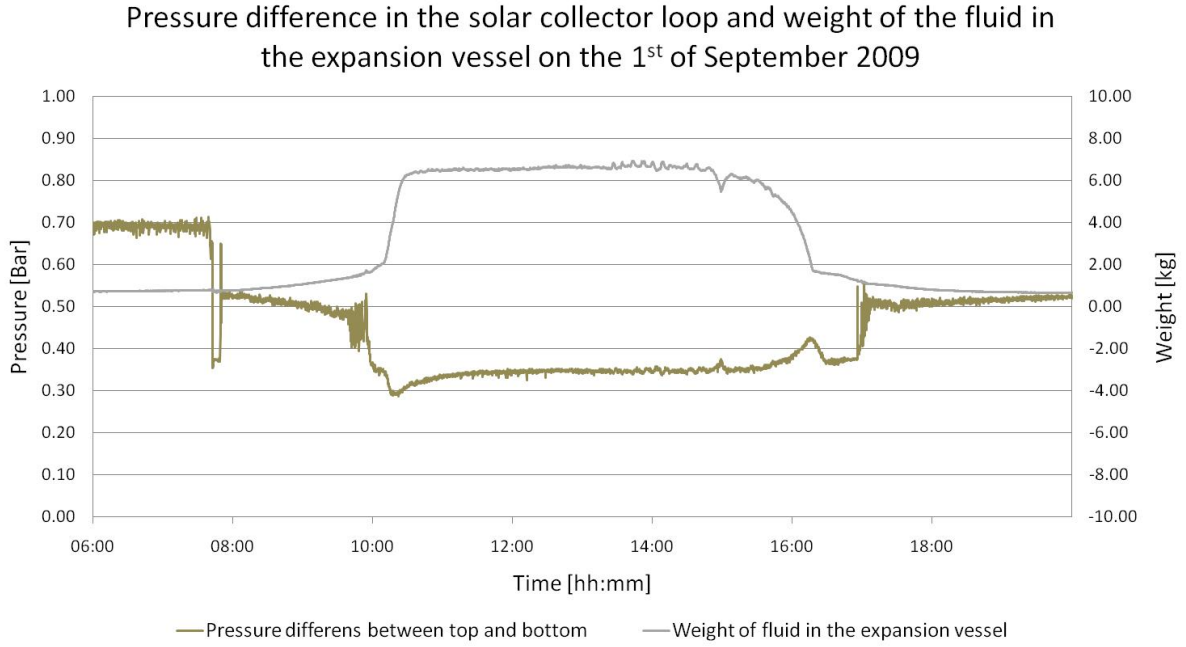

Figure 7.10 Weight of fluid in the expansion vessel and pressure difference between top and bottom in the collector loop on the 1st of September 2009.

The temperatures in the collector loop, from the expansion vessel to the inlet to the collectors are shown in Figure 7.11. As soon as the pump is turned off, high temperatures in the solar collectors are prevented from reaching any vital components of the collector loop. The fluctuations seen close to the inlet of the collectors are due to a continuous change of the level of the interface between gas and fluid in the collectors, resulting in changing fluid flow directions in the inlet pipe to the collectors.

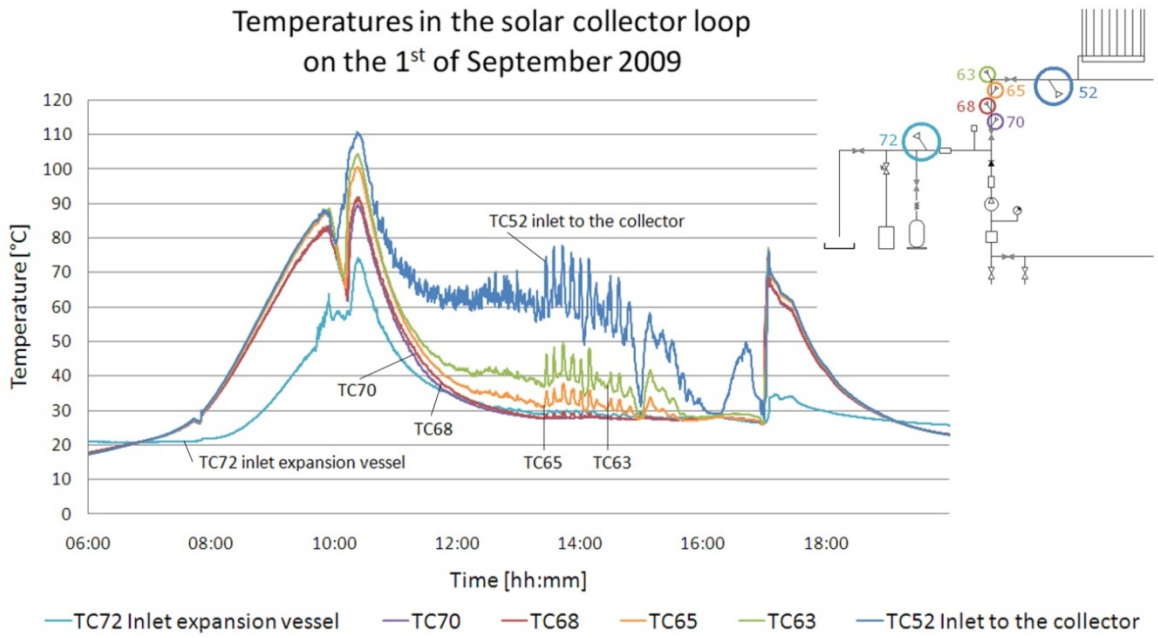

Figure 7.11 Temperatures in the collector loop from the expansion vessel to the inlet to the collectors on the 1st of September 2009.

The temperatures in the collector loop from the outlet of the collector to the expansion vessel can be seen in Figure 7.12. Again as soon as the pump is turned off the transfer of high temperatures is stopped. The temperature at the outlet from the collectors is high during the whole stagnation period and does not begin to fall until the pump starts working again.

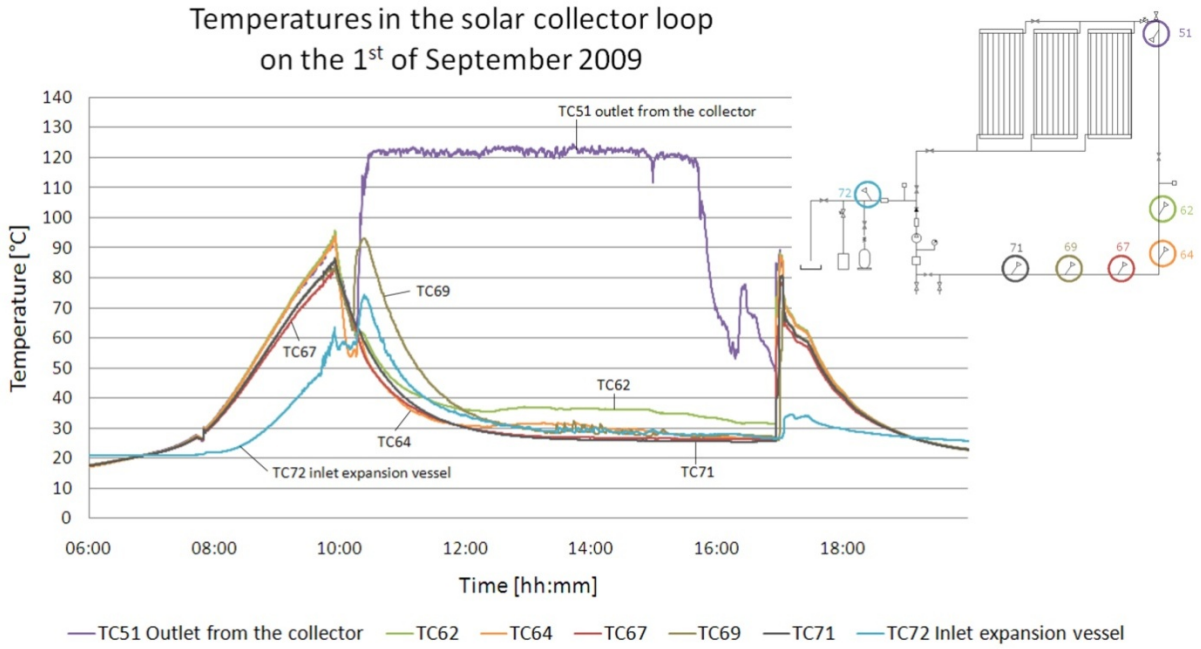

Figure 7.12 Temperatures in the collector loop from outlet of the collectors to the expansion vessel on the 1st of September 2009.

Based on the investigations it is concluded that the principle with a large expansion vessel and a control system turning the circulation pump off at a high temperature level will result in a durable solar collector loop as long as solar collectors with a good emptying behaviour and a propylene glycol water mixture without inhibitors are used.

7.3.3 Dimension sheet for installers

A dimensioning tool for installers for dimensioning the expansion vessel was constructed. An excel-sheet was prepared based on a detailed investigation of the theory of stagnation and validation of a simulation model by means of measurements, [Chen et al. 2009]. The input to the excel-sheet is: Number of collectors, fluid content of collectors, inner pipe diameter of the top part of the collector loop, pipe length of the top part of the collector loop, total volume of solar collector fluid in the system, propylene glycol percentage of the solar collector fluid, max. acceptable temperature for the solar collector fluid, vertical distance between the collectors and the expansion vessel, pre-pressure of the expansion vessel and the system filling pressure. Though the excel sheet was created based on measurements from Denmark, the excel sheet can also be used for Greenlandic locations. This is because the maximum temperature in solar collector is an input to the excel sheet, and in a sense gives the worst conditions for the solar heating system and thereby the dimensioning conditions for the expansion vessel. It is important to state that the excel sheet can only be used for solar collectors with a good emptying behaviour, as the BA22 and BA30, which means inlet at the bottom and outlet at the top.

In Figure 7.13 the volume of the expansion vessel can be determined for a specific system for different pre-pressures of the expansion vessel and system filling pressures.

Figure 7.13 shows the calculations for:

> 1 BA30 collector, max. temperature = 150 °C, distance between top of collector loop and expansion vessel 6 m, pipe length of top collector loop 3.5, inner diameter in collector loop 0.013 m, propylene glycol percent 50 %, fluid content in collector loop 10 l.

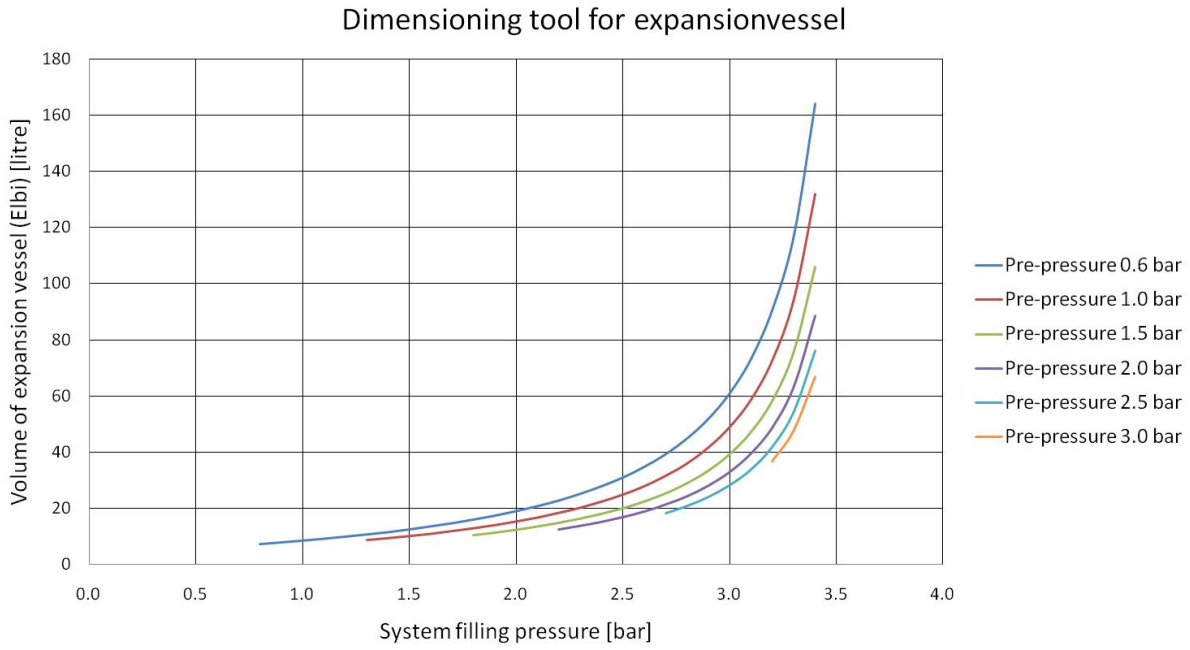

Figure 7.13 Example of dimensioning tool for expansion vessel.

7.4 Discussion

Investigations have shown that during stagnation the solar collector fluid in the top of the solar collectors evaporates and expands. This expansion pushes collector fluid into the inlet pipe and into the expansion vessel. During the stagnation high temperatures are maintained in the collectors, while the temperatures in the solar collector loop are relatively low. This is independent of the different setups with different numbers of collectors and different inlet connections. The volume pushed into the expansion vessel varies from 90% to 109% of the fluid volume in the collectors with the different setups, pre-pressures of the expansion vessel and filling pressures of the system.

During the measuring period 97 stagnation periods were recorded. The solar collector fluid maintained a propylene glycol percentage of 32 % during the whole measuring period, and the PH-value of the fluid kept at a value of 7 throughout the period.

The investigations showed that a control system turning off the pump at high temperatures, and a large pressurized expansion vessel will secure a solar heating system from critically high temperatures and secured the durability of the solar collector fluid, as long as the collectors have a good emptying behaviour, and a propylene glycol water mixture without additives is used as solar collector fluid.

The principle will also secure the solar heating system from damage in sunny periods with power outage, therefore making it attractive for Greenland.

Chapter 8 Conclusions

8.1 Conclusion on the mathematical modelling of solar radiation

Analysis of the global and diffuse radiation measurements in Sisimiut show that the diffuse correlations methods developed by 'Erbs et al.' and 'Orgill and Hollands' underestimate the diffuse radiation and overestimate the beam radiation. Of the two correlations 'Orgill and Hollands' is the most accurate, underestimating the diffuse radiation by 3.3 % and thereby overestimating the beam radiation by 2.7 %.

The investigations of four different radiation models show that for the conditions in Greenland it is not suitable to take circumsolar diffuse radiation and horizontal brightening diffuse radiation into account. Of the four models the 'Liu and Jordan' model – the simple isotropic model - is the most accurate.

Measurements showed that snow reflects solar radiation as a mirror. The effective albedo is therefore a function of the difference between the solar azimuth and the surface azimuth. Equations for the effective albedo were determined for each month of the year based on the measurements. The equations can be used as input for simulation models.

8.2 Conclusion on the potential and practical experience of solar heating in Greenland

The collector area for solar domestic hot water system in Greenland should be proportional to the daily hot water consumption, approximately 1 m^2 for a daily hot water consumption of 40 l. A reasonable assumption of the hot water consumption is 35-50 l per person. For a family of four this results in a hot water consumption of 140 – 200 l and a collector area between 3.5 – 5.0 m^2. The orientation of the collectors should not deviate more than ± 30° from the optimum orientation. The tilt should not deviate more than 15° from the optimum.

The solar heating systems respectively in the Low Energy House and at the Knud Rasmussen Folk High School have both provided practical experience of operation and performance of solar heating systems in an Arctic climate.

The experience from the systems regarding the installation of solar heating systems shows that having trained installers is of vital importance. This is both in terms of installing new systems and in connection with repair of existing systems. Both systems experienced problems during the installation, which affected the performance of the systems and could have been avoided with better education of the

installers. The importance of using pre-fabricated components of solar heating systems must be mentioned. By using such components the risk of installation errors are reduced.

The operation of the solar heating system at the Low Energy House showed that thermosyphoning proved to be a problem during the cold winters. Thermosyphoning can be prevented by installing a non return valve on the return from the collectors, or a magnetic valve controlled by the pump in the solar collector loop.

The system in the Low Energy House reached a yearly solar fraction of 46 % in 2010 after several corrections had been made to the system. The system as it is now still leaves room for improvement, by utilizing the energy sent to the radiator in a better way, which opens up the possibility for even higher solar fractions.

The thermal performance of the system at the Knud Rasmussen Folk High School is difficult to evaluate, because of electrical faults in the system. The measurements from the system have shown that the system is capable of covering most of the hot water consumption for four months during the summer, while also providing energy to the space heating loop. During the 17 months investigated the system produced 15.2 MWh of useful energy, which is much lower than anticipated.

Both system have pressurised solar collector loops with expansion vessel, and have proved that this design works well under Arctic conditions, where the power-outage is more frequent leaving the system at risk if this happens during sunny periods when the pump in the solar collector loop is not working. This is supported by the investigation carried out at the Technical University of Denmark, of the pressure and temperature development in solar collectors and solar collector loops during stagnation. The investigation showed that the volume of solar collector fluid which is pushed into the expansion vessel varies from 90% to 109% dependent on the different collector areas, pre-pressures of the expansion vessel and filling pressures of the system. When the temperature drops in the solar collectors the fluid is pushed back into the solar collectors.

During the measuring period at the test facility at the Technical University of Denmark 97 stagnation periods were recorded. The solar collector fluid maintained a propylene glycol percentage of 32 % during the whole measuring period, and the PH-value of the fluid kept at a value of 7 throughout the period. The investigation also showed that good emptying behavior of the solar collector is of importance.

This has proven to be a problem for the flat plate solar collectors installed at the Knud Rasmussen Folk High School, where solar collector fluid is ‘trapped’ during stagnation and causes the pressure in the system to build up with the potential for damaging the system.

8.3 Outlook

It is recommended to continue measurement of the diffuse and global radiation in Sisimiut, and install similar measuring devices at other locations in Greenland. This will provide data from which a diffuse correlation method suitable for the conditions in Greenland can be derived.

It is also recommended to continue measuring the total and reflected radiation in different directions at other locations, in order to elucidate how the reflection from the ground is affected by the latitude. Further, measurements of the reflection for both direct and diffuse radiation are recommended.

The data will provide input for radiation models, so that the solar radiation on different tilted and oriented surfaces in Greenland can be determined with improved accuracy.

In terms of monitoring solar heating systems installed in Greenland it is recommended that this continues for the system in the Low Energy House and at the Knud Rasmussen Folk High School, and that the newly installed system at the schools dormitory is included in the monitoring process. It is also recommended that this system is thoroughly checked, so that any faults are found and corrected as soon as possible.

Continuing to educate installers is important for both the maintenance of the existing systems but also to further increase the number of installed solar heating systems in Greenland, and thereby decreasing emissions of CO_2.

Chapter 9 References

Chen, Z., Dragsted, J., Furbo, S., Perers, B., 2010. Theoretical study on a solar collector loop during stagnation. Eurosun 2010. Graz, Austria.

Choudhury, B. J., Chang, A. T. C., 1981. On the angular variation of solar reflectance of snow. Journal of geophysical research Vol. 86, pp. 465-472.

Dragsted, J., Furbo, S., Fan, J., 2008. Solar heating systems in the Arctic. Conference Proceedings: Sustainable energy supply in the Arctic, Sisimiut, Greenland, 2008.

Dragsted, J., Furbo, S., Bengt, P., Ziqian, C., 2009. Solfangerkreds med stor ekspansionsbeholder og fordampning i solfanger ved faretruende høje temperaturer til sikring af solfangervæske og anlæg. Department of Civil Engineering at the Technical University of Denmark. Rapport SR 10-04.

Duffie, J. A., Beckman, W. A., 1991. Solar engineering of thermal processes, Second ed. John Wiley & Sons, INC., New York.

Erbs, D.G., Klein, S. A., Duffie, J. A., 1981. Estimation of the diffuse radiation fraction for hourly, daily and monthly-average global radiation. Solar Energy. Vol. 28, pp 293-302.

Furbo, S., 1982. Test procedures for heat storages for solar heating systems. International Journal of Solar Energy Vol. 1, pp. 419-429.

Furbo, S., Berg, P., 1990. Calculation the thermal performance of small hot water solar heating systems using low flow operation. Conference Proceedings North Sun 1990, Reading, United Kingdom.

Furbo, S., Shah, L., 2002. Lavenergihuset i Sisimiut – Solvarmeanlæg. Bagrund og forslag. Department of Civil Engineering at the Technical University of Denmark. Rapport SR 02-22.o

Furbo, S., Shah, J. L., 2003. Thermal advantages for solar heating systems with a glass cover with antireflection surfaces. Solar Energy, Volume 74, pp.513-523.

Furbo, s., 2004. Low flow solar heating systems. Department of Civil Engineering at the Technical University of Denmark. Educational note U-067.

Hausner, R., Fink, C., 2000. Stagnation behaviour of thermal solar systems. Eurosun 2000 Congress proceedings, Copenhagen, Denmark.

Hay, J. E., Davies, J. A., 1978. Calculation of the solar radiation incident on an inclined surface. First Canadian Solar Radiation Data Workshop. Canadian Atmospheric Environment Service and the National Research Council of Canada.

Jensen, K. F., Lauritsen, D., 2006. Solstråling under arktiske forhold, Department of Civil Engineering,Technical University of Denmark.

Klucher, T. M., 1978. Evaluation of models to predict insolation on tilted surfaces. Solar Energy Vol. 23, pp. 111-114.

Knudsen, S., 2004. Investigation and optimization of heat storage tanks for low-flow SDHW systems. Department of Civil Engineering at the Technical University of Denmark. PhD thesis, Report R-075.

Koenderink, J. J., W. A. Richards, 1992. Why is snow so bright?.Journal of the Optical Society of America A, Vol. 9, Issue 5, pp. 643-648.

Kotol, M., Rode, C., Vladykova, P., Furbo, S., Borchersen, E., 2010. Low-energy house in Sisimiut – Annual report of Low-energy house performance July 2009 to June 2010. Department of Civil Engineering at the Technical University of Denmark. Rapport SR 10-10.

Krag, J., Nielsen, T. R., Svendsen, S., 2002. Grønlandsk vejrdata Nuuk Uummannaq. Department of Civil Engineering at the Technical University of Denmark. Rapport November 2002.

Liu, B. Y. H., Jordan, R. C., 1963. The long-term average performance of flat-plate solar-energy collectors. Solar Energy. Vol. 7, pp. 53-74.

Orgill, J. F., Hollands, K. G. T., 1977. Correlation equation for hourly diffuse radiation on a horizontal surface. Solar Energy. Vol. 19, pp. 357-359.

Perers, B., Lorenz, K., Rönnelid, M., 2003. Partiell f¨0rångning I solfångarsystem. Överhettningsskyld för värmebäraren (främst glycol). Centrum för solenergiforskning Solar energy research center. December 2003. ISSN 1401-7555.

Perez, R., Seals, R., Ineichen, P., Stewart, R., Menicucci, D., 1987. A new simplified version of the Perez diffuse irradiance model for tilted surfaces. Solar Energy Vol. 39, pp. 221-231.

Pirazzini, R., 2004. Surface albedo measurements over Antarctic sites in summer. Journal of Geophysical Research, Volume 109.

Psiloglou, B. E., Balaras, C. A., Santamouris, M., Asimakopoulos,D. N., 1997. Calculation of ground albedo for the estimation of global radiation on tilted surfaces, for four European locations. International Journal of Solar Energy, Volume 18, pp. 231-258.

Rode, C., Borchersen, E., Fan, J., Furbo, S., Kragh, J., 2006. Lavenergihuset i Sisimiut – Årsrapport for lavenergihusets ydeevne juli 2005 til juni 2006. Department of Civil Engineering at the Technical University of Denmark. Rapport SR 06-12.

Rode, C., Borchersen, E., Fan, J., Furbo, S., Kragh, J., 2007. Lavenergihuset i Sisimiut – Årsrapport for lavenergihusets ydeevne juli 2006 til juni 2007. Department of Civil Engineering at the Technical University of Denmark. Rapport SR 07-10.

Rode, C., Borchersen, E., Fan, J., Furbo, S., Kragh, J., 2008. Lavenergihuset i Sisimiut – Årsrapport for lavenergihusets ydeevne juli 2007 til juni 2008. Department of Civil Engineering at the Technical University of Denmark. Rapport SR 08-03.

Rode, C., Kragh, J., Borchersen, E., Vladykova, P., Furbo, S., Dragsted, J., 2009. Performance of the Low-energy House in Sisimiut. Cold Climate HVAC.

Shah, J. L., Furbo, S., 1996. Optimization of mantle tanks for low flow solar heating systems. Conference Proceedings EuroSun 1996, Freiburg, Germany.

Shah, L. J., 1999. Investigation and modeling of thermal conditions low flow SDHW systems. Department of Civil Engineering at the Technical University of Denmark. PhD thesis, Report R-034.

Shah, J. L., 2000. Heat transfer correlations for vertical mantle heat exchangers. Solar Energy, Volume 69, pp.157-171.

Shah, L., Furbo, S., 2005. Modeling shadows on evacuated tubular collectors with cylindrical absorbers. Journal of Solar energy engineering, Volume 127, pp. 333-342.

Temps, R. C., Coulson, K. L., 1977. Solar radiation incident upon slopes of different orientations. Solar Energy Vol. 19, pp. 179-184.

Vladykova, P., Borchersen, E., Rode, C., Furbo, S., 2009. Low-energy house in Sisimiut – Annual report of Low-energy house performance July 2008 to June 2009. Department of Civil Engineering at the Technical University of Denmark. Rapport SR 09-06.

Wang, Z., Barlage, M. Zeng, X., 2005. The solar zenith angle dependence of desert albedo. Geophysical research letters, Volume 32.

Wang, X., Zender, C. S., 2010. MODIS snow albedo bias at high solar zenith angles relative to theory and to in-situ observations in Greenland, Remote sensing of environment, Volume 114, pp. 563-575.

Warren, S. G., 1982. Optical properties of snow. Reviews of geophysics and space physics, Vol. 20, No. 1, 67-89.

Wiscombe, W. J., Warren, S. G., 1980. A model for spectral albedo of snow. I: Pure snow. Journal of the atmospheric sciences, Volume 37.

Yamanouchi, T., 1983. Variations of the incident solar flux and snow albedo on the solar zenith angle and cloud cover, at Mizuho Station, Antarctica. Journal of the Metrological society of Japan Vol. 61, No. 6.

Ørbæk, A., Halpin, F., Dahl, J., 2010. Solar collectors in the Arctic – Field Report. 41420 Arctic Technology Course. Department of Civil Engineering at the Technical University of Denmark. Student Report 2010.

Solar energy is a clean and natural energy source. The solar radiation on earth – including at Arctic latitudes – is so large that it is possible to utilize solar energy on a large scale. Using solar energy means reducing the use of fossil fuels. In the Arctic several conditions must be taken into account in terms of solar radiation at these latitudes. The sun is positioned low on the sky, which means that the optimum tilt angle of a receiving surface will increase. Also most solar radiation appears in the summertime, where there, at latitudes above the Arctic Circle, is solar radiation 24 hours a day and radiation from all directions. The reflection from the snow will increase the solar radiation on tilted surfaces. The use of solar energy varies from country to country, as does the design of the solar heating systems.

The purpose of this study is to investigate the solar radiation potential in Greenland, and to investigate how a solar heating system for Greenland should be designed.

DTU Civil Engineering
Department of Civil Engineering
Technical University of Denmark

Brovej, Building 118
2800 Kgs. Lyngby
Telephone 45 25 17 00

www.byg.dtu.dk

ISBN: 978877973203
ISSN: 1601-2917